



Laporan Akhir Projek Penyelidikan Jangka Pendek

**Digital Image Thumbnail To Represent
Images With Poor Quality**

by

Assoc. Prof. Dr. Haidi Ibrahim

Dr. Dzati Athiar Ramli

2015

Please use this checklist to self-assess your report before submitting to RCMO.
Checklist should accompany the report.

Digital Image Thumbnail to Represent Images with Poor Quality

1001/PELECT/814169

Assoc. Prof Dr Haidi Ibrahim & Dr Dzati Athiar Ramli



NO.	ITEM	PLEASE CHECK (✓)		
		PI	JKPTJ	RCMO
1	Completed Final Report Form	✓	✓	
2	Project Financial Account Statement (e-Statement)	✓	✓	
3	Asset/Inventory Return Form (<i>Borang Penyerahan Aset/Inventori</i>)	✓	✓	
4	A copy of the publications/proceedings listed in Section D(ii) (Research Output)	✓	✓	
5	Comprehensive Technical Report	✓	✓	
6	Other supporting documents, if any	-NA-		
7	Project Leader's Signature	✓	✓	
8	Endorsement of PTJ's Evaluation Committee	✓	✓	
9	Endorsement of Dean/ Director of PTJ's	✓	✓	



RU GRANT FINAL REPORT FORM

Please email a softcopy of this report to rcmo@usm.my



A	PROJECT DETAILS								
i	Title of Research: Digital Image Thumbnail to Represent Images with Poor Quality								
ii	Account Number: 1001/PELECT/814169								
iii	Name of Research Leader: Dr. Haidi Ibrahim								
iv	Name of Co-Researcher: 1. Dr. Dzati Athiar Ramli								
v	Duration of this research: <table style="margin-left: 20px;"> <tr> <td>a) Start Date</td> <td>: 15 July 2012</td> </tr> <tr> <td>b) Completion Date</td> <td>: 14 July 2015</td> </tr> <tr> <td>c) Duration</td> <td>: 3 years</td> </tr> <tr> <td>d) Revised Date (if any)</td> <td>: -</td> </tr> </table>	a) Start Date	: 15 July 2012	b) Completion Date	: 14 July 2015	c) Duration	: 3 years	d) Revised Date (if any)	: -
a) Start Date	: 15 July 2012								
b) Completion Date	: 14 July 2015								
c) Duration	: 3 years								
d) Revised Date (if any)	: -								
B	ABSTRACT OF RESEARCH								
	<p><i>(An abstract of between 100 and 200 words must be prepared in Bahasa Malaysia and in English. This abstract will be included in the Report of the Research and Innovation Section at a later date as a means of presenting the project findings of the researcher/s to the University and the community at large)</i></p> <p><i>Thumbnail images are widely used in electronic devices to help user to scan through original high resolution images. Therefore, it is important to represent the thumbnail image correspondingly to the original image. A low quality image should not appear to be a high quality image in thumbnail form. The quality of an image can be affected by noise and blur. Noise is characterized by high frequency components, but blur is by low frequency components. It is worth noting that to embed a vast information into a limited data space is a challenging task. Therefore, in this project, more concentrations are given towards embedding blur information into the thumbnail. The proposed method has three stages, which are the preliminary processes, blur detection, and down-sampling. The thumbnail image with blur information is generated using the average edge width as a weight to integrate blur information. The results show that the proposed method is better than five other thumbnail generation methods.</i></p>								

Imej lakaran kenit digunakan secara meluas dalam peranti elektronik untuk membantu pengguna mengimbas imej asal yang beresolusi tinggi. Oleh itu, adalah penting untuk mewakili imej kecil yang bersepadanan dengan imej asal. Imej yang berkualiti rendah tidak sepatutnya kelihatan seperti imej yang berkualiti tinggi dalam bentuk imej lakaran kenit. Kualiti imej boleh dipengaruhi oleh hingar dan kekaburan. Hingar mempunyai ciri-ciri komponen tinggi frekuensi, tetapi kekaburan adalah komponen rendah frekuensi. Perlu diingat bahawa untuk membenamkan banyak maklumat ke dalam ruang data yang terhad adalah satu tugas yang mencabar. Oleh itu, dalam projek ini, lebih tumpuan diberikan ke arah menerapkan maklumat kekaburan ke dalam imej lakaran kenit. Kaedah yang dicadangkan mempunyai tiga peringkat, yang merupakan proses awal, pengesanan kabur, dan persampelan-menurun. Imej lakaran kenit dengan maklumat yang kabur dihasilkan menggunakan purata lebar pinggir sebagai pemberat untuk mengintegrasikan maklumat kabur. Hasil kajian menunjukkan bahawa kaedah yang dicadangkan adalah lebih baik daripada lima kaedah penghasilan lakaran kenit yang lain.

C BUDGET & EXPENDITURE

i **Total Approved Budget** : RM 147,835.00

Yearly Budget Distributed

Year 1 : RM 56,245.00

Year 2 : RM 48,245.00

Year 3 : RM 43,345.00

Total Expenditure : RM143,873.90

Balance : RM 3,961.10

Percentage of Amount Spent (%) : 97.3206%

Please attach final account statement (eStatement) to indicate the project expenditure

ii **Equipment Purchased Under Vot 35000**

No.	Name of Equipment	Amount (RM)	Location	Status
1	DSLR Camera	RM 4,200.00	School of Electrical & Electronic Engineering	Returned

Please attach the Asset/Inventory Return Form (Borang Penyerahan Aset/Inventori) – Appendix 1

D RESEARCH ACHIEVEMENTS

i **Project Objectives (as stated/approved in the project proposal)**

No.	Project Objectives	Achievement
1	To developed a new down-sampling algorithm, by manipulating image in transformed domain.	One method based on fractal has been developed. This method able to emphasize bright structures on the image.
2	To developed a new down-sampling algorithm, by manipulating image data in spatial domain.	Two methods have been developed. Both are using edge width analysis

3	To optimize the implementation of the algorithm so that it can be implemented in real-time, or near-real-time imaging system.	Implementation for noise reduction has been carried out. Yet, in order to further simplify the method, noise detector is excluded from the final method.
---	---	--

ii Research Output

a) Publications in ISI Web of Science/Scopus

No.	Publication (authors,title,journal,year,volume,pages,etc.)	Status of Publication (published/accepted/ under review)
1.	Boon Tatt Koik and Haidi Ibrahim, "Thumbnail with Integrated Blur Based on Edge Width Analysis" Journal of Sensors (Impact factor 2014: 1.182)	Under review (major revision)
2.	Boon Tatt Koik and Haidi Ibrahim, "Thumbnail Image with Blurry Edge Information Utilizing Half Factor Rules," Mathematical Problems in Engineering, vol. 2014, Article ID 651353, 9 pages, 2014. doi:10.1155/2014/651353 (Impact factor 2013: 1.383)	Published
3.	Sin Hoong Teoh and Haidi Ibrahim, "Robust algorithm for broad impulse noise removal utilizing intensity distance and intensity height methodologies", Signal, Image and Video Processing, vol. 8, no. 2, pp. 223-242, 2014. (Impact factor 2013: 0.409)	Published
4.	Haidi Ibrahim and Seng Chun Hoo, "Local Contrast Enhancement Utilizing Bidirectional Switching Equalization of Separated and Clipped Subhistograms," Mathematical Problems in Engineering, vol. 2014, Article ID 848615, 10 pages, 2014. doi:10.1155/2014/848615 (Impact Factor 2013: 1.383)	Published

b) Publications in Other Journals

No.	Publication (authors,title,journal,year,volume,pages,etc.)	Status of Publication (published/accepted/ under review)
1	Sin Hoong Teoh, Boon Tatt Koik, and Haidi Ibrahim, "Exploration of Current Trend on Median Filtering Methods Utilized in Digital Grayscale Image Processing", International Journal of Materials, Mechanics and Manufacturing, vol. 1, no. 1, pp. 50-54, February 2013.	Published
2.	Nicholas Sia Pik Kong, Haidi Ibrahim, and Seng Chun Hoo, "A Literature Review on Histogram Equalization and Its Variations for Digital Image Enhancement", International Journal of Innovation, Management and Technology, vol. 4, no. 4, pp. 386-389, August 2013.	Published
3.	Sin Hoong Teoh and Haidi Ibrahim, "Variations on Impulse Noise Model in Digital Image Processing Field: A Survey on Current Research Inclination", International Journal of Innovation, Management and Technology, vol. 4, no. 4, pp. 393-396, August 2013.	Published
4.	Boon Tatt Koik and Haidi Ibrahim, "Exploration of Current Trend on Blur Detection Method Utilized in Digital Image Processing", Journal of Industrial and Intelligent Information, vol. 1, no. 3, pp. 143-147, September 2013.	Published

c) Other Publications
(book, chapters in book, monograph, magazine, etc.)

No.	Publication (authors, title, journal, year, volume, pages, etc.)	Status of Publication (published/accepted/ under review)

d) Conference Proceeding

No.	Conference (conference name, date, place)	Title of Abstract/Article	Level (International/National)
1	First International Conference on Artificial Intelligence, Modelling and Simulation (AIMS2013), Kota Kinabalu, Sabah, 3-5 December 2013.	A Literature Survey on Blur Detection Algorithms for Digital Image	International
2	2014 IEEE International Conference on Control System, Computing and Engineering, Penang, 28-30 November 2014.	Image Thumbnail Based on Fusion for Better Image Browsing	International
3	The 3rd International Conference on Computer Engineering and Mathematical Sciences (ICCEMS 2014), Langkawi, 4-5 December 2014.	Accentuate of Bright Structures onto Image Thumbnail using Dilated Intensity Projection	International

Please attach a full copy of the publication/proceeding listed above

iii Other Research Output/Impact From This Project
(patent, products, awards, copyright, external grant, networking, etc.)

-none-

E HUMAN CAPITAL DEVELOPMENT**a) Graduated Human Capital**

Student	Nationality (No.)		Name
	National	International	
PhD			
MSc	3		1. Teoh Sin Hoong 2. Hoo Seng Chun 3. Koik Boon Tatt
Undergraduate	5		1. Lim Chiou Shi 2. Tan Ping Yang 3. Lee Zhe Heng 4. Cheah Tatt Wei 5. Yeoh Hoon Boon

b) On-going Human Capital

Student	Nationality (No.)		Name
	National	International	
PhD			1. 2.
MSc			1. 2.
Undergraduate			1. 2.

c) Others Human Capital

Student	Nationality (No.)		Name
	National	International	
Post Doctoral Fellow			1. 2.
Research Officer	1		1. Koik Boon Tatt 2.
Research Assistant	1		1. 2.
Others (.....)	1		1. 2.

F COMPREHENSIVE TECHNICAL REPORT

Applicants are required to prepare a comprehensive technical report explaining the project. The following format should be used (this report must be attached separately):

- Introduction
- Objectives
- Methods
- Results
- Discussion
- Conclusion and Suggestion
- Acknowledgements
- References

G	PROBLEMS/CONSTRAINTS/CHALLENGES IF ANY
	<p><i>(Please provide issues arising from the project and how they were resolved)</i></p> <p>- None-</p>
H	RECOMMENDATION
	<p><i>(Please provide recommendations that can be used to improve the delivery of information, grant management, guidelines and policy, etc.)</i></p> <p>It would be better if USM has a system that allows researchers to update their progress online. The system should be opened not only to the main researcher, but to the co-researchers as well. An online system will help on filing, sharing information among the researcher of the project, and also promoting sustainability as it reduces the use of paper.</p>

Project Leader's Signature:



Name : Associate Professor Dr Haidi Ibrahim

Date : 18 February 2016

DR HAIDI IBRAHIM
 Associate Professor
 School of Electrical & Electronic Engineering,
 Engineering Campus, Universiti Sains Malaysia,
 14300 Nibong Tebal, Penang, Malaysia.
 Tel: +604-599 5822 Fax: +604-594 1023
 Email: haidi@usm.my / haidi_ibrahim@ieeee.org

COMMENTS, IF ANY/ENDORSEMENT BY PTJ'S RESEARCH COMMITTEE

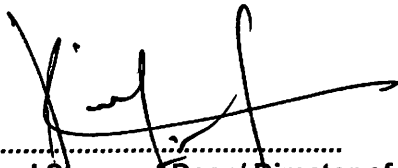
Very good research output.

PROFESOR DR. MOHD. FADZIL BIN AIN
Timbalan Dekan
(Penyelidikan, Siswazah dan Jaringan)
Pusat Pengajian Kejuruteraan Elektrik & Elektronik
Kampus Kejuruteraan
Universiti Sains Malaysia

Signature and Stamp of Chairperson of PTJ's Evaluation Committee

Name :

Date : 22/2/2016



Signature and Stamp of Dean/ Director of PTJ
PROFESOR DR. MOHD RIZAL ARSHAD

Name : Dean
School of Electrical & Electronic Engineering

Date : Engineering Campus
Universiti Sains Malaysia

23/2/16



BORANG PENYERAHAN ASET / INVENTORI

A. BUTIR PENYELIDIK

1. NAMA PENYELIDIK :...PM DR HAIDI BIN IBRAHIM.....
2. NO STAF :...AE50286.....
3. PTJ :...PPK ELEKTRIK & ELEKTRONIK.....
4. KOD PROJEK :... 1001/PELECT/814169.....
5. TARIKH TAMAT PENYELIDIKAN :.....14 Julai 2015.....

B. MAKLUMAT ASET / INVENTORI

BIL	KETERANGAN ASET	NO HARTA	NO. SIRI	HARGA (RM)
1	Gn Canon DSLR EOS 60D Camera	AK00007029	2481409574	4200

C. PERAKUAN PENYERAHAN

Saya dengan ini menyerahkan aset/ inventori seperti butiran B di atas kepada pihak Universiti:


.....

(PM DR HAIDI BIN IBRAHIM)

Tarikh: 18/02/2016

DR HAIDI IBRAHIM
Associate Professor
School of Electrical & Electronic Engineering,
Engineering Campus, Universiti Sains Malaysia,
14300 Nibong Tebal, Penang, Malaysia.
Tel: +604-599 5822 Fax: +604-594 1023
Email: haidi@usm.my / haidi_ibrahim@ieeee.org

D. PERAKUAN PENERIMAAN

Saya telah memeriksa dan menyemak setiap alatan dan didapati :


Lengkap

Rosak

Hilang : Nyatakan.....

Lain-lain : Nyatakan *Diserahkan kepada Unit multimedia EG*

Diperakukan Oleh :


.....

Tandatangan
Pegawai Aset PTJ

KHAIRUL ANUAR BIN AB. RAZAK
Penolong Jurutera
Pusat Pengajian Kejuruteraan Elektrik & Elektronik
Universiti Sains Malaysia
Kampus Kejuruteraan

Nama :

Tarikh : *18/2/2016*

***Nota :** Sesalanan borang yang telah lengkap perlulah dikemukakan kepada Unit Pengurusan Harta, Jabatan Bendahari dan Pejabat RCMO untuk tujuan rekod.



UNIVERSITI SAINS MALAYSIA

JABATAN BENDAHARI

PENYATA PERBELANJAAN SEHINGGA 30 NOVEMBER 2015

Tarikh Cetakan : 07/01/2016

Projek :

No. Akaun : 1001.PELECT.814169.

Vot	Nama Fot	Peruntukan Projek	Perbelanjaan Terkumpul Sehingga Thn Lalu	Baki Peruntukan Tahun Lalu	Peruntukan Thn Semasa	Jumlah Peruntukan Thn Semasa	Tanggung Semasa	Bayaran Thn Semasa	Jum Belanja Thn Semasa	Baki Projek
111	GAJI	34,021.05	0.00	34,021.05	0.00	34,021.05	0.00	17,022.18	17,022.18	16,998.87
113	SUMBANGAN MAJIKAN	0.00	0.00	0.00	0.00	0.00	0.00	72.85	72.85	-72.85
115	LAIN-LAIN EMOLUMEN	-1,000.00	0.00	-1,000.00	0.00	-1,000.00	0.00	1,000.00	1,000.00	-2,000.00
221	PERJALANAN DAN SARA HIDUP	4,908.95	0.00	4,908.95	0.00	4,908.95	0.00	2,070.20	2,070.20	2,838.75
223	PERHUBUNGAN DAN UTILITI	720.00	0.00	720.00	0.00	720.00	0.00	0.00	0.00	720.00
226	BEKALAN BAHAN MENTAH	4,500.00	0.00	4,500.00	0.00	4,500.00	0.00	0.00	0.00	4,500.00
227	BEKALAN DAN BAHAN LAIN	4,339.70	0.00	4,339.70	0.00	4,339.70	0.00	774.50	774.50	3,565.20
229	PERKHIDMATAN IKTISAS & HOSPITALITI	-14,609.42	0.00	-14,609.42	0.00	-14,609.42	0.00	8,779.45	8,779.45	-23,388.87
335	HARTA MODAL	800.00	0.00	800.00	0.00	800.00	0.00	0.00	0.00	800.00
Jumlah		33,680.28	0.00	33,680.28	0.00	33,680.28	0.00	29,719.18	29,719.18	3,961.10

Penyata ini adalah cetakan komputer tiada tandatangan diperlukan

Penyata ini adalah dianggap tepat jika tiada maklumbalas dalam tempoh masa 14 hari dari tarikh penyata

Research University Individual (RUI) Grant
Comprehensive Technical Report

1001/PELECT/814169

Digital Image Thumbnail to Represent Images with Poor Quality

by

**Associate Professor Dr Haidi Ibrahim
&
Dr Dzati Athiar Ramli**

School of Electrical & Electronic Engineering, Engineering
Campus, Universiti Sains Malaysia, 14300 Nibong Tebal,
Penang.

15 July 2012 - 14 July 2015

1
2
3
4
5
6
7
8
9
10
11
12
13
14
15
16
17
18
19
20
21
22
23
24
25
26
27
28
29
30
31
32
33
34
35
36
37
38
39
40
41
42
43
44
45
46
47
48
49
50
51
52
53
54
55
56
57
58
59
60
61
62
63
64
65
66
67
68
69
70
71
72
73
74
75
76
77
78
79
80
81
82
83
84
85
86
87
88
89
90
91
92
93
94
95
96
97
98
99
100

To RCMO, USM

Contents

Contents	i
1 Introduction	3
1.1 Background	3
1.2 Objective of the Research	6
2 Thumbnail Image Using Transformed Domains	7
2.1 Methodology	7
2.2 Results and Discussions	9
2.3 Remarks	10
3 Thumbnail Image Using Spatial Domain	11
3.1 Noise Detection	11
3.1.1 Methodology	14
3.1.1.1 Intensity Distance Differential Method	14
3.1.1.2 Intensity Height Differential Method	17
3.1.1.3 The Proposed Noise Detection Scheme	19
3.1.2 Optimization for Implementation	21
3.1.3 Results and Discussions	25
3.1.3.1 False Positive Detection Rate	25
3.1.3.2 False Negative Detection Rate	29
3.1.3.3 Processing Time	32
3.1.4 Remarks	34
3.2 Thumbnail Image Generation Method	34
3.2.1 Methodology	38
3.2.2 Results and Discussions	41
3.2.3 Remarks	45
4 Conclusion and Future Works	47
4.1 Summary and Conclusion	47
4.2 Future Works	48

Bibliography

51

R
E
F
E
R
E
N
C
E
S

Acknowledgements

With the completion of this project, we would like to express our gratitude to all persons who contributed and assisted us in this research. First of all, we would like to thank USM, especially to RCMO, for offering and opening RUI grants to the USM's researchers. This grant has helped us a lot with our research work.

We also would like to thank our former Dean, Prof. Dr Mohd Zaid Abdullah, and our former Deputy Dean (Research), Prof. Dr Nor Ashidi Mat Isa, for the approval of our grant proposal at department level. We are also would like to thank our current Dean, Prof. Dr Mohd Rizal Arshad, and the current Deputy Dean (Research), Prof. Dr Mohd Fadzil Ain, for their good support.

We also would like to thanks our students who were involved and contributed to this research. They are Mr Teoh Sin Hoong, Mr Hoo Seng Chun, Mr Koik Boon Tatt, Mrs Lim Chiou Shi, Mr Tan Pin Yang, Mr Lee Zhe Heng, Mr Cheah Tatt Wei, and Mr Yeoh Hoon Boon. We also appreciate the discussions with Dr Ng Theam Foo, Dr Wan Amir Fuad Wajdi, Dr Shahrel Azmin Suandi, Mr Nicholas Sia Pik Kong, Dr Aeizal Azman Abd Wahab and Dr Teoh Soo Siang.

Chapter 1

Introduction

1.1 Background

The demand and usage of digital pictures in our daily life is showing an increasing trend. Digital pictures are cheaper, easier to distribute, store, and share, and they are also never degrade. Furthermore, the process of taking digital pictures is faster and cheaper, if compared with the traditional film based photography [56]. Moreover, the price of digital camera and camcorder is now affordable for most people. As to follow this trend, in addition to the camera and camcorder, most of the state-of-art consumer electronic products, such as smart-phone and printer, are now been equipped with the ability to capture and display digital images. In order to function as a "what you see is what you get (WYSIWYG)" system, most of these consumer imaging products utilize image thumbnail to allow the user to easily browse the pictures that have been stored in the digital storage of the product. This approach is also been used due to the small size of the display screen equipped with these electronic products [12, 9].

As shown in Figure 1.1, image thumbnail represents the original image, but in smaller size. The definition of an image thumbnail is [15]:

An image thumbnail is produced after the partitioning of an image into rectangular (usually square) blocks of pixels and constructing a thumbnail image comprising blocks, of single pixel-size or larger, of uniform pixel value. The blocks in the thumbnail are uniformly scaled with respect to those of the image.

The original image is with high spatial resolution, whereas the image thumbnail has low spatial resolution. Therefore, the task of developing an accurate thumbnail is challenging, as a vast amount of information need to be embedded into a limited space of data. That is why if the generated image thumbnail is too small, it would be difficult for the user to extract the actual information from it [81].



Figure 1.1: Example of image thumbnails

Image thumbnail is used to allow the user to roughly inspect the picture's composition. Image thumbnail also normally been used by the user to judge the quality of taken picture in general. For example, during a digital photography session, the user normally will judge the quality of the acquired picture based on the image thumbnail after each shoot. Then, based on this rough judgement, the user will decide whether he want to keep the picture, or to delete it and has a reshoot [69]. Some of the users tend to take more than one shoot for the same scene as they are not confident enough with the displayed thumbnail. The result from this is the waste of time, battery power, and storage.

However, most of the current image thumbnail algorithms are not designed to accurately indicate the real quality of the taken picture. Standard image thumbnail represents the good pictures, blur pictures and noisy pictures as clean and sharp. Therefore, it is difficult for the user to know the real quality of the pictures. If the image thumbnail mislead the user to think bad quality picture as having good quality, this condition mostly will lead to the user's frustration when the picture is printed, or displayed on higher resolution equipment.

Although the image thumbnail can be constructed by many ways, there are not many literatures available for this research field. The commonly used method is the standard image thumbnail, whihc is known as Pixel-based Down Sampling with Anti-aliasing Filter (PDAF) [68, 24]. The implementation of PDAF has two stages. The first stage is the low-pass filtering process, and the second stage is down-sampling process. This method uses low pass filter to limit the frequency components of the picture, in order to preserve noise information as the noise is mostly dominated in high frequency components of the original picture. Thus, PDAF cannot indicate the presence of noise correctly as its generated image thumbnail is always appears clean [68]. It is also worth noting that although PDAF smoothes slightly the image thumbnail [24], some of the blurry regions in the original pictures are not represented correctly by PDAF [68].

Other image thumbnail algorithm, which is known as Direct Pixel-based Down-sampling (DPD) creates the image thumbnail by down-sample the original picture directly, without applying any filtering process [24]. When the original picture is being down-sampled by a factor L , DPD selects one out of every $L \times L$ pixels to be included inside the thumbnail. Image thumbnail generated by DPD is sharper than the one by PDAF because there are higher picture frequency components inside it. However, similar to PDAF, DPD cannot indicate correctly the presence of blur in the original picture.

In order to increase the apparent resolution of an LCD display, a similar method to DPD, which is called Direct Sub-pixel-based Down-sampling (DSD) has been proposed by Daly [16]. Yet this method works only for color digital images. In this method, the information of red, green and blue (RGB) for each pixel in thumbnail is taken from three consecutive pixels on the original image. Although the implementation of both DPD and DSD are relatively simple, these methods suffer from aliasing artifact. Furthermore, DPD produces image thumbnails with chrominance distortion.

Fang and Au [24] proposed the use of Min-Max Directional Error (MMDE) in order to reduce the color fringing artifact while increases the apparent resolution. Unfortunately, the implementation of MMDE needs unique software to be used and direct implementation of this method failed to produce any output as it is very high in computational cost. Therefore, MMDE with Visual Relaxation (MMDE-VR) and MMDE with Edge Relaxation (MMDE-ER) have been proposed. Yet, both methods still require long processing time, and therefore are not suitable to be implemented in consumer electronic products.

It is worth noting that all the abovementioned methods deal with the works on producing sharper image thumbnail. None of them are developed with the ability to embed blur and noise information. Therefore, those thumbnail cannot present the actual quality of the acquired picture. As noisy images still appear as clean images on the image thumbnails, and blur images still appear as sharp images in the image thumbnails, browsing and searching using these image thumbnails might lead to errors and inefficiency.

Therefore, Samadani et. al [68, 67, 69] proposed an image thumbnail scheme which is able to present blur and noisy pictures. The proposed method is divided into two stages. In the first stage, a blur map is used to present the local blur information. This map is created by inspecting the intensity ranges within image blocks from eleven blurred thumbnail versions. During the second stage, the noise information is added to the thumbnail obtained from stage one by using a modified wavelet based soft thresholding de-noiser.

Ibrahim [37] presents a new method to embed blur information of the original picture inside the image thumbnail. This method is simple to be implemented in electronic products. This method uses two small images, which are the direct down-sampled image, and the corresponding smoothed image version. Although the method is superior to other well known image thumbnail methods in presenting blur information, the sensitivity of the method towards blur and noise is depending on three parameters.

In works by Trentacoste et. al [89], perceptual-based model to down-sample an image is build to create a down-sampled version of the image that gives the same impression as the original image version. This study has been conducted to find out how much blur must be present in the down-sampled image, as it can be perceived as the same as the original image. Matthew et. al used the modified version of Samadani et. al's work to conduct their experiment. New appearance-preserving algorithm has been used to alter blur magnitude locally, to create a smaller image. The blur magnitude is analysed as a function of spatial frequency.

1.2 Objective of the Research

The main objective of this proposed research is to develop a new method that is able to embed the blur and noise information inside the image thumbnail. Several goals have been identified in order to achieve the main objectives. They are:

1. To develop a new down-sampling algorithm, by manipulating image in transformed domain.
2. To develop a new down-sampling algorithm, by manipulating image data in spatial domain.
3. To optimize the implementation of the algorithm so that it can be implemented in real-time, or near-real-time imaging system.

Chapter 2

Thumbnail Image Using Transformed Domains

In this research work, for generating image thumbnail in transformed domain, several domains have been explored, including wavelet domain, Fourier domain, and fractal domain. However, in this report, we only concentrate on fractal domain. Fractal is normally used in the field of image compression. This domain assumes that natural and most artificial images has similar and repeating patterns, which are redundant in the image [2]. Therefore, by reducing this redundancy, the image can be stored in much smaller size. Similarly, the same concept can be applied for generating thumbnail image. The redundancy within $L \times L$ pixels block can be removed, by using the concept of fractals, so that this block can be represented by a single pixel.

2.1 Methodology

Cohen [13, 14] created thumbnail image by using fractal theory. First, the original image F is first downsampled using PDAF method to find the initial thumbnail image f . This method used $L = 4$ for its implementation. Next, image f is then up-sampled (i.e., zoomed-in) by factor $L = 4$ in order to obtain the actual spatial resolutions. The image is up-sampled using nearest neighbour interpolation [82]. Then, the 4×4 correction matrix C is found. The values within f will be iteratively updated, until minimum C is found.

The method proposed by Cohen [13, 14] can be considered as a slight improvement towards PDAF method. Similar to PDAF method, this method does not consider the noise and blur information. By obtaining smaller value of C , the thumbnail image will become clean, and not sensitive to outliers or noise. Therefore in this research, a modifications has been done by introducing grayscale morphology in the process.

If F is with resolution $M \times N$ pixels, f is with resolution $m \times n$ pixels (i.e, $m = M/L$ and $n = N/L$). Therefore, in generating the thumbnail image, the aim of this procedure

is to project $M \times N$ pixels onto $m \times n$ grid. In other words, the procedure wants to accurately project $L \times L$ pixels from image F to one single pixel on image f . This is shown by Figure 2.1.

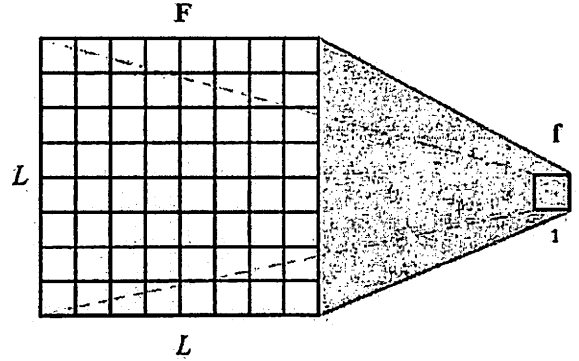


Figure 2.1: Projecting information from high spatial resolution grid to lower resolution grid

The proposed method consists of two stages. The first stage is the accentuation of bright structures by using grayscale morphology operation. The second stage is the down-scaling process. In order to emphasize bright structure in the image, the method uses grayscale morphological operations, which is erosion operation \ominus , to obtain dilated image D . This operation is given as [28]:

$$D(x, y) = [F \oplus S](x, y) = \max_{(x', y') \in S} \{F(x - x', y - y')\} \quad (2.1)$$

where S is the structuring element. This work uses a flat structuring element, with size of $L \times L$ pixels. This is because the proposed method wants to have equal contributions from all samples within the block. The method sets the structuring element to size of $L \times L$ pixels because it want to completely cover the area defined by the down-sampling factor L , as shown by Figure 2.1.

The second stage of this method is to down sample image D . This process is given as:

$$f(x, y) = D(xL, yL) \quad (2.2)$$

The method can be used for grayscale and also color images. If the image is color image, the proposed method will process each color channel independently.

It is noted from Equation (2.2), the proposed method only takes use one pixel from image D to assign it to image f . Thus, in order to reduce the processing time and to optimize this method for reduced computational requirements, Equation (2.1) can be simplified as follows:

$$D(x, y) = \begin{cases} [F \oplus S](x, y) & : x = 0, L, 2L, 3L, \dots \text{ and } y = 0, L, 2L, 3L, \dots \\ 0 & : \text{otherwise} \end{cases} \quad (2.3)$$

By using Equation (2.3) instead of Equation (2.1), the computational requirement of the proposed method is reduced significantly.

2.2 Results and Discussions

In this experiment, two test images have been used. The first result, which is obtained by using *Test Image 1*, is shown in Figure 2.2(a). The original size of *Test Image 1* is 3456×2304 pixels. The down-sampling factor used in this experiment is set to value 8 (i.e., $L = 8$). Based on the down-sampling factor used, the output thumbnail image is at size 432×288 pixels.

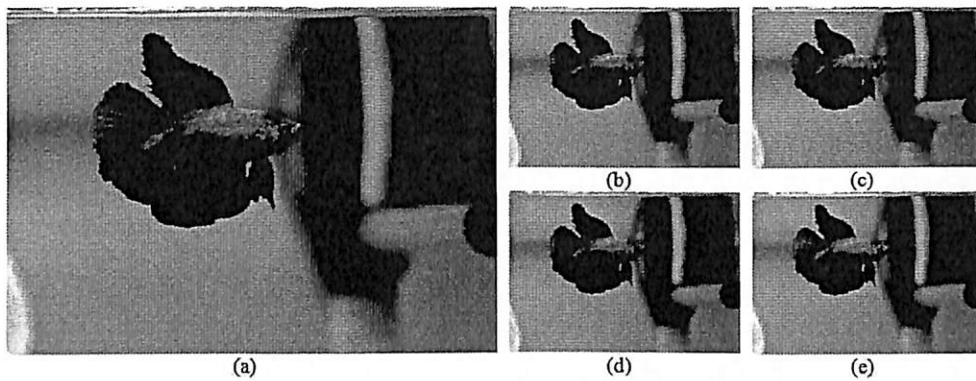


Figure 2.2: *Test image 1*. (a) Input image. (b) Output from PDAF. (c) Output from DPD. (d) Output from DSD. (e) Output from the proposed method.

As shown by Figure 2.2, all methods successfully generate the thumbnail versions of the original images. The basic structure and the composition of the original image can be represented by all thumbnail images. Yet, the proposed method successfully emphasizes the bright structure of the image. This can be observed by comparing the body and tail of the fish in Figure 2.2(e) with other subfigures.

The second result, which is using *Test Image 2*, is shown in Figure 2.3. The original size of *Test Image 2* is 3456×5184 pixels. The down-sampling factor used in this experiment is set to value 8 (i.e., $L = 8$). Thus, the output thumbnail image is at size 432×648 pixels.

Similar to the results obtained in Figure 2.2, the same observation can be obtained from Figure 2.3. All thumbnail versions can give a basic idea to the users, regarding to the basic composition of the original image. However, the proposed method successfully emphasizes the bright structure on the image, as what can be seen from Figure 2.2(e). In this figure, the white hen appears brighter in this thumbnail, as compared with other thumbnail images.

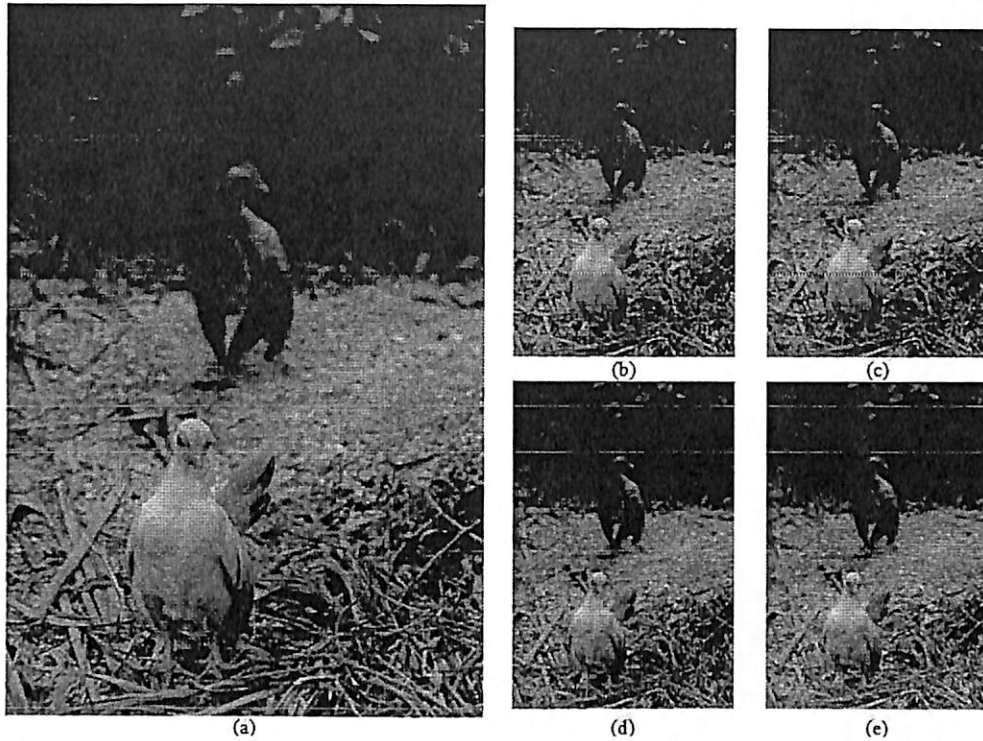


Figure 2.3: *Test image 2.* (a) Input image. (b) Output from PDAF. (c) Output from DPD. (d) Output from DSD. (e) Output from the proposed method.

2.3 Remarks

A new method, utilizing grayscale mathematical morphological dilation operation, has been proposed in this subsection, as an improvement to the fractal method. The method is simple and easy to be implemented. Compared to other thumbnail image algorithms, the proposed method has better ability to highlight bright structure onto the thumbnail images.

Chapter 3

Thumbnail Image Using Spatial Domain

This chapter deals with the development of thumbnail image generating method in the spatial domain. At the beginning, the initial methodology of the proposed method is given by Figure 3.1. As shown by this figure, the proposed method will detect noise on the original image, in order to embed it to the thumbnail image. Similarly, detection of the blur will also be carried out. The methodology for each stage, and its results will be presented by the following subsections.

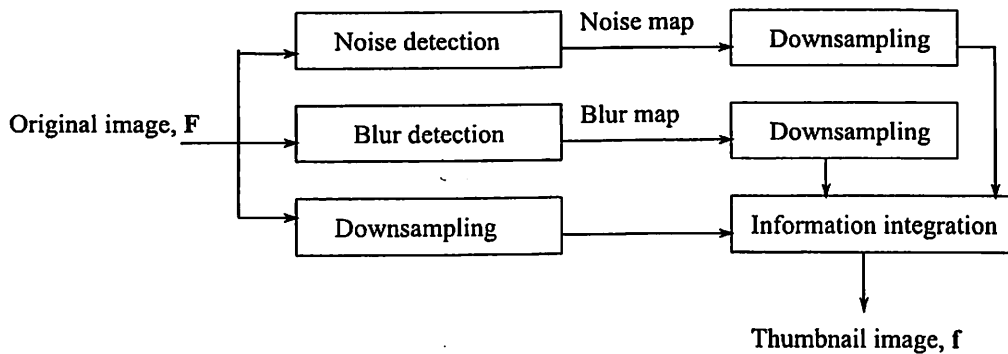


Figure 3.1: The initial methodology of the proposed method for generating image thumbnail.

3.1 Noise Detection

The noise that is considered in this research is the impulse noise. Impulse noise is considered as an additive noise [50, 64, 49, 86, 87, 88, 28]. The additive noise is defined as follows. If (x, y) are the spatial coordinates on the image, and $C = \{C(x, y)\}$ is the

ideal uncorrupted and clean image, the damaged image by additive noise $\mathbf{D} = \{D(x, y)\}$ can be described as:

$$\mathbf{D} = \begin{cases} \mathbf{C} & : \text{ with probability } 1 - P \\ \mathbf{C} + \mathbf{N} & : \text{ with probability } P \end{cases} \quad (3.1)$$

where P (i.e., $0 \leq P \leq 1$) presents the noise density, and \mathbf{N} is the noise intensity value or the noise amplitude. In this equation, \mathbf{N} can have a positive or a negative value.

Impulse noise can be characterized by a long-tail probability distribution* of N , and thus impulse noise can be considered as an additive long-tailed noise [26, 54, 79, 44]. The probability density function p for impulse noise can be modelled by some skewed distributions. Furutsu and Ishida in 1961 [26] used a combinations of Poisson distributions to present impulse noise. In 1988, Lin and Willson Jr [54] presented impulse noise by using a log-normal distribution as given as:

$$p(|N|) = \frac{1}{\sqrt{2\pi|\bar{N}|}} \exp\left(-\frac{1}{2} \ln^2\left(\frac{|N| \exp(0.5)}{|\bar{N}|}\right)\right) \quad (3.2)$$

where $|\bar{N}|$ is the average value of $|N|$. However, the popularity of impulse noise models that are described by skewed probability distributions, such as the work by [26] and [54], are decreasing in recent research papers.

From Equation (3.1), for the case of the corrupted pixels, the results of $\mathbf{C} + \mathbf{N}$ actually can take any value because \mathbf{N} is a random value. Therefore, in recent literatures, Equation (3.1) has been simplified and replaced with Equation (3.3)[†][74, 1, 43].

$$\mathbf{D} = \begin{cases} \mathbf{C} & : \text{ with probability } 1 - P \\ \mathbf{N} & : \text{ with probability } P \end{cases} \quad (3.3)$$

This Equation shows that for most of the current impulse noise models, the corrupted pixels are directly replaced with the noise intensity values [73, 52, 71, 4, 94]. Unlike Equation (3.1), in this Equation, the value of \mathbf{N} is restricted to positive values only. If the image is quantized into L intensity levels, \mathbf{N} can take any values between 0 to $L - 1$ [52].

The distribution p of noise \mathbf{N} in Equation (3.3) can be defined in many ways. Some researchers define p as a uniform distribution, which is:

$$p(N) = P/L \quad 0 \leq N \leq L - 1 \quad (3.4)$$

For this case, the noise amplitudes occupy all possible intensity values, from 0 to $L - 1$. This type of impulse noise is widely known as random-valued impulse noise. Random-valued impulse noise have been studied in many works, such as [52, 71, 6, 19, 62, 11, 48, 96, 97].

*A long-tailed probability distribution is a distribution which has relatively high probability regions far from the mean or median values.

[†]Due to this simplification, in some literatures, impulse noise is neither considered as an additive noise nor a multiplicative noise, but as another class of its own.

Other widely used practical impulse noise model is known as fixed-valued impulse noise. In this model, N in Equation (3.3) is restricted to the minimum or the maximum intensity value (i.e. 0 or $L - 1$)[‡]. As the noise with intensity 0 appears as black pixels on the image, this noise is referred as pepper noise. On the other hand, the noise with intensity $L - 1$ appears as white pixels on the image. This type of noise is referred as salt noise. Therefore, fixed-valued impulse noise is also known as salt-and-pepper noise[§]. If D is the intensity of image D , fixed-valued impulse noise is given by the following probability density function:

$$p(D) = \begin{cases} \frac{1}{2}P & : \text{pepper}; D = 0 \\ 1 - P & : \text{noise free pixels}; 0 \leq D \leq L - 1 \\ \frac{1}{2}P & : \text{salt}; D = L - 1 \end{cases} \quad (3.5)$$

Because of its simplicity and practicality, this noise model is the most popular impulse noise model used in literatures, such as the works in [32, 27, 72, 21, 39, 46, 84, 5, 65, 18, 36, 42, 22, 77, 75, 57, 33, 61, 3, 60, 59, 91].

A simple modification can be done to Equation (3.5) by allowing unequal densities of salt noise and pepper noise, as given as:

$$p(D) = \begin{cases} P_1 & : \text{pepper}; D = 0 \\ 1 - P & : \text{noise free pixels}; 0 \leq D \leq L - 1 \\ P_2 & : \text{salt}; D = L - 1 \end{cases} \quad (3.6)$$

where $P_1 + P_2 = P$. This noise model has been used in some recent literatures, such as [97, 75, 57, 33, 61, 3, 60, 59, 91]. This type of noise is called unipolar when either P_1 or P_2 is zero [29].

A variation to Equation (3.6) is obtained by allowing salt noise and pepper noise to be presented by two intensity ranges. Salt noise occupies high intensity range, while pepper noise occupies low intensity range. Each range is presented by m intensity levels. This noise model is given as:

$$p(N) = \begin{cases} P_1/m & : \text{pepper}; 0 \leq N < m \\ 1 - P & : \text{noise free pixels}; 0 \leq N \leq L - 1 \\ P_2/m & : \text{salt}; L - 1 - m < N \leq L - 1 \end{cases} \quad (3.7)$$

Some example of works that are using this noise model can be found in [97, 61, 3, 60, 59, 91].

Equation (3.7) can be simplified by assuming that the density of salt noise is equal to the density of pepper noise. This is given as:

$$p(D) = \begin{cases} P/2m & : \text{pepper}; 0 \leq D < m \\ 1 - P & : \text{noise free pixels}; 0 \leq D \leq L - 1 \\ P/2m & : \text{salt}; L - 1 - m < D \leq L - 1 \end{cases} \quad (3.8)$$

[‡]It is easier to understand the idea behind this noise model by using equation (3.1). In this equation, impulse noise N can take positive or negative value. It is assumed that the magnitude of N is very large, such that $C(i, j) + N(i, j)$ will produce values either greater than $L - 1$ or lower than 0. Due to quantization process, these values are truncated to $L - 1$ or 0 [29].

[§]Sometimes, this type of noise also been referred as data-drop-out or spike noise [29].

Actually, when m is equal to one, this equation is equivalent to Equation (3.5), which is fixed-valued impulse noise. On the other hand, when m is equal to $L/2$, this model resembles Equation (3.4), which is random-valued impulse noise. This noise model has been used in [61, 3, 60, 59, 91].

3.1.1 Methodology

Boundary discriminative noise detection (BDND) method, which has been proposed by Ng and Ma [61], will be chosen as the base of the proposed method in this research work. BDND method not only good in detecting fixed-valued impulse noise as defined in Equation (3.5), but also a wide range of impulse noise models, including the models defined by Equations (3.6) to (3.8).

The common problem of noise detection stage is the wrong classification of the image pixels. Some uncorrupted pixels might be detected as noise pixel candidates, and otherwise. If the uncorrupted pixels are treated as noise pixel candidates, they will be unnecessarily been processed in the noise cancellation stage, makes the object details become blur. This problem always happen when processing the object edges in the image. On the other hand, if the noise pixels are treated as uncorrupted pixels, they will not be processed in the noise cancellation stage. As a consequence, the noise pixels will not be removed successfully from the image. This problem always happen when the corruption level is high, where the number of noise pixels in the image is huge. Therefore, to reduce the faulty noise detection and to increase the efficiency of the impulse noise reduction filter, a method which focus on the misdetection and wrong detection should be designed.

The proposed noise detection scheme employs two techniques, known as intensity distance differential method, and intensity height differential method. To ease the understanding, the basic concept of intensity distance differential method is first introduced in Subsection 3.1.1.1. Next, the concept of intensity height differential method is briefly described in Subsection 3.1.1.2. Then, the proposed noise detection scheme will be properly described in Subsection 3.1.1.3.

3.1.1.1 Intensity Distance Differential Method

Many studies have been done by other researchers in recent years to improve the noise detection process. This is because the successfulness of the detection stage is indeed a very crucial factor to produce a more accurate result of F , with less unwanted pixel alterations and better local contents preservation. One of the successful noise detection techniques has been introduced in BDND [61]. BDND has been designed to deal with a wide range of impulse noise models, from the noise model described by Equation (3.5) to the noise model described by Equation (3.8). By assuming that the intensities presenting the impulse noise are not the same as the intensities for the uncorrupted clean pixels, and the intensity of the noise located at the right most and left most regions of the image

histogram as shown in Figure 3.2, BDND tries to estimate the noise ranges for both ends by finding two intensity boundaries. The noise boundary 1 (B_0) is the boundary for the lower impulse noise, while the noise boundary 2 (B_1) is the boundary for the upper impulse noise. Then, BDND uses these two intensity boundaries to separate the clean pixels from the corrupted pixels.

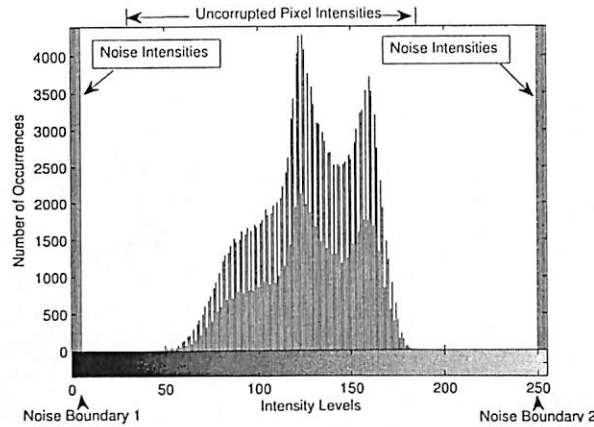


Figure 3.2: Example of image histogram corrupted by impulse noise, with well defined noise boundaries

BDND uses a method known as the *intensity distance differential method*, to detect the impulse noise boundaries in the histogram. To further explain the basic concept of this methodology, an example for intensity distance differential method is given in Figure 3.3. Figure 3.3(a) highlights an image area defined by a sliding window of size 9×9 pixels[¶]. The pixel of interest $X(i, j)$, which is the pixel located at the centre of the window, is indicated by orange coloured cell. This pixel of interest has intensity value of 255, and for this example, it is a noise pixel. The aim of the noise detection stage is to mark this pixel as one of noise pixel candidates, so it will be filtered out in the next processing stage, which is noise reduction stage.

In order to find the impulse noise boundaries, the original work by Ng and Ma [61] uses sorting algorithm. First, the method sorts the samples defined by the sliding window in ascending order, and the median value is found. This sorted samples are saved as vector \vec{v}_O . For the example shown in Figure 3.3(a), this vector is:

$$\vec{v}_O = \left\{ \begin{array}{l} 66, 66, 66, 66, 66, 66, 66, 66, 66, 66, 66, 66, 66, 66, 66, 66, 66, 66, \\ 66, 66, 66, 66, 66, 66, 66, 66, 66, 66, 66, 66, 66, 66, 66, 66, 66, 66, \\ 72, 72, 72, 72, \boxed{72}, 72, 72, 72, 72, 72, 72, 72, 74, 74, 74, 74, 80, 80, \\ 88, 88, 88, 88, 88, 88, 90, 90, 90, 90, 95, 95, 95, 95, 98, 98, 98, 98, \\ 128, 128, 130, 130, 135, 135, 140, 140, 255 \end{array} \right\} \quad (3.9)$$

[¶]Although the filter of size 9×9 pixels is used in this example, in real implementation of BDND, filters of size 21×21 pixels and 3×3 pixels are used. It is worth noting that in the proposed method, only filter of size 21×21 pixels is employed.

(i.e. $v_D(36) = 6$). The corresponding v_O^* is $v_O(36)$ which has intensity 66. Therefore, for this example, B_0 is 66.

Similar approach has been used to determine the upper impulse noise boundary B_1 . However, the searching involves the intensities between the median value to the maximum intensity value of the sample. In this case, the maximum v_D^* is at the 80th sample (i.e. $v_D(80) = 155$). The corresponding v_O^* is 140 (i.e. $v_O(80) = 144$). Therefore, $B_1 = 144$. The pixel of interest $X(i, j)$ will be classified as noise-free pixel candidate if its intensity value is in between B_0 and B_1 . Otherwise, $X(i, j)$ will be considered as a noise pixel candidate. For the example shown in Figure 3.3(a), $X(i, j)$ is a noise pixel candidate because its value is greater than B_1 (i.e. $X(i, j) = 255$ is greater than $B_1 = 140$). Thus, in this example, $X(i, j)$ is successfully marked as the noise pixel candidate.

When the detection filter size is big, the original intensity distance differential method requires a long processing time to create v_O^* and v_D^* . To generate v_O^* , sorting algorithm is used. To generate v_D^* , the difference between each pair of samples need to be determined. Therefore, in order to reduce the computational time requirement by the intensity distance differential method, the implementation will be based on the local histogram. As already described in Section 3.1.2, local histogram can be obtained quickly with proper implementation.

Figure 3.3(b) shows the distribution of the pixels defined by the window in Figure 3.3(a) in histogram form. This histogram can adequately present v_O^* from Equation (3.9). However, the information obtained from the histogram is easier to be interpreted. By using histogram, the requirement for creating v_D^* can be diminished. Through this figure, a set of intensity distance differential values can be determined. The intensity distance differential value can be defined as the gap value between two successive non-empty histogram bins. The method determines the lower impulse noise boundary value B_0 (i.e. for pepper noise) by finding the intensity value in the range from intensity 0 to the median value, which generates the maximum intensity distance differential value. Therefore, in this example, B_0 is equal to 66, with intensity distance differential value equal to 6. Similarly, BDND finds the higher impulse noise boundary value B_1 (i.e. for salt noise) by searching for the maximum intensity distance differential value from the median value (i.e. intensity 72 for this example) to the maximum intensity (i.e. intensity 255). Thus, for this example, B_1 is equal to 140, with intensity distance differential value equal to 150. Therefore, the utilization of local histogram will give the same values for B_0 and B_1 , but with less computational time.

3.1.1.2 Intensity Height Differential Method

Although the intensity distance differential method is able to detect the impulse noise boundary, it is only effective when the noise intensities are unique and differ from the intensities of the uncorrupted pixels, as shown in Figure 3.2. However, when the regions of impulse noise with uncorrupted pixels are overlapped with each other in the histogram, intensity distance differential method mostly will fail to detect the impulse

noise boundaries. This regions overlapped condition might be happen when the noise spread factor m in Equations (3.7) or (3.8) is large (as shown in Figure 3.4(a)) or when the uncorrupted pixel intensities occupy the whole dynamic range (as shown in Figure 3.4(b)).

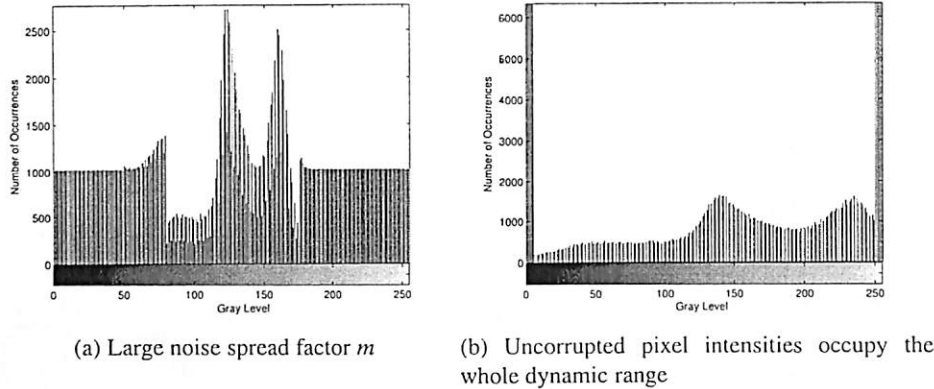


Figure 3.4: Examples of image histogram corrupted by impulse noise, with unclear impulse noise intensity boundaries

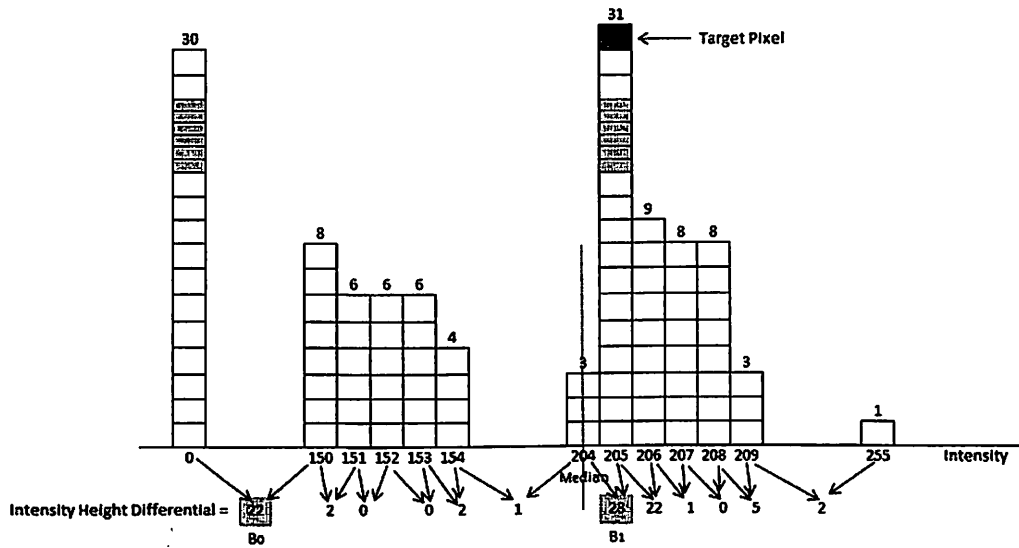
In order to deal with the situations as shown in Figure 3.4, a method known as *intensity height differential method* has been introduced in this work. This approach is actually similar to the intensity distance differential method, except that the intensity height difference is defined as the bin's height difference between two successive non-empty histogram bins. Figure 3.5 will be used to explain the basic concept of this approach. In this example, the image portion is highly corrupted by the impulse noise. The highlighted area in Figure 3.5(a) indicates the region defined by a sliding detection window of size 11×11 pixels. The pixel of interest $X(i, j)$ is a noise pixel, with intensity 205.

Figure 3.5(b) shows the distribution of the sampled intensities in Figure 3.5(a) in histogram form. As shown by this histogram, the intensity of $X(i, j)$ is not the highest intensity value within the samples. The intensity is also located near to the median value. If the detection is using intensity distance differential approach, B_0 will be equal to 0 and B_1 will be equal to 209. With detected impulse noise boundaries, $X(i, j)$ will be considered as an uncorrupted pixel. As a consequence, this pixel will remain unchanged, as it will not be filtered in the next processing stage. Thus, the impulse noise will still be remained in the image.

Therefore, intensity height differential method is used to reduce the number of mis-detected noise pixels. Through Figure 3.5(b), a set of intensity height differential values can be determined. The lower impulse noise boundary B_0 is determined based on the intensity index from intensity 0 to the median intensity value (i.e. intensity 204 for this example), where the intensity height differential value is maximum. In this case, B_0 is found to be 0. On the other hand, the upper impulse noise boundary B_1 is determined based on the intensity index from the median intensity value (i.e. intensity 204 for this

205	205	205	205	205	205	205	205	0	0	0	0	0	0
205	205	205	205	208	208	208	208	206	204	204	204	204	0
205	205	205	205	208	208	208	208	206	204	204	204	204	0
205	205	205	205	208	208	208	208	206	204	204	204	204	0
205	205	205	205	153	152	151	152	150	204	204	204	204	0
205	205	205	205	153	150	150	150	152	204	204	204	204	0
205	205	205	205	153	150	150	150	152	204	204	204	204	0
205	205	205	205	153	152	151	152	153	204	204	204	204	0
205	205	205	205	153	154	154	207	207	206	206	206	206	0
205	205	205	205	153	154	154	207	207	206	206	206	206	0
205	205	205	205	206	206	207	207	207	206	206	206	206	0
205	205	205	205	205	205	205	205	205	205	205	205	0	0

(a) Image portion defined by window of size 11 × 11 pixels



(b) Representation of the data in (a) as histogram

Figure 3.5: Examples for intensity height differential method

example) to the highest intensity value (i.e. intensity 255), where the intensity height differential value is maximum. In this example, B_1 is equal to 204. As the value of $X(i, j)$ is not in between the range between B_0 to B_1 (i.e. the condition $B_0 < X(i, j) < B_1$ is not been met), as desired, $X(i, j)$ is successfully detected as a noise pixel candidate.

3.1.1.3 The Proposed Noise Detection Scheme

For salt-and-pepper noise, or fixed-valued impulse noise defined by equation (3.5), this type of noise can be easily handled by intensity distance differential approach. This is because, the noise is always located at the most right and the most left of the histogram bars. For an 8-bit gray scale images, the salt-and-pepper noise only has intensity 0

and 255. Therefore, the noise will always successfully been included as noise pixel candidates by this method. However, when the noise spread factor m is not equal to 1, the histogram of image D might be similar to the one shown in Figure 3.4(a) or Figure 3.4(b)¹¹. For this case, intensity height differential methodology is more suitable for detecting the potential noise pixels.

Following the basic methodology of a switching median filter, as shown in Figure 3.6, the output of the noise detection stage is a noise mask M . This mask will be used to indicate which pixels are noise pixel candidates, and which pixels are noise-free pixel candidates. The following notation is used:

$$M(i, j) = \begin{cases} 1 & : \text{ impulse noise candidate} \\ 0 & : \text{ otherwise} \end{cases} \quad (3.11)$$

From this equation, $M(i, j)$ is set to 1 for noise candidate, and 0 for noise-free candidate. The overall block diagram of the proposed noise detection scheme, for detecting an impulse noise at coordinates (i, j) , is summarized by Figure 3.7.

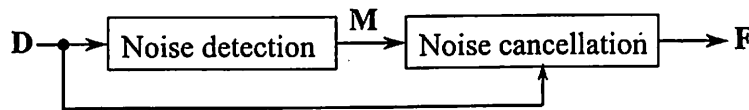


Figure 3.6: Block diagram presenting switching median filter

The proposed impulse noise detection process in this method uses two detection window; a coarse noise detection window, and a fine noise detection window. The coarse noise detection window is of size 21×21 pixels. This size of detection window has been chosen to be exactly the same as the one used in BDND [61] and other BDND median filtering based methods, such as DSMFBDNDE [60]. On the other hand, the fine noise detection window is of size 3×3 pixels. This small window size is chosen in order to maintain the locality of the image information.

In Figure 3.7, noise borders with subscript 0 correspond to the lower intensity impulse noise borders, whereas noise border with subscript 1 correspond to the higher intensity impulse noise borders. Noise borders with subscript *Distance* are obtained from intensity distance differential method, while subscript *Height* presents intensity height differential method. Subscript *Coarse* presents the borders obtained using a detection window of size 21×21 pixels, and subscript *Fine* presents the borders from a detection window of size 3×3 pixels. For example, $B_{0_Distance_Coarse}$ is a lower impulse noise boundary, obtained from intensity distance differential approach, using the coarse detection window.

The noise detection process as shown by the flowchart in Figure 3.7 has been designed in order to successfully detect various type of impulse noise. Unlike BDND

¹¹For example, for an 8-bit grayscale image (i.e. $L = 256$), if the noise spread factor m is equal to 10, this means that the impulse noise intensities are presented by two intensity ranges, which are from 0 to 9, and from 246 to 255.

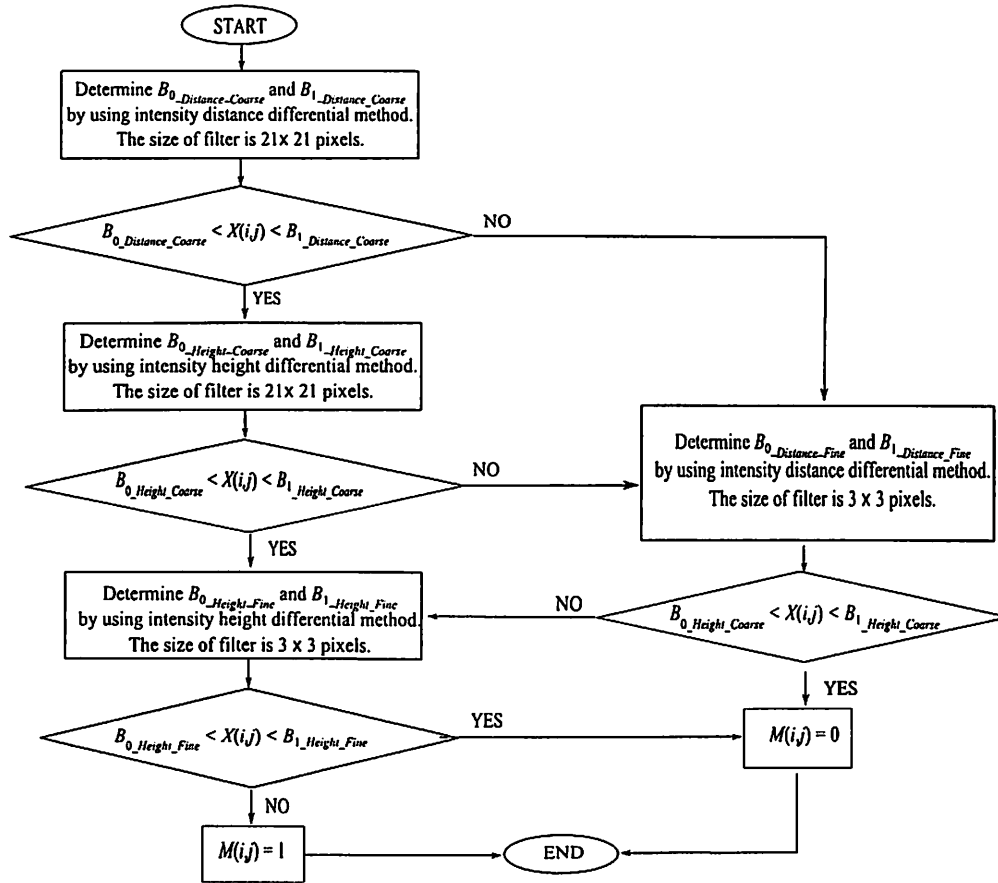
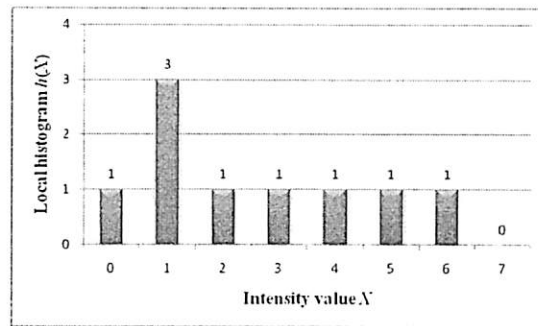


Figure 3.7: Block diagram presenting the noise detection process for pixel $X(i, j)$

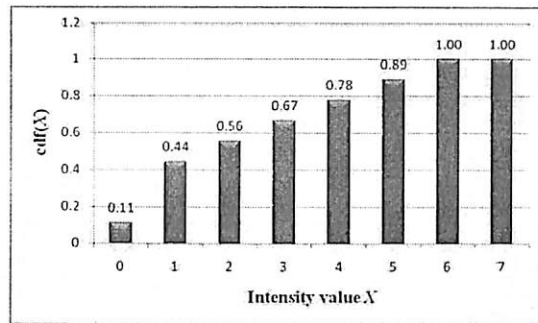
method [61], the proposed method uses both intensity distance differential method and intensity height differential method. As the process starts with intensity distance differential approach, it can be assumed that the proposed method does the detection for the salt-and-pepper noise first. The method then refines the finding to avoid noise miss-detection. This is carried out by using the smaller noise detection window, or detecting impulse noise with larger noise spread factor m using intensity height differential approach. Using this new noise detection scheme, a pixel will go through at least two, and at most three, noise detection windows before it is classified as a noise pixel candidate or a noise free pixel candidate. Therefore, an optimization approach described in Section 3.1.2 has been designed and implemented. This method requires a continuous window sliding for local histogram creation, but create local histograms with low computational burden. Therefore, some processing time can be saved by this approach.

3.1.2 Optimization for Implementation

Most of the median filtering techniques have long processing time. As an example, the switching median filter with boundary discriminative noise detection (BDND) tech-



(a) Local histogram



(b) The corresponding cdf

Figure 3.9: The local histogram and cdf defined by the window shown in Figure 3.8

where n_s is the number of samples within the contextual region that contribute to the calculation of the median value. In this example, n_s is equal to 9 (i.e. 3×3). The median value is identified as the intensity value X where the cdf first reaching the value equal or greater to 0.5. For the example shown in Figure 3.9(b), the median value is equal to 2.

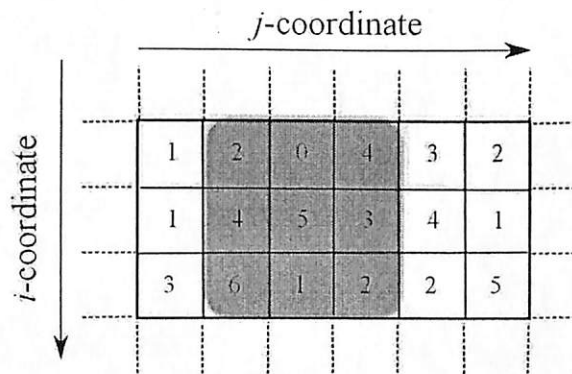


Figure 3.10: The image in Figure 3.8 when the filter is shifted one pixel to the right

The utilization of local histograms can avoid the usage of sorting operations, and thus can save a significant processing time. This can be observed clearly when the image is being filtered by a filter with a big dimensions, such as of size 21×21 pixels. Besides,

the creation of the local histogram is simple, when the filter is being moved one pixel per time. Figure 3.10 show the same image portion as shown in Figure 3.8, but when the filter is moved one pixel to the right side.

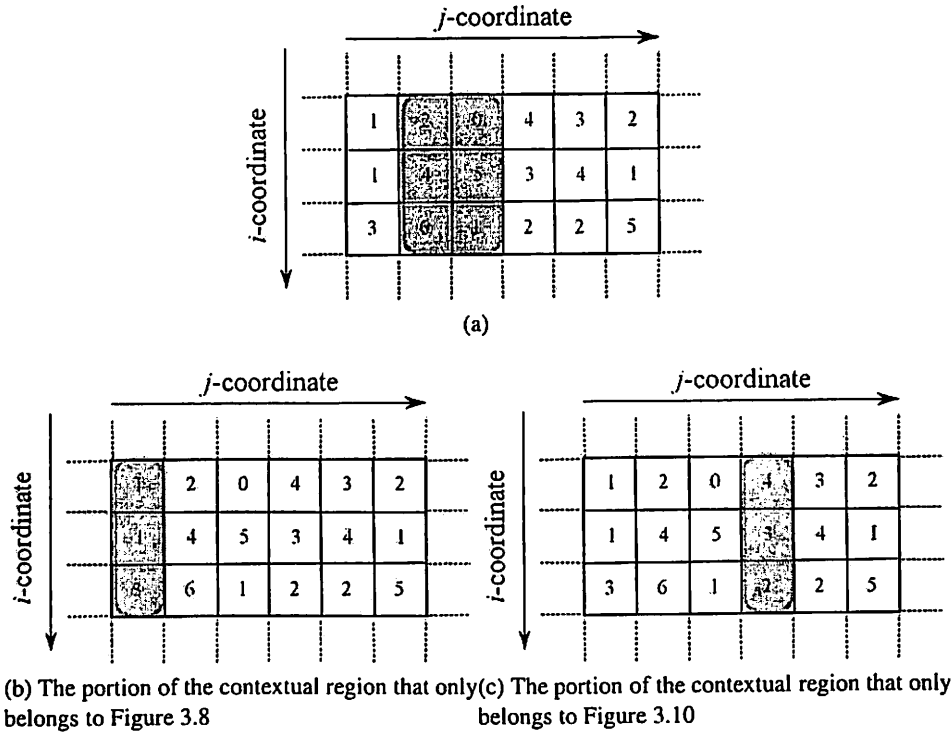


Figure 3.11: Sub-regions defined by Figures 3.8 and 3.10

Figure 3.11 shows the common region and the differences between Figures 3.8 and 3.10. Using the example shown by these figures, the samples defined by the contextual region in Figure 3.10 actually can be initiated based on the samples in Figure 3.8 with added samples from Figure 3.11(c) and deducted samples from Figure 3.11(b). The samples in Figure 3.8 are {0, 1, 1, 1, 2, 3, 4, 5, 6}. Therefore, the samples in Figure 3.10 can be defined as:

$$\{0, 1, 1, 1, 2, 3, 4, 5, 6\} + \{2, 3, 4\} - \{1, 1, 3\} = \{0, 1, 2, 2, 3, 4, 4, 5, 6\} \quad (3.13)$$

Thus, the local histogram can be updated by considering only two columns at one time. As a consequence, this can save a lot of processing time.

The processing time can be reduced further if the window slides continuously, where the current local histogram can be created from the previous local histogram. Therefore, in the implementation of the proposed method, the window slides from left to right for the odd numbered rows, and from right to left for the even numbered rows. The calculation of median value by using this method is faster than if the new local histogram is developed from the whole contextual region.

3.1.3 Results and Discussions

In order to present a wide range of images, the test image used in this experiment is a composite image. This test image is created by using 13 individual standard greyscale images that are normally used in digital image noise reduction field. These standard test images can be obtained from [92]. There are four images with size 256×256 pixels, seven images with size 512×512 pixels, and two images with size 1024×1024 pixels. Therefore, the test image can be considered to represent images of different sizes. As shown by this figure, the content of each figure is also different from each other. For example, *Baboon* image contains more details as compared with *Peppers* image, and *Lena* image is darker than *Stephanie* image. Thus, the test image represents a wide range of image details. The composite image, which is the test image, is shown in Figure 3.12. The size of this image is 2048×2048 pixels, which is equivalent to 4 Megapixels image.

Three quality measures have been used in this research work to evaluate the performance of the proposed noise detection method as compared with seven other detection approaches from median filtering techniques. These measures are the false positive detection, false negative detection, and processing time. The results are presented in the following subsections in the form of surface plots. Each surface plot is obtained by using 90 test images generated from the combinations of noise density $P = \{0\%, 10\%, 20\%, 30\%, 40\%, 50\%, 60\%, 70\%, 80\%, 90\%\}$ with noise spread factor $m = \{1, 16, 32, 48, 64, 80, 96, 112, 128\}$.

3.1.3.1 False Positive Detection Rate

False positive detection happens when a clean, uncorrupted pixel has been classified as a noisy pixel candidate, when the noise reduction filter processes the corrupted image D . As a consequence, the intensity value of this wrongly identified pixel will be altered during noise cancellation stage. As the intensity value of this pixel is unnecessarily been changed, this condition produces a difference between the filtered image F with the ideal clean image C . Therefore, this condition should be avoided, as F may lost some of the image details.

False positive detection rate is used in this work to evaluate the performance of noise detection ability of the method. This measure is defined as:

$$\text{False positive detection} = \frac{N_p}{J \times K} \times 100\% \quad (3.14)$$

where N_p is the number of clean pixels wrongly detected as noise. Thus, as a good noise reduction method should minimize its false positive, a good noise reduction method should have a low false positive detection rate.

In order to determine false positive detection rate of an image, three noise masks (i.e. M_1 , M_2 , and M_3) are created. The values of these masks are initially set to 0. During the creation of image D , for each coordinates (i, j) where noise is added to image C , mask M_1 is marked true (i.e. $M_1(i, j) = 1$). During the noise detection process on image D ,

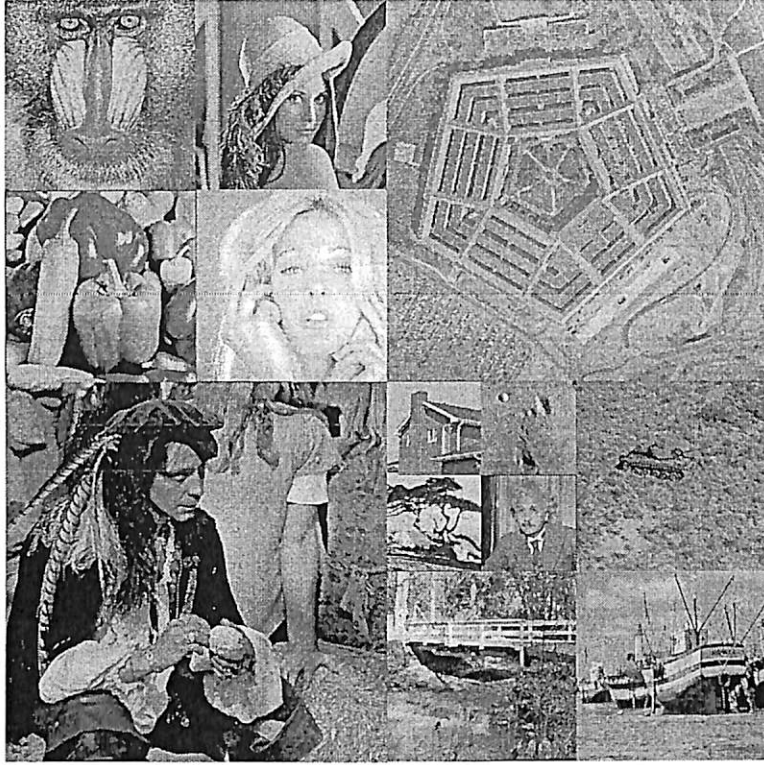


Figure 3.12: The composite image used as the test image in this work

M_2 is marked true (i.e. $M_2(i, j) = 1$) for each detected noise pixel candidates. After these two noise masks are created, mask M_3 is defined as:

$$M_3(i, j) = \begin{cases} 1 & : M_1(i, j) = 0 \text{ and } M_2(i, j) = 1 \\ 0 & : \text{otherwise} \end{cases} \quad (3.15)$$

Then, the number of clean pixels wrongly detected as noise pixel candidates, which will be used in Equation (3.14), can be determined as follow:

$$N_p = \sum_{i=1}^J \sum_{j=1}^K M_3(i, j) \quad (3.16)$$

Surface plots for false positive rates are shown in Figure 3.14. As shown by this figure, SMF3 has the highest false positive rate. This is because, SMF3 treats all pixels in \mathbf{D} as noisy pixel candidates. Therefore, as can be observed in Figure 3.14a, SMF3 has high false positive rate when P is low, and low false positive rate when P is high. Regardless the value of m , the value of false positive rate for SMF3 is approximately equal to $100 - P$.

PCINRF, IMF, AFSF, and MDBUTMF have relatively low false positive detection rate. The magnitude of false detection rate for these methods, for all tested samples, is less than 5%. Although low false detection rate is desired, further investigation should

still be carried out, by using other quality measures. This is to check whether the low false positive detection rate is not because the method does not filter the image.

As shown in Figures 3.13f to 3.13h, ABDND, DSMFBDNDE, and the proposed method has higher false positive detection rate when P is low. This is mostly because these methods are designed to deal with high level of corruption. Therefore, at lower corruption level, these methods tend to consider pixels as noise pixel candidates. ABDND has higher false positive detection rate for random-valued impulse noise (i.e. when m is equal to 128), while DSMFBDNDE has higher false positive detection rate for salt-and-pepper noise (i.e. when m is equal to 1). On the other hand, the proposed method has low false positive detection rate for salt-and-pepper noise. As compared with ABDND, the proposed method has a smoother false positive detection rate surface.

Filter	False Positive Detection								
	m=1			m=64			m=128		
	P=20	P=50	P=90	P=20	P=50	P=90	P=20	P=50	P=90
SMF3	80.0000	50.0000	10.0000	80.0000	50.0000	10.0000	80.0000	50.0000	10.0000
PCINRF	0.7184	0.4202	0.0888	0.9061	0.5978	0.1745	1.2636	0.8149	0.2546
IMF	0.4585	0.4181	0.0901	0.4864	0.4408	0.0932	0.5577	0.4505	0.0936
AFSF	1.9015	2.9074	1.0778	2.1005	3.2491	1.2440	2.4280	4.0508	1.5582
MDBUTMF	0.7352	0.4606	0.0908	0.7357	0.4593	0.0932	0.7349	0.4580	0.0936
ABDND	0.7527	0.4700	0.0916	22.1768	1.6084	0.1390	14.8436	20.9072	5.9380
DSMFBDNDE	8.4187	7.5440	6.6865	4.4716	1.3319	0.3533	5.7349	2.0229	0.5626
Proposed	1.0248	0.5774	0.3995	14.6147	6.1895	1.2310	16.1419	8.3607	2.0475

Figure 3.13: Summary table for discussed filter, p=noise density, m=noise spread factor

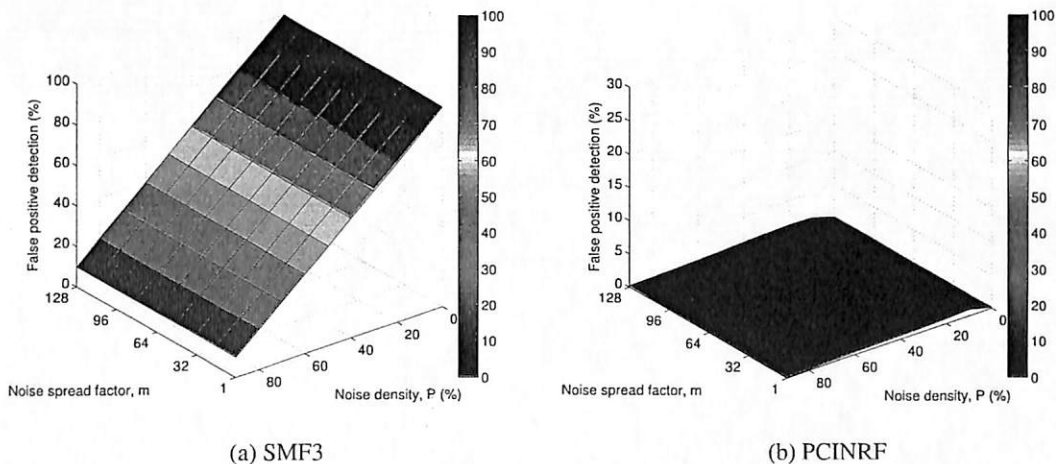
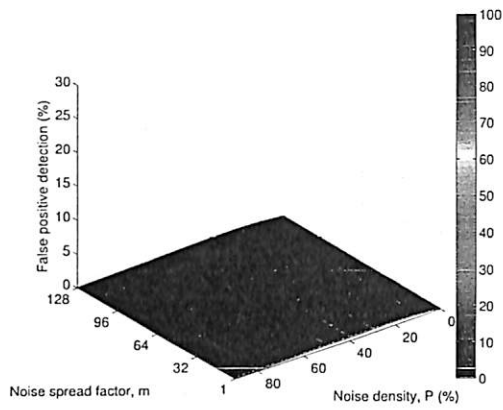
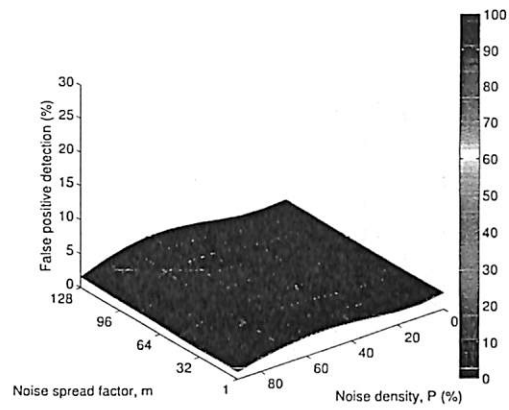


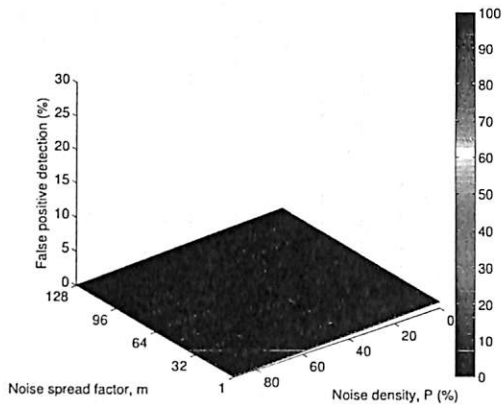
Figure 3.14: False positive detection surface plots



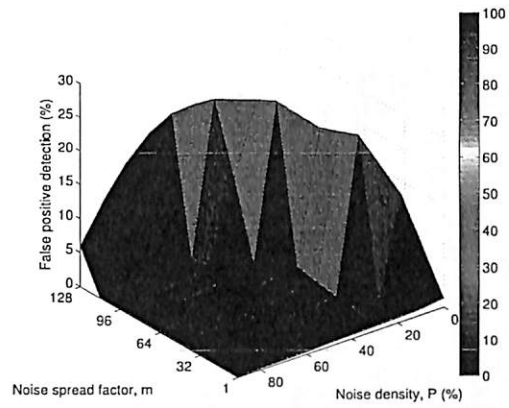
(c) IMF



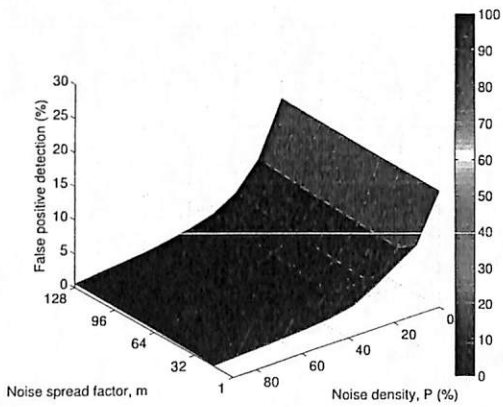
(d) AFSF



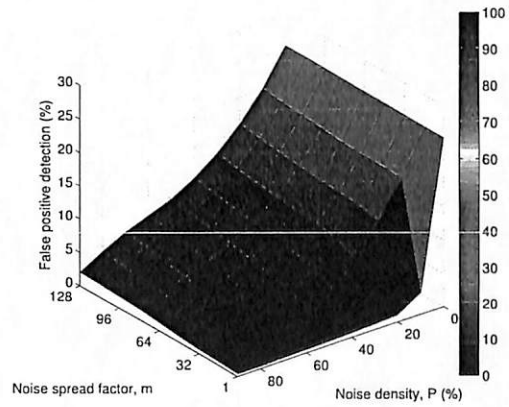
(e) MDBUTMF



(f) ABDND



(g) DSMFBDNDE



(h) Proposed method

Figure 3.13: Continued

3.1.3.2 False Negative Detection Rate

False negative detection happens when the method failed to detect corrupted pixels in damaged image D . As a consequence of false negative detection, not all the noisy pixels will be cleaned up during noise cancellation process. Therefore, similar to false positive detection rate, false negative detection rate is also can be used to evaluate the performance of noise detection ability of the method. False negative detection rate is defined as:

$$\text{False negative detection} = \frac{N_n}{J \times K} \times 100\% \quad (3.17)$$

where N_n is the number of undetected noisy pixel. Thus, as a good noise reduction method should minimize its false negative, a good noise reduction method should have a low false negative detection rate.

In order to determine false positive detection rate of an image, three noise masks (i.e. M_1 , M_2 , and M_3) are created. The values in masks M_1 and M_2 are set exactly the same as described in Section 3.1.3.1. However, mask M_3 is defined as:

$$M_3(i, j) = \begin{cases} 1 & : M_1(i, j) = 1 \text{ and } M_2(i, j) = 0 \\ 0 & : \text{otherwise} \end{cases} \quad (3.18)$$

Then, the number of undetected noisy pixels, which will be used in Equation (3.17), can be determined as follow:

$$N_n = \sum_{i=1}^J \sum_{j=1}^K M_3(i, j) \quad (3.19)$$

Surface plots for false negative detection rate are shown in Figure 3.14. As shown by this figure, false negative detection rate for SMF3 is always zero. This is because SMF3 treats all pixels in image D as noise pixels. Therefore, all of the actual noise pixels are successfully marked as noisy pixel candidates by SMF3.

In contrary with the results on false positive detection rate, all tested method, except SMF3, have high false negative detection rate when the noise density P is high. This is because when P is high, the number of noise pixels in D is also high. Therefore, the probability that the noise pixels will be undetected by the noise detection methods is also increased.

As observed from Figures 3.14b, 3.14c, and 3.14d, when $m \neq 1$ (i.e. except salt-and-pepper noise), the false negative detection rate for PCINRF, IMF, and MDBUTMF is almost can be represented as $100 - P$. However, the false positive detection rate for these methods, as can be observed in the corresponding subfigures in Figure 3.14, are very small. These situations indicate that PCINRF, IMF, and MDBUTMF are only work well for salt-and-pepper noise. The similar trend can also be observed in DSMFBDNDE.

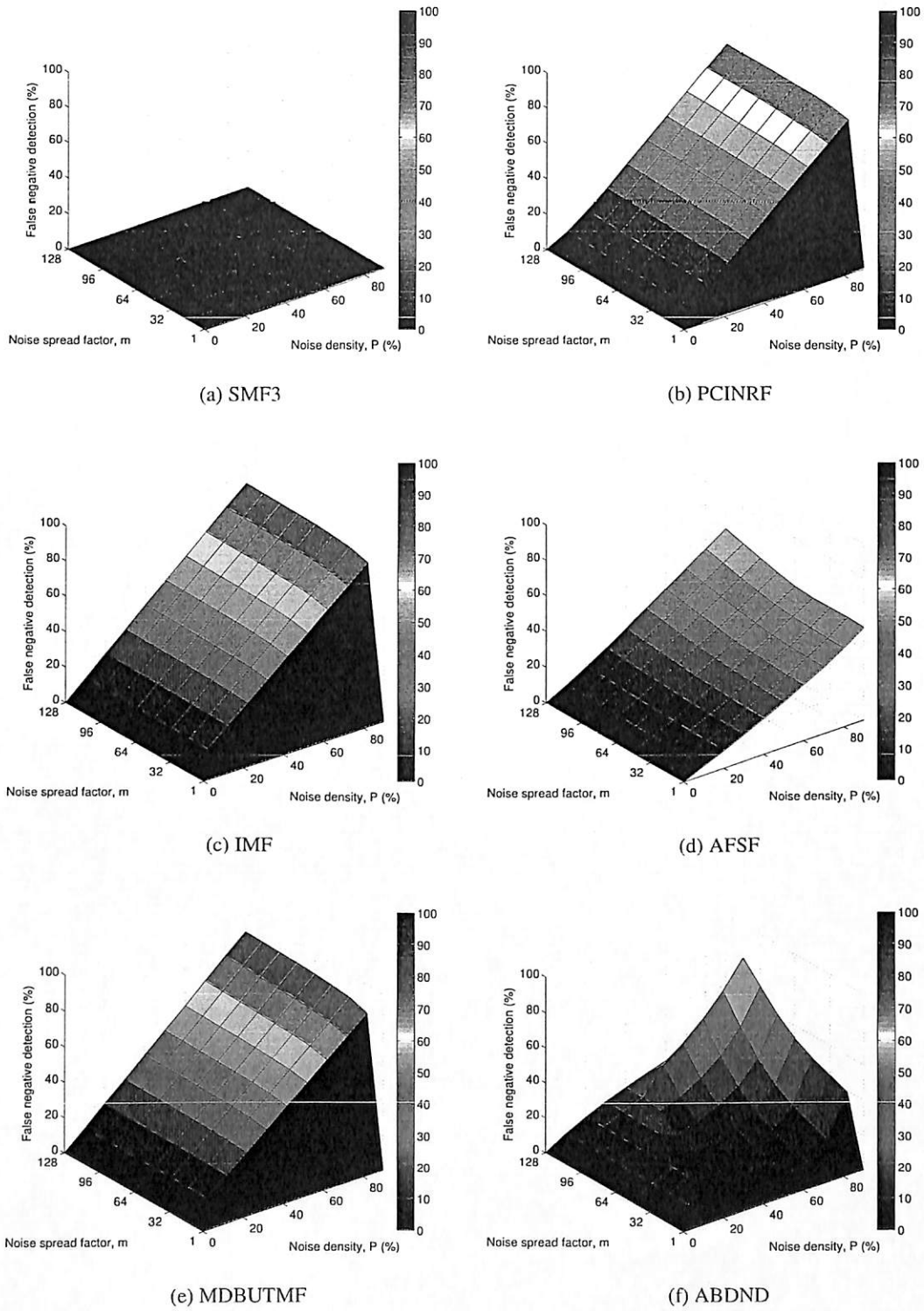


Figure 3.14: False Negative detection surface plots

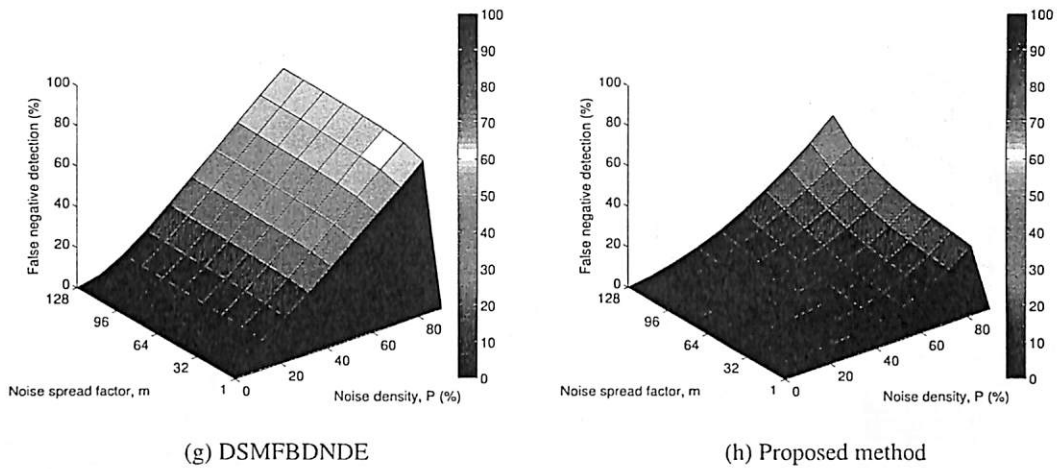


Figure 3.13: Continued

In Figure 3.14, it is shown that AFSF, ABDND, and the proposed method have low false negative detection rate values. AFSF, as shown in Figure 3.13d, also has low false positive detection rate. The surface of false negative detection rate for AFSF does not differentiate salt-and-pepper noise, and thus the surface is more even as compared to others. However, amongst these three methods, the proposed method has the lowest false negative detection rate at most of the tested samples. Furthermore, similar to ABDND, the proposed method has the high false negative detection rate for highly corrupted random-valued impulse noise. This is may be due that the intensity of the corrupted pixel in **D** is similar to the actual noise free pixel in image **C**.

Filter	False Negative Detection								
	m=1			m=64			m=128		
	P=20	P=50	P=90	P=20	P=50	P=90	P=20	P=50	P=90
SMF3	0.0000	0.0000	0.0000	0.0000	0.0000	0.0000	0.0000	0.0000	0.0000
PCINRF	0.9701	0.5766	0.7348	13.3287	41.9898	81.4776	14.2891	42.4127	81.8546
IMF	0.1810	0.1400	0.2182	19.6893	49.2193	88.5937	19.8446	49.6095	89.2969
AFSF	10.1350	25.8128	52.2977	10.7321	27.8028	52.7004	12.2833	32.9374	62.3161
MDBUTMF	0.0000	0.0000	0.0000	19.6875	49.2188	88.5937	19.8437	49.6094	89.2969
ABDND	0.0000	0.0000	0.0000	12.1203	10.5895	52.8102	12.8886	25.7833	40.1561
DSMFBDNDE	0.0000	0.0000	0.0000	7.3017	33.8915	72.7873	8.6489	34.9759	73.7214
Proposed	0.0000	0.0000	0.0000	1.5507	7.6760	29.8365	4.4220	17.9944	50.1878

Figure 3.14: Summary table for discussed filter, p=noise density, m=noise spread factor

3.1.3.3 Processing Time

Processing time, which is the time needed to complete the filtering process, is used in this work as a measure to indicate the complexity of the method. More complex method requires more processing time. Shorter processing time is desired.

Surface plots of processing time are shown in Figure 3.15. As shown by this figure, all methods, except DSMFBDNDE and the proposed method, require less than 5 seconds to complete the filtering process. However, as indicated by the corresponding subfigures in Figures 3.14 and 3.14, this short processing time might be due to the failure of the noise detection stage in identifying noisy pixels. Most of these methods have very low false positive detection rate, and high false negative detection rate. This situation indicates that these methods only mark a few pixels as noise pixel candidate. As a consequence, the noise cancellation stage only processes these few pixels, and thus requires only a short processing time.

Figure 3.14g shows that DSMFBDNDE requires the longest processing time. Most of the test samples require more than 2000 seconds (i.e. more than 30 minutes) to be processed by DSMFBDNDE. This is mostly because DSMFBDNDE uses sorting algorithm for finding median value, and uses relatively large noise detection filter, which is of size 21×21 and 5×5 pixels. On the other hand, as shown by Figure 3.14h, although the proposed method requires relatively high processing time compared to the other six noise filtering methods, the proposed method still has significantly shorter processing time as compared with DSMFBDNDE. Each test sample require less than 50 seconds to be processed completely by the proposed method.

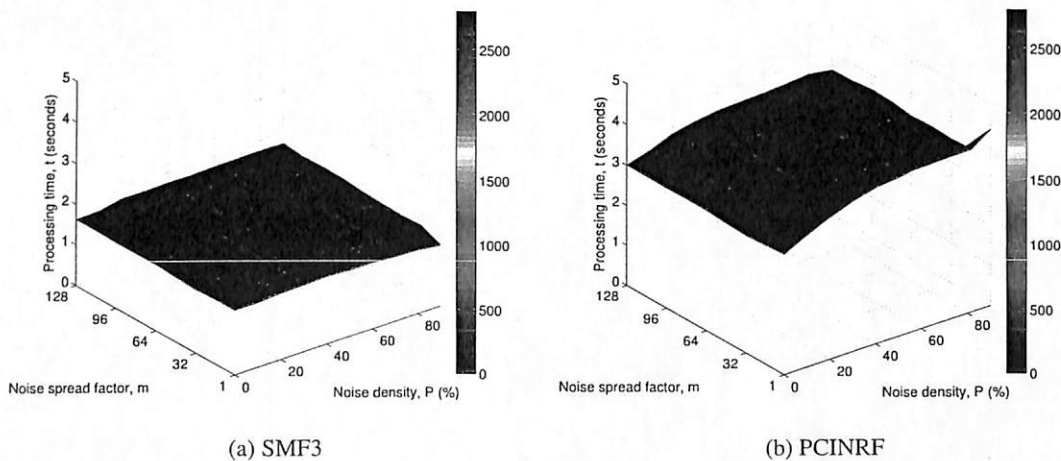
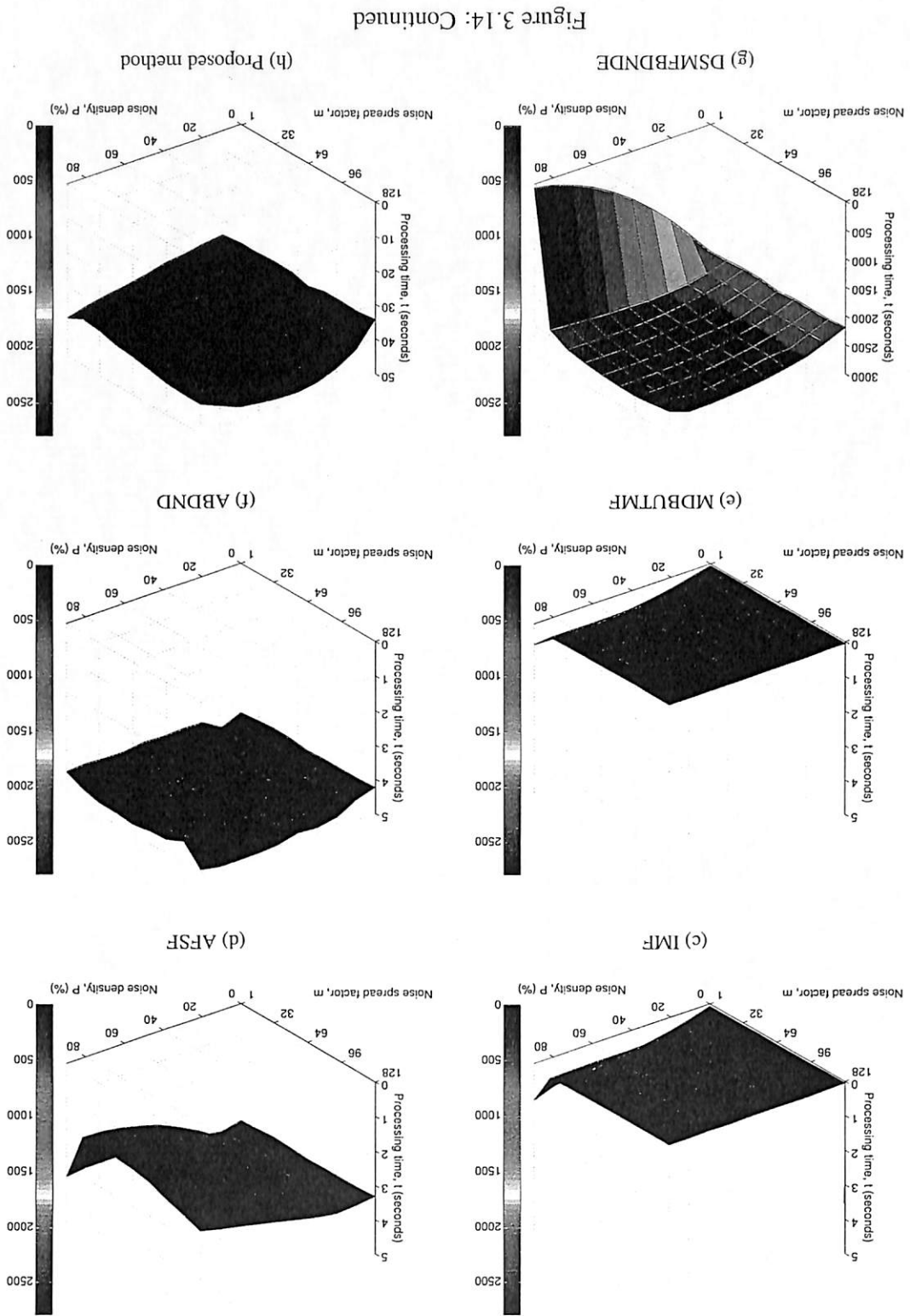


Figure 3.15: Processing time surface plots



Filter	Processing Time(s)								
	m=8			m=64			m=128		
	p=20	p=50	p=90	p=20	p=50	p=90	p=20	p=50	p=90
SMF3	1.6275	1.6174	1.5231	1.6255	1.6277	1.6281	1.7431	1.7457	1.7462
PCINRF	3.5123	4.0312	4.2314	3.4057	3.6171	3.5989	3.3123	3.5987	3.6018
IMF	0.2243	0.3561	1.0367	0.0456	0.0461	0.0482	0.0458	0.0486	0.0501
AISF	3.0798	2.5671	3.2091	2.5712	2.3965	1.9856	3.2856	3.0123	2.7921
MOBUTMF	0.3921	0.4157	0.4203	0.0491	0.0502	0.0517	0.0493	0.0512	0.0512
ABDND	3.8712	3.9891	4.2123	4.7981	4.8194	4.8241	4.2876	4.9871	4.9921
DSMFBDND	1821.6731	918.9831	131.6730	2287.6780	2512.9832	2601.6792	2257.8210	2819.3471	2791.7534
Proposed	30.0215	35.9832	38.6582	38.9261	39.0213	39.6762	34.9854	48.9853	41.9839

Figure 3.15: Summary table for discussed filter, p=noise density, m=noise spread factor

3.1.4 Remarks

This chapter presents the evaluations of the proposed noise detection method, as compared to other seven state-of-the-art methods. The evaluations have been carried out objectively. In terms of false positive detection rate, the proposed method is the second highest, just behind SMF3. However, the good performances of other methods in false positive detection might be due to the inefficiency of the noise detection stage of the methods, where majority of the pixels will not be classified as noise pixel candidate, even though the pixel is actually a noise pixel. This can be proven by inspecting the false negative detection rate. Among the switching median filtering methods used in this work (i.e. excluding SMF3), the proposed methods has the lowest false negative detection rate, portraying its good noise detection ability. However, the proposed method require a slightly longer processing time as compared to the majority of the method. It needs around 40 to 50 seconds (which is less than one minute) to completely process one 4-Megapixels image. Therefore, as the processing time required is still considered long, this process is excluded from the thumbnail generation method that will be designed next.

3.2 Thumbnail Image Generation Method

Blur can be generally classified into complete blur or partial blur. Complete blur of image can be caused by camera shake, which undesirably distorts the whole image taken. Complete blur of image also can be due to Gaussian blur operation. Sometimes, this is done on purpose in photography. Another type of blur, which is the partial blur, happens normally when a fast moving object is captured by a relatively slower shutter speed of the camera [80].

Blurring of images can be disadvantageous or advantageous, depending on purpose of the image being used. For example, partial blur image can be used to emphasize

object of interest (OOI) in the image. This type of image has a blurred background with a distinct foreground object (i.e., OOI). Furthermore, partial motion blurred image of the main object in image can create a sense of motion effect in the image, such as in 100 meters short run competition. The disadvantages of wholly blur and partial blur image is obvious, which prevent user to fully interpret the meaning of image due to lack or distorted information in image.

Motion blur can be caused by camera shake or movement of the object in the image. Camera shake can cause a complete blur for the image captured while object movement in the image will cause partial blur. Camera shake is normally due to handheld camera, therefore a tripod can be a solution for this situation. Typical motion blur is due to relative motion between the captured scene and camera during exposure time of images [34].

Depth of field is the distance between the nearest and the furthest objects that give an image judged to be in focus in a camera. Depth of field is affected by lens's aperture in camera [83]. A lens's aperture is the opening in the diaphragm that determines the amount of focused light passing through the lens. Large aperture will introduce a low depth of field, which mean only near object in front of the camera is focused while object of further distance in the image will be blurred. Small aperture will enable high depth of field, which means further object in the image relative to the camera will be sharply captured. In other words, image is in focus within a range of distances from the lens, called depth of field.

Out of focus blur in image is caused by improper focus on the object in the image. Camera autofocus nowadays depends on contrast to perform focusing mechanism accurately. If there is only slight contrast in the image to be taken, the focusing mechanism might not be working properly [95].

Blur detection is one of the important research branches in digital image processing field. From the literatures based on the approach used, recent blur detection algorithms can be roughly classified into the following six groups:

1. Bayes discriminant function.
2. Extraction of low depth of field (DOF) with emphasize on characteristics.
3. Non-reference (NR) block.
4. Lowest directional high frequency energy (for motion blur).
5. Wavelet-based Histogram and Support Vector Machine (SVM).
6. Edge width analysis.

In the work by Ko and Kim in 2009 [45], Bayes discriminant function is constructed based on the statistic of the gradients of the input image. Mean and standard deviation's statistics are taken for all blur and clear regions. Blur image tends to have a smaller value of mean and standard deviation in the distribution compared with clear image.

By utilizing this concept, blur region in images can be detected for further de-blurring processes.

Low depth of field blur causes blur due to large aperture of the camera during the capture of digital image. This blur detection method is suitable for low DoF image, where the center image containing focused object with out-of-focus background. For this type of image, object of interest (OOI) can be extracted through works by Kim [7] and Wang et al. [41].

In the work of Kim [7], low-DOF image is transformed into appropriate feature space such as spatial distribution of high frequency. Higher order statistic (HOS) computation is performed afterwards for all pixels in low-DOF image. HOS is simplified by using morphological filter operation by reconstruction (dilation and erosion operations), which eliminates the dark holes and bright patches in input image. The differences of this method compared with three other methods, which are segmentation through variable order surface fitting by Besl et al. [63], image segmentation based on extreme intensity by Lifshitz et al. [53] and robust analysis of feature space of color image segmentation by Comaniciu et al. [20] are: Kim's method performs morphological and region merging method perform computation of higher order statistic, morphological operations, region merging and thresholding. These processes are to segment out the OOI image from the input while three other mentioned methods used properties of image intensity and texture to detect clear and blur region.

Sometimes, in researches regarding to digital image processing, there is a need to measure the degree of blur introduced into the image after certain type of process was applied. Therefore, blur degree can become one of the qualitative measures to evaluate the quality of an image. The degree of blur is important for researcher to evaluate the robustness and effectiveness of the image processing algorithms. If the measurement requires both the processed and the original sharp image, this measurement method is known as full-reference (FR) method.

No reference block based blur detection method does not require any of the original signal information which is more convenience in real scenario, compared with full-reference (FR) and reduced-reference (RR) block based. Image blur region is obtained via averaging the local blur of macro blocks in the images. Texture influence of the image is reduced via a content dependent weighting scheme and the local blur is defined as the distance between the two pixels with maximum and minimum luminance values. This method has lower complexity, higher robustness for variety of image contents compared with typical edge based blur metrics [17].

No reference block-based blur detection calculates the local blur at the boundaries and averaging the magnitudes to get the blur of the image. To reduce the influence from the texture, a content dependent weighting scheme is employed. The basic approach of no reference quality measurement is the extraction of the decoded video feature and relationship built between the extracted features and the decoded visual quality. Blur detection based on no reference block often compared with typical edge based blur met-

ric. No reference block-based method has advantages over edge-based as block-based method does not need edge detection, which means the blur detection is not in limited region like edge-based method and it has more accurate results in estimate the local blur.

The proposed direction estimation is based on measurement of lowest directional high frequency energy [8]. Motion blur detection based on lowest directional high frequency energy has less computational cost without the usage of point spread function estimation. The main contribution of this paper is that a closed-form solution is derived. This method detect the blur region by analyzing high frequency energy and estimate the motion direction of the image blocks, making it more accurate and more robust compared with other learning-based methods like the work by Liu et al. [66].

The main idea of wavelet-based histogram and support vector machine is on discrimination of the gradient distributions between blurred and non-blurred image regions [85]. The proposed algorithm does not need the prior knowledge about the input image and is oriented to out-of-focus blur, unlike motion blur detection as described in the previous sections. This algorithm works on feature extraction in wavelet space by applying wavelet decomposition of input image, calculating wavelet gradient map and construction of gradient histograms.

Blur detection based on edge intensity profile is works by analysing the edge of the objects on the image. The intensity profile of the input image being conducted to check whether there is potential blur image region in the image.

The example on how the blur effects to the gradient of the object's edges is shown in Figure 3.16. Notice that the sharp image, as shown in Figure 3.16(a), has steep gradients (i.e., step edge). On the other hand, blur image, as shown in Figure 3.16(c), contains a relatively smaller edge gradients (i.e., ramp edge) [23]. By having a larger gradient in image, the sharp image will looks more distinct compared with the blurred image, which the gradient already being smoothed. By using this concept, blur detection can be carried out by analyzing the edge gradient from the image data. Steep edge and ramp edge gradient regions being segmented out from the input image and ramp edge gradient region have high potential in representing the blur region [76].

In Figure 3.16, the intensity profile of the edge of sharp image (Figure 3.16 (b)) is very steep, while the blurred image's intensity profile (Figure 3.16 (d)) has a relatively smoother rising and falling edges. For both Figure 3.16 (a) and (c), since the same pattern of image is being used, comparisons between blurred and clear image can be done in a more comprehensive way. In the work of Chung et al. [10], the blur measure is estimated by inspecting the contrast of the edges in image. Weighted average between local standard deviation of the edge gradient's magnitude and the edge gradient's magnitude is performed in their works. The standard deviation is perceived as the width of the edge and the edge gradient magnitude is included to make their algorithm more reliable. Experiment on natural scene has shown that their works can effectively describe the blurriness in the input image.

In order to embed blur information into the thumbnail, blur detection methods were

studied. Blur detection methods are mainly area based analysis, rather than more on specific points of interest. From all possible blur detection researches, edge width analysis is being considered for this research project. Analysis based on edge width is more effective as its scope is narrowed to the pixel level of an image, as compared to area based analysis. Furthermore, currently there is no thumbnail generation method using edge width analysis approach.

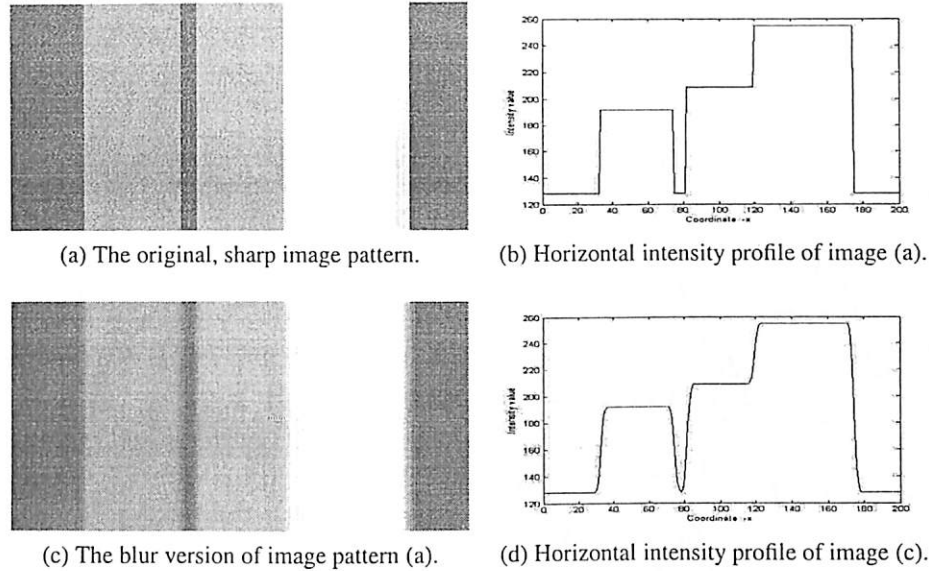


Figure 3.16: Example of blur edges. (a) The original, sharp image. (b) Horizontal intensity profile of image (a). (c) The blur version of image (a). (d) Horizontal intensity profile of image (c).

3.2.1 Methodology

Most of the image thumbnails tend to ignore information regarding the noise and blur content of the originally high resolution input image F . Therefore, in this thesis, a new image thumbnail generation algorithm has been developed. This gives more emphasize on blur regions, and thus named as Thumbnail with Blur Information (TBI). The idea of this proposed method is to preserve the blur information, especially for the blurs on the edges on image F , to its corresponding image thumbnail f . To achieve this aim, blur detection algorithm has been employed to image F . In TBI method, blur detection algorithm used is based on the work proposed by Chung et al. [10] in 2004. Then, after the blur detection process is performed, TBI down-samples image F by using the blur information. Each layers of R,G, and B color will be processed separately and then combined back in the end process during thumbnail generation stage to ensure less complicated computation coding.

In this proposed TBI method, similar to other image thumbnail algorithms, the user

only need to input the down-sampling factor L . If the original input image \mathbf{F} is of size $M \times N$, its thumbnail version \mathbf{f} is of size $m \times n$. The dimensions of m and n are defined as:

$$m = \left\lfloor \frac{M}{L} \right\rfloor \quad \text{and} \quad n = \left\lfloor \frac{N}{L} \right\rfloor \quad (3.20)$$

where $\lfloor \cdot \rfloor$ stands for floor value (e.g., $\lfloor 2015.9254 \rfloor = 2015$). This means that truncation approach has been chosen in the implementation of TBI.

Generally, the originally high-resolution acquired image \mathbf{F} can be described by the following equation [51] [30]:

$$\mathbf{F} = \mathbf{B} \otimes \mathbf{C} \quad (3.21)$$

where \mathbf{B} is the space-varying blur, whereas \mathbf{C} is the ideal clean and sharp image. The symbol \otimes in this equation presents a 2-dimensional convolution operation.

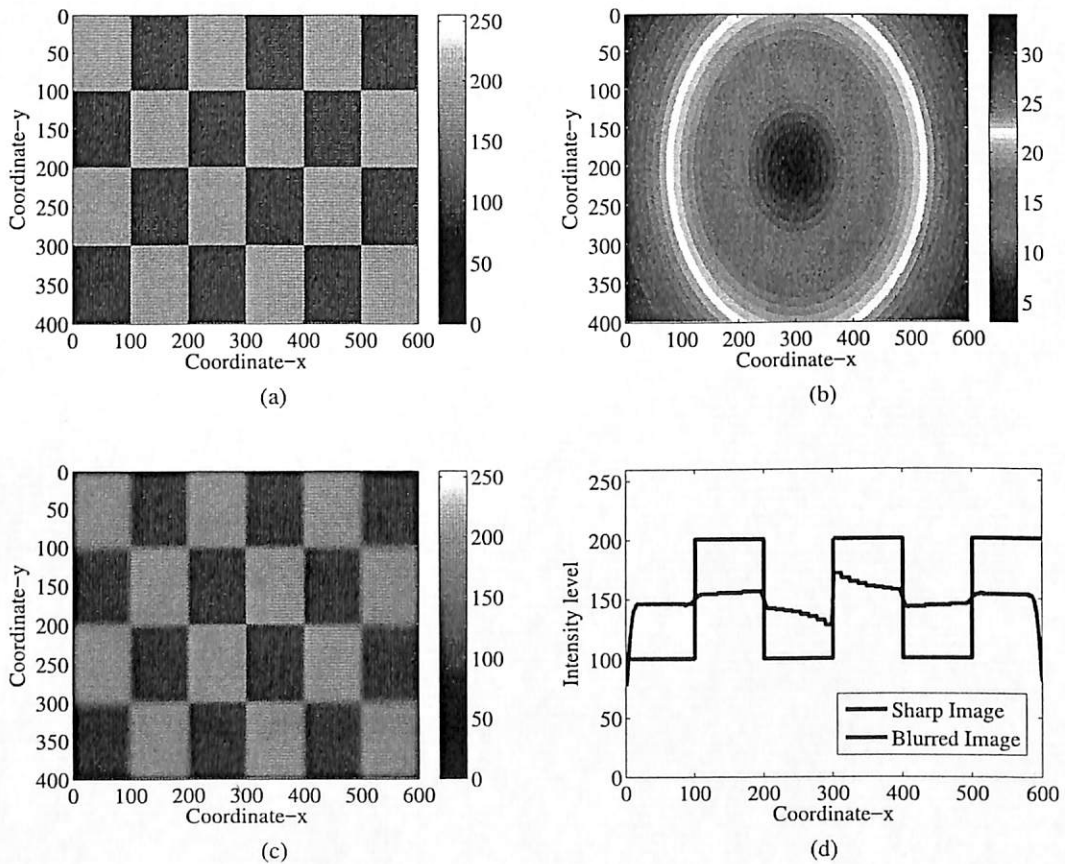


Figure 3.17: (a) An ideal clean image \mathbf{C} . (b) The blur \mathbf{B} as a function of the radius B_r of the blur kernel. (c) A blurred image \mathbf{F} according to equation (3.21). (d) Image profile of \mathbf{C} and \mathbf{F} along x -axis, at $y = 199$.

To clarify equation (3.21), an example is given in Figure 3.17. Image \mathbf{F} shown by Figure 3.17(c) is obtained by convolving image \mathbf{C} (i.e., Figure 3.17(a)) with blur function

B (i.e., Figure 3.17(b)). In this example, **B** is a space-varying blur function, described by 2-dimensional Gaussian function [93]:

$$\text{Gaussian}(y, x) = \exp\left(-\frac{y^2 + x^2}{2\sigma^2}\right) \quad (3.22)$$

where σ is the standard deviation of the distribution.

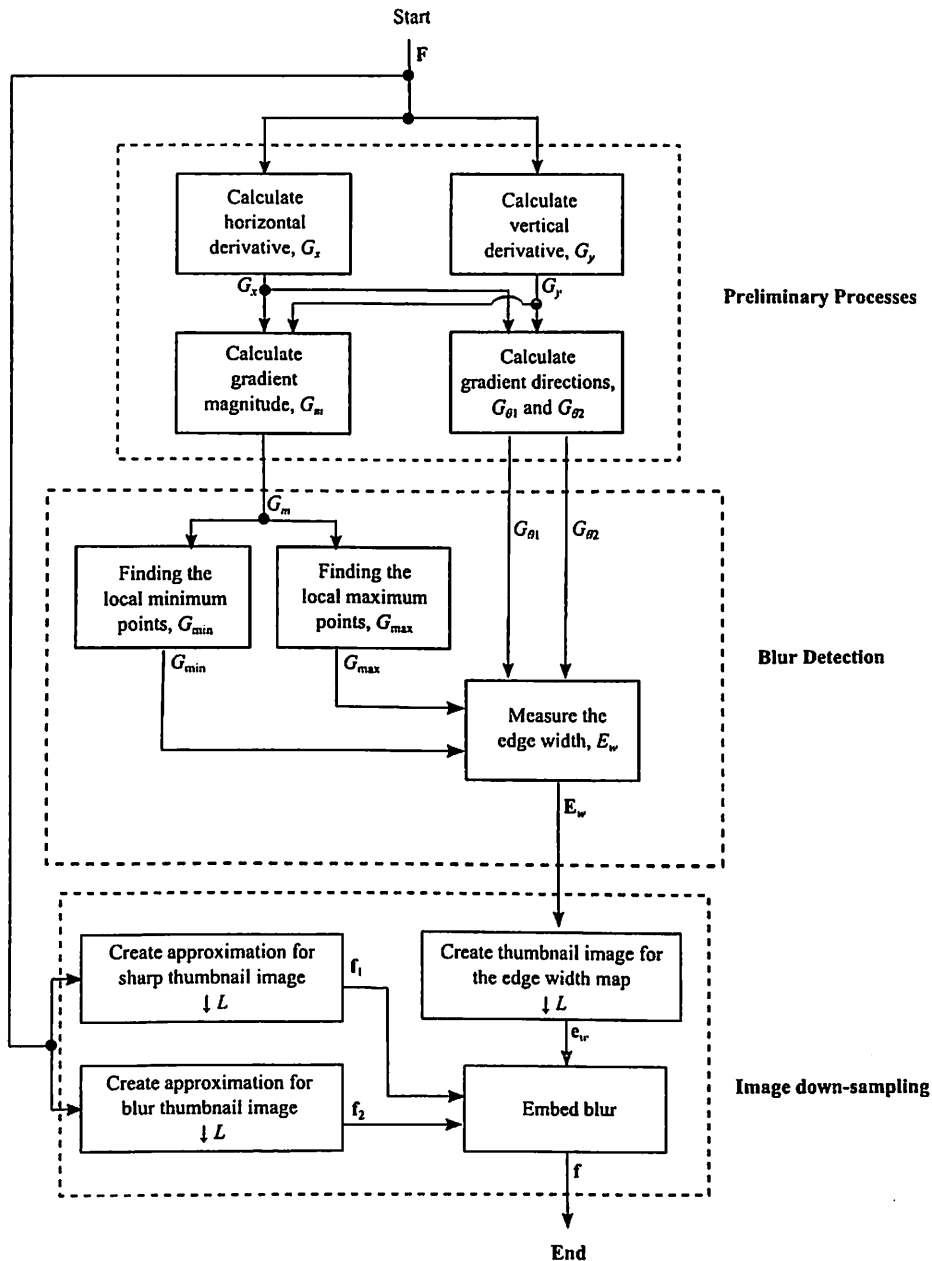


Figure 3.18: Overview of the process involved in TBI algorithm.

Assuming that the Gaussian filter applied is a square filter, with odd size, defined as

$(2B_r + 1) \times (2B_r + 1)$, then σ can be written as [78]:

$$\sigma = \frac{B_r}{\sqrt{-2.0 \times \ln(\xi)}} \quad (3.23)$$

where, in this example, ξ is set to value 0.0001. Variable B_r in this formula stands for the radius of the blur kernel. Therefore, the Gaussian filter in equation (3.22) can be expressed in terms of the filter's size.

Therefore, the blur function \mathbf{B} in Figure 3.17(b) is defined as a function of B_r . As shown by this figure, the size of the blur filter kernel applied to the pixels located at the center of the image is small, and the filter's size is gradually increasing towards the border of the image. Blur filter with larger size gives more blur to the image, as compared to blur filter with smaller size. As a consequence, in Figure 3.17(c), the image appears relatively sharper at the center region (i.e., regions where blur filters with small size are applied), as compared with the regions on the border (i.e., regions where blur filters with larger size are applied).

By inspecting the image profiles shown in Figure 3.17(d), the effect of the blur filter can be observed. When comparing the profile from the sharp image \mathbf{C} with the blurred image \mathbf{F} , it is shown that blur filter changes the step edges in \mathbf{C} to become ramp edges in \mathbf{F} . This figure also shows that the slope of the edges becoming more gradual when the size of the blur filter applied is bigger (i.e., when the blur effect become more serious).

Therefore, the degree of blurs can be observed by inspecting the edges on the image. Sharp regions have narrow edge width, while blur regions have wider edge width. This is the main approach used by TBI in detecting the blur regions.

Figure 3.18 shows the general view of TBI. As shown by this figure, the proposed method has three main blocks. These blocks are; (1) Preliminary processes, (2) Blur detection, and (3) Image down-sampling. TBI algorithm takes the information from the blur detection stage, and use it in its image down-sampling stage, so that more blur informations from \mathbf{F} can be embedded into \mathbf{f} .

3.2.2 Results and Discussions

In order to evaluate the performance of TBI properly, five other thumbnail image algorithms are implemented and used as benchmarks. The methods that are included for comparisons are DPD method [25] [40], DSD method [55], PDAF method with averaging filter [31], TBNI method [38] and DIB method [70]. The input dataset used consists of twelve raster images obtained from the database provided by Trentacoste et al. [90] as it contains various partial blur images suitable to be input data for discussion purposes. These images are shown in Figure 3.2.2. In order to ensure the "completeness" of the test data, the image suffers from various degree and types of blurs. The image size is also varies.

The images used in this experiment are color image with bit-depth of 24 bits. The image format is JPEG, which is a common compression scheme used for digital image.

As the input image has three color layers, the processing of TBI is done separately on each color layer.



Figure 3.19: Example of input images.

In this section the analysis is done based on survey, conducted with all 12 test images with down-sampling factor L is set to four and eight. For each of the test image, at a specific L value, each of the data set consists of thumbnail images of DPD, DSD, PDAF,

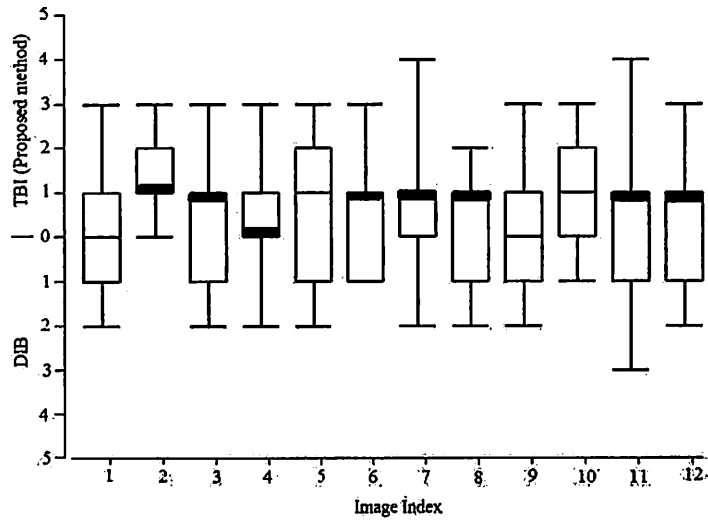
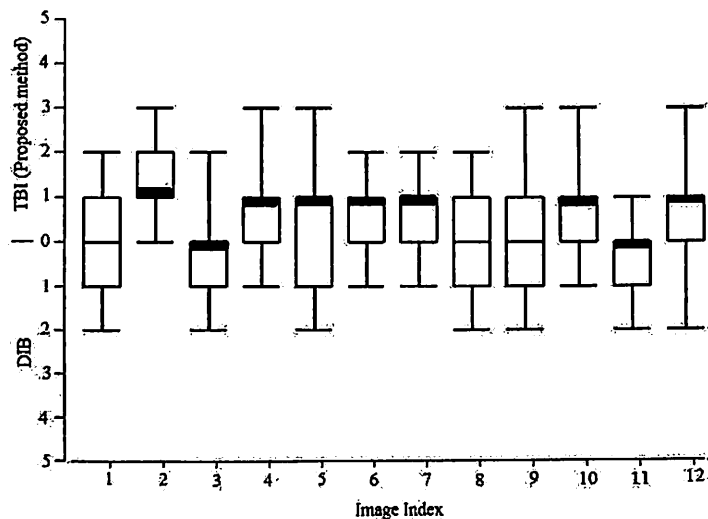
(a) Box-and-whisker plot for TBI vs. DIB for $L=4$.(b) Box-and-whisker plot for TBI vs. DIB for $L=8$.

Figure 3.20: Box-and-whisker plot for TBI Vs. DIB thumbnail images survey.

Box-and-whisker plots is useful for indicating whether a distribution is skewed and whether there are potential unusual observations (outliers) in the data set. It is also very useful when large numbers of observations are involved and when two or more data sets are being compared. This type of graph is used to show the shape of the distribution, its central value, and its variability. In box-and-whisker plots, the ends of the box are the upper and lower quartiles, so the box spans the interquartile range. Besides, the median is marked by a horizontal line inside the box and the whiskers are the two lines outside the box that extend to the highest and lowest observations.

Figure 3.20 shows box-and-whisker plot for TBI vs. DIB thumbnail images survey.

Analyzing from the median, it is obvious that TBI method is chosen over DIB method with a very high tendency from volunteers for both Figure 3.20 (a) and Figure 3.20 (b).

Quartile 1 and quartile 3 also show that the choice is favourable towards TBI. The extreme minority value also shows tendency towards TBI method for both $L=4$ and $L=8$. Therefore, from this survey, TBI method outperformed DIB with high preference from volunteers.

3.2.3 Remarks

The results and discussions via graphs and survey have shown that TBI obtained satisfactory thumbnail results. TBI thumbnail method is successful in a way that it proposed a new way of generating thumbnail image based on edge width analysis. Normal down-sampling like DPD and DSD is a direct down-sampling method, without pre-analysis of the image. PDAF method with averaging filter shows smoother results, sometimes not correspond to the sharp original image. Overall, TBI has shown a satisfactory result of down sampling method based on edge analysis, which might not be an obvious better way, but it is a new approach for a down-sampling method.

Chapter 4

Conclusion and Future Works

This last chapter will give an overall project performance. Section 4.1 concludes the findings of this project, which reflects the objectives of this research. Next, Section 4.2 put forwards several suggestions, as a general guideline for future works related to this project.

4.1 Summary and Conclusion

The project carried out in this work is regarding the development of the algorithm for image thumbnail. This project has been executed successfully, where a thorough literature survey has been carried out, a new method has been designed properly and was evaluated extensively with other thumbnail methods. In general, even though this does not give a very obvious visual improvement compared with its peer's methods, it does contribute to the idea of new algorithm of thumbnail generation based on edge width analysis which has never been done by other researchers. In short, this project is on the right path in developing a more advanced thumbnail generation method.

To inspect the achievement of the project in more detail, with respect to the project objectives, the following points are given:

1. The algorithm based on domain transform has been explored. In this research, one image thumbnail generation method has been developed based on the idea captured from the fractal transform. The results shows that the proposed method is better in embedding high intensity structures into the image thumbnail.
2. Development of method in spatial domain has been carried out. Noise detection method has been successfully designed, but unfortunately its take very long computational time. Therefore, only blur information is emphasize in this project. The proposed method (i.e., TBI) has been developed by inspecting the blur informa-

tion. The degree of blur is decided by the edge width analysis. The results shows that the proposed method is better than some common image thumbnail methods.

3. The work on optimization has been done. First, the implementation of the impulse noise detector has been optimized by manipulating the information from local sliding window. However, the processing time for this approach is still relatively high and not suitable for real time application. Therefore, the second optimization is by ignoring the problem by noise, and this project only concentrated on embedding blur information into the thumbnail.

4.2 Future Works

Indeed, there are lots of improvements that can be carried out in the future for the betterment of the project. These suggestions are not only related to the improvement of the proposed Thumbnail with Blur Information (TBI) alone, but also included for the benefits of this project in the future. These suggestions are listed as follow:

1. The improvements on input datasets.
In the future, it is much better if the input dataset are carried out independently for each type of blur images like out of focus blur, low depth of field blur and motion blur. Each type of blur can have different execution processes based on its blur properties. It is because analysis of each type of blur independently might brings unexpected research outcome for future research purposes. For this purposes, dataset need to be collected in vast amount and more algorithms need to be implemented for this intensive purposes.
2. The improvements on the acquisition device.
In the future, variety of camera should be used for data collection purpose. For instance, professional camera still have different image properties compared with normal point and shoot camera or handphone camera. Therefore, this future work enable variety of input devices, hence potentially making the future work more robust and better.
3. The improvements in terms of the input media.
In the current project, the input datasets are from still images. In the future, one should also consider the usage of digital video as the input. Video stream in thumbnail form is a potential future research work for further algorithm enhancement. One of the applications of thumbnail video output is at security room for surveillance system.
4. Investigations on more down-sampling method
Variety of downsizing factor need to be included for more down-sampling factor L . Variety of L parameter in research will help to further investigate and evaluate

the potential of the down-sampling algorithm. Further research need to be done for high down-sampling factor thumbnail image, as less information from original image embed into the thumbnail, making the future research work more interesting and challenging.

Bibliography

- [1] Tinku Acharya and Ajoy K. Ray. *Image Processing: Principles and Applications*. John Wiley & Sons, Hoboken, New Jersey, 2005. [cited at p. 12]
- [2] A. Al-Fahoum and B. Harb. A combined fractal and wavelet angiography image compression approach. *The Open Medical Imaging Journal*, 7:9–18, 2013. [cited at p. 7]
- [3] K. K. Anisha and M. Wilsy. Impulse noise removal from medical images using fuzzy genetic algorithm. *Signal & Image Processing: An International Journal (SIPIJ)*, 2(4):173–186, December 2011. [cited at p. 13, 14]
- [4] Ali Said Awad and Hong Man. Similar neighbor criterion for impulse noise removal in images. *AEU-International Journal of Electronics and Communications*, 64(10):904–915, October 2010. [cited at p. 12]
- [5] Soon Ting Boo, Haidi Ibrahim, and Kenny Kal Vin Toh. An improved progressive switching median filter. In *Proceedings of the International Conference on Future Computer and Communication (ICFCC 2009)*, pages 136–139, 2009. [cited at p. 13]
- [6] Raymond H. Chan, Chen Hu, and Mila Nikolova. An iterative procedure for removing random-valued impulse noise. *IEEE Signal Processing Letters*, 11(12):921–924, 2004. [cited at p. 12]
- [7] Kim Changick. Segmenting a Low-depth-of-field Image Using Morphological Filters and Region Merging. *IEEE Transactions on Image Processing*, 14(10):1503–1511, 2005. [cited at p. 36]
- [8] Xiaogang Chen, Jie Yang, Qiang Wu, and Jiajia Zhao. Motion blur detection based on lowest directional high-frequency energy. *Image Processing (ICIP) 2010 17th IEEE International Conference*, pages 2533–2536, September 2010. [cited at p. 37]
- [9] J. Chun, S. H. Han, H. Im, and Y. S. Park. A method for searching photos on a mobile phone by using the fisheye view technique. *International Journal of Industrial Ergonomics*, 41:280–288, 2011. [cited at p. 3]
- [10] Yun Chung, Jung Ming Wang, Robert R. Bailey, Sei Wang Chen, and Shyang Lih Chang. Non-parametric Blur Measure based on Edge Analysis for Image Processing Applications. In *Cybernetics and Intelligent Systems*, pages 356–360. IEEE, 2004. [cited at p. 37, 38]

- [11] Pinar Civicioglu. Removal of random-valued impulsive noise from corrupted images. *IEEE Transactions on Consumer Electronics*, 55(4):2097–2104, November 2009. [cited at p. 12]
- [12] H. A. Cohen. Access and retrieval from image databases using image thumbnails. In *Fourth International Symposium on Signal Processing and Its Applications (ISSPA 96)*, pages 427–428, 1996. [cited at p. 3]
- [13] H. A. Cohen. Fractal image coding for thumbnail based image access. In *1996 Fourth International Signal Processing and Its Applications (ISSPA 96)*, pages 158–161, 1996. [cited at p. 7]
- [14] H. A. Cohen. Thumbnail-based image coding utilising the fractal transform. In *1996 Proceedings of International Conference on Image Processing*, pages 145–148, 1996. [cited at p. 7]
- [15] H. A. Cohen. Note: Retrieval and browsing of images using image thumbnails. *Journal of Visual Communication and Image Representation*, 8(2):226–234, 1997. [cited at p. 3]
- [16] S. J. Daly. Analysis of subtriad addressing algorithms by visual system models. In *Symposium on Digital Technical Papers (SID)*, pages 1200–1203, 2001. [cited at p. 5]
- [17] Liu Debing, Chen Zhibo, Ma Huadong, Xu Feng, and Gu Xiaodong. No reference block based blur detection. In *Quality of Multimedia Experience, QoMEx. International Workshop*, pages 75–80, July 2009. [cited at p. 36]
- [18] S. Deivalakshmi, S. Sarath, and P. Palanisamy. Detection and removal of salt and pepper noise in images by improved median filter. In *2011 IEEE Recent Advances in Intelligent Computational Systems (RAICS)*, pages 363–368, 2011. [cited at p. 13]
- [19] Yuqi Dong and Shufang Xu. A new directional weighted median filter for removal of random-valued impulse noise. *IEEE Signal Processing Letters*, 14(3):193–196, 2007. [cited at p. 12]
- [20] Comaniciu Dorin and Peter Meer. Robust analysis of feature spaces: Color image segmentation. In *IEEE Conference Computer Vision and Pattern Recognition*, pages 750–755, 1997. [cited at p. 36]
- [21] How-Lung Eng and Kai-Kuang Ma. Noise adaptive soft-switching median filter. *IEEE Transactions on Image Processing*, 10(2):242–251, 2001. [cited at p. 13]
- [22] S. Esakkirajan, T. Veerakumar, Adabala N. Subramanyam, and C. H. PremChand. Removal of high density salt and pepper noise through modified decision based unsymmetric trimmed median filter. *IEEE Signal Processing Letters*, 18(5):287–290, May 2011. [cited at p. 13]
- [23] Feng Xiao Fan, Hao Pan, and Scott Daly. Comparisons of Motion Blur Assessment Strategies for Newly Emergent LCD and Backlight Driving Technologies. *Journal of The Society for Information Display*, 16(10):981–988, 2008. [cited at p. 37]
- [24] L. Fang and O. C. Au. Subpixel-based image down-sampling with min-max directional error for stripe display. *IEEE Journal of Selected Topics in Signal Processing*, 5(2):240–251, 2011. [cited at p. 4, 5]

- [25] Lu Fang, Au Oscar, Ketan Tang, Xing Wen, and Wang Hanli. Novel 2-D MMSE subpixel-based image down-sampling. *Circuits and Systems for Video Technology, IEEE Transactions on*, 22(5):740–753, 2012. [cited at p. 41]
- [26] K. Furutsu and T. Ishida. On the theory of amplitude distribution of impulsive random noise. *Journal of Applied Physics*, 32(7):1206–1221, July 1961. [cited at p. 12]
- [27] Roman Garnett, Timothy Huegerich, Charles Chui, and Wenjie He. A universal noise removal algorithm with an impulse detector. *IEEE Transactions on Image Processing*, 14(11):1747–1754, November 2005. [cited at p. 13]
- [28] R. C. Gonzalez and R. E. Woods. *Digital Image Processing*. Pearson Prentice Hall, 3rd edition, 2008. [cited at p. 8, 11]
- [29] Rafael C. Gonzalez and Richard E. Woods. *Digital Image Processing*. Pearson Prentice Hall, Upper Saddle River, New Jersey, USA, 3rd edition, 2008. [cited at p. 13]
- [30] Liu Guangcan, Chang Shiyu, and Ma Yi. Blind image deblurring using spectral properties of convolution operators. *arXiv preprint arXiv:1209.2082*, 2014. [cited at p. 39]
- [31] Juan Ramón Hernández, Fernando Perez-Gonzalez, Jose Rodriguez, and Gustavo Nieto. Performance analysis of a 2-d-multipulse amplitude modulation scheme for data hiding and watermarking of still images. *Selected Areas in Communications, IEEE Journal on*, 16(4):510–524, 1998. [cited at p. 41]
- [32] Cheng-Hsing Hsieh and Po-Chin Huang. Impulse noise removal with modified BDND and adaptive switching median filter. In Shengyong Chen and Qing Li, editors, *Proceedings of the 8th WSEAS International Conference on Applied Computer and Applied Computational Science (ACACOS'09)*, pages 106–111. WSEAS Press, 2009. [cited at p. 13]
- [33] Cheng-Hsiung Hsieh, Po-Chin Huang, and Sheng-Yung Hung. Noisy image restoration based on boundary resetting BDND and median filtering with smallest window. *WSEAS Transactions on Signal Processing*, 5(5):178–187, May 2009. [cited at p. 13]
- [34] Kuihua Huang, Haozhe Liang, Weiya Ren, and Jun Zhang. Motion blur identification using image statistics for coded exposure photography. In *Emerging Technologies for Information Systems, Computing, and Management*, pages 461–468. Springer New York, 2013. [cited at p. 35]
- [35] Thomas S. Huang, George J. Yang, and Gregory Y. Tang. A fast two-dimensional median filtering algorithm. *IEEE Transactions on Acoustics, Speech and Signal Processing*, 27(1):13–18, February 1979. [cited at p. 22]
- [36] Ying Huang, Mei Xie, Weisheng Li, and Lifang Zhou. Research on k-means median filter. *Journal of Information & Computational Science*, 8(6):961–968, 2011. [cited at p. 13]
- [37] H. Ibrahim. Image thumbnail with blur and noise information to improve browsing experience. *Advances in Multimedia - An International Journal (AMIJ)*, 2(3):39–48, 2011. [cited at p. 5]
- [38] Haidi Ibrahim. Image thumbnail with blur and noise information to improve browsing experience. *Advances in Multimedia*, 2(3):39–48, 2011. [cited at p. 41]

- [39] Haidi Ibrahim, Nicholas Sia Pik Kong, and Theam Foo Ng. Simple adaptive median filter for the removal of impulse noise from highly corrupted images. *IEEE Transactions on Consumer Electronics*, 54(4):1920–1927, November 2008. [cited at p. 13]
- [40] N. Jagadeesan and R. M. S Parvathi. An efficient image downsampling technique using genetic algorithm and discrete wavelet transform. *Journal of Theoretical and Applied Information Technology*, 61(3), 2014. [cited at p. 41]
- [41] Wang James, Jia Li, Robert M. Gray, and Gio Wiederhold. Unsupervised multi-resolution segmentation for images with low depth of field. *PAMI*, 23(1):85–90, 2001. [cited at p. 36]
- [42] V. Jayaraj, D. Ebenezer, and V. R. Vijayakumar. A noise free estimation switching median filter for detection and removal of impulse noise in images. *European Journal of Scientific Research*, 51(4):563–581, 2011. [cited at p. 13]
- [43] S. Jayaraman, S. Esakkirajan, and T. Veerakumar. *Digital Image Processing*. Tata McGraw-Hill Education, New Delhi, India, 2009. [cited at p. 12]
- [44] S. Kalavathy and R. M. Suresh. A switching weighted adaptive median filter for impulse noise removal. *International Journal of Computer Applications*, 28(9):8–13, 2011. [cited at p. 12]
- [45] Jaeseung Ko and Changick Kim. Low cost blur image detection and estimation for mobile devices. *Advanced Communication Technology . International Conference on Advanced Computing Technologies*, 3(1):1605–1610, February 2009. [cited at p. 35]
- [46] Nicholas Sia Pik Kong and Haidi Ibrahim. The effect of shape and weight towards the performance of simple adaptive median filter in reducing impulse noise level from digital images. In *Proceedings of the 2nd International Conference on Education Technology and Computer (ICETC)*, volume 5, pages 118–121, 2010. [cited at p. 13]
- [47] Nicholas Sia Pik Kong and Haidi Ibrahim. Multiple layers block overlapped histogram equalization for local content emphasis. *Computer and Electrical Engineering*, 37:631–643, 2011. [cited at p. 22]
- [48] Ryosuke Kubota and Noriaki Suetake. Distribution distance-based threshold auto-tuning method for switching median filter. *IEICE Electronics Express*, 7(17):1310–1316, 2010. [cited at p. 12]
- [49] Yau-Hwang Kuo, Chang-Shing Lee, and Chao-Lieh Chen. High-stability AWFm filter for signal restoration and its hardware design. *Fuzzy Sets and Systems*, 114(2):185–202, September 2000. [cited at p. 11]
- [50] Chang-Shing Lee, Yau-Hwang Kuo, and Pao-Ta Yu. Weighted fuzzy mean filters for image processing. *Fuzzy Sets and Systems*, 89(2):157–180, July 1997. [cited at p. 11]
- [51] Anat Levin, Rob Fergus, Fredo Durand, and William Freeman. Image and depth from a conventional camera with a coded aperture. In *ACM Transactions on Graphics (TOG)*, volume 26, page 70. ACM, 2007. [cited at p. 39]
- [52] Sheng-Fu Liang, Shih-Mao Lu, Jyh-Yeong Chang, and Chin-Teng Lee. A novel two-stage impulse noise removal technique based on neural networks and fuzzy decision. *IEEE Transactions on Fuzzy Systems*, 16(4):863–873, 2008. [cited at p. 12]

- [53] Lifshitz, Lawrence M., and Stephen M. Pizer. A multi-resolution hierarchical approach to image segmentation based on intensity extrema. *PAMI IEEE*, 12(6):529–540, June 1990. [cited at p. 36]
- [54] Ho-Ming Lin and Alan N. Willson Jr. Median filters with adaptive length. *IEEE Transactions on Circuits and Systems*, 35(6):675–690, June 1988. [cited at p. 12]
- [55] Fang Lu, Oscar Au, Ngai Man Cheung, Aggelos Katsaggelos, Houqiang Li, and Feng Zou. Luma-chroma space filter design for subpixel-based monochrome image downsampling. *Image Processing, IEEE Transactions on*, 22(10):3818–3829, 2013. [cited at p. 41]
- [56] M. McCandless. Digital photography: a farewell to “cheese”. *IEEE Intelligent Systems and Their Applications*, 13(2):16–17, 1998. [cited at p. 3]
- [57] Kapila M. Moon, M. D. Patil, and Bhavesh Parmar. Image restoration using adaptive switching median filter. In *2010 IEEE International Computational Intelligence and Computing Research (ICIC)*, pages 1–4, 2010. [cited at p. 13]
- [58] Oyelami Olufemi Moses. Improving the performance of bubble sort using a modified diminishing increment sorting. *Scientific Research Essays*, 4(8):740–744, August 2009. [cited at p. 22]
- [59] Madhu S. Nair and G. Raju. A new fuzzy-based decision algorithm for high-density impulse noise removal. *Signal, Image and Video Processing*, DOI:10.1007/s11760-010-0186-4:(17 pages), [In Press]. [cited at p. 13, 14]
- [60] A. Nasimudeen, Madhu S. Nair, and Rao Tatavarti. Directional switching median filter using boundary discriminative noise detection by elimination. *Signal, Image and Video Processing*, 6(4):613–624, 2012. [cited at p. 13, 14, 20]
- [61] Pei-Eng Ng and Kai-Kuang Ma. A switching median filter with boundary discriminative noise detection for extremely corrupted images. *IEEE Transactions on Image Processing*, 15(6):1506–1516, June 2006. [cited at p. 13, 14, 15, 20, 21, 22]
- [62] Rajoo Pandey. An improved switching median filter for uniformly distributed impulse noise removal. *Proceedings of World Academy of Science, Engineering and Technology*, 38:349–351, 2008. [cited at p. 12]
- [63] Besl Paul and Ramesh Jain. Segmentation through variable order surface fitting. *IEEE Trans. Pattern Anal. Mach. Intell.*, 10(3):167–192, March 1988. [cited at p. 36]
- [64] Maria Petrou and Panagiota Bosdogianni. *Image Processing: The Fundamentals*. John Wiley & Sons, West Sussex, England, 1999. [cited at p. 11]
- [65] Wei Ping, Li Junli, Lu Dongming, and Chen Gang. A fast and reliable switching median filter for highly corrupted images by impulse noise. In *IEEE International Symposium on Circuits and Systems, 2007 (ISCAS 2007)*, pages 3427–3430, 2007. [cited at p. 13]
- [66] Liu Renting, Zhaorong Li, and Jiaya Jia. Image partial blur detection and classification. *Computer Vision and Pattern Recognition*, pages 1–8, June 2008. [cited at p. 37]
- [67] R. Samadani. A fast algorithm for preserving noise while reducing image size. In *IEEE International Conference on Image Processing (ICIP 2008)*, pages 2824–2827, 2008. [cited at p. 5]

- [68] R. Samadani, S. H. Lim, and D. Tretter. Representative image thumbnails for good browsing. In *IEEE International Conference on Image Processing (ICIP 2007)*, pages II–193–II–196, 2007. [cited at p. 4, 5]
- [69] R. Samadani, A. M. Mauer, D. M. Berfanger, and J. H. Clark. Image thumbnail that represent blur and noise. *IEEE Transactions on Image Processing*, 19(2):363–373, 2010. [cited at p. 4, 5]
- [70] Ramin Samadani, Timothy Mauer, and Berfanger. Image thumbnails that represent blur and noise. *Image Processing, IEEE Transactions on*, 19(2):363–373, 2010. [cited at p. 41]
- [71] V. Saradhadevi and V. Sundaram. A novel two-stage impulse noise removal technique based on neural networks and fuzzy decision. *International Journal of Computer Applications*, 21(3):31–42, May 2011. [cited at p. 12]
- [72] V. Saradhadevi and W. Sundaram. An adaptive fuzzy switching filter for images corrupted by impulse noise. *Global Journal of Computer Science and Technology*, 11(4):29–33, March 2011. [cited at p. 13]
- [73] Stefan Schulte, Valerie De Witte, Mike Nachtegael, Dietrich Van der Weken, and Etienne E. Kerre. A new fuzzy multi-channel filter for the reduction of impulse noise. In Jorge Marques, Nicolas Perez de la Blanca, and Pedro Pina, editors, *Pattern Recognition and Image Analysis*, volume 3522 of *Lecture Notes in Computer Science*, pages 619–668. Springer Berlin / Heidelberg, 2005. [cited at p. 12]
- [74] Stefan Schulte, Valerie De Witte, Mike Nachtegael, Dietrich Van der Weken, and Etienne E. Kerre. A novel histogram based fuzzy impulse noise restoration method for color images. In Jacques Blanc-Talon, editor, *Proceedings of the 7th International Conference on the Advanced Concepts for Intelligent Vision Systems (ACIVS 2005)*, pages 626–633, 2005. [cited at p. 12]
- [75] P. Shanmugavadivu and P. S. Eliahim Jeevaraj. Fixed-value impulse noise suppression for images using PDE based adaptive two-stage median filter. In *International Conference on Computer, Communication and Electrical Technology (ICCCET 2011)*, pages 290–295, 2011. [cited at p. 13]
- [76] Leslie Smith. Estimating an image’s blur kernel from edge intensity profiles. *Naval Research Lab Washington D.C. Applied Optics Branch*, No. NRL/MR/5660–12-9393, 2012. [cited at p. 37]
- [77] Younghun Song, Yunsang Han, and Sangkeun Lee. Pixel correlation-based impulse noise reduction. In *2011 17th Korea-Japan Joint Workshop on Frontiers of Computer Vision (FCV)*, pages 1–4, 2011. [cited at p. 13]
- [78] Milan Sonka, Vaclav Hlavac, and Roger Boyle. *Image processing, Analysis, and Machine Vision*. Cengage Learning, 2014. [cited at p. 41]
- [79] E. Srinivasan and D. Ebenezer. New nonlinear filtering strategies for eliminating short and long tailed noise in images with edge preservation properties. *International Journal of Information and Communication Engineering*, 4(3):175–181, 2008. [cited at p. 12]
- [80] D. J. Stavely. Apparatus and Method for Reducing Image Blur in A Digital Camera. US Patent 7,787,015, 2010. [cited at p. 34]

- [81] T. Suga, K. Muto, K. Yagi, K. Asai, and K. Kondo. Relation between image detection time and thumbnail image size for satellite-based telemedicine. In *18th International Conference on Knowledge-Based and Intelligent Information & Engineering Systems - KES2014*, pages 1513–1518, 2014. [cited at p. 3]
- [82] K. K. Teoh, H Ibrahim, and S. K. Bejo. Investigation on several basic interpolation methods for the use in remote sensing application. In *Proceedings of the 2008 IEEE Conference on Innovative Technologies in Intelligent Systems and Industrial Applications*, pages 60–65, 2008. [cited at p. 7]
- [83] Georgiev Todor and Andrew Lumsdaine. Depth of field in plenoptic cameras. *Eurographics*, 1(1), 2009. [cited at p. 35]
- [84] Kenny Kal Vin Toh, Haidi Ibrahim, and Muhammad Nasiruddin Mahyuddin. Salt-and-pepper noise detection and reduction using fuzzy switching median filter. *IEEE Transactions on Consumer Electronics*, 54(4):1956–1961, November 2008. [cited at p. 13]
- [85] Kanchev Tonchev and Ognian Boumbarov. Blurred image regions detection using wavelet-based histograms and svm. *Intelligent Data Acquisition and Advanced Computing Systems (IDAACS) IEEE 6th International Conference*, 1(2):457–461, September 2011. [cited at p. 37]
- [86] Abdullah Toprak and Inan Guler. Suppression of impulse noise in medical images with the use of fuzzy adaptive median filter. *Journal of Medical Systems*, 30(6):465–471, 2006. [cited at p. 11]
- [87] Abdullah Toprak and Inan Guler. Impulse noise reduction in medical images with the use of switch mode fuzzy adaptive median filter. *Digital Signal Processing*, 17(4):711–723, July 2007. [cited at p. 11]
- [88] Abdullah Toprak, Mehmet Sirac Ozerdem, and Inan Guler. Suppression of impulse noise in MR images using artificial intelligent based neuro-fuzzy adaptive median filter. *Digital Signal Processing*, 18(3):391–405, May 2008. [cited at p. 11]
- [89] M. Trentacoste, R. Mantiuk, and W. Heidrich. Blur aware image downsampling. In *Computer Graphics Forum*, pages 573–582, 2011. [cited at p. 6]
- [90] Matthew Trentacoste, Rafal Mantiuk, and Wolfgang Heidrich. Blur-aware image down-sampling. Available from world wide web: <http://www.cs.ubc.ca/nest/imager/tr/2011/BlurAwareDownsize/ap-resizing-validation/index.html> [Accessed on 01 April 2014]., 2011. [cited at p. 41]
- [91] A. K. Tripathi, U. Ghanekar, and S. Mukhopadhyay. Switching median filter: Advanced boundary discriminative noise detection algorithm. *IET Image Processing*, 5(7):598–610, 2011. [cited at p. 13, 14]
- [92] Signal & Image Processing Institute University of Southern California. The USC-SIPI Image Database [Online]. Available from World Wide Web: <http://sipi.usc.edu/database/> [Accessed 16th August 2010]. [cited at p. 25]
- [93] Nguyen Vu and Michael Blumenstein. An application of the 2d gaussian filter for enhancing feature extraction in off-line signature verification. *Document Analysis and Recognition (ICDAR), 2011 International Conference*, pages 339–343, June 2011. [cited at p. 40]

- [94] Yi Wan, Qiqiang Chen, and Yan Yang. Robust impulse noise variance estimation based on image histogram. *IEEE Signal Processing Letters*, 17(5), May 2010. [cited at p. 12]
- [95] Gerhard Winkler. *Image Analysis, Random Fields and Markov Chain Monte Carlo methods: A Mathematical Introduction*, volume 27. Springer Science & Business Media, 2003. [cited at p. 35]
- [96] Jian Wu and Chen Tang. PDE-based random-valued impulse noise removal based on new class of controlling functions. *IEEE Transactions on Image Processing*, 20(9):2428–2438, September 2011. [cited at p. 12]
- [97] Junying Xia, Jiulong Xiong, Xiaoquan Xu, and Qi Zhang. An efficient two-state switching median filter for the reduction of impulse noises with different distributions. In *Proceedings of 2010 3rd International Congress on Image and Signal Processing (CISP2010)*, pages 639–644, 2010. [cited at p. 12, 13]

Thumbnail With Integrated Blur Based on Edge Width Analysis

Boon Tatt Koik · Haidi Ibrahim

Received: date / Accepted: date

Abstract Thumbnail image is widely used in electronic devices to help the user to scan through original high resolution images. Hence, it is essential to represent the thumbnail image correspondingly to the original image. A blur image should not appear to be a clear image in thumbnail form, where this situation might mislead the perceptual analysis of user. The main purpose of this research work is to develop a down-sampling algorithm to create a thumbnail image which includes blur information. The proposed method has three stages involved to obtain the proposed output thumbnail which are preliminary processes, blur detection and lastly image down-sampling. For preliminary processes, Sobel first order derivatives, gradient magnitude and gradient orientation are determined. In blur detection stage, local maximum, local minimum and gradient orientation are utilized to calculate the edge width. The thumbnail image with blur information is generated using the average edge width map as a weightage to integrate blur information. This proposed method has achieved satisfying results and have high potential to be applied as one of the thumbnail generation options for photo viewing.

Keywords Thumbnail image · image down-sample · blur width analysis · integrated blur image · image browsing

1 Introduction

For an image, generally it is important that an image is clear and sharp. However, there are also occasions where the blur is done purposely to make the image captured more meaningful, such as motion blur in a photo of a runner that is about to cross the ending line (i.e., motion blur on the body but clear on facial expression). Be it as it may, blur image in most

B. T. Koik
School of Electrical and Electronic Engineering, Engineering Campus, Universiti Sains Malaysia, 14300
Nibong Tebal, Penang, Malaysia
E-mail: btkoik@gmail.com

H. Ibrahim
School of Electrical and Electronic Engineering, Engineering Campus, Universiti Sains Malaysia, 14300
Nibong Tebal, Penang, Malaysia
E-mail: haidi_ibrahim@ieee.org

occasions, is unwanted and many researches have magnificent works in this blur image branch. In this paper, blur analysis and thumbnail generation based on blur analysis will be emphasized.

There are few fundamental thumbnail generation methods available such as Direct Pixel-based Down-sampling (DPD) [1], Direct Sub-pixel-based Down-sampling (DSD) [2], and Pixel-based Down Sampling with Anti-aliasing Filter (PDAF) [3]. Direct Pixel-based Down-sampling (DPD) is a method of generating thumbnail image without any filtering method. In method that employ DPD technique, one corresponding pixel of the original image is taken to represent the single pixel in thumbnail image [4]. DPD method generally generate a sharper image compared with the original image. Direct Sub-pixel-based Down-sampling (DSD) is the extension of DPD down-sampling method. DSD uses a similar concept to DPD, but instead of using information from just one pixel, one thumbnail image's pixel by DSD uses three pixel values from the original image [1]. These three pixels correspond to the red R, green G, and blue B color channel. Therefore, DSD is only applicable for color images [1]. Pixel-based Down Sampling with Anti-aliasing Filter (PDAF) utilizes the usage of filtering method, which is low pass filter. Low pass filter band-limit the frequency component of the initial high resolution original image, therefore the resulting thumbnail image unlikely to retain noise very well. As noise normally occupies the high frequency components in image, the resulting thumbnail image from PDAF method will appear to be smoother and clean from noise [2].

Blur analysis is the process where the image is analyzed in terms of bluriness of edge or bluriness of a certain region in image with quantitative parameter. Example of blur analysis is edge width analysis where the degree of blur is assumed to be proportional to the edge width [5]. Edge width data is mapped for the original image and the data can be used for further process, such as de-deblurring and re-sampling of the image. Other examples of blur analysis are Bayes discriminant analysis [6] which researches on gradient statistic of the blur object in image. There is also researches on calculation of local blur at boundary and blur magnitude averaging of an image using non-reference block based analysis [7].

The works of others researchers have enriched blur analysis research area. Samadani et al. [8][9] have come out with an idea to embed blur and noise information into thumbnail images, thumbnail with integrated blur method(DIB). This is because in normal thumbnail image, the blur and noise information is lost due to the filtering and sub-sampling. Their work consists of two stages: blur detection stage, and noise detection stage. In works of Trentacoste et al. [10], perceptual-based model to down-sample an image is build to create a down-sampled version of the image that gives the same impression as the original. A study has been conducted to find out how much blur must be present in down-sampled image to perceived the same as the original. Trentacoste et al. uses the modified version of Samadani's work [8][9] to conduct their experiment. New appearance-preserving algorithm has incorporated to alter blur magnitude locally to create a smaller image corresponding to the original image. The blur magnitude is analysed as a function of spatial frequency. For other down-sampling method[4], thumbnail with blur and noise information (TBNI), two temporary thumbnail images are combined to generate thumbnail image that retain the original image's bluriness and noise(TBNI). This propose thumbnail scheme is actually an extension to DPD method, with DPD thumbnail is used as the base thumbnail. The selection of the information to be embedded into the final thumbnail is based on blur extend parameter. This parameter controls the sensitivity of the algorithm towards noise and blur.

In this paper, a new down-sampling algorithm is proposed based on edge width analysis to embed the blur information of the original high resolution image into thumbnail image. The methodology will be further described in the next Section.

2 Preliminary Concept of Thumbnail With Integrated Blur based on Edge Width Analysis

In this proposed method, similar to other image thumbnail algorithms, the user need to input the down-sampling factor L . If the original input image F is of size $M \times N$, its thumbnail version f is of size $m \times n$. Generally, the originally high-resolution acquired image F can be described by the following equation [11] [12]:

$$F = B \otimes C \quad (1)$$

where B is the space-varying blur, whereas C is the ideal clean and sharp image. The symbol \otimes in this equation presents a 2-dimensional convolution operation.

To clarify equation (1), an example is given in Figure 1. Image F shown by Figure 1(c) is obtained by convolving image C (i.e., Figure 1(a)) with blur function B (i.e., Figure 1(b)). In this example, B is a space-varying blur function, described by 2-dimensional Gaussian function [13]:

$$\text{Gaussian}(y, x) = \exp\left(-\frac{y^2 + x^2}{2\sigma^2}\right) \quad (2)$$

where σ is the standard deviation of the distribution. Assuming that the Gaussian filter applied is a square filter, with odd size, defined as $(2B_r + 1) \times (2B_r + 1)$, then σ can be written as [14]:

$$\sigma = \frac{B_r}{\sqrt{-2.0 \times \ln(\xi)}} \quad (3)$$

where, in this example, ξ is set to value 0.0001. Variable B_r in this formula stands for the radius of the blur kernel. Therefore, the Gaussian filter in equation (2) can be expresses in terms of the filter's size.

Therefore, the blur function B in Figure 1(b) is defined as a function of B_r . As shown by this figure, the size of the blur filter kernel applied to the pixels located at the center of the image is small, and the filter's size is gradually increasing towards the border of the image. Blur filter with larger size gives more blur to the image, as compared to blur filter with smaller size. As a consequence, in Figure 1(c), the image appears relatively sharper at the center region (i.e., regions where blur filters with small size are applied), as compared with the regions on the border (i.e., regions where blur filters with larger size are applied).

By inspecting the image profiles shown in Figure 1(d), the effect of the blur filter can be observed. When comparing the profile from the sharp image C with the blurred image F , it is shown that blur filter changes the step edges in C to become ramp edges in F . This figure also shows that the slope of the edges becoming more gradual when the size of the blur filter applied is bigger (i.e., when the blur effect become more serious).

Therefore, the degree of blurs can be observed by inspecting the edges on the image. Sharp regions have narrow edge width, while blur regions have wider edge width. This is the main approach used by this proposed method in detecting the blur regions.

Figure 2 shows the general view of this proposed method. As shown by this figure, the proposed method has three main blocks. These blocks are; (1) Preliminary processes, (2) Blur detection, and (3) Image down-sampling. The propose method takes the information from the blur detection stage, and use it in its image down-sampling stage, so that more blur informations from F can be embedded into f .

2.1 Preliminary processes

As mentioned in previous section, determination of the degree of blurs is by inspecting the edges on the image. It is well known that the edges can be enhanced by calculating its gradient value. Therefore, the main purpose of this preliminary processes is to emphasize the edges from F . As shown by Figure 3, the input for this stage is the original image F , while the output from this stage are the gradient magnitude G_m and two gradient directions $G_{\theta 1}$ and $G_{\theta 2}$.

2.1.1 Determination of Gradient Components

At this stage, the gradient values (i.e., G_x and G_y) of the input image F at every spatial coordinates (i, j) , within the matrix of size $M \times N$ pixels, are calculated. These gradient values are obtained by applying 2-dimensional directional derivatives as given by equation (4).

$$\begin{bmatrix} G_x(i, j) \\ G_y(i, j) \end{bmatrix} = \begin{bmatrix} \frac{d}{dx} F(i, j) \\ \frac{d}{dy} F(i, j) \end{bmatrix} \quad (4)$$

where G_x is the first order derivative in x -direction (i.e., horizontal direction), and G_y is the first order derivative in y -direction (i.e., vertical direction).

Sobel filter [15] is used to find the approximation to the gradient values at each point (i, j) in F . Sobel operators are chosen because they have lower sensitivity towards the image noise, as compared with the Robert cross filter or Laplacian filter [16]. Therefore, this condition brings an advantage to proposed method's algorithm. This is because Sobel operators enable this method to give more focus on blur issue, which is the main concern of this thesis.

Calculation of Gradient Magnitude The gradient magnitude G_m combines the information from G_x and G_y using the following equation:

$$|G_m(i, j)| = \sqrt{|G_x(i, j)|^2 + |G_y(i, j)|^2} \quad (5)$$

Figure 4 shows the calculated G_m . As presented by this figure, G_m shows the locations of the edges on image F . The gradient magnitude is higher at sharper region, as compared to blurred regions. This figure also shows that the width of the edges becomes wider when the blurs are serious.

2.1.2 Calculation of Gradient Orientations

Gradient orientation, or edge direction, indicates the direction of the vector normal to the edge point, with respect to the horizontal direction (i.e., x -axes). In the implementation of this proposed method, the gradient orientation $G_{\theta 1}$ is defined using a function called as "atan2", which calculates the value of arctangent of all four quadrants as shown in Figure 5.

This "atan2" function calculates the arctangent value by taking two arguments, which are G_x and G_y :

$$G_{\theta 1}(i, j) = \text{atan2}(G_y(i, j), G_x(i, j)) \quad (6)$$

The function of "atan2" returns the value of the angle in radians, in the range between $-\pi$ to π . This means that $-\pi \leq G_{\theta}(i, j) \leq \pi$.

In the implementation of this proposed method, the edge orientation as defined by $G_{\theta_1}(i, j)$ is considered as bi-directional. This characteristic is important for the width measurement of the blurry edges, used in the blur detection stage. This means that the direction defined by $G_{\theta_1}(i, j)$ is taken to be the same as the angle defined in the opposite direction (i.e., $G_{\theta_1}(i, j) \pm \pi$ or $G_{\theta_1}(i, j) \pm 180^\circ$). This is shown by the example given in Figure 6.

In order to fulfil the abovementioned requirement, in the implementation of this proposed method, an additional edge orientation $G_{\theta_2}(i, j)$ is defined using equation (7).

$$G_{\theta_2}(i, j) = G_{\theta_1}(i, j) + \pi \quad \text{or} \quad G_{\theta_2}(i, j) = G_{\theta_1}(i, j) + 180^\circ \quad (7)$$

An example of the gradient orientation G_{θ_1} is shown in Figure 7. In Figure 7(a), because G_{θ_1} is defined in between $-\pi$ to π radians, this gradient orientation has both positive and negative values. On the other hand, in Figure 7(b), the directions are now turned 180° against the original direction, where G_{θ_2} is defined in between 0 to 2π radians. Therefore, as shown by this subfigure, all G_{θ_2} values are positive values.

2.2 Blur detection

In this blur detection stage, proposed method takes G_m , G_{θ_1} and G_{θ_2} from the preliminary processing stage, as its input. The output from this stage is an edge width map E_w , which brings the information regarding to the width of the edges on the image. A general block diagram for this blur detection stage is shown by Figure 8. The calculation of the edge width starts on the edge, which is indicated by the local maximum points on the gradient magnitude G_m . The process, which is guided by G_{θ_1} and G_{θ_2} , stops on the uniform regions, which can be identified from the local minimum points on G_m . Therefore, in this blur detection stage, the proposed method needs to find the locations of the local maximum points and the local minimum points of G_m before it can proceed to the edge width calculation process.

2.2.1 Local Maximum and Local Minimum

In order to find the local maximum points, the definitions for the local maximum are needed. Thus, in this research, Figure 9 shows this definition. As shown by this figure, there are three definitions for the local maximum locations:

1. Defined at the gradient edge, from a region with constant value, moving towards lower gradient values (i.e., $G_m(i-1) = G_m(i) > G_m(i+1)$).
2. Defined at the actual peak, where current gradient value is greater than the neighboring gradient values (i.e., $G_m(i-1) < G_m(i) > G_m(i+1)$).
3. Defined at the edge, from a region with increasing gradient value, to a region with constant gradient value (i.e., $G_m(i-1) < G_m(i) = G_m(i+1)$).

Similarly, the definitions for the local minimum point are needed in order to search the local minimum locations. Figure 10 gives this definitions for these local minimum points used in this thesis. There are three definitions used to define the local minimum locations, as presented by this figure:

1. Defined at the edge, from a region with decreasing gradient value, to a region with constant gradient value (i.e., $G_m(i-1) > G_m(i) = G_m(i+1)$).
2. Defined at the gradient edge, from a region with constant value, moving towards higher gradient values (i.e., $G_m(i-1) = G_m(i) < G_m(i+1)$).

3. Defined at the actual valley, where current gradient value is the smallest when compared to the neighboring gradient values (i.e., $G_m(i-1) > G_m(i) < G_m(i+1)$).

For local minimum, some of the data locations are failed to be detected, and therefore create some "fragmented" regions in G'_{\min} . As a consequence, this will lead to inaccurate edge width calculation. In order to reduce this problem, in this proposed method, a binary mathematical dilation has been utilized. This operation has been selected as it can combine "fragmented" areas. The binary mathematical dilation \odot is defined as [14]:

$$G_{\min} = G'_{\min} \odot S = \{z(\hat{S})_z \cap G'_{\min} \neq \emptyset\} \quad (8)$$

where S is the structuring element and z is a set of points.

2.2.2 Measure the Edge Width

In order to measure the edge width E_w , the idea based on the work by [5] is implemented in this stage of proposed method. This idea is depicted in Figure 11. By inspecting the gradient maximum locations provided by G_{\max} , the location of the edge is identified. The coordinates (i, j) is defined as the location of the edge when $G_{\max}(i, j)$ has value of 1, or logical "true". Then, this algorithm takes this location as the starting point for the edge width measure. From this point, the algorithm traverses to search the location of the gradient magnitude local minimum in G_{\min} , which is the location where G_{\min} has values 1. First, the method traverses on the "left side" of the edge. The distance between the location of the local maximum and the location of the local minimum is defined as E_l . Then, the same traversing process is applied again from the edge (i.e., starting point) to the local minimum location, but now in the opposite direction, which is on the "right side" of the edge. The distance found on this side is defined as E_r . The width of the edge blur E_w is the distance between the two local minimums. This can be defined using the following equation:

$$E_w = E_r + E_l + 1 \quad (9)$$

In this equation, value 1 is added because the edge point was not included during the measurement of E_r and E_l .

The idea presented in Figure 11 is actually the simplified concept, as it only shows how the method works for 1-dimensional data. Because an image is a 2-dimensional data, the edge width calculation process is not as simple as presented in the previous paragraph. For a 1-dimensional data, it is easy to define "left side" and "right side" as there are only two neighboring elements need to be considered. For a 2-dimensional data, the elements now has eight neighboring elements. Therefore, for 2-dimensional data, the definitions for "left side" and "right side" are guided by the gradient orientations G_{θ_1} and G_{θ_2} .

In order to ease the process of the traversing, two functions are defined. These two functions are index_x and index_y , which are based on the eight neighboring elements as shown in Figure 12. These two functions take angle θ as their input, and are given by equations (10) and (11), respectively.

$$\text{index}_x(\theta) = \begin{cases} -1 : \left(\frac{5}{8}\pi \leq \theta \leq \pi\right) \text{ OR } \left(\pi \leq \theta \leq \frac{9}{8}\pi\right) \text{ OR } \left(-\pi \leq \theta \leq -\frac{5}{8}\pi\right) \\ 1 : \left(0 \leq \theta \leq \frac{3}{8}\pi\right) \text{ OR } \left(\frac{13}{8}\pi \leq \theta \leq 2\pi\right) \text{ OR } \left(-\frac{3}{8}\pi \leq \theta \leq 0\right) \\ 0 : \text{otherwise} \end{cases} \quad (10)$$

$$\text{index}_y(\theta) = \begin{cases} -1 : \left(-\frac{7}{8}\pi \leq \theta \leq -\frac{\pi}{8}\right) \text{ OR } \left(\frac{9}{8}\pi \leq \theta \leq \frac{15}{8}\pi\right) \\ 1 : \left(\frac{\pi}{8} \leq \theta \leq \frac{7}{8}\pi\right) \\ 0 : \text{otherwise} \end{cases} \quad (11)$$

Figure 13 shows the flowchart used by this proposed method to determine the edge width E_w . It is worth noting that this process is executed only when $G_{\max}(i, j)$ is equal to 1 (i.e., at the edge element). As shown by this figure, the process of edge width calculation can be divided into three main stages:

1. Finding the value of E_l .
2. Finding the value of E_r .
3. Assign values to E_w .

The process of finding the value of E_l is almost the same as the process of finding E_r , except the latter gives more priority towards $G_{\theta 2}$.

As shown by the flowchart in Figure 13, 2-dimensional array **mask** is used in the process. If the input image F is of size $M \times N$ pixels, the size of **mask** is also of size $M \times N$ pixels. This array is used to mark the locations that are involved with the traversing process. Other variables, which are *left*, *right*, *top* and *bottom*, define the region of interest (ROI). This ROI is a rectangle identified from two coordinates, which are $(y_1, x_1) = (\text{top}, \text{left})$ and $(y_2, x_2) = (\text{bottom}, \text{right})$. Coordinates (y, x) presents the current location, while (y', x') are the temporary locations. In addition to the conditions shown in this flowchart, the traversing process on each "side" will also be terminated if the method pointing to the element located outside the area defined by the image.

Figure 14(a) shows the edge width calculated by using G'_{\min} . As shown by this figure, the obtained edge width is not accurate, as the values are significantly higher at the uniform region as compared to the regions near the edges. This is because the traversing process during the calculation "leaks" through the discontinuities of local minimum points defined by G'_{\min} .

On the other hand, by improving G'_{\min} through mathematical morphological dilation operation, G_{\min} is obtained. The edge width E_w obtained from G_{\min} is presented in Figure 14(b). As shown by this figure, the obtained values are more accurate because it is proportional to the blur kernel function shown in Figure 1(b).

2.3 Image down-sampling

If a down-sampling factor L is used, each element in e_w is presented by $L \times L$ elements in E_w :

$$e_w(i, j) \leftarrow \begin{bmatrix} E_w(i, j) & E_w(i, j+1) & \dots & E_w(i, j+L-1) \\ E_w(i+1, j) & E_w(i+1, j+1) & \dots & E_w(i+1, j+L-1) \\ \vdots & \vdots & \ddots & \vdots \\ E_w(i+L-2, j) & E_w(i+L-2, j+1) & \dots & E_w(i+L-2, j+L-1) \\ E_w(i+L-1, j) & E_w(i+L-1, j+1) & \dots & E_w(i+L-1, j+L-1) \end{bmatrix} \quad (12)$$

In this algorithm, the thumbnail image e_w for the edge width map E_w is obtained by the averaging process. Yet, because e_w presents the width of the blur in the thumbnail image,

it is worth noting that as E_w is down-sampled by using a down-sampling factor L , the edge width also will be scaled by $\frac{1}{L}$. Therefore, the value for the e_w at coordinates (i, j) is defined by using the following formula:

$$e_w(i, j) = \frac{1}{L} \left\{ \frac{1}{L^2} \sum_{k=0}^{L-1} \sum_{j=0}^{L-1} E_w(i+k, j+l) \right\} = \frac{1}{L^3} \sum_{k=0}^{L-1} \sum_{j=0}^{L-1} E_w(i+k, j+l) \quad (13)$$

Embed blur In the implementation of this proposed method, the blur is embedded into f by combining image f_1 with image f_2 using a weighted average approach. This process is shown in Figure 15, and can be expressed by Equation (14).

$$f(i, j) = \omega_1(i, j)f_1(i, j) + \omega_2(i, j)f_2(i, j) \quad (14)$$

where ω_1 and ω_2 are the space-varying weight values. Here, $0 \leq \omega_1 \leq 1.0$ and $0 \leq \omega_2 \leq 1.0$. In order to make sure that the intensity values in f are in the correct intensity range, the following restriction is applied:

$$\omega_1(i, j) = 1.0 - \omega_2(i, j) \quad (15)$$

This restriction implies that when more emphasize is given to $f_1(i, j)$ less emphasize will be given to $f_2(i, j)$, and vice-versa.

Thumbnail image f gives higher values of ω_2 to the regions with blurs, while gives higher values of ω_1 to the sharp regions. Therefore, in this proposed method, the weight $\omega_2(i, j)$ is made related to the edge width map $e_w(i, j)$. The higher the value of $e_w(i, j)$, the higher the value of will be given to $\omega_2(i, j)$ as the blur is expected to be more serious. Thus, $\omega_2(i, j)$ is defined as:

$$\omega_2(i, j) = \begin{cases} e_w(i, j) & : e_w(i, j) < 1.0 \\ 1.0 & : \text{otherwise} \end{cases} \quad (16)$$

When $e_w(i, j)$ is greater than 1.0, this condition indicates a serious blur. This is because the blur here is not in sub-pixel level, but it size is bigger than one pixel. Therefore, $f(i, j)$ will takes only the value of $f_2(i, j)$ for this condition.

An example of the thumbnail image f for the edge width map is shown in Figure 16(a). This thumbnail is obtained from Figure 14(b), with down-sampling factor L equal to 8. The differences between image f with f_1 and f_2 are shown in Figure 16(b) and Figure 16(c), respectively. These differences shows that image f is unique.

3 Results and Discussions

This section presents the evaluations of the experimental results obtained from the proposed thumbnail algorithm. The performances of the algorithm are evaluated qualitatively, and also quantitatively. This section is divided into two subsections.

3.1 Qualitative Evaluation Based on Visual Inspection

In this section, in order to evaluate the performance of the proposed method, four other thumbnail image algorithms are implemented and used as benchmarks. The methods that are included for comparisons are DPD method [1], DSD method [2], PDAF method with averaging filter [3], and thumbnail with blur and noise information (TBNI)[4]. Two test images F_1 and F_2 are used. Both images are with dimensions 1500×1000 pixels.

The results from downsampling image F_1 is shown in Figure 17. Figure 17(a) shows the original, high resolution image. Notice that the lion in this image is blurred, while the tree trunks in front of it are sharp. Figure 17(c) to (f) show the five thumbnail images, including the thumbnail image from the proposed method. The downsampling factor L used is set to 10. The thumbnail images are with dimensions 150×100 pixels. As shown in Figure 17, thumbnail images from DPD, DSD, and TBNI are sharp, but noisy. Thumbnail image from PDAF and the proposed method (i.e., TBI) are smoother, and more accurately represent the original image.

The results from downsampling image F_2 is shown in Figure 18. The original high resolution image is shown in Figure 18(a). As shown in this figure, the object, which is the crocodile, is blurred. Figure 17(c) to (f) show the five thumbnail images versions. Same with the results from Figure 17, the downsampling factor L used is also been set to 10. As shown by this figure, TBI method produces thumbnail image which is more accurately represent the original image.

3.2 Quantitative Evaluation Based on Survey

In order to evaluate the performance of proposed method properly, five other thumbnail image algorithms are implemented and used as benchmarks. The methods that are included for comparisons are DPD method [1], DSD method [2], PDAF method with averaging filter [3], thumbnail with blur and noise information (TBNI)[4], and thumbnail with integrated blur method(DIB)[8].

In this section, the analysis is done based on survey, conducted using 12 test images obtained from [17]. The down-sampling factor L is set to 4 and 8. The survey questions asked on preference on choosing between:

1. TBI thumbnail image and DPD thumbnail image
2. TBI thumbnail image and DSD thumbnail image
3. TBI thumbnail image and PDAF thumbnail image
4. TBI thumbnail image and TBNI thumbnail image
5. TBI thumbnail image and DIB thumbnail image

For each of the question, only one answer is being chosen. Each question will test on volunteer's preference on two thumbnail images, which are judged based on the original image. Volunteer will choose the preferred thumbnail (e.g. left thumbnail or right thumbnail) and put a scale (i.e., scale from 0 to 5) on how much the thumbnail being chosen is more corresponds to the original image, as compared with another thumbnail. Scale of "0" will be selected if the two thumbnails being compared are of the same quality. The scale below shows scale indication as references:

- **Scale "5-left"**: The thumbnail on the left side is totally different to the thumbnail on the right side. Almost 90 percent of the blur or clear regions of the left thumbnail image are shown better corresponding to the original image.

- Scale "4-left": The thumbnail on the left side is different to the thumbnail on the right side. Almost 70 percent of the blur or clear regions of the left thumbnail image are shown better corresponding to the original image.
- Scale "3-left": The thumbnail on the left side is different to the thumbnail on the right side. Almost 50 percent of the blur or clear regions of the left thumbnail image are shown better corresponding to the original image.
- Scale "2-left": The thumbnail on the left side is almost similar to the thumbnail on the right side. Almost 30 percent of the blur or clear regions of the left thumbnail image are shown better corresponding to the original image.
- Scale "1-left": The thumbnail on the left side is almost similar to the thumbnail on the right side. Less than 10 percent of the blur or clear regions of the left thumbnail image are shown better corresponding to the original image.
- Scale "0": The thumbnail on the right is of the same quality as thumbnail on the left corresponding to the original image.
- Scale "1-right": The thumbnail on the right side is almost similar to the thumbnail on the left side. Less than 10 percent of the blur or clear regions of the right thumbnail image are shown better corresponding to the original image.
- Scale "2-right": The thumbnail on the right side is almost similar to the thumbnail on the left side. Almost 30 percent of the blur or clear regions of the right thumbnail image are shown better corresponding to the original image.
- Scale "3-right": The thumbnail on the right side is different to the thumbnail on the left side. Almost 50 percent of the blur or clear regions of the right thumbnail image are shown better corresponding to the original image.
- Scale "4-right": The thumbnail on the right side is different to the thumbnail on the left side. Almost 70 percent of the blur or clear regions of the right thumbnail image are shown better corresponding to the original image.
- Scale "5-right": The thumbnail on the right side is totally different to the thumbnail on the left side. Almost 90 percent of the blur or clear regions of the right thumbnail image are shown better corresponding to the original image.

Each of the section of the question consists of five preference questions. There are twelve sections for each set of questionnaire. There are two sets of questionnaire available. The total question for each survey is 120 questions (i.e., 12 images \times 2 L /image \times 5 comparisons/ L , average completion time is 35 minutes including 5 minutes rest time in between the switching of L values. Each question estimated answering time is 15 seconds. For data compilation, graphs of box-and-whisker are plotted for comparisons of proposed TBI method with other methods with respective parameter L . Briefing is given to every volunteer prior to the survey process. The volunteer will chose one of the two thumbnails in each comparison question (e.g., TBI or DPD) and put a scaling of their choice, depending on their preferences.

Number of volunteer is 51, the volunteer's age range from 20 year-old to 40 year-old, consists of both male and female in various faculties across the campus. Volunteers are given briefing prior to the start of the survey and being placed 60cm in front of the 15.6 inches monitor screen of 1366 \times 768 resolutions. The survey is done in a closed room, without any noise of sound. After the survey, box-and-whisker plots are generated to show the overall tendency of volunteers towards the thumbnail methods.

Box and whisker plots are ideal for comparing distributions because the centre, spread and overall range are immediately apparent. A box and whisker plot is a way of summarizing a set of data measured on an interval scale. It is often used in explanatory statistical data analysis.

Box-and-whisker plots is useful for indicating whether a distribution is skewed and whether there are potential unusual observations (outliers) in the data set. It is also very useful when large numbers of observations are involved and when two or more data sets are being compared. This type of graph is used to show the shape of the distribution, its central value, and its variability. In box-and-whisker plots, the ends of the box are the upper and lower quartiles, so the box spans the interquartile range. Besides, the median is marked by a horizontal line inside the box and the whiskers are the two lines outside the box that extend to the highest and lowest observations.

Figure 19 shows the box-and-whisker plot for TBI vs. DPD thumbnail images. The median value for both Figure 19 (a) and Figure 19 (b) show that the overall volunteer tendency towards choosing TBI is slightly higher than DPD image for $L=8$ and the tendency is roughly the same for $L=4$. Most of the inter-quartile range falls between "0" and "1" towards TBI indicate slight preference of user in choosing TBI. This tendency happens for both $L=4$ and $L=8$. The extreme value in this scattered around value of "2" and "3", for both $L=4$ and $L=8$. Generally, the tendency of user towards the comparisons between TBI and DPD is slightly towards TBI thumbnail. Therefore, proposed TBI is slightly better than DPD in this survey analysis.

Figure 20 shows the box-and-whisker plot for TBI vs. DSD thumbnail images survey. The median value in the plot for Figure 20 (a) and Figure 20 (b) show that the tendency of volunteer to choose over TBI method and DSD method is the same for both $L=4$ and slightly towards TBI thumbnail for $L=8$.

For $L=4$, there are preferences in choosing TBI thumbnail and DSD thumbnail, counteracting each other in term of tendency. For $L=8$, the preference is given slightly towards TBI thumbnail. Quartile 1 and quartile 3 also show the roughly same tendency of liking from the survey with some tendency of DPD counteract with TBI. Extreme error bar for both Figure 20 (a) and Figure 20 (b) range mostly from value of "2" and "3", for both TBI and DSD. Overall, TBI and DSD have the same performance tendency in survey's perspective for $L=4$ but for $L=8$, the tendency is slightly given to TBI.

Figure 21 shows box-and-whisker plot for TBI vs. PDAF thumbnail images survey. Overall value of median shows that TBI is slightly chosen over PDAF thumbnail image by the volunteer for both Figure 21 (a) and Figure 21 (b).

The quartile 1 is mostly of value "0" while quartile 3 has value "1" as majority, for both $L=4$ and $L=8$. The extreme error bar value has low fluctuations range (e.g., value of "1" and "2") for Figure 21 (a) and Figure 21 (b), indicating the preference of the survey in this comparison is quite stable. Overall, the tendency of choosing proposed TBI image in this survey is slightly higher than PDAF.

Figure 22 shows box-and-whisker plot for TBI vs. TBNI thumbnail images survey. The median of the plots show that both TBI and TBNI has the same tendency from the volunteer's choice for both $L=4$ and $L=8$. Both median of $L=4$ and median of $L=8$ counteracting each other in term of preferences.

From quartile 1 and quartile 3, TBNI method shows roughly the same tendency compared with TBI for Figure 22 (a) but the tendency is slightly higher for TBI in Figure 22 (b). The error bar value for Figure 22 is high, indicating there are extreme preference from volunteers for both TBI and TBNI. From this survey, overall TBI shows slightly higher results than TBNI for $L=8$ but the tendency for both TBI and TBNI is roughly the same for $L=4$.

Figure 23 shows box-and-whisker plot for TBI vs. DIB thumbnail images survey. Analyzing from the median, it is obvious that TBI method is chosen over DIB method with a very high tendency from volunteers for both Figure 23 (a) and Figure 23 (b).

Quartile 1 and quartile 3 also show that the choice is favourable towards TBI. The extreme minority value also shows tendency towards TBI method for both $L=4$ and $L=8$. Therefore, from this survey, TBI method outperformed DIB with high preference from volunteers.

4 Conclusion

The results and discussions have shown that this proposed method has obtained satisfactory thumbnail results. This method successful in a way that it proposed a new method of generating thumbnail image based on edge analysis. Normal down-sampling like DPD and DSD is a direct down-sampling method, without pre-analysis of the image. PDAF method with averaging filter shows smoother results, sometimes not correspond to the sharp original image. DIB method shows more blurred thumbnail image, which does not correspond to the original image perceptually while TBNI shows a roughly equal visual performance with proposed method in this analysis. Overall, proposed method has shown a satisfactory result of down-sampling method based on edge analysis, which might not in obvious better way, but it is a new approach for a down-sampling method.

5 Acknowledgement

This work was supported in part by the Universiti Sains Malaysia's Research University Individual (RUI) Grant with account number 1001/PELECT/814169.

References

1. Lu Fang, C. Au Oscar, Ketan Tang, XingWen, andWang Hanli. Novel 2-D MMSE subpixel-based image down-sampling. *Circuits and Systems for Video Technology*, IEEE Transactions on, 22(5):740-753, 2012.
2. Lu Fang and C. Au Oscar. Subpixel-based image down-sampling with min-max directional error for stripe display. *Selected Topics in Signal Processing*, IEEE Journal, 5(2):240-251, 2011.
3. Juan Ramn Hernández, Fernando Perez-Gonzalez, Jose M. Rodriguez, and Gustavo Nieto. Performance analysis of a 2-D-multi-pulse amplitude modulation scheme for data hiding and watermarking of still images. *Selected Areas in Communications*, IEEE Journal on, 16(4):510-524, 1998.
4. Haidi Ibrahim. Image thumbnail with blur and noise information to improve browsing experience. *Advances in Multimedia*, 2(3):39-48, 2011.
5. Y. Chung, J.Wang, R. Bailey, S. Chen, and S. Chang. Non-parametric Blur Measure based on Edge Analysis for Image Processing Applications. In *Cybernetics and Intelligent Systems*, pages 356-360. IEEE, 2004.
6. Jaeseung Ko, and Changick Kim. Low cost blur image detection and estimation for mobile devices. *Advanced Communication Technology*. International Conference on Advanced Computing Technologies, 3(1):1605-1610, February 2009.
7. Liu Debing, Chen Zhibo, Ma Huadong, Xu Feng, and Gu Xiaodong. No reference block based blur detection. In *Quality of Multimedia Experience, QoMEx*. International Workshop, pages 75-80, July 2009.
8. Ramin Samadani, Timothy A. Mauer, M. David Berfanger, and H. James. Image thumbnails that represent blur and noise. *Image Processing*, IEEE Transactions on, 19(2):363-373, 2010.
9. Ramin Samadani, Suk Hwan Lim, and Daniel Tretter. Representative image thumbnails for good browsing. In *Image Processing, 2007. ICIP 2007*. IEEE International Conference on, volume 2, pages IIC193. IEEE, 2007.
10. Matthew Trentacoste, Rafal Mantiuk, and Wolfgang Heidrich. Blur-aware image downsampling. In *Computer Graphics Forum*, volume 30, pages 573-582. Wiley Online Library, 2011.
11. Anat Levin, Rob Fergus, Frdo Durand, and William T Freeman. Image and depth from a conventional camera with a coded aperture. In *ACM Transactions on Graphics (TOG)*, volume 26, page 70. ACM, 2007.

12. Guangcan Liu, Shiyu Chang, and Yi Ma. Blind image deblurring using spectral properties of convolution operators. arXiv preprint arXiv:1209.2082, 2014.
13. Vu Nguyen and Michael Blumenstein. An application of the 2D Gaussian filter for enhancing feature extraction in off-line signature verification. Document Analysis and Recognition (ICDAR), 2011 International Conference, pages 339-343, June 2011.
14. Milan Sonka, Vaclav Hlavac, and Roger Boyle. Image Processing, Analysis, and Machine Vision. Cengage Learning, 2014.
15. Ramesh Jain, Rangachar Kasturi, and Brian G. Schunck. Machine Vision, volume 5. McGraw-Hill New York, 1995.
16. G. T Shrivakshan, and C. Chandrasekar. A comparison of various edge detection techniques used in image processing. IJCSI International Journal of Computer Science Issues, 9(5):269-276, 2012.
17. Matthew Trentacoste, Rafal Mantiuk, and Wolfgang Heidrich. Blur aware image down-sampling. Available from world wide web: <http://www.cs.ubc.ca/nest/imager/tr/2011/BlurAwareDownsize/ap-resizingvalidation/index.html> [Accessed on 01 April 2014], 2011.

6 Figures

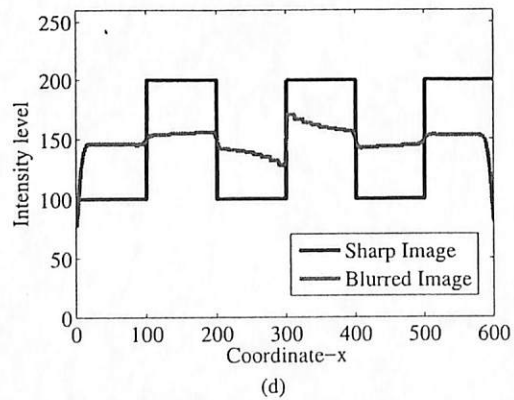
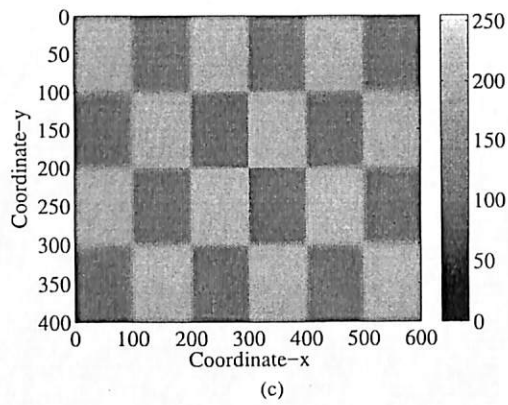
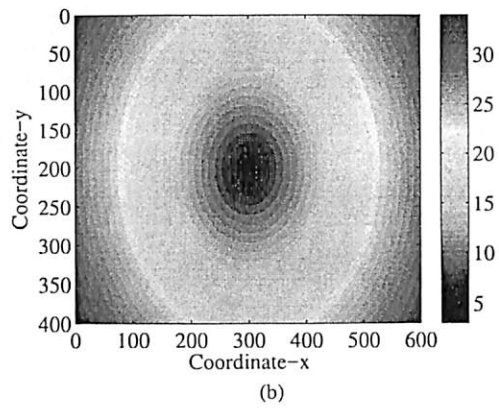
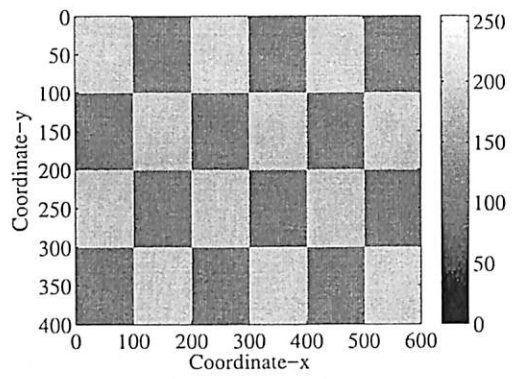


Fig. 1 (a) An ideal clean image C . (b) The blur B as a function of the radius B_r of the blur kernel. (c) A blurred image F according to equation (1). (d) Image profile of C and F along x -axis, at $y = 199$.

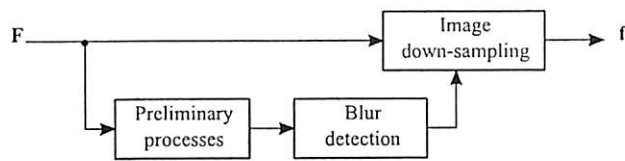


Fig. 2 Overview of the process involved in this proposed method.

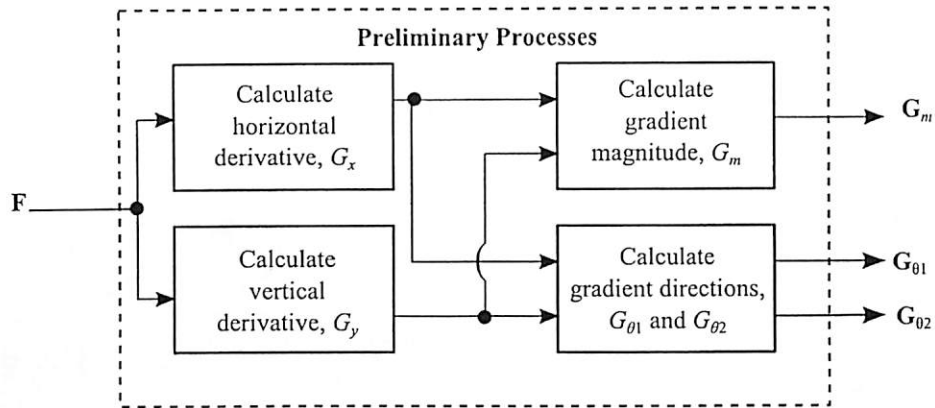


Fig. 3 The block diagram for the preliminary processes.

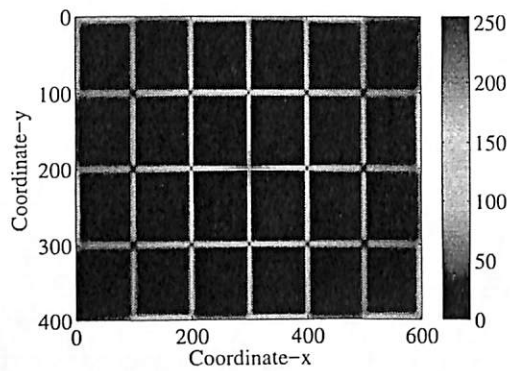


Fig. 4 Gradient magnitude G_m calculated from the gradient components G_x and G_y .

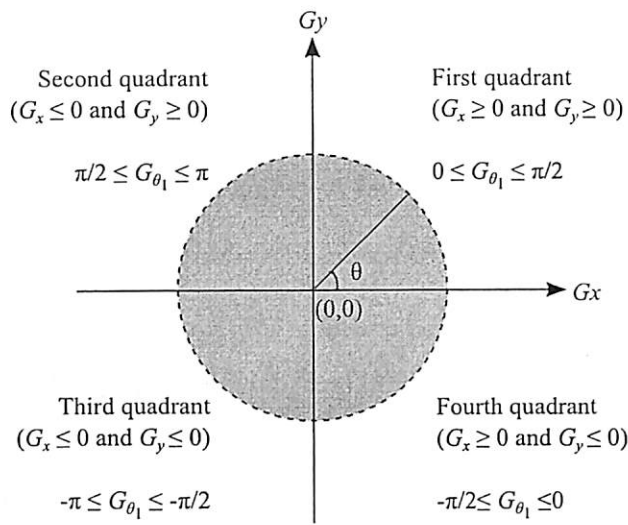


Fig. 5 Gradient direction G_{θ_1} returned by the "atan2" function.

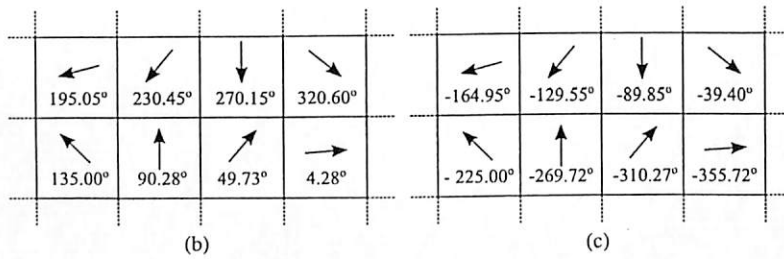
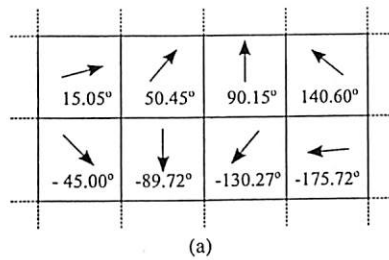


Fig. 6 Gradient orientation G_{θ_1} (in unit degrees) and its equivalent directions. (a) G_{θ_1} . (b) $G_{\theta_1} + 180^\circ$. (c) $G_{\theta_1} - 180^\circ$.

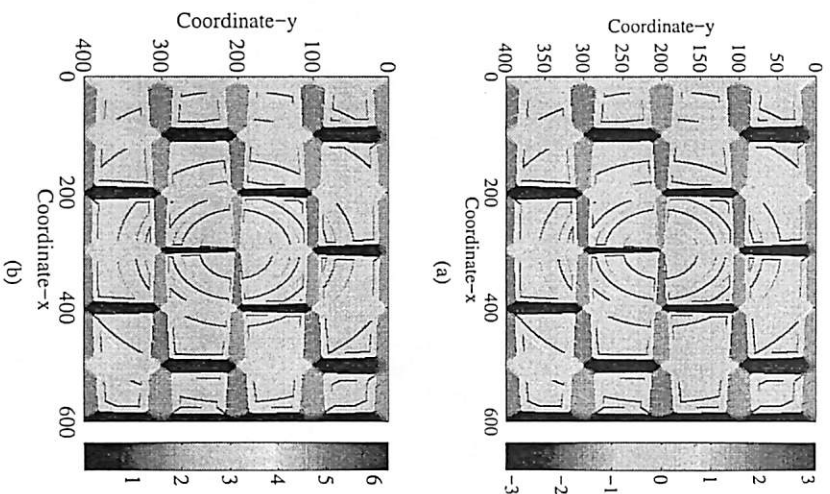


Fig. 7 Gradient orientation (in radians) obtained from the gradient components. (a) The original gradient orientation, G_{01} . (b) The modified gradient orientation, G_{02} .

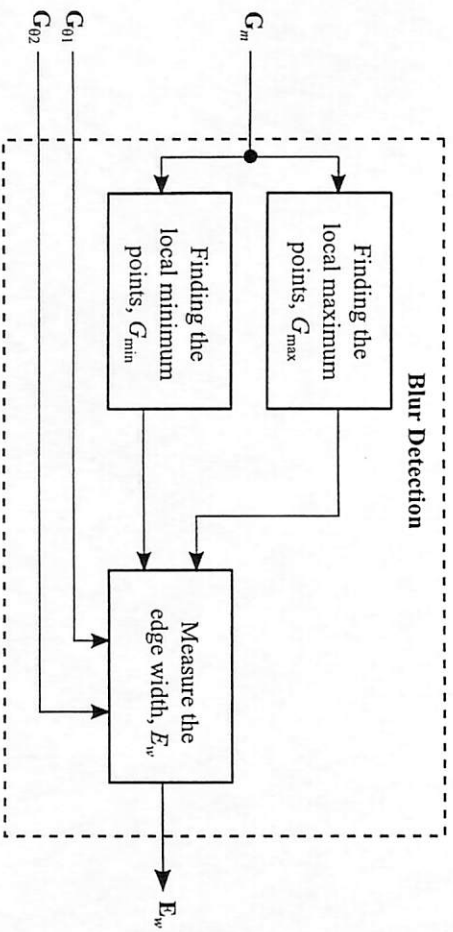


Fig. 8 The details block diagram for the blur detection stage.

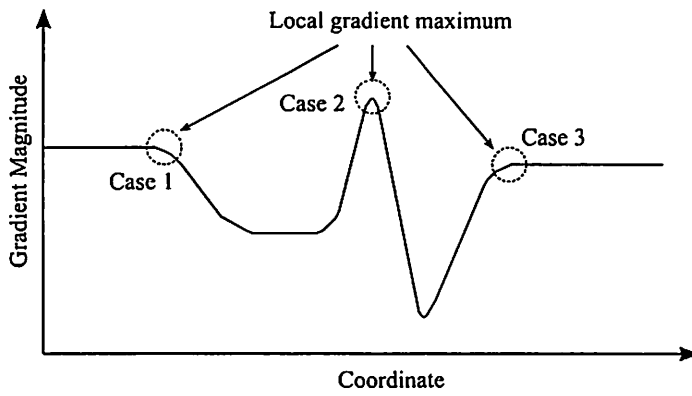


Fig. 9 The definitions for local maximum locations.

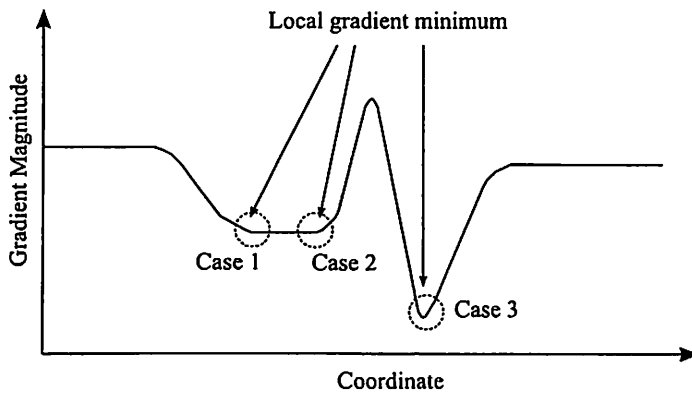


Fig. 10 The definition for local minimum.

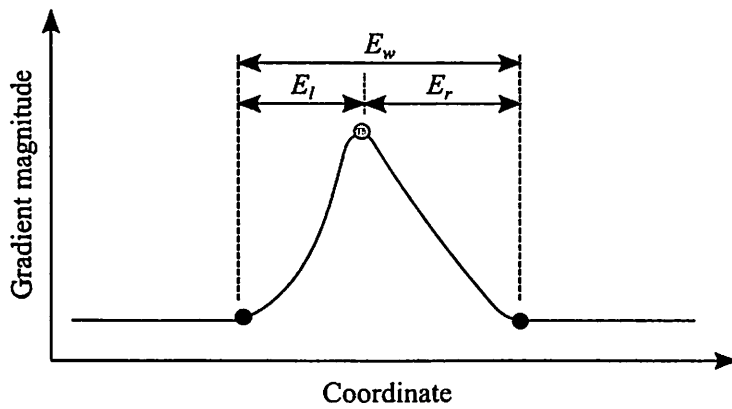


Fig. 11 The basic idea used in the calculation of the edge width. The green circle presents the location of the local maximum, whereas the red circles presents the locations of the local minimum.

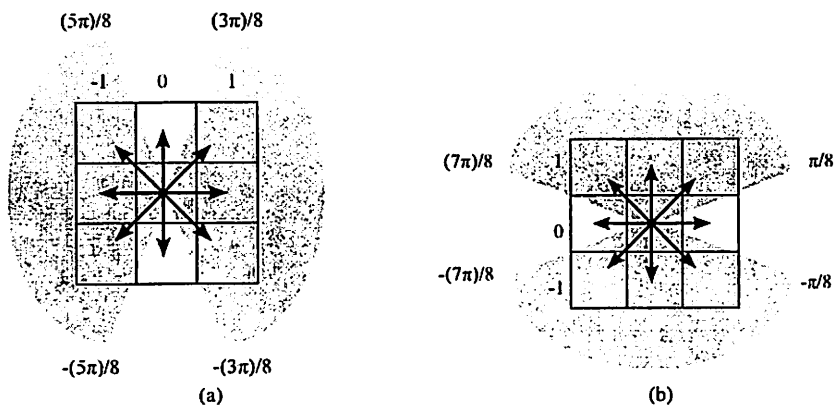


Fig. 12 (a) Definition for index_r . (b) Definition for index_y .

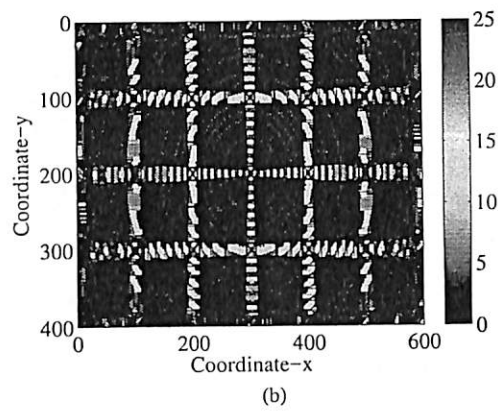
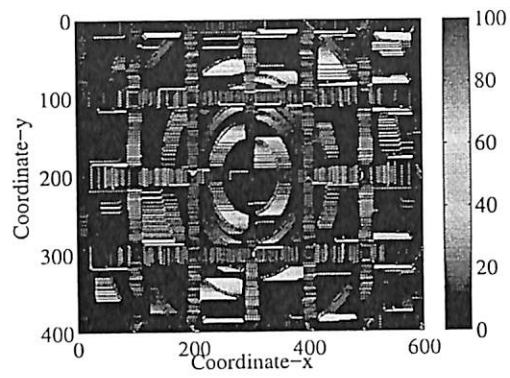


Fig. 14 (a) Edge width calculated from G'_{\min} . (b) Edge width E_w obtained from G'_{\min} .

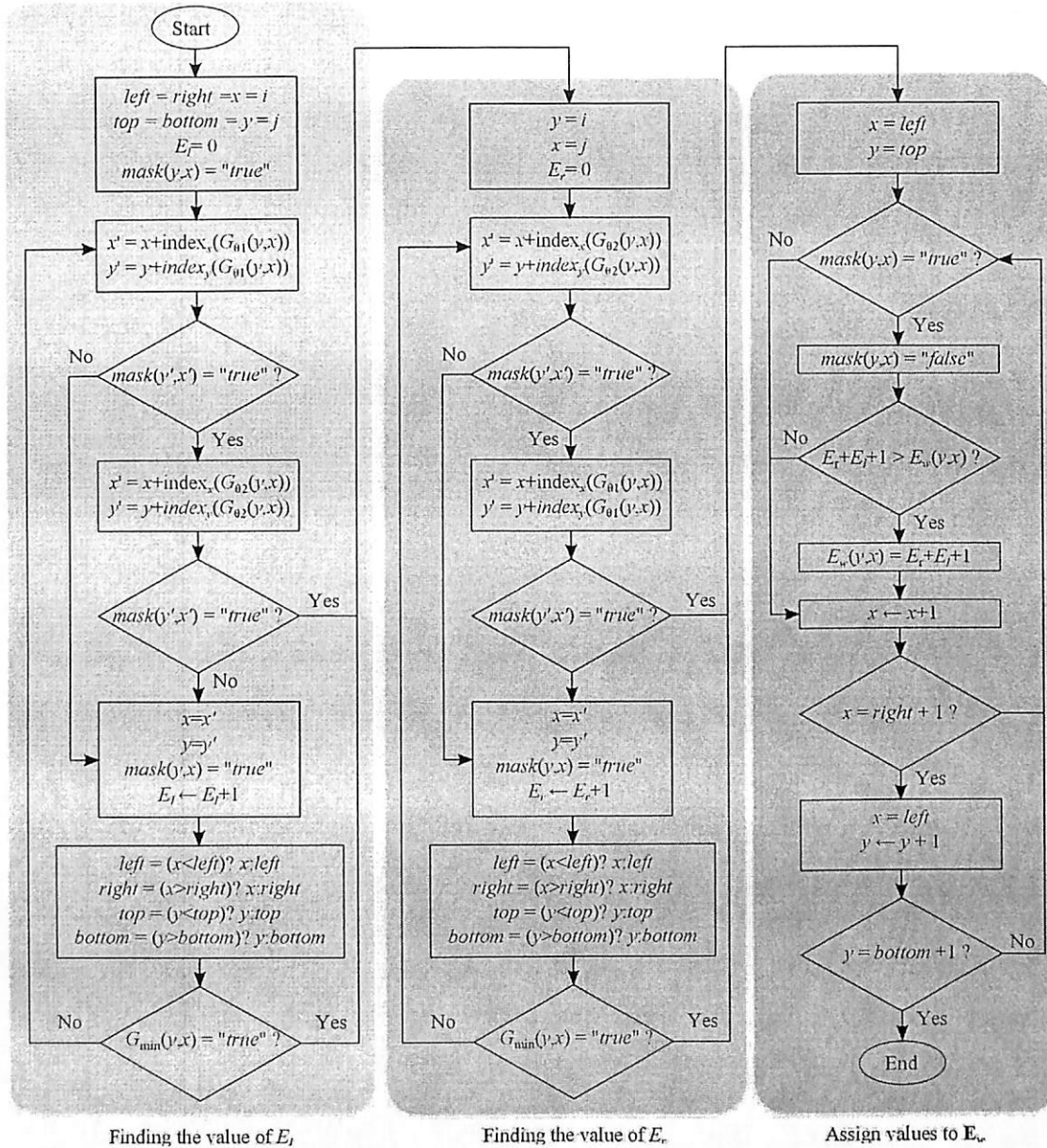


Fig. 13 Flowchart for the edge width calculation.

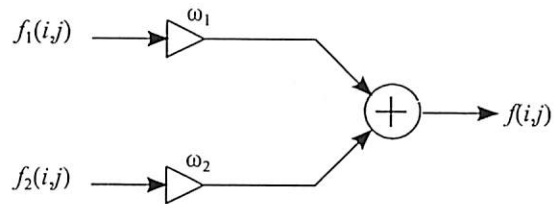


Fig. 15 Block diagram for blur embedding process.

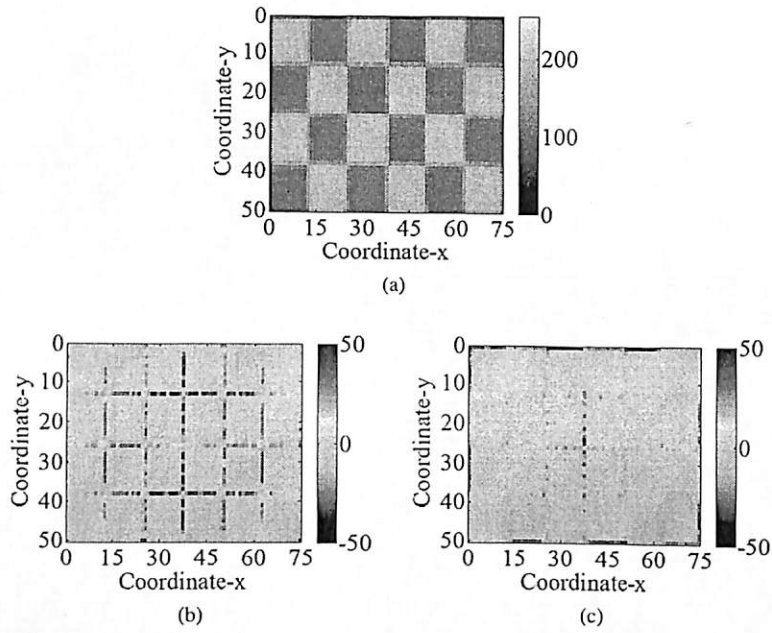
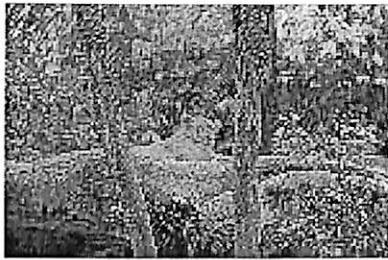


Fig. 16 (a) Thumbnail image f . (b) Array of $f-f_1$. (c) Array of i.e., $f-f_2$.



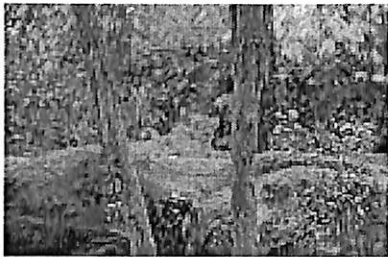
(a) Original image



(b) DPD [1]



(c) DSD [2]



(d) PDAF [3]



(e) TBNI [4]



(f) Proposed TBI

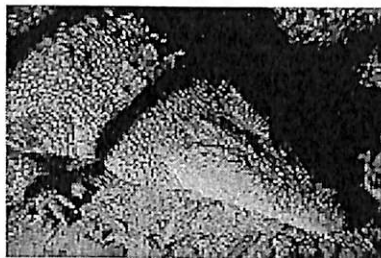
Fig. 17 F_1 . Comparison of proposed method with other methods with down-sampling factor of 10.



(a) Original image



(b) DPD [1]



(c) DSD [2]



(d) PDAF [3]

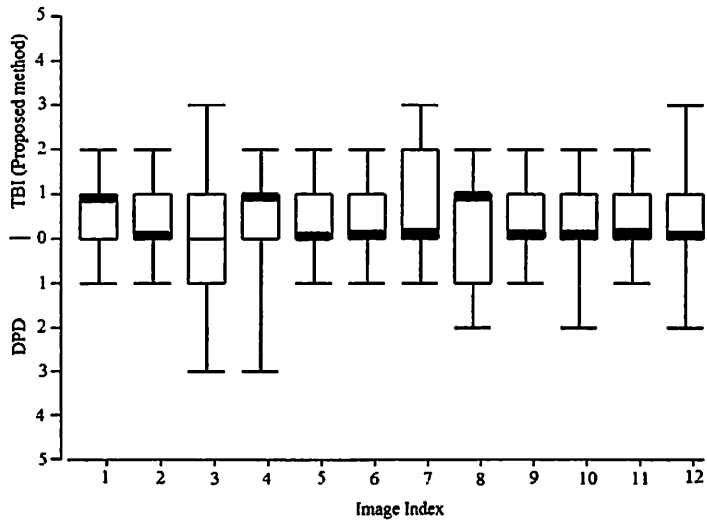


(e) TBNI [4]

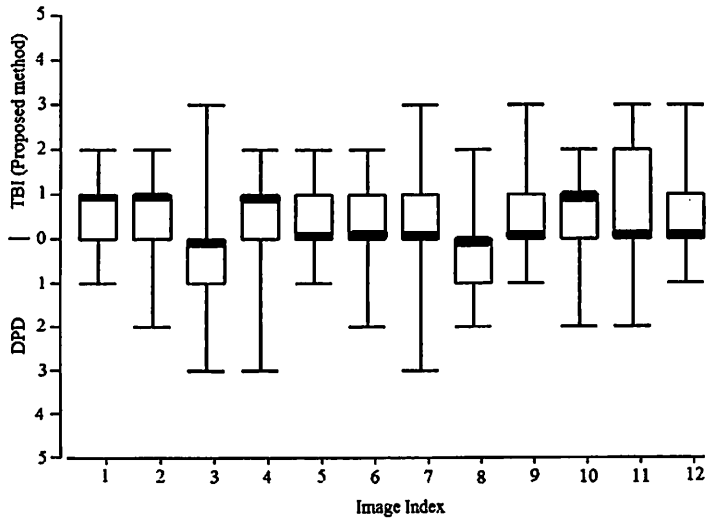


(f) Proposed TBI

Fig. 18 F_2 . Comparison of proposed method with other methods with down-sampling factor of 10.

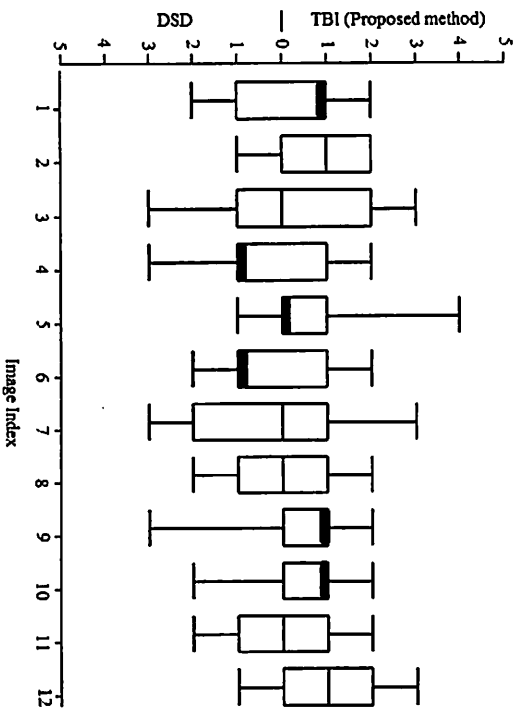


(a) Box-and-whisker plot for TBI vs. DPD for $L=4$.

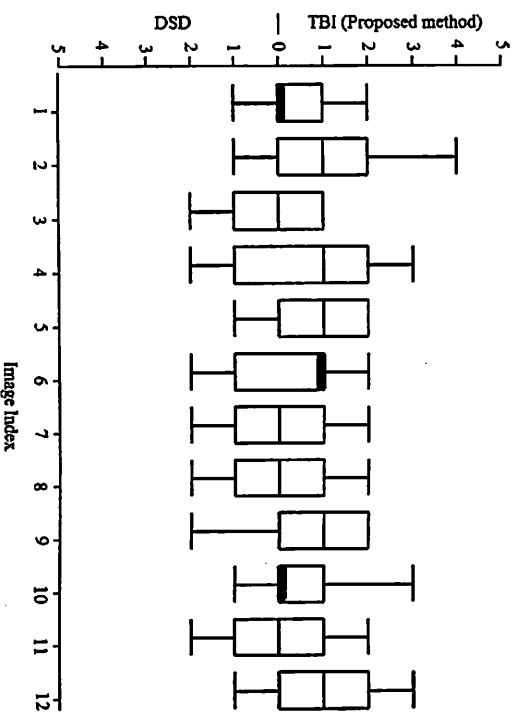


(b) Box-and-whisker plot for TBI vs. DPD for $L=8$.

Fig. 19 Box-and-whisker plot for TBI Vs. DPD thumbnail images survey.

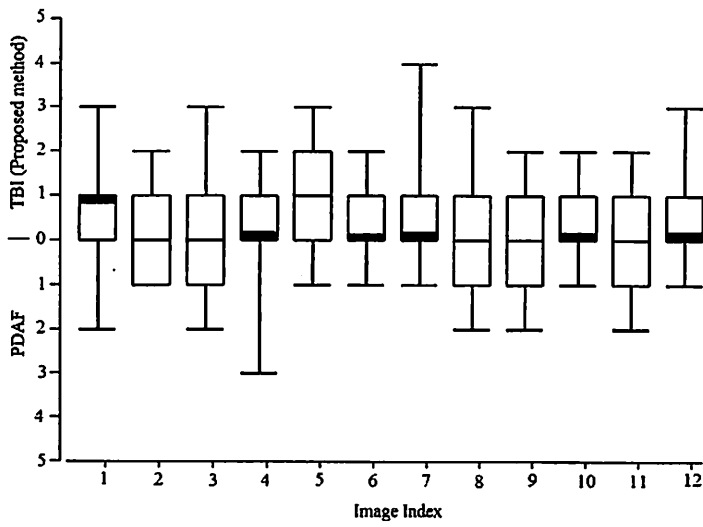


(a) Box-and-whisker plot for TBI vs. DSD for $L=4$.

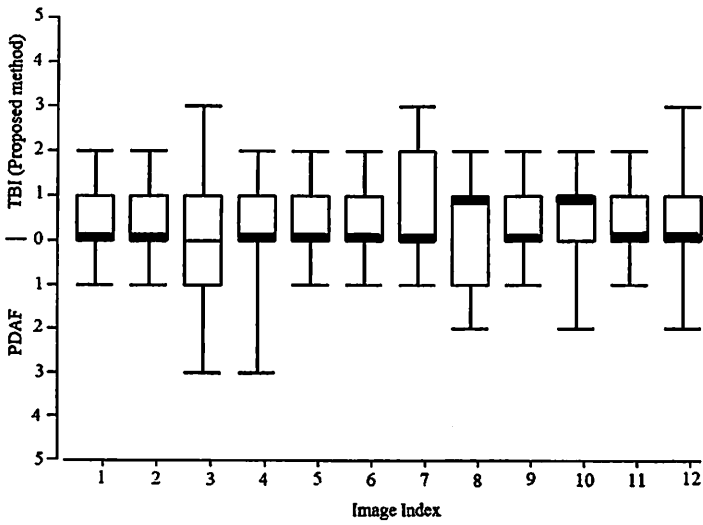


(b) Box-and-whisker plot for TBI vs. DSD for $L=8$.

Fig. 20 Box-and-whisker plot for TBI Vs. DSD thumbnail images survey.

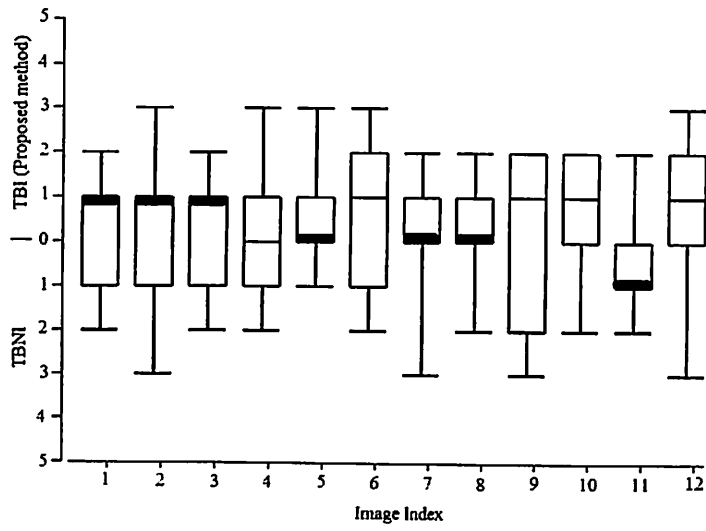


(a) Box-and-whisker plot for TBI vs. PDAF for $L=4$.

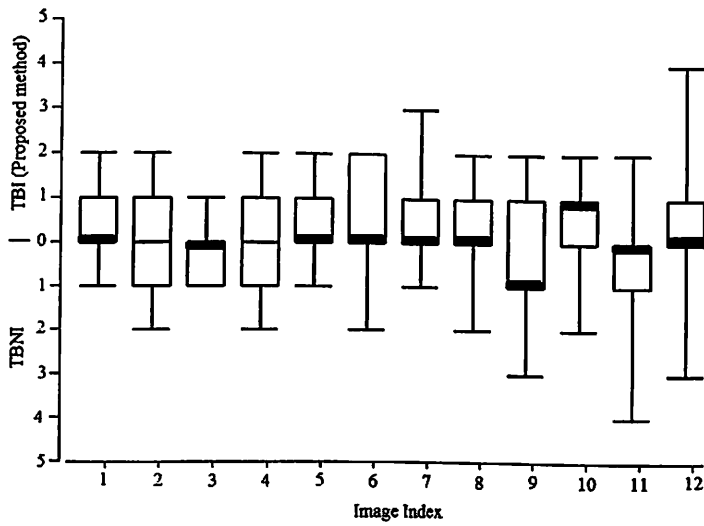


(b) Box-and-whisker plot for TBI vs. PDAF for $L=8$.

Fig. 21 Box-and-whisker plot for TBI Vs. PDAF thumbnail images survey.

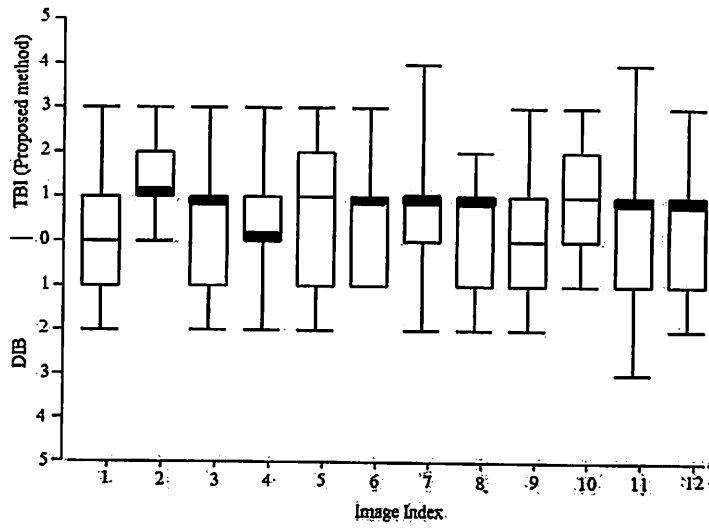


(a) Box-and-whisker plot for TBI vs. TBNI for $L=4$.

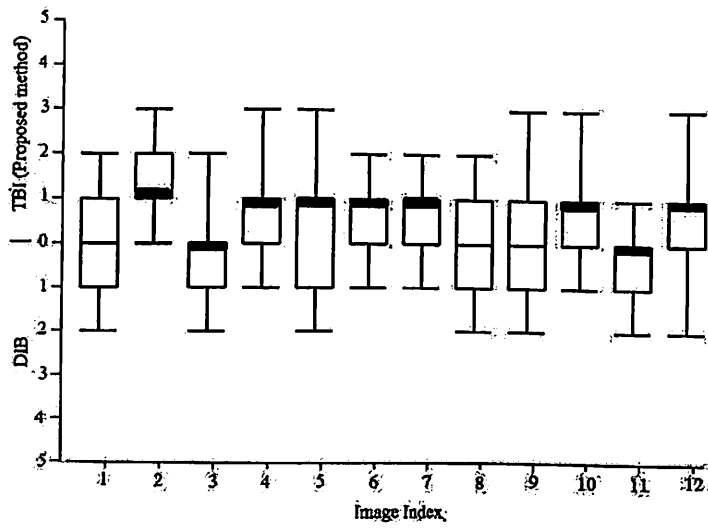


(b) Box-and-whisker plot for TBI vs. TBNI for $L=8$.

Fig. 22 Box-and-whisker plot for TBI Vs. TBNI thumbnail images survey.



(a) Box-and-whisker plot for TBI vs. DIB for $L=4$.



(b) Box-and-whisker plot for TBI vs. DIB for $L=8$.

Fig. 23 Box-and-whisker plot for TBI Vs. DIB thumbnail images survey.

Research Article

Thumbnail Image with Blurry Edge Information Utilizing Half Factor Rules

Boon Tatt Koik and Haidi Ibrahim

School of Electrical & Electronic Engineering, Universiti Sains Malaysia, Engineering Campus, 14300 Nibong Tebal, Penang, Malaysia

Correspondence should be addressed to Haidi Ibrahim; haidi_ibrahim@ieee.org

Received 6 August 2014; Accepted 14 December 2014; Published 31 December 2014

Academic Editor: Sabri Arik

Copyright © 2014 B. T. Koik and H. Ibrahim. This is an open access article distributed under the Creative Commons Attribution License, which permits unrestricted use, distribution, and reproduction in any medium, provided the original work is properly cited.

Thumbnail image with blurry edge information has attracted much attention in recent years. Thumbnail image, which is a tiny version of the original image, enables user to scan through a large proportion of image data for elimination of blurry image or picking up a sharp and a nice image in user's perspective. The thumbnail image is being utilized commonly in camera, smart phone, and other computing devices. In this paper, a method to embed blurry edge information in thumbnail images is proposed. This method is straight forward and simple to be implemented in electronic products. The image will undergo edge width measurement process by finding the local maximum and local minimum locations based on its edge magnitude. This is obtained after the implementation of horizontal and vertical first order derivatives of the original high resolution input image. The blur edges will be emphasized by utilizing edge width information during downsampling process to enable users to identify blurry edge image distinctively. Experimental results show a satisfactory outcome in embedding blurry characteristics of the original image to thumbnail image on the proposed method.

1. Introduction

Photo capturing by digital camera is very convenient for most consumers, be it the process of photo taking or viewing the photo after the image is captured [1]. Today, the digital camera has become a routine tool, especially when it is integrated into the smart phone with social media applications. Furthermore, digital image becomes easily accessible through consumer electronics such as laptop and tablet. In year 2011, Americans have captured 80 billion photographs and more than 250 million photographs are being posted daily on Facebook. This number is expected to be increased each year [2]. While the camera manufacturers continue to improve photo quality and increase the resolution of the image captured by their products, the consumers are drowning in digital visual contents [3]. Thus, there is a need to determine ways to review and check the quality of the captured digital photograph.

Thumbnail images are normally being used in electronic devices, such as computer, and handheld electronic product,

such as a smart phone. Thumbnail image, which is a smaller version of the original image, is normally being displayed in batches. It enables users to scroll through a bunch of images more effectively. How a blurry image is displayed by the thumbnail image is important, so that the users can conveniently filter out those unwanted blur images in a batch of thumbnails [4].

Thumbnail image enables the user to judge the original image in an effective way; whether an image quality or intrinsic value is worth keeping. Unfortunately, most of the image thumbnail technologies are unable to depict the real blur information from the original image. This drawback makes the quality judgment of an image through thumbnail image hard and not accurate. As a consequence, this situation creates inconveniences and leads to frustrations, especially when the user made a mistake in judging blurry image as a sharp, clear image [5].

Currently, there are several ways to create thumbnail images. The most common method is pixel-based downsampling with antialiasing filter (PDAF). PDAF uses low-pass

filter to bandlimit the frequency components of the original image, so that aliasing problem after signal resampling process can be avoided. However, this method is not able to retain noise information very well. This is because the noise mostly occupies high frequency image components. Therefore, thumbnail image which resulted from PDAF always appears to be rather clean from the noise [6, 7].

Direct pixel-based downsampling (DPD) is a method of generating thumbnail image without the need of any filtering. In this method, direct downsampling is employed, and this means that the pixel value of the thumbnail image takes one of the corresponding pixel values from the original high resolution image. The DPD thumbnail image is sharper than PDAF thumbnail image because it contains higher frequency components [8]. Another thumbnail image method is direct subpixel-based downsampling (DSD). DSD uses a similar concept to DPD, but instead of using information from just one pixel, one thumbnail image's pixel by DSD uses three pixel values from the original image. These three pixels correspond to the red (R), green (G), and blue (B) color channel. Therefore, DSD is only applicable for color images [9].

It is worth noting that none of the downsampling algorithms mentioned above are designed to embed the blur information from the original high resolution image to the thumbnail image. Therefore, thumbnail with blur information (TBI) is proposed in this paper. The purpose of this new algorithm is to assist the user to perceptually identify an image of good quality based on the thumbnail image. From there, the user will be able to select wanted or unwanted blur images in a bulky image folder.

This paper is arranged as follows. Section 2 describes the preliminary concept of blur detection. This useful concept is used in TBI in order to emphasize the blur. Next, Section 3 describes the processes involved in TBI in detail. Section 4 presents the experimental results where the performance of the proposal TBI method is compared with a few other well-known thumbnail image algorithms. This paper ends with Section 5 which summarizes the findings.

2. Preliminary Concept of Blur Detection

One of the concepts used in the proposed method, TBI, is presented in Figure 1. This figure presents an example to show the effect of blur towards the slope of the object's edges in the image. Sharp images as shown by Figures 1(a) and 1(b) contain step edges. However, when the image becomes blurred, the step edges are becoming ramp edges. The degree of blurring is increasing from Figure 1(a) to Figure 1(c) to Figure 1(e). Hence, the resultant intensity profiles are generated from these three grayscale images decreasing from sharper image (i.e., Figure 1(a)) to the most blurred image (i.e., Figure 1(e)). Noting that the "merging effect" between the edges at distance 600 along the profile is getting more serious when the image is getting more blurred. This phenomenon is more prevalent when the edges are located near to each other. Figure 1 shows that the slope of the edges is depending on the degree of blurring. Therefore, the measure of blurring can be estimated by using the information from the object's edges [10].

The proposed TBI method uses the estimated edge width to estimate the blur extent. This proposed method has been categorized into few processes, which are as follows.

- (i) Stage 1: Calculate horizontal and vertical derivative of the image.
- (ii) Stage 2: Find local maximum and local minimum of edge magnitude.
- (iii) Stage 3: Determine the direction of blur and calculate the edge width.
- (iv) Stage 4: Generate the downsampled image.

3. Thumbnail with Blur Information

Figure 2 shows the methodology of the TBI. Gradient maps are obtained after the horizontal and vertical first order derivatives are performed to the input image. The edge magnitude calculation is done using the data obtained in the first order derivative. After the edge magnitude map is obtained, edge blur direction map is generated. With the combination of the local maximum, local minimum, and edge magnitude data, the blur width map in the image can be estimated.

3.1. Horizontal and Vertical Derivative of Image. At the initial stage, the gradient, Δ , of the input image at any pixel is calculated by applying 2D directional derivative as given by

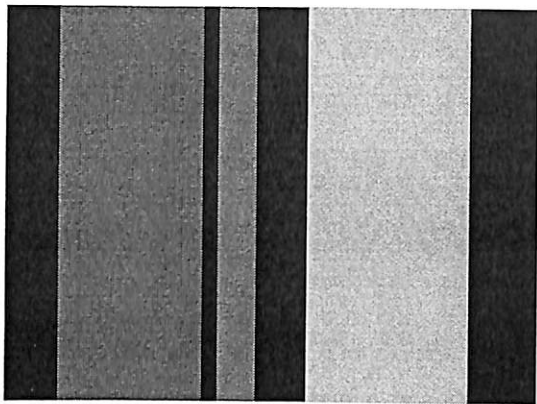
$$\begin{bmatrix} G_x(i, j) \\ G_y(i, j) \end{bmatrix} = \begin{bmatrix} \frac{d}{dx} I(i, j) \\ \frac{d}{dy} I(i, j) \end{bmatrix}, \quad (1)$$

where G_x is first order derivative in x direction, G_y is first order derivative of y direction, I is the original image, and (i, j) are the spatial coordinates of the pixel.

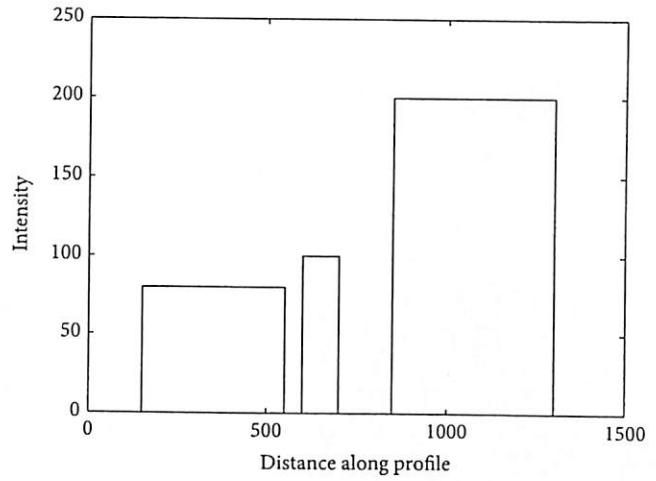
In the implementation of TBI, Sobel filter [11] is used at this stage in order to find the 2D directional derivatives. Sobel filter is used to calculate the gradient magnitude at each point in each 2D image channel. Sobel operator is chosen as it is less sensitive to the noise as compared to the Roberts cross filter or Laplacian filter [10]. Thus, this gives an advantage to the TBI method because a Sobel filter will enable TBI to give more emphasis on blur issue, which is the main concern for this method. Derivative in both x and y directions is executed separately for each R, G, and B color channel of the original image. Equation (2) is the equations for calculating first order derivatives using Sobel horizontal and Sobel vertical derivative kernel [12] as follows:

$$\begin{aligned} G_x &= \begin{bmatrix} -1 & 0 & 1 \\ -2 & 0 & 2 \\ -1 & 0 & 1 \end{bmatrix} \otimes I, \\ G_y &= \begin{bmatrix} 1 & 2 & 1 \\ 0 & 0 & 0 \\ -1 & -2 & -1 \end{bmatrix} \otimes I, \end{aligned} \quad (2)$$

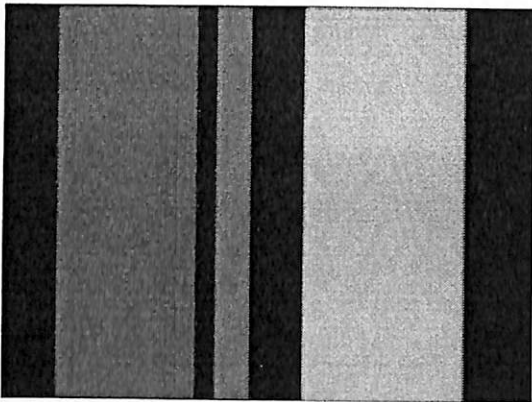
where \otimes represents a convolution process.



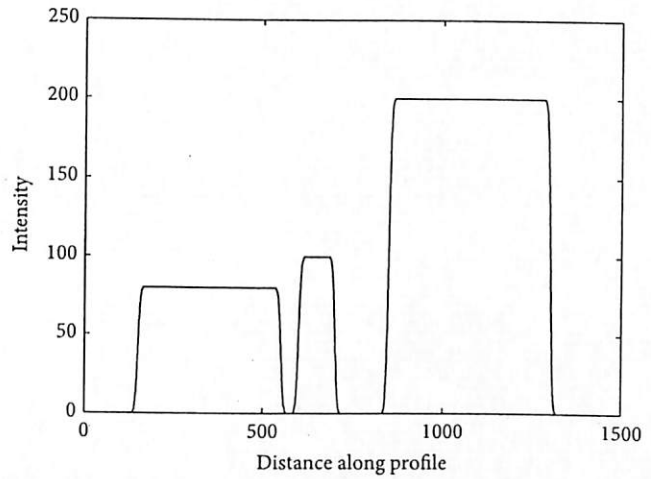
(a)



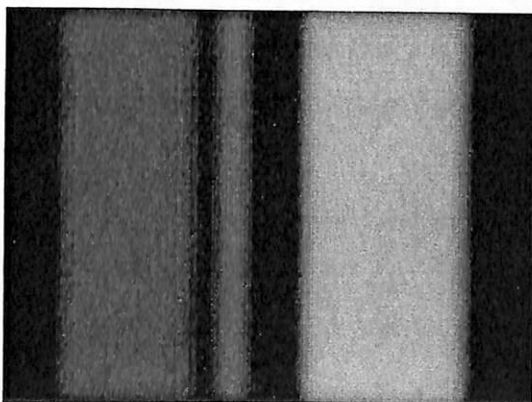
(b)



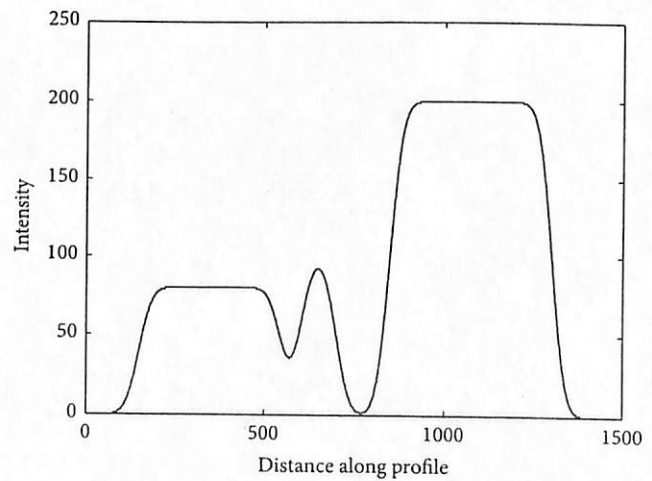
(c)



(d)



(e)



(f)

FIGURE 1: Examples of blur edges. (a) The original, sharp image. (b) Horizontal profile of image (a). (c) Slightly blur image. (d) Horizontal profile of image (c). (e) Seriously blurred image. (f) Horizontal profile of image (e).

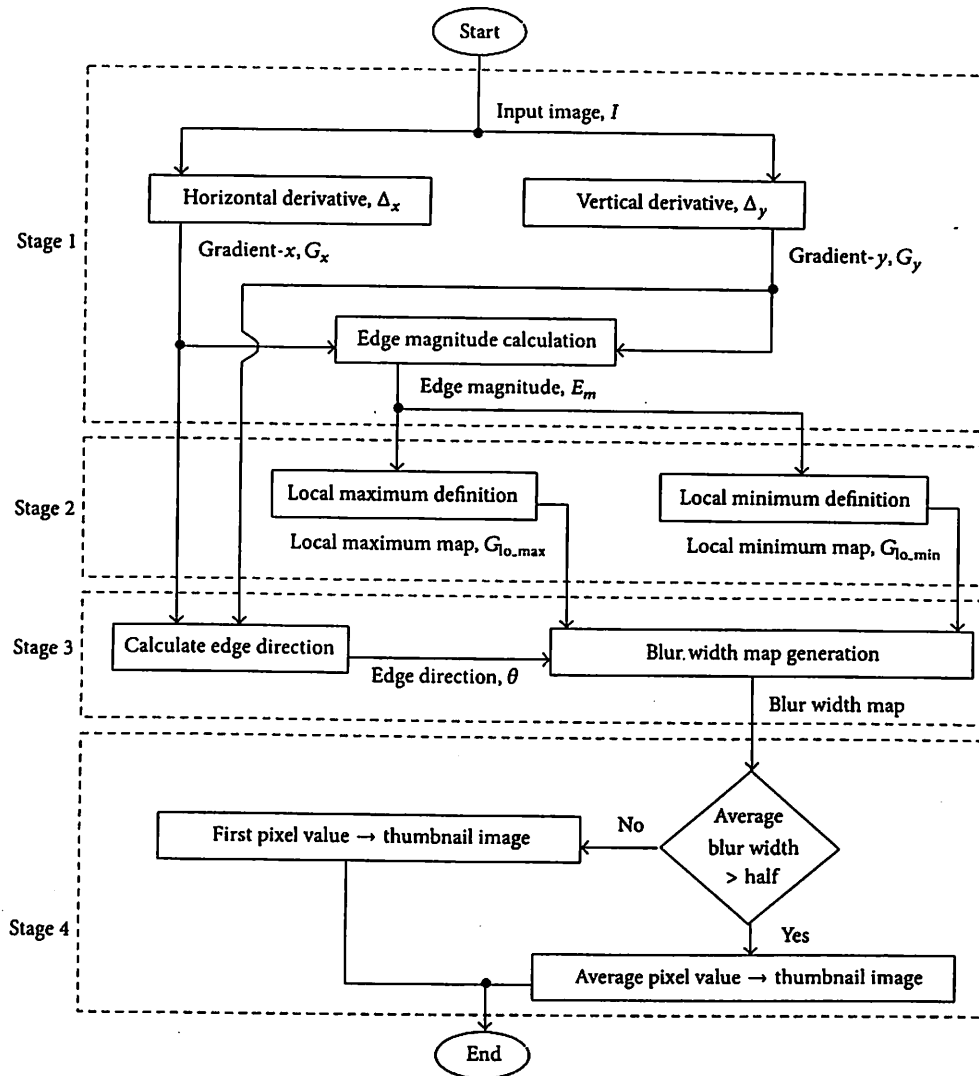


FIGURE 2: Flowchart for methodology of TBI.

3.2. Edge Magnitude, Local Maximum, and Local Minimum. Edge magnitude, E_m , is calculated using data obtained from $G_x(i, j)$ and $G_y(i, j)$ by

$$|E_m(i, j)| = \sqrt{|G_x(i, j)|^2 + |G_y(i, j)|^2}. \quad (3)$$

Edge magnitude is needed in TBI in order to find local maximum and local minimum. To find the local maximum and minimum, we use the concept of peak and valley analysis from the edge magnitude data. The usage of the local minimum and local maximum point will be utilized in defining the edge width in the following subsection. Equation (4) summarizes how the local minimum and maximum are defined based on edge magnitude values as follows:

$$G_{lo,max}(i, j) = \begin{cases} 1, & E_m(i, j-1) \leq E_m(i, j) \\ & \& E_m(i, j) > E_m(i, j+1) \\ 1, & E_m(i, j-1) < E_m(i, j) \\ & \& E_m(i, j) \geq E_m(i, j+1) \\ 0, & \text{otherwise,} \end{cases}$$

$$G_{lo,min}(i, j) = \begin{cases} 1, & E_m(i, j-1) \geq E_m(i, j) \\ & \& E_m(i, j) < E_m(i, j+1) \\ 1, & E_m(i, j-1) > E_m(i, j) \\ & \& E_m(i, j) \leq E_m(i, j+1) \\ 0, & \text{otherwise,} \end{cases} \quad (4)$$

where $\&$ is logical "AND" and $G_{lo,min}$ and $G_{lo,max}$ are the local minimum and local maximum map, respectively.

Notice that (4) only shows the processes in y direction. A similar process to define the local maximum and local minimum in x direction needs to be performed using the same concept. All the local maximum and minimum will be embedded in a new masking map, $G_{lo,min}$ and $G_{lo,max}$, respectively. Local maximum, $G_{lo,max}$, will be used to denote the initial edge location in this method, whereas local minimum, $G_{lo,min}$, will be defined as the ending point. Both local maximum and local minimum will be used to estimate edge width in the next stage.

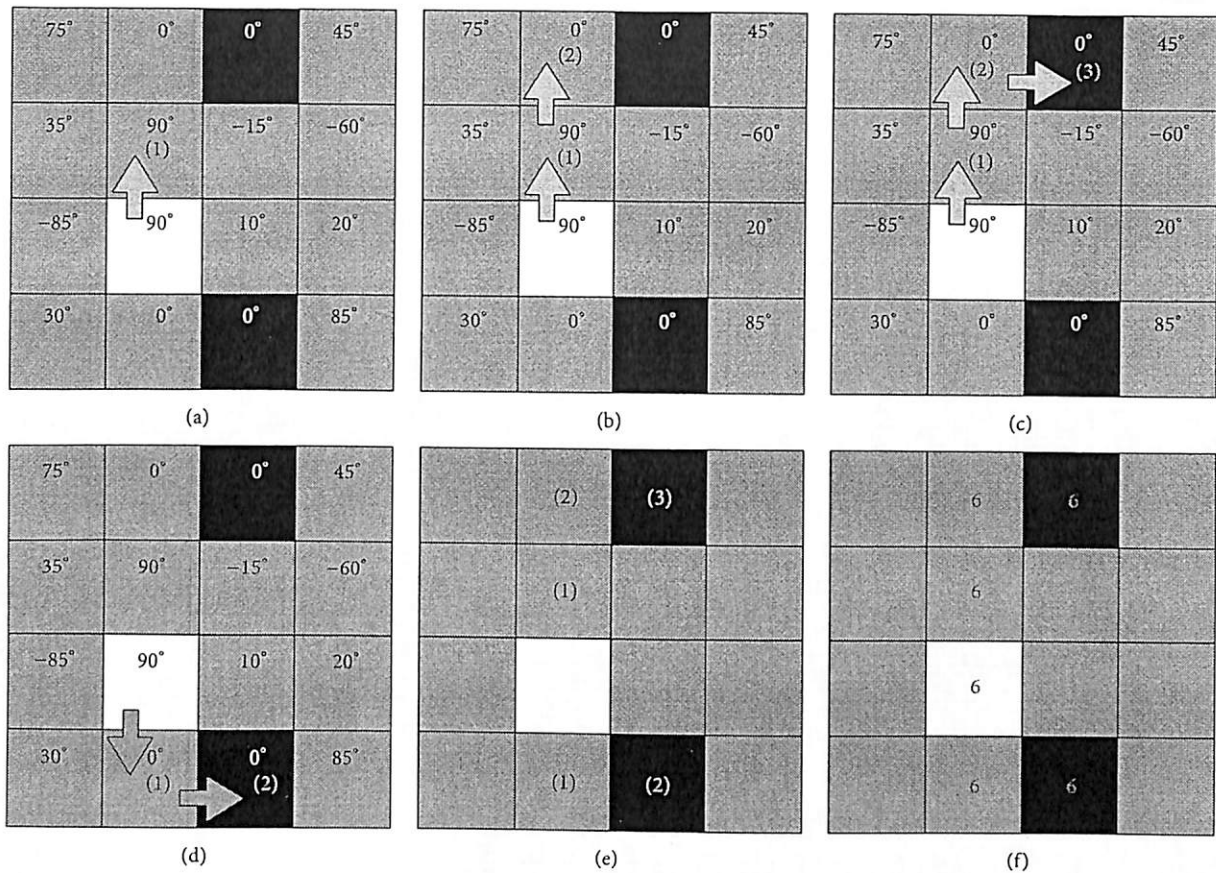


FIGURE 3: Illustration of edge width estimation.

3.3. Determine the Edge Blur Direction and Edge Width. Edge blur direction that indicates the direction of the normal to the edge point with respect to the x -axes is defined using atan2 function as in

$$\theta(i, j) = \text{atan2}(G_y(i, j), G_x(i, j)). \quad (5)$$

The data obtained from the atan2 in (5), whose values are in the range of $-\pi$ to π , is used in TBI to denote the direction of the blur edge in the width calculation process. The edge blurs direction is bidirectional, which means that $\theta(i, j) = \theta(i, j) \pm 180^\circ$. TBI uses the idea from Chung et al. [10] to determine the edge width. The process of calculating the edge width starts at a local maximum. At each local maximum point, the algorithm traverses, guided by $\theta(i, j)$, until it found a local minimum point on the "left side" of the edge. Then, the algorithm starts again at the same local maximum point until it found another local minimum point on the "right side" of the edge. The width of the image blur is then defined as the distance between these two local minimums.

Figure 3 shows an example of how the edge width is being determined. In this example, we use an image of size 4×4 pixels, where the coordinates $(i, j) = (0, 0)$ are located at the left top corner. The value shown inside each pixel presents the gradient direction θ . The white box at coordinates $(2, 1)$ presents the local maximum point, whereas the black boxes at coordinates $(0, 2)$ and $(3, 2)$ present the

local minimum points. The local maximum point acts as the initial starting position for the calculation of the edge width. The explanations of this example are as follows.

- (a) The value of θ will guide the algorithm to traverse into one of the eight neighboring pixels. In this case, at position $(2, 1)$, the value of θ is equal to 90° . Therefore, the algorithm moves to coordinates $(1, 1)$. Count "1" will be mapped at this location as (1).
- (b) The pixel at $(1, 1)$ is not a local minimum. Thus, this pixel becomes the current pixel. At this position, the value of θ is equal to 90° . The algorithm moves to coordinates $(0, 1)$. The distance between these coordinates with the starting point $(2, 1)$ is 2 pixels, and thus, count "2" will be mapped at this location as (2).
- (c) The current pixel is now at coordinates $(0, 1)$. The value of θ at this position is 0° . Thus, the algorithm moves to coordinates $(0, 2)$. Count "3" will be mapped at this location as (3). Because pixel at coordinates $(0, 2)$ is a local minimum point, this indicates the termination point for the blur edge on the "right side."
- (d) The algorithm needs to find the width of the blur edge located on the "left side." Thus, the algorithm starts again at coordinates $(2, 1)$. But, by using bidirectional property, θ is now equal to -90° . Therefore, it will

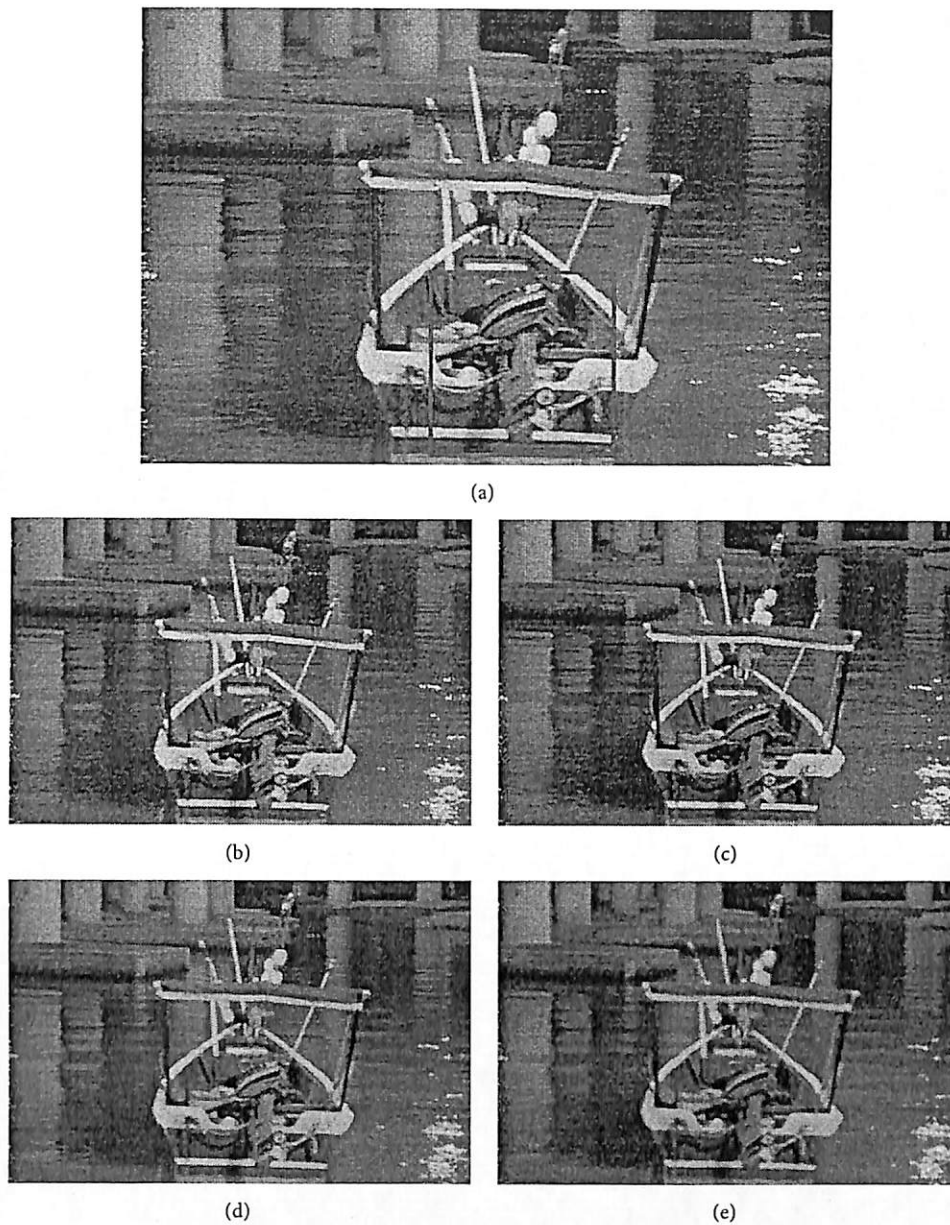


FIGURE 4: (a) Original image of "The Boat." (b) Image thumbnail generated by DPD. (c) Image thumbnail generated by DSD. (d) Image thumbnail generated by PDAF. (e) Image thumbnail generated by the proposed method.

move to coordinates (3, 1). Then, at coordinates (3, 1), θ is equal to 0° , which leads to the local minimum point at (3, 2). Thus, the traversing process terminates at this position.

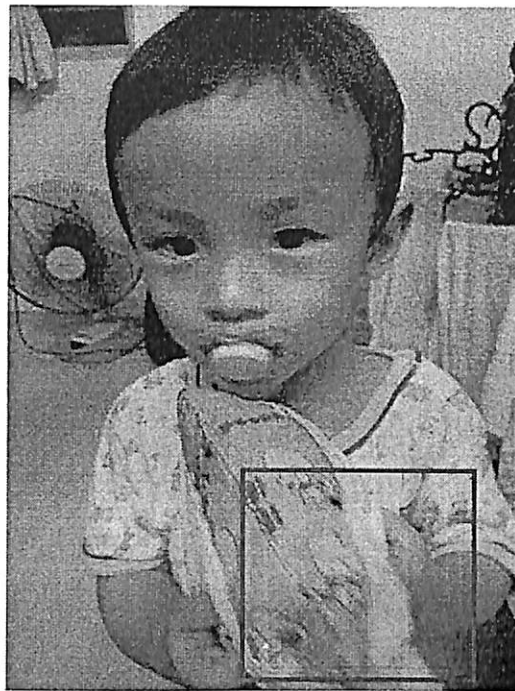
- (e) The resultant from this process is a counting map. From this counting map, the width of the edges can be calculated. In this example, the width of the edge is equal to 3 (i.e., the width of the "right side") + 2 (i.e., the width of the "left side") + 1 (i.e., the local maximum point) = 6 pixels.
- (f) The edge width map will be generated by the algorithm by putting the edge width value to every pixel that was involved with the traversing process.

3.4. TBI Downsampling of Image. Let assume that the original image is being downsampled using a factor L . Thus, the size of the downsampling window for this process is $L \times L$ pixels. If the local edge width values contained in this downsampling window area are

$$\text{Local blur width map} = \begin{bmatrix} a_{1,1} & a_{1,2} & \dots & a_{1,L} \\ a_{2,1} & a_{2,2} & \dots & a_{2,L} \\ \vdots & \vdots & \ddots & \vdots \\ a_{L,1} & a_{L,2} & \dots & a_{L,L} \end{bmatrix}, \quad (6)$$

then the average blur edge width value w is defined as

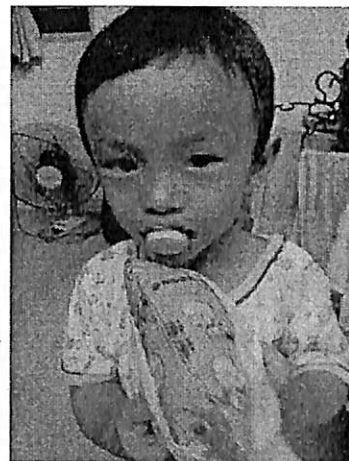
$$w = \frac{1}{L^2} \sum_{i=1}^L \sum_{j=1}^L a_{i,j}. \quad (7)$$



(a)



(b)



(c)



(d)



(e)

FIGURE 5: (a) Original image of "The Boy." (b) Image thumbnail generated by DPD. (c) Image thumbnail generated by DSD. (d) Image thumbnail generated by PDAF. (e) Image thumbnail generated by the proposed method.

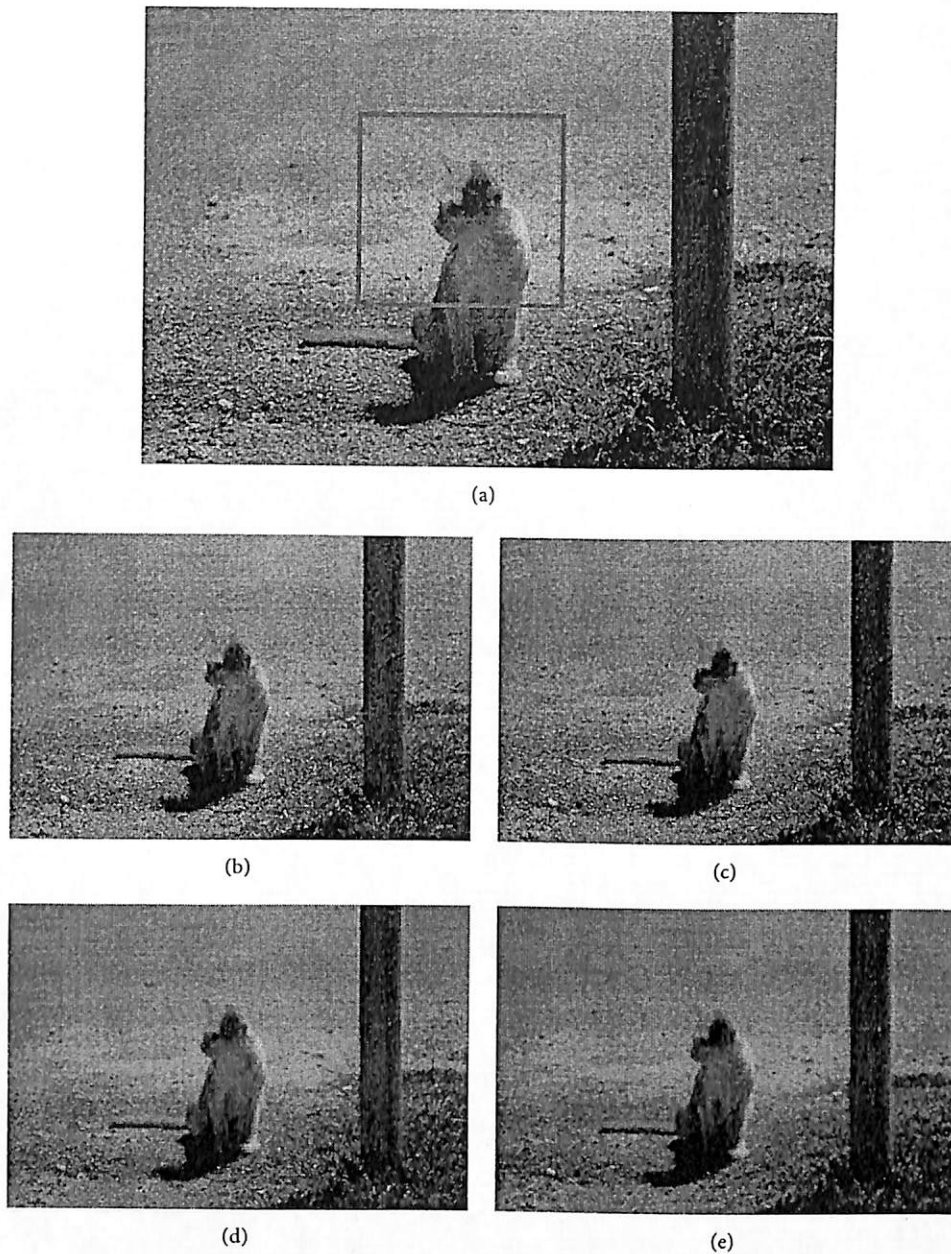


FIGURE 6: (a) Original image of “The Cat.” (b) Image thumbnail generated by DPD. (c) Image thumbnail generated by DSD. (d) Image thumbnail generated by PDAF. (e) Image thumbnail generated by the proposed method.

TBI downsampling process uses either the first pixel value (i.e., using the same method as DPD method) or the average intensity value, depending on the value of the local average blur width w . The thumbnail image will use the average pixel value when w fulfills the half factor rule. The half factor rule is a process implemented when the average width of a certain region is greater than half of the downsampling factor. This average value is obtained from an averaging process of a 2D matrix that is initiated on the image thumbnail itself, using a window of size 3×3 pixels. On the other hand, the first pixel value is used when the average blurs width is less or equal to half of the downsampling factor.

4. Experimental Results

In order to evaluate the performance of TBI, thumbnail images from TBI are compared with the outputs from PDAF, DPD, and DSD methods. Three test images have been used. These images are color images and in JPEG format. All images have been acquired using a phone camera, Samsung GT-I9100. The dimensions of the acquired original images are 2448×3264 pixels. The downsampling factor L used is set to 8, and therefore, the thumbnail images are at size 432×288 pixels.

Figure 4 shows the results using one of the test images. This test image “The Boat” shows an image of a boat, captured

during night time under dim light. This image appears yellowish because the scene was illuminated by yellow street lights. As shown by Figure 5(a), there is a slightly blurred region of the boat's engine, as indicated by a red rectangle. In this figure, the results show that DPD and DSD produce sharper thumbnail images, when compared to the output from PDAF and also the proposed TBI. Yet, these methods failed to emphasize the blurs on the boat's engine. The proposed method produces a much better thumbnail image, as it carries the blur information of the original image in the most accurate way.

Figure 5(a) shows the test image that we named as "The Boy." The red rectangle on this image, which covers a part of a pillow, indicates the region that suffers from motion blur. From Figure 5, we can observe that DPD, DSD, and PDAF produce almost the same thumbnail images. On the other hand, the proposed TBI method successfully embeds distinctive blur information into its thumbnail image.

Figure 6(a) is a test image, which shows an image of a cat. This test image suffers from out-of-focus blur. The blur region is indicated by a red rectangle. From Figure 6, we can notice that DPD and DSD methods produce much sharper thumbnail images, as compared with PDAF and TBI. But DPD and DSD failed to give emphasis on the blur region. PDAF and the proposed method successfully embed blur characteristic into their thumbnail images. By comparing Figure 6(d) with Figure 6(e), we can see that TBI is more effective in embedding blur information.

5. Conclusion

In this paper, a new thumbnail image algorithm (TBI) has been proposed. Experimental results by using three test images suggest that the proposed method has successfully embedded blur information into thumbnail image. The complexity of TBI is low, and the method is simple. Therefore, TBI can be suggested as one of the digital display options for consumer electronics. TBI potentially can prevent the hassle in filtering away low quality or unwanted pictures.

Conflict of Interests

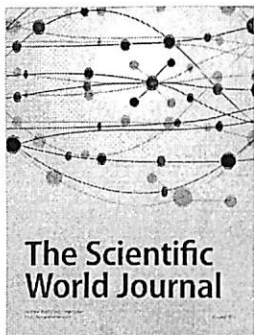
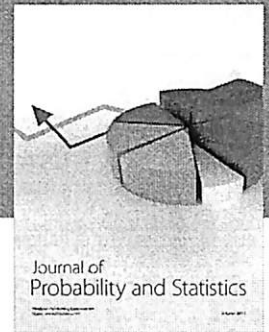
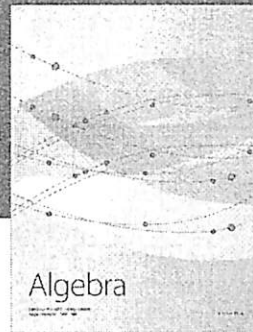
The authors declare that there is no conflict of interests regarding the publication of this paper.

Acknowledgments

The authors would like to thank the reviewers for their constructive comments. They also would like to thank Mr. Rostam Affendi Hamzah and Miss Kam Chai Mei for helping them in proofreading this paper. This work was supported in part by the Universiti Sains Malaysia's Research University Individual (RUI) Grant with account no. 1001/PELECT/814169.

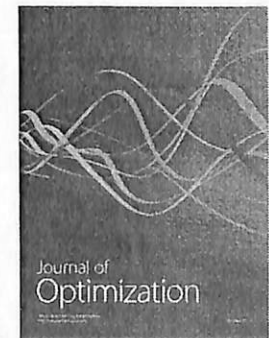
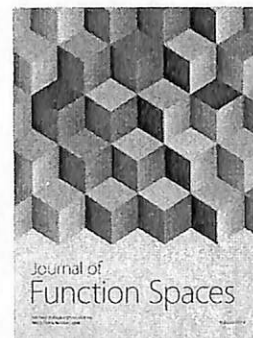
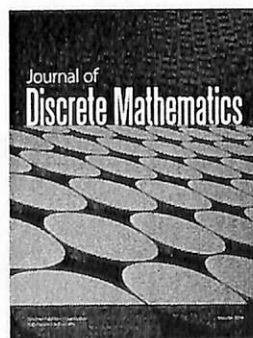
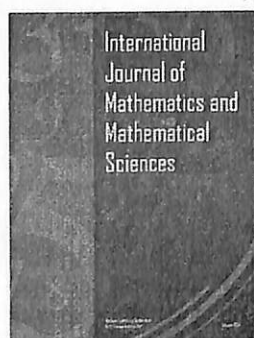
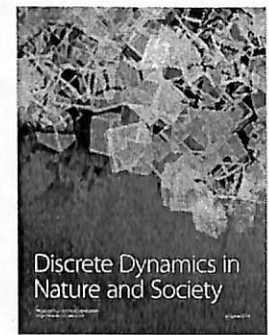
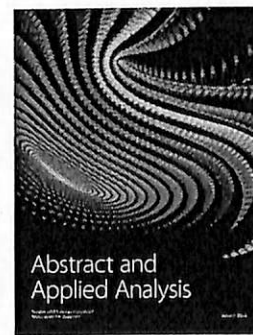
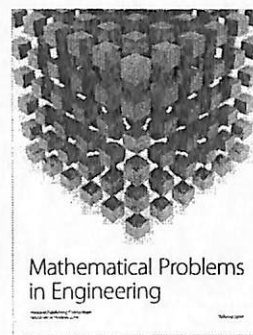
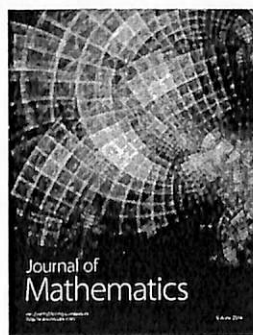
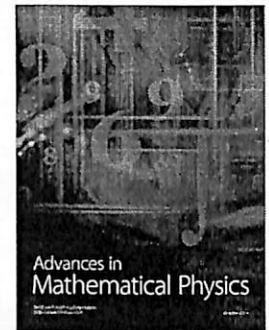
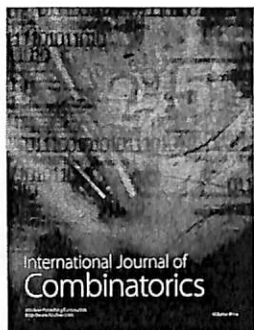
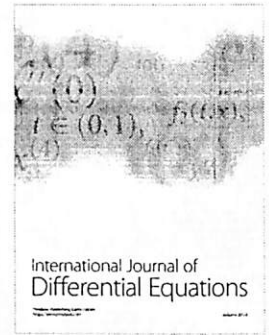
References

- [1] A. Levin, "Blind motion deblurring using image statistics," in *Proceedings of the 20th Annual Conference on Neural Information Processing Systems (NIPS '06)*, pp. 841–848, December 2006.
- [2] P. Andrews and M. Langford, *Langford's Starting Photography: The Guide to Create Great Images*, Taylor & Francis, 2014.
- [3] L. L. Hinthorne, "Using digital and instant film photography for research documentation: a research note," *Qualitative Research*, vol. 14, no. 4, pp. 508–519, 2014.
- [4] C. Dainty, "Film photography is dead: long live film: What can digital photography learn from the film era?" *IEEE Consumer Electronics Magazine*, vol. 1, no. 1, pp. 61–64, 2012.
- [5] L. Fang, K. Tang, O. C. Au, and A. K. Katsaggelos, "Anti-aliasing filter for subpixel down-sampling based on frequency analysis," in *Proceedings of the 36th IEEE International Conference on Acoustics, Speech, and Signal Processing (ICASSP '11)*, pp. 1117–1120, Prague, Czech Republic, May 2011.
- [6] Y. Ling, O. C. Au, K. Tang, J. Pang, J. Zeng, and L. Fang, "An analytical study of subpixel-based image down-sampling patterns in frequency domain," in *Proceedings of the IEEE International Conference on Visual Communications and Image Processing (VCIP '13)*, pp. 1–6, IEEE, Kuching, Malaysia, November 2013.
- [7] R. Samadani, T. A. Mauer, D. M. Berfanger, and J. H. Clark, "Image thumbnails that represent blur and noise," *IEEE Transactions on Image Processing*, vol. 19, no. 2, pp. 363–373, 2010.
- [8] H. Ibrahim, "Image thumbnail with blur and noise information to improve browsing experience," *Advances in Multimedia*, vol. 2, no. 3, pp. 39–48, 2011.
- [9] L. Fang, O. C. Au, K. Tang, X. Wen, and H. Wang, "Novel 2-D MMSE subpixel-based image down-sampling," *IEEE Transactions on Circuits and Systems for Video Technology*, vol. 22, no. 5, pp. 740–753, 2012.
- [10] Y.-C. Chung, J.-M. Wang, R. R. Bailey, S.-W. Chen, and S.-L. Chang, "A non-parametric blur measure based on edge analysis for image processing applications," in *Proceedings of the IEEE Conference on Cybernetics and Intelligent Systems*, pp. 356–360, December 2004.
- [11] G. T. Shrivakshan, "An analysis of SOBEL and GABOR image filters for identifying fish," in *Proceedings of the International Conference on Pattern Recognition, Informatics and Mobile Engineering (PRIME '13)*, pp. 115–119, February 2013.
- [12] R. Maini and H. Aggarwa, "Study and comparison of various image edge detection techniques," *International Journal of Image Processing (IJIP)*, vol. 3, no. 1, pp. 1–11, 2009.



Hindawi

Submit your manuscripts at
<http://www.hindawi.com>



Robust algorithm for broad impulse noise removal utilizing intensity distance and intensity height methodologies

Sin Hoong Teoh & Haidi Ibrahim

Signal, Image and Video Processing

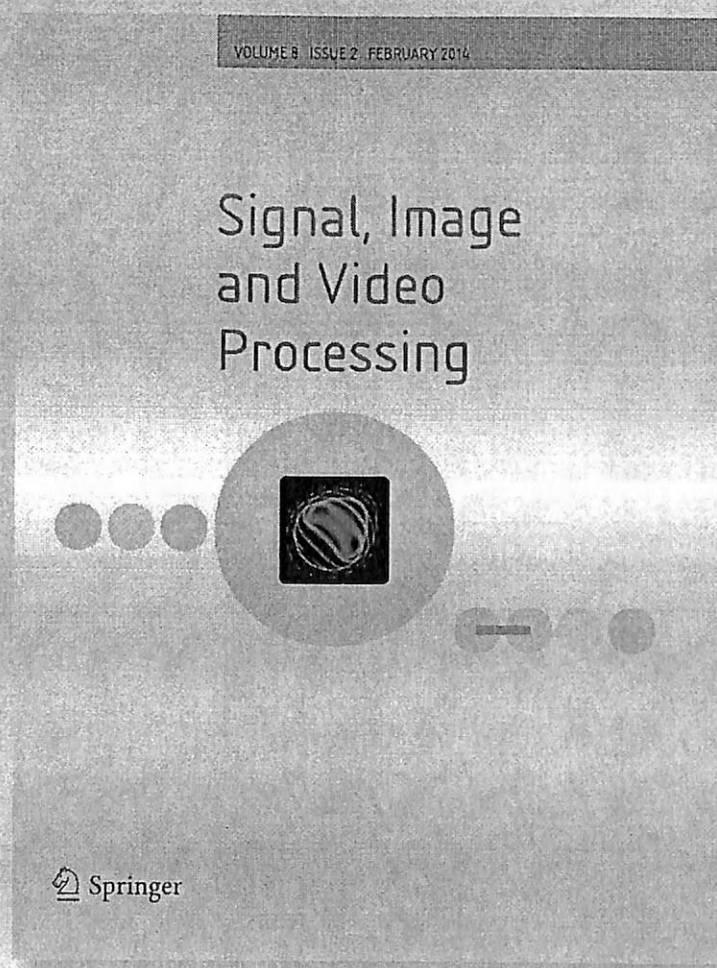
ISSN 1863-1703

Volume 8

Number 2

SIVIP (2014) 8:223-242

DOI 10.1007/s11760-013-0538-y



 Springer

Your article is protected by copyright and all rights are held exclusively by Springer-Verlag London. This e-offprint is for personal use only and shall not be self-archived in electronic repositories. If you wish to self-archive your article, please use the accepted manuscript version for posting on your own website. You may further deposit the accepted manuscript version in any repository, provided it is only made publicly available 12 months after official publication or later and provided acknowledgement is given to the original source of publication and a link is inserted to the published article on Springer's website. The link must be accompanied by the following text: "The final publication is available at link.springer.com".



Robust algorithm for broad impulse noise removal utilizing intensity distance and intensity height methodologies

Sin Hoong Teoh · Haidi Ibrahim

Received: 26 January 2013 / Revised: 19 June 2013 / Accepted: 8 August 2013 / Published online: 24 August 2013
© Springer-Verlag London 2013

Abstract In this manuscript, a new algorithm to reduce impulse noise from digital images has been proposed. This algorithm is based on switching median filtering approach, and therefore, it can be generally divided into two main stages; impulse noise detection stage and impulse noise cancellation stage. Modifications towards a well-known boundary discriminative noise detection method have been made. First, rather than using any sorting algorithm, we determine the local median values from manipulated local histograms. This solution makes the execution of the algorithm faster. Next, in the noise detection stage, in addition to the originally proposed intensity distance differential approach, the new method includes intensity height differential approach to reduce false detection rate. Then, instead of using adaptive approach in noise cancellation stage, our approach uses iterative approach, which has better local content preservation ability. Broad impulse noise model has been employed in this experiment. Based on the evaluations from root mean square error, false positive detection rate, false negative detection rate, mean structure similarity index, processing time, and visual inspection, it is shown that the proposed method is the best method when compared with seven other state-of-the-art median filtering techniques.

Keywords Digital image processing · Impulse noise · Salt-and-pepper noise · Switching median filter · Impulse noise detection · Impulse noise cancellation

1 Introduction

Impulse noise appears as a sprinkle of bright and dark spots on digital images. Normally, these spots have relatively high contrast towards the relatively clean, uncorrupted surrounding area [1]. Even at low corruption level, impulse noise can significantly degrade the appearance and quality of the image [2]. Several impulse noise models can be found in the literature. Each of these impulse noise models are presented by unique mathematical equations. Examples of impulse noise models are salt-and-pepper impulse noise and uniform impulse noise [3].

A popular solution to deal with impulse noise is by using rank-order filters, also known as order-statistic filters. These type of filters are nonlinear and work in spatial domain. They use a sliding window approach, where at each sliding iteration, only the restored value for the pixel corresponding to the centre of the window is determined. This restored value is obtained from the ordered intensity values of the pixel samples contained within the area defined by the sliding window [4]. To facilitate ordered intensity values, sorting algorithm, which sorts the sample into an ascending or descending order, mostly were used [5].

Among the rank-order filters, median-based filters are the most popular techniques to reduce impulse noise. Generally, median filters use the median value in its filtering process [4]. The median value \tilde{X} of a sample is defined as [6]:

$$\tilde{X} = \begin{cases} X_{(n_s+1)/2} & : n_s \text{ is odd} \\ 0.5 (X_{n_s/2} + X_{(n_s+1)/2}) & : n_s \text{ is even} \end{cases} \quad (1)$$

where X_1, X_2, \dots, X_{n_s} are the intensity values, arranged in either increasing or decreasing order, and n_s is the size of the sample.

Standard median filter (SMF), or also known as median smoother, has been introduced by Tukey in 1971 [7]. The

S. H. Teoh · H. Ibrahim (✉)
School of Electrical and Electronic Engineering, Engineering Campus,
Universiti Sains Malaysia, 14300 Nibong Tebal, Penang, Malaysia
e-mail: haidi_ibrahim@ieee.org

filtered image $\mathbf{F} = \{F(i, j)\}$ from SMF can be defined by the following equation [4]:

$$F(i, j) = \text{median}_{(k,l) \in W_{h,w}} \{D(i+k, j+l)\} \quad (2)$$

where \mathbf{D} is the image affected by impulse noise, and $W_{h,w}$ is a sliding window of size $h \times w$ pixels centred at coordinates (i, j) . The median value is calculated by using Eq. (1) with $n_s = h \times w$. Although SMF is able to remove impulse noise, it requires a large filter size when the corruption level is high. Unfortunately, this condition will result in a significant distortion to the image [8]. Furthermore, because SMF does not differentiate between uncorrupted from corrupted pixels, all pixels within the image will be processed. As the uncorrupted pixels are also modified, SMF produces unnecessary changes. Local details, especially thin lines and sharp corners, will be destroyed [9].

In order to improve the performance of SMF, many types of modification towards median filtering have been proposed. Research on impulse noise suppression using median filters are expanding at a very rapid pace. Many new median filtering systems have been proposed in recent years. In general, these modifications can be classified into seven common frameworks [10]. They are weighted median filter, iterative median filter, recursive median filter, directional median filter, switching median filter, adaptive median filter, and median filter incorporating artificial intelligence, including fuzzy logics. However, most of the current median filter methods utilize more than one filtering framework.

Pixel correlation-based impulse noise reduction filter (PCINRF) has been introduced by Song et al. [11]. This method follows the switching median filter methodology, and thus, its implementation can be divided into two stages: impulse noise detection and impulse noise cancellation. Its noise mask is generated from a comparison between an SMF filtered image \mathbf{E} with the input noise affected image \mathbf{D} and binary mathematical morphology operation. The impulse noise cancellation stage utilizes adaptive median filtering framework, where the size of the filter gradually increases from 3×3 pixels until there is at least one uncorrupted pixel candidate within the filtering samples. The restored value given to the corrupted pixel candidate is either the arithmetic mean or the median value, depending on the correlation between the pixels at that position. Yet, as the noise detection stage employs local intensity minimum and maximum values, this method is effective towards salt-and-pepper noise only.

Improved Median Filter (IMF) has been developed by Deivalakshmi et al. [12]. This filter also uses the switching median filtering framework. The main aim of this filter is to restore digital images, which have been corrupted by a severe degree of salt-and-pepper noise. IMF targets to reduce false positive detection of noise candidates in its first stage.

By doing so, it is expected that this noise filtering filter is able to maintain most of the image details. However, IMF is only suitable for salt-and-pepper noise because only pixels with intensity values 0 and 255 are evaluated during its noise detection stage.

Adaptive fuzzy switching filter (AFSF) is a new improvement of median filter introduced by Saradhadevi and Sundaram [13]. First, fuzzification process of the corrupted image \mathbf{D} is carried out. Using the directional median filtering framework, at each location (i, j) , AFSF convolves the image with four one-dimensional Laplacian operators of size five pixels and produces four values. The minimum absolute value obtained from this convolution is assigned to fuzzy noise value, which will be used for impulse detection process. Unfortunately, this noise detection scheme is only useful when the noise pixel has a significant contrast towards its neighbours.

Modified decision-based un-symmetric trimmed median filter (MDBUTMF) has been introduced by Esakkirajan et al. [14]. MDBUTMF is also can be considered as a switching median filter. This filter is simple and named as trimmed median filter because the noise candidate samples are not included in the filtering process. It is named un-symmetric because the amount of salt noise mostly will not be equal to the amount of pepper noise within the filtering window, which results in unequal trimming at the end of the sorted sample. Because MDBUTMF takes only pixels with intensity value 0 and 255 as its noise candidates, same as IMF, this method is not fit for all types of impulse noise, but only good for salt-and-pepper noise.

Advanced boundary discriminative noise detector (ABDND) has been introduced by Tripathi et al. [15]. This filter was designed to deal with a wide range of impulse noise models. ABDND is actually an improved version of a well-known technique developed by Ng and Ma in 2006, called switching median filter with boundary discriminative noise detection (BDND) [16]. Both ABDND and BDND are switching median filtering methods. In its impulse noise detection scheme, ABDND first estimates the global noise range from the image histogram. Next, noise candidates are determined from the local maximum and local minimum values, using a sliding window of size 11×11 pixels. Then, ABDND further refine the impulse noise detection by using an adaptive filtering approach. In its noise cancellation stage, an adaptive filtering approach, as suggested by Nallaperumal et al. [17] has been implemented.

Recently, a new impulse noise reduction technique known as directional switching median filter using boundary discriminative noise detection by elimination (DSMFBDNDE) has been introduced by Nasimudeen et al. [18]. Similar to ABDND, this method is also an extension from BDND method proposed by Ng and Ma [16] and is a switching median filter method. In its noise detection stage, DSMFBD-

NDE uses intensity distance differential approach as used in BDND. The intensity distance differential approach will be presented in Sect. 2.2.1. Furthermore, similar to BDND, its impulse noise cancellation process also utilizes an adaptive filtering scheme. Yet, a directional median filtering framework is also included into this stage. Due to the complexity of the algorithm, DSMFBDNDE will mostly require long processing times.

In this paper, we present a further modification towards BDND method. BDND scheme has been selected as we deal with a wide range of impulse noise models and not only limited to salt-and-pepper noise. We improve the noise detection stage by complementing intensity distance differential approach with a new noise border detection scheme, which we call intensity height differential approach. Modifications to the noise cancellation process have also been included in order to maintain local information contents. This research methodology will be explained in Sect. 2. Then, the experimental results and discussions are given in Sect. 3. Finally, Sect. 4 concludes our findings.

2 Methodology

In general median filtering techniques, in order to produce the filtered image F , the filter processes and alters every pixel in the corrupted image D , even if the pixel is originally clean from noise. As a consequence, this process always causes unnecessary pixel replacement and might further degrades the image. Therefore, to avoid unnecessary pixel alterations, an improved version of median filtering technique is proposed in this paper. From our literature survey, we found that the switching median filtering framework is able to reduce this problem. This approach divides the filtering process into two stages, which are: a noise detection stage and a noise cancellation stage. The output of the noise detection stage is a noise mask M , which is used to indicate the potential noise pixels. The advantages of using this approach as compared to other approaches are the preservation of the local image contents including lines and edges, and also the reduction in processing time for images corrupted by low level of impulse noise. Due to these advantages, a switching median filter approach will be used in the proposed methodology.

In order to ease the presentation of the methodology, this section has been divided into three main subsections. The first section, which is Sect. 2.1, explains the technique implemented in this work to reduce the processing time for calculating the local median values. This basic technique is important as it can reduce the processing time, significantly. The modifications towards BDND have been done in both the

noise detection stage and the noise cancellation stage. These modifications are presented in Sects. 2.2 and 2.3, respectively.

2.1 Faster local median values determination

Most of the median filtering techniques have long processing time. As an example, the switching median filter with boundary discriminative noise detection (BDND) technique, which was originally proposed by Ng and Ma [16], is a computational expensive method. This condition is mostly contributed by the following three main factors [19]:

1. In both the noise detection stage and the noise correction stage, the sorting operations have been employed to determine the local median values.
2. In the noise detection stage, BDND uses two detection windows, which are of size 21×21 pixels and 3×3 pixels, to classify the input pixels to either noise pixel candidates, or noise-free pixel candidates. As the detection process is involving sorting and local median value calculation, and the detection window is relatively large, this process requires long processing time.
3. In noise correction stage, BDND employs an adaptive median filter approach. The filtering window is not been fixed to a certain size, but changing accordingly to the local noise density.

In order to reduce the problems as given by points 1 and 2, sorting operations should be avoided. Even though sorting algorithm can be easily implemented, sorting procedure requires long computational time especially when $W_{h,w}$ is a large filter because the number of pixel samples (i.e., $n_s = w \times h$) is big [20].

In our implementation, we decided to exploit the local histograms in order to find the local median values [21]. At each filter's position (i, j) , a local histogram $H(X)$ is created. Histogram $H(X)$ presents the number of occurrences of intensity X within the contextual region defined by the sliding window at position (i, j) . Then, a local cumulative density function (cdf) is determined. The cdf is defined as:

$$\text{cdf}(X) = \frac{1}{n_s} \sum_{x=0}^X H(x) \quad (3)$$

where n_s is the number of samples within the contextual region that contribute to the calculation of the median value. The median value is identified as the intensity value X where the cdf is first reaching the value equal or greater to 0.5. The process of finding \bar{X} from $\text{cdf}(X)$ is presented by Algorithm 1.

Algorithm 1 Median Value from Local Histogram

Require: Accumulator = Acc_{cdf} .
 Number of samples = n_s .
Input: Local histogram H using the pixel intensity samples defined by the sliding window of size $h \times w$ pixels at position (i, j) .
Output: Local median value \bar{X} .
Note: This is for the case of an 8-bit-depth grayscale image.
 {Calculate n_s }
 1: $n_s = h \times w$, {Find \bar{X} }
 2: $Acc_{cdf} = 0$,
 3: $\bar{X} = 0$,
 4: **for** $X = 0 \rightarrow 255$ **do**
 5: $Acc_{cdf} \leftarrow Acc_{cdf} + H(X)$
 6: **if** $Acc_{cdf} \geq 0.5 \times n_s$ **then**
 7: $\bar{X} = X$,
 8: **Break**,
 9: **end if**
 10: **end for**

The processing time can be reduced further if the window slides continuously, where the current local histogram can be created from the previous local histogram. The time required to form local histogram can be reduced by using a method proposed by Huang et al. [22], which only updates the changes between two successive contextual regions. Thus, instead of updating $h \times w$ samples, only $2h$ samples need to be updated in each sliding iteration. In order to ensure a continuous trail of the sliding window, in our implementation, the window moves from left to right for the odd numbered rows, and from right to left for the even numbered rows. The calculation of the median value by using this method is faster than when the new local histogram is developed from the whole contextual region.

2.2 Impulse noise detection stage

The common problem of noise detection stage is the wrong classification of the image pixels. Some uncorrupted pixels might be detected as noise pixel candidates. If the uncorrupted pixels are treated as noise pixel candidates, they will then be unnecessarily processed at the noise cancellation stage, making the object details become blur. This problem always happens when processing the object edges in the image. On the other hand, if the noise pixels are treated as uncorrupted pixels, they will not be processed in the noise cancellation stage. As a consequence, the noise pixels are not been removed successfully from the image. This can be observed when the corruption level is high, where the number of noise pixels in the image is huge. Therefore, to reduce the faulty noise detection and to increase the efficiency of the impulse noise reduction filter, a method which focuses on the wrong detections and missed detections should be designed.

The proposed noise detection scheme employs two techniques, known as intensity distance differential approach,

and intensity height differential approach. To ease the understanding, the basic concept of intensity distance differential approach is first introduced in Sect. 2.2.1. Next, the concept of intensity height differential method is briefly described in Sect. 2.2.2. Then, the proposed noise detection scheme will be properly described in Sect. 2.2.3.

2.2.1 Intensity distance differential approach

Many studies have been done by other researchers in recent years to improve the noise detection process. This is because the successfulness of the detection stage is indeed a very crucial factor to produce a more accurate result of F , with less unwanted pixel alterations and better local contents preservation. One of the successful noise detection techniques has been introduced in BDND [16]. BDND has been designed to deal with a wide range of impulse noise models, and utilizing intensity distance differential approach in its impulse noise detection stage.

This approach assumes that the intensity values representing the impulse noise pixels are unique and different from the intensity values presenting the uncorrupted clean pixels. It also assumes that the noise intensities are located at the extreme both left and right regions of the histogram of the damaged image D , as shown in Fig. 1. Based on these assumptions, by using a sliding impulse noise detection window, at each position (i, j) , the intensity distance differential approach estimates the noise ranges for both ends by finding two intensity boundaries. The noise boundary 0 (B_0) is the boundary for the lower impulse noise, while the noise boundary 1 (B_1) is the boundary for the upper impulse noise. Then, the approach uses these two boundaries to separate the clean pixels from the corrupted pixels.

In order to find the impulse noise boundaries, the original work by Ng and Ma [16] uses a sorting algorithm. First,

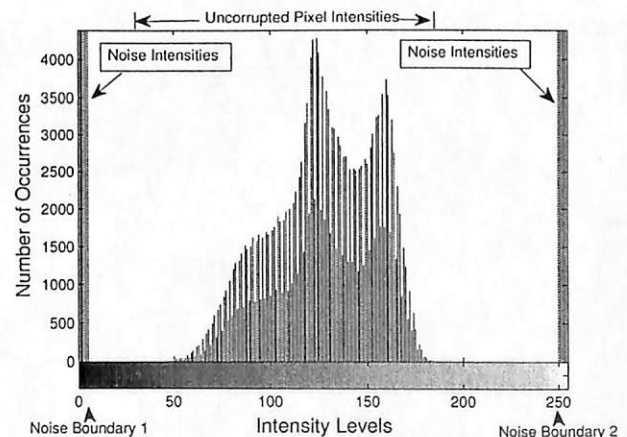


Fig. 1 Example of image histogram with well-defined noise boundaries

the method sorts the samples defined by the sliding window in ascending order, and the median value \bar{X} is found. This sorted samples are saved as vector v_O . Next, the difference vector v_D is then obtained from v_O . Vector v_D is defined as the intensity difference between each pair of adjacent pixels in v_O (i.e., $v_D(i) = v_O(i + 1) - v_O(i)$). The length of v_D is one sample less than v_O . After that, the intensity distance differential method inspects the samples in v_O with intensities between 0 to \bar{X} , and search for the maximum value in v_D within the same range. The intensity value that fulfils this condition is defined as the lower impulse noise boundary value B_0 . Similar approach has been used to determine the upper impulse noise boundary B_1 . However, the searching involves the intensities between \bar{X} to the maximum intensity value of the sample.

When the detection filter size is big, the original intensity distance differential method requires a long processing time to create v_O and v_D . To generate v_O , sorting algorithm is used. To generate v_D , the difference between each pair of samples need to be determined. Therefore, in order to reduce the computational time requirement by the intensity distance differential method, the implementation will be based on the local histogram. As already described in Sect. 2.1, local histograms can be obtained quickly with proper implementation.

As in our implementation we utilize local histograms $H(X)$ to find \bar{X} , vector v_O is been replaced by $H(X)$. Furthermore, the requirement to generate v_D is can also be removed. From $H(X)$, a set of intensity differential values Δ_X is determined. This value is defined as a gap value between two successive non-empty histogram bins. Next, the approach determines the lower impulse noise boundary value B_0 by finding the intensity value X , in the range from intensity 0 to \bar{X} , which generates the maximum Δ_X value. Similarly, the method finds the higher impulse noise boundary value B_1 by searching for the maximum Δ_X from \bar{X} to the maximum intensity value within the sample. As this solution does not require a sorting operation, and the size of Δ_X is smaller than v_D , the utilization of local histograms will give the same values for B_0 and B_1 , but with less computational time. This process is summarized by Algorithm 2.

2.2.2 Intensity height differential approach

Although the intensity distance differential method is able to detect the impulse noise boundary, it is only effective when the noise intensities are unique and differ from the intensities of the uncorrupted pixels, as shown in Fig. 1. However, when the regions of impulse noise with uncorrupted pixels overlap with each other in the histogram, intensity distance differential methods mostly fail to detect the impulse noise boundaries. This condition might happen when the noise spread factor m is large or when the uncorrupted pixel intensities

Algorithm 2 Intensity Distance Differential Approach

Require: Previous non-empty histogram bin = H_p .
 Current non-empty histogram bin = H_c .
 Intensity differential value = Δ_X .
 Maximum difference = \max_{Δ} .
Input: Local histogram H and median value \bar{X} using the pixel intensity samples defined by the sliding window of size $h \times w$ pixels at position (i, j) .
Output: Lower impulse noise boundary B_0 and higher impulse noise boundary B_1 .
Note: This is for the case of an 8-bit-depth grayscale image.
 {Initialize H_p .}
 1: for $X = 0 \rightarrow \bar{X}$ do
 2: if $H(X) \neq 0$ then
 3: $H_p = X$,
 4: Break;
 5: end if
 6: end for
 {Find B_0 .}
 7: $\max_{\Delta} = 0$,
 8: $B_0 = \bar{X}$,
 9: for $X = H_p + 1 \rightarrow \bar{X}$ do
 10: if $H(X) \neq 0$ then
 11: $H_c = X$,
 12: $\Delta_X = H_c - H_p$,
 13: if $\Delta_X > \max_{\Delta}$ then
 14: $\max_{\Delta} \leftarrow \Delta_X$,
 15: $B_0 \leftarrow H_p$,
 16: end if
 17: $H_p \leftarrow H_c$,
 18: end if
 19: end for
 {Reinitialization of H_p .}
 20: for $X = 255 \rightarrow \bar{X}$ do
 21: if $H(X) \neq 0$ then
 22: $H_p = X$,
 23: Break;
 24: end if
 25: end for
 {Find B_1 .}
 26: $\max_{\Delta} = 0$,
 27: $B_1 = 255$,
 28: for $X = 255 \rightarrow \bar{X}$ do
 29: if $H(X) \neq 0$ then
 30: $H_c = X$,
 31: $\Delta_X = H_c - H_p$,
 32: if $\Delta_X > \max_{\Delta}$ then
 33: $\max_{\Delta} \leftarrow \Delta_X$,
 34: $B_1 \leftarrow H_c$,
 35: end if
 36: $H_p \leftarrow H_c$,
 37: end if
 38: end for

occupy the whole dynamic range of the histogram, as shown in Fig. 2.

In order to deal with the situations as shown in Fig. 2, an approach known as intensity height differential has been introduced in this work. This approach is presented as Algorithm 3. This approach is actually similar to the intensity distance differential approach, except that the intensity height difference Δ_H is defined as the bin's height difference

Algorithm 3 Intensity Height Differential Approach

```

Require: Previous non-empty histogram bin =  $H_p$ .
Current non-empty histogram bin =  $H_c$ .
Intensity height difference =  $\Delta_H$ .
Maximum difference =  $\max_{\Delta}$ .
Input: Local histogram  $H$  and median value  $\bar{X}$  using the pixel intensity samples defined by the sliding window of size  $h \times w$  pixels at position  $(i, j)$ .
Output: Lower impulse noise boundary  $B_0$  and higher impulse noise boundary  $B_1$ .
Note: This is for the case of an 8-bit-depth grayscale image.
{Initialize  $H_p$ .}
1: for  $X = 0 \rightarrow \bar{X}$  do
2:   if  $H(X) \neq 0$  then
3:      $H_p = X$ ,
4:     Break;
5:   end if
6: end for
{Find  $B_0$ .}
7:  $\max_{\Delta} = 0$ ,
8:  $B_0 = \bar{X}$ ,
9: for  $X = H_p + 1 \rightarrow \bar{X}$  do
10:  if  $H(X) \neq 0$  then
11:     $H_c = X$ ,
12:     $\Delta_H = H(H_c) - H(H_p)$ ,
13:    if  $\Delta_H > \max_{\Delta}$  then
14:       $\max_{\Delta} \leftarrow \Delta_H$ ,
15:       $B_0 \leftarrow H_p$ ,
16:    end if
17:     $H_p \leftarrow H_c$ ,
18:  end if
19: end for
{Reinitialization of  $H_p$ .}
20: for  $X = 255 \rightarrow \bar{X}$  do
21:  if  $H(X) \neq 0$  then
22:     $H_p = X$ ,
23:    Break;
24:  end if
25: end for
{Find  $B_1$ .}
26:  $\max_{\Delta} = 0$ ,
27:  $B_1 = 255$ ,
28: for  $X = 255 \rightarrow \bar{X}$  do
29:  if  $H(X) \neq 0$  then
30:     $H_c = X$ ,
31:     $\Delta_H = H(H_c) - H(H_p)$ ,
32:    if  $\Delta_H > \max_{\Delta}$  then
33:       $\max_{\Delta} \leftarrow \Delta_H$ ,
34:       $B_1 \leftarrow H_c$ ,
35:    end if
36:     $H_p \leftarrow H_c$ ,
37:  end if
38: end for
    
```

between two successive non-empty histogram bins. Therefore, this approach complements the weakness associated with the intensity distance differential approach.

2.2.3 The proposed impulse noise detection method

Following the basic methodology of a switching median filter, the output of the impulse noise detection stage is a noise

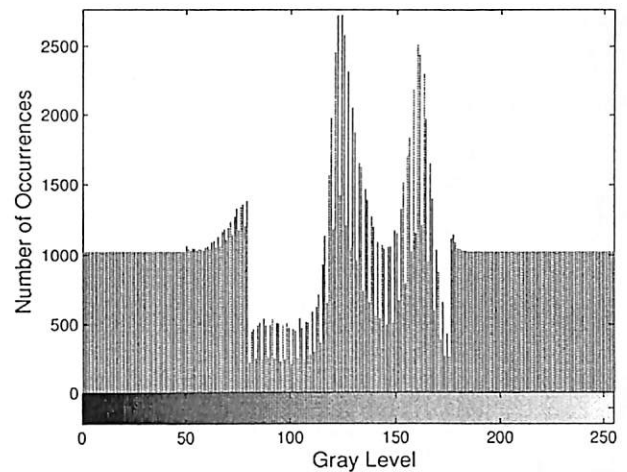


Fig. 2 Examples of image histogram with unclear impulse noise intensity boundaries

mask M , which classifies the pixels into either noise pixel or noise-free pixel candidates. In our implementation, $M(i, j)$ is set to 1 for noise candidate, and 0 for noise-free candidate. The overall block diagram of the proposed noise detection scheme, for detecting an impulse noise from image D at coordinates (i, j) , is summarized by Fig. 3.

The proposed impulse noise detection process in this method uses two detection windows: a coarse noise detection window and a fine noise detection window. The coarse noise detection window is of size 21×21 pixels. This size of detection window has been chosen to be exactly the same as the one used in BDND [16] and other BDND median filtering based methods, such as DSMFBDNDE [18]. On the other hand, the fine noise detection window is of size 3×3 pixels. This small window size is chosen in order to maintain the locality of the image information.

In Fig. 3, noise borders with subscript 0 correspond to the lower intensity impulse noise borders, while noise border with subscript 1 correspond to the higher intensity impulse noise borders. Noise borders with subscript $_Distance$ are obtained from intensity distance differential method, whereas subscript $_Height$ presents intensity height differential method. Subscript $_Coarse$ presents the borders obtained using a detection window of size 21×21 pixels, and subscript $_Fine$ presents the borders from a detection window of size 3×3 pixels. For example, $B_{0_Distance_Coarse}$ is a lower impulse noise boundary, obtained from intensity distance differential approach, using the coarse detection window.

The noise detection process as given by the flowchart in Fig. 3 has been designed in order to successfully detect various type of impulse noise. Unlike the original BDND method [16], the proposed method uses both intensity distance differential method and intensity height differential method. As the

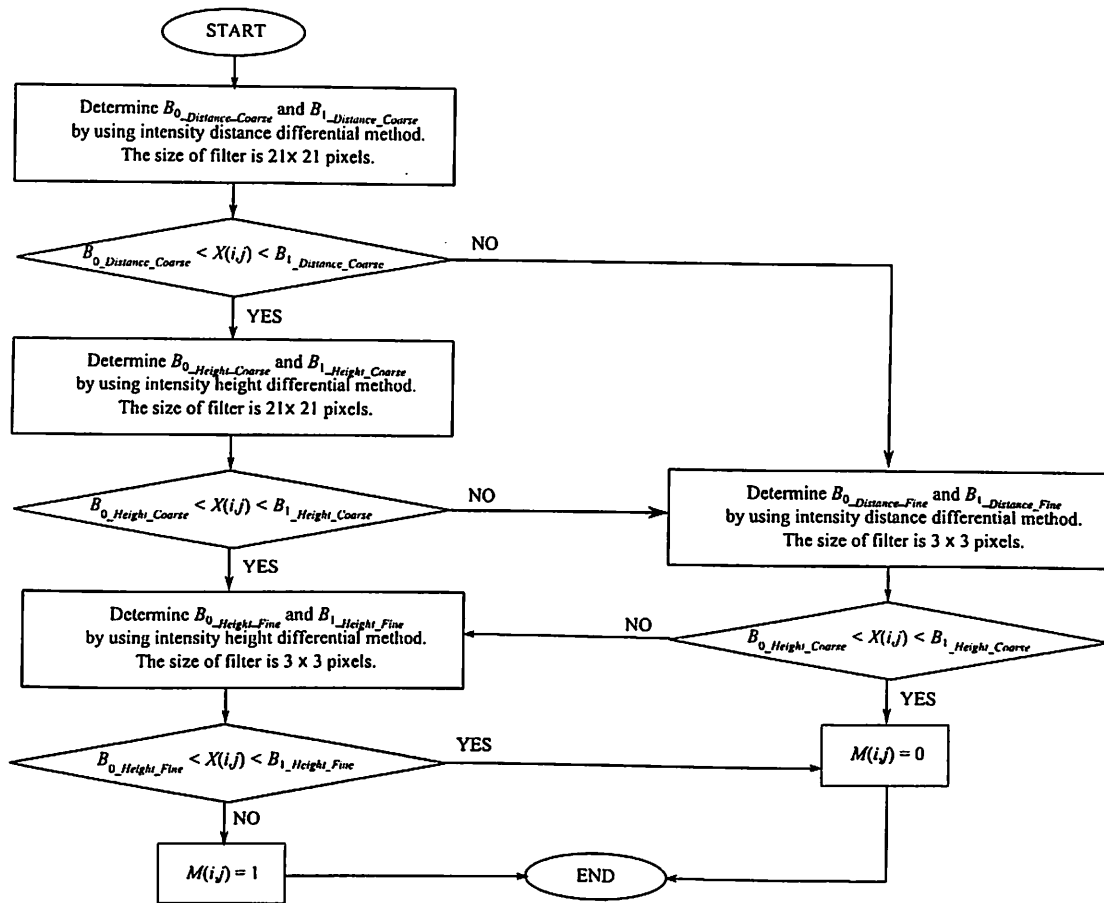


Fig. 3 Block diagram presenting the noise detection process for pixel $D(i, j)$

process starts with intensity distance differential approach, it can be assumed that the proposed method does the detection for the salt-and-pepper noise first. The method then refines the finding to avoid noise miss-detection. This is carried out by using the smaller noise detection window, or detecting impulse noise with larger noise spread factor m using intensity height differential approach. Using this new noise detection scheme, a pixel will go through at least two, and at most three, noise detection windows before it is classified as a noise pixel candidate or a noise-free pixel candidate. Yet, the approach described in Sect. 2.1 has been implemented. This method requires a continuous window sliding for local histogram creation, but creates local histograms with low computational burden. Therefore, some processing time can be saved by this approach.

2.3 Impulse noise cancellation stage

Although BDND filtering method [16], and its derivative methods such as ABDND [15] and DSMFBDNDE [18] use adaptive median filtering approach in their noise cancellation

stage, the proposed method utilizes iterative median filtering method. As compared to adaptive filtering approach, iterative approach normally uses small filter therefore needs shorter processing time. Furthermore, small filter size enables the method to maintain local features and corners in the image.

In this proposed method, noise cancellation filter of size 3×3 has been used. At the beginning of the execution of this stage, the method is required to check whether all pixels in the image are clean pixels or not. This can be verified by inspecting M . If there is no noise pixel candidate found on the image, the following condition is obtained:

$$\sum_{i=0}^J \sum_{j=0}^K M(i, j) = 0 \tag{4}$$

which means that there is 0% of impulse noise candidate on the image. With this initial condition, the output image F then is the input image D itself, as no correction is required to be done.

When the condition given by Eq. (4) is not met, noise cancellation process needs to be carried out. First, a temporary noise mask M' is created, as a copy to the original noise mask

M. Mask **M** is used to determine noise-free pixel candidates for the median calculation, while **M'** is used to mark those pixels that have been processed in that iteration.

In this process, by following the basic framework of the switching median filter, only pixels marked as noise candidates (i.e., $M'(i, j) = 1$) will be processed by the noise cancellation filter of size 3×3 pixels. The restored value to **F** is calculated as the median value of the noise-free candidates (i.e., indicated by $M(i, j) = 0$) within the filtering window. Then, $M'(i, j)$ is set to 0, to indicate that the pixel has been cleaned. However, if the samples defined by the filtering window at coordinates (i, j) are all noise pixel candidates, then, the pixel will be processed on the next iteration. For this case, $M'(i, j)$ maintains its original value, which is value 1. At the end of each iteration, the content of **M'** is copied back to **M**. Next, the method checks whether there is still unprocessed noise pixel candidate by using Eq. (4). If there is still unprocessed noise pixel, **D** takes the values from **F**, and the cycle repeated until there is no more unprocessed noise pixel left.

3 Experimental results and discussions

This section presents the restoration results obtained by using the proposed method that has been explained in Sect. 2. In addition to the proposed method, seven other state-of-the-art median filtering based methods were also been implemented for the purpose of benchmarking. These methods are SMF of size 3×3 pixels (SMF3) [4], PCINRF [11], IMF [12], AFSF [13], MDBUTMF [14], ABDND [15], and DSMFBDNDE [18]. A brief introduction to these methods has been given in Sect. 1.

This chapter has been divided into four main sections. First, Sect. 3.1 presents the noise model used in this experiment. Next, the test image used for this evaluation purpose is presented in Sect. 3.2. Then, the performances of the proposed method are judged objectively by using several quality measures in Sect. 3.3. Finally, in Sect. 3.4, the output images are judged subjectively based on visual inspection.

3.1 Impulse noise model

Impulse noise can be modelled by several equations [3]. However, in this research work, a broad impulse noise model has been used. This broad impulse noise model is defined as:

$$p(D) = \begin{cases} P/2m & : \text{pepper}; 0 \leq D < m \\ 1 - P & : \text{noise-free pixels}; 0 \leq D \leq L - 1 \\ P/2m & : \text{salt}; L - 1 - m < D \leq L - 1 \end{cases} \quad (5)$$

where P (i.e., $0 \leq P \leq 1$) presents the noise density, $p()$ is the probability density function, and L is the quantization level of the image. For an 8-bit-depth grayscale image, L

is equal to 256. This equation allows the impulse noise to be presented by two intensity ranges, where each range is presented by m intensity levels. In this paper, m is called as the noise spread factor.

The reason why we choose this noise model is because Eq. (5) is able to cover a wide range of impulse noise models. When m is equal to 1, this impulse noise is equal to the salt-and-pepper noise. On the other hand, when m is equal to $L/2$ (or 128 for this work), this impulse noise is equivalent to the random-valued impulse noise. In addition to m , this noise model also allows P to be tuned. In this experiment, we had tried all the ninety possible combinations between ten P values (i.e., $P = 0, 10, 20, 30, \dots, 90\%$) with nine m values (i.e., $m = 1, 16, 32, 48, 64, 80, 96, 112, 128$). It is worth noting that as far as our concern, there is no other literature up to date that does such thorough evaluation as we did in this paper.

3.2 Input test image data

In order to present a wide range of images, the test image used in this experiment is a composite image. This test image is created by using 13 individual standard grayscale images that are normally used in digital image noise reduction field. This composite image is shown in Fig. 4. The size of this image is 2048×2048 pixels, which is equivalent to 4 Megapixels image. There are four images with size 256×256 pixels, seven images with size 512×512 pixels, and two images with size 1024×1024 pixels. Therefore, the test image is adequate to represent images of different sizes. As shown by

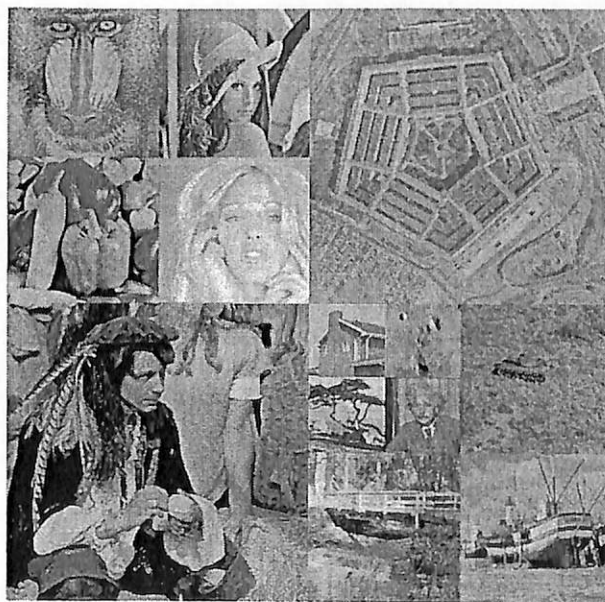


Fig. 4 The composite image used as the test image in this work

this figure, the content of each figure is also different from each other. For example, *Baboon* image contains more details as compared with *Peppers* image, and *Lena* image is darker than *Tiffany* image. Thus, the test image also presents a wide range of image details.

3.3 Evaluations based on qualitative measures

Five quality measures have been used in this work to evaluate the performance of the proposed method as compared with seven other median filtering techniques. These measures are the root mean square error (RMSE), false positive detection, false negative detection, mean structure similarity index

(MSSIM), and processing time. The results are presented in the following subsections.

3.3.1 Root mean square error (RMSE)

Root mean square error (RMSE) is one of the popular objective measures used in digital image noise reduction researches. This measure indicates how much the similarity between the filtered image F , as compared to the ideal clean image C . In this experiment, image C , which has been shown in Fig. 4, is corrupted by impulse noise with different degree of P and m , produces damaged image D . Then, by filtering image D by noise reduction filter, image F is obtained.

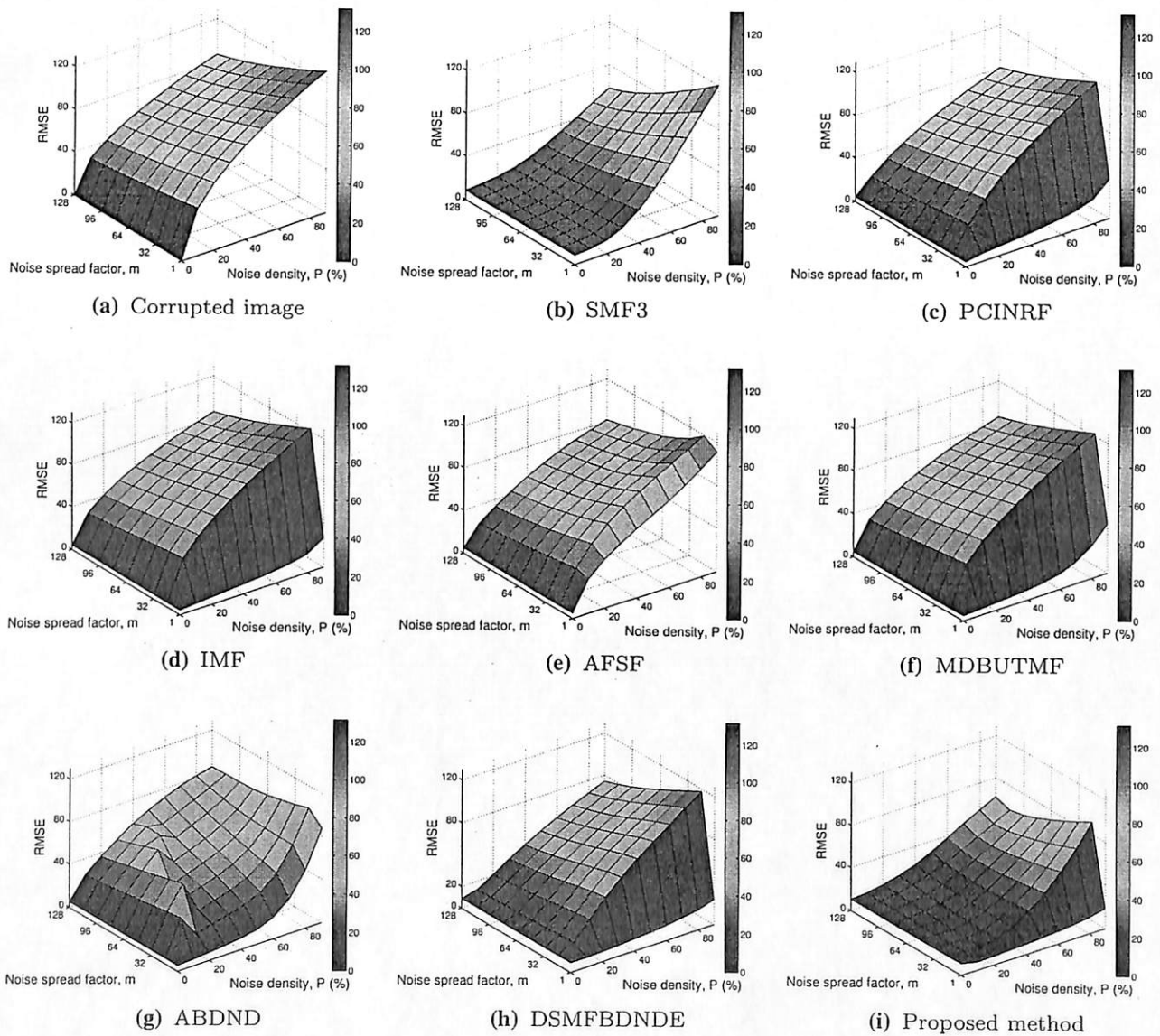


Fig. 5 RMSE surface plots

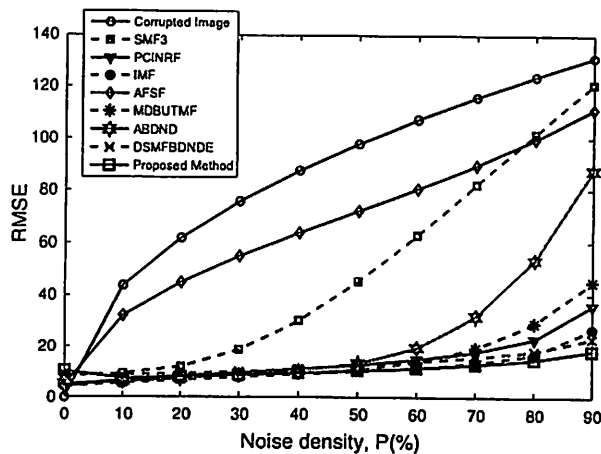


Fig. 6 Plot of RMSE values when $m = 1$

For image with size $J \times K$ pixels, RMSE is defined as:

$$RMSE = \sqrt{\frac{1}{J \times K} \sum_{j=1}^J \sum_{i=1}^K |F(i, j) - C(i, j)|^2} \quad (6)$$

A good impulse noise reduction technique will restore image D so that the filtered image F will be closely resemble image C . This similarity makes the difference between F and C small. Therefore, a good impulse noise reduction technique will produce a small RMSE value.

The surface plots of RMSE values are shown in Fig. 5. All of these surface plots are using the same scale. Figure 5a is the surface plot for the corrupted image D . This is obtained by replacing $C(i, j)$ by $D(i, j)$ in Eq. (6). In this figure, as expected, RMSE values are relatively small when P is low, and exponentially increased when P increased. This is because, when P is small, only a few pixels are altered and not having the same intensity values with C . When P is equal to zero, there is no corruption, and therefore, D is equal to C . As a consequence, as shown by Fig. 5a, RMSE values for this case are equal to zero. As P increased, the number of pixels with different intensity values from C is also increased and therefore increases the RMSE value.

It is worth noting that in Fig. 5, all of the evaluated methods in this paper, have non-zero RMSE values when P equal to zero. This situation indicates that the methods do the unnecessary alterations on the image, even though the image is clean from noise. This shows the weaknesses of the method to identify the noise pixel candidates correctly.

Comparing Fig. 5c, d, f, h, with a, we can see that PCINRF, IMF, MDBUTMF, and DSMFBNDDE do not change the RMSE value significantly for $m \neq 1$. Figure 5e shows that AFSF fails to reduce the RMSE value. Therefore, AFSF is the worst method tested in this section. On the other hand, as shown in Fig. 5g, i, ABDND and the proposed method drastically reduce the RMSE value. However, in general, the

proposed method has the lowest RMSE values for most of the tested samples.

However, as shown in Figs. 5 and 6, all evaluated method in this paper, except SMF and AFSF, have better performance in terms of RMSE, for salt-and-pepper noise. The values of RMSE when m equal to 1 are significantly low. This is mostly because the pixel corrupted by salt-and-pepper noise is easier to be identified due to its intensity contrast.

3.3.2 False positive detection rate

False positive detections happen when a clean, uncorrupted pixel has been classified as a noisy pixel candidate, when the noise reduction filter processes the corrupted image D . As a consequence, the intensity value of this wrongly identified pixel will be altered during noise cancellation stage. As the intensity value of this pixel is unnecessarily changed, this condition produces a difference between the filtered image F with the ideal clean image C . Therefore, this condition should be avoided, as F may lose some of the image details.

The false positive detection rate is used in this work to evaluate the performance of noise detection ability of the method. This measure is defined as:

$$\text{False positive detection} = \frac{N_c}{J \times K} \times 100\% \quad (7)$$

where N_c is the number of clean pixels wrongly detected as noisy pixels. Thus, as a good noise reduction method should minimize the number of false positives, a good noise reduction method should have a low false positive detection rate.

In order to determine the false positive detection rate of an image, three noise masks (i.e., M_1 , M_2 , and M_3) are created. The values of these masks are initially set to 0. During the creation of image D , for each coordinates (i, j) where noise is added to image C , mask M_1 is marked true (i.e., $M_1(i, j) = 1$). During the noise detection process on image D , M_2 is marked true (i.e., $M_2(i, j) = 1$) for each detected noise pixel candidates. After these two noise masks are created, mask M_3 is defined as:

$$M_3(i, j) = \begin{cases} 1 & : M_1(i, j) = 0 \text{ and } M_2(i, j) = 1 \\ 0 & : \text{otherwise} \end{cases} \quad (8)$$

Then, the number of clean pixels wrongly detected as noise pixel candidates, which will be used in Eq. (7), can be determined as follow:

$$N_c = \sum_{i=1}^J \sum_{j=1}^K M_3(i, j) \quad (9)$$

Surface plots for false positive rates are shown in Fig. 7. As shown by this figure, SMF3 has the highest false positive rate. This is because, SMF treats all pixels in D as noisy

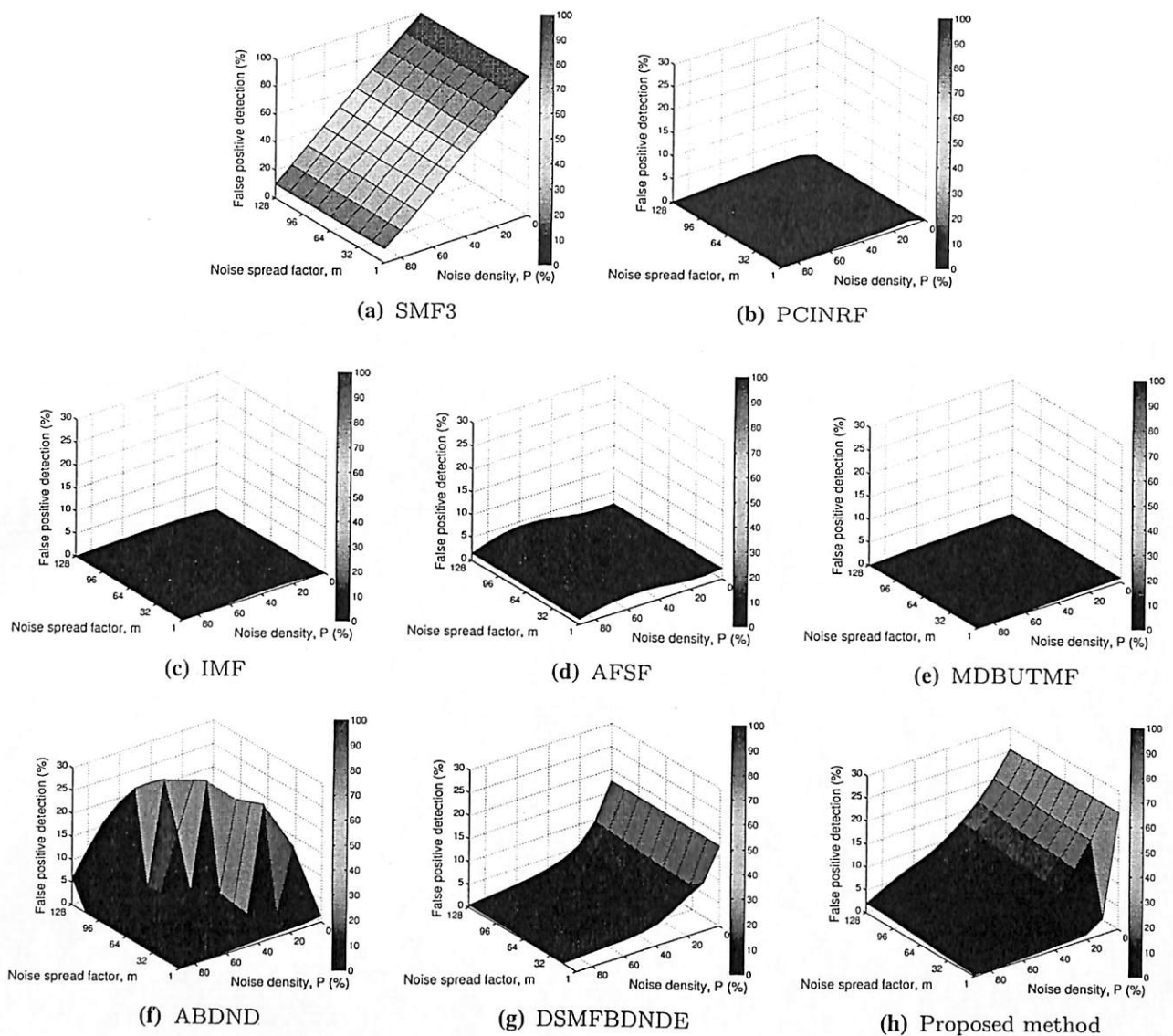


Fig. 7 False positive detection surface plots

pixel candidates. Therefore, as can be observed in Fig. 7a, SMF3 has high false positive rate when P is low, and low false positive rate when P is high. From this surface plot, we can observe that regardless the value of m , the value of false positive rate for SMF3 is approximately equal to $100 - P$.

PCINRF, IMF, AFSF, and MDBUTMF have relatively low false positive detection rate. The magnitude of false detection rate for these methods, for all tested samples, is less than 5%. Although low false detection rate is desired, further investigation should still be carried out, by using other quality measures. This is to check whether the low false positive detection rate is not because the method does not filter the image.

As shown in Fig. 7f–h, ABDND, DSMFBDNDE, and the proposed method has higher false positive detection rate when P is low. This is mostly because these methods are designed to deal with a high level of corruption. Therefore, at a lower corruption level, these methods tend to consider pixels as noise pixel candidates. ABDND has higher false positive detection rate for random-valued impulse noise (i.e., when m is equal to 128), while DSMFBDNDE has higher false positive detection rate for salt-and-pepper noise (i.e., when m is equal to 1). On the other hand, the proposed method has low false positive detection rate for salt-and-pepper noise. As compared with ABDND, the proposed method has a smoother false positive detection rate surface.

3.3.3 False negative detection rate

False negative detection happens when the method failed to detect corrupted pixels in damaged image **D**. As a consequence of false negative detection, not all the noisy pixels will be cleaned up during noise cancellation process. Therefore, similar to false positive detection rate, false negative detection rate is also used to evaluate the performance of noise detection ability of the method. False negative detection rate is defined as:

$$\text{False negative detection} = \frac{N_n}{J \times K} \times 100\% \tag{10}$$

where N_n is the number of miss-detected noisy pixel. Thus, as a good noise reduction method should minimize its false

negative, a good noise reduction method should have a low false negative detection rate.

In order to determine false positive detection rate of an image, three noise masks (i.e., M_1 , M_2 , and M_3) are created. The values in masks M_1 and M_2 are set exactly the same as described in Sect. 3.3.2. However, mask M_3 is defined as:

$$M_3(t, j) = \begin{cases} 1 & : M_1(t, j) = 1 \text{ and } M_2(t, j) = 0 \\ 0 & : \text{otherwise} \end{cases} \tag{11}$$

Then, the number of undetected noisy pixels, which will be used in Eq. (10), can be determined as follow:

$$N_n = \sum_J \sum_{j=1}^K M_3(t, j) \tag{12}$$

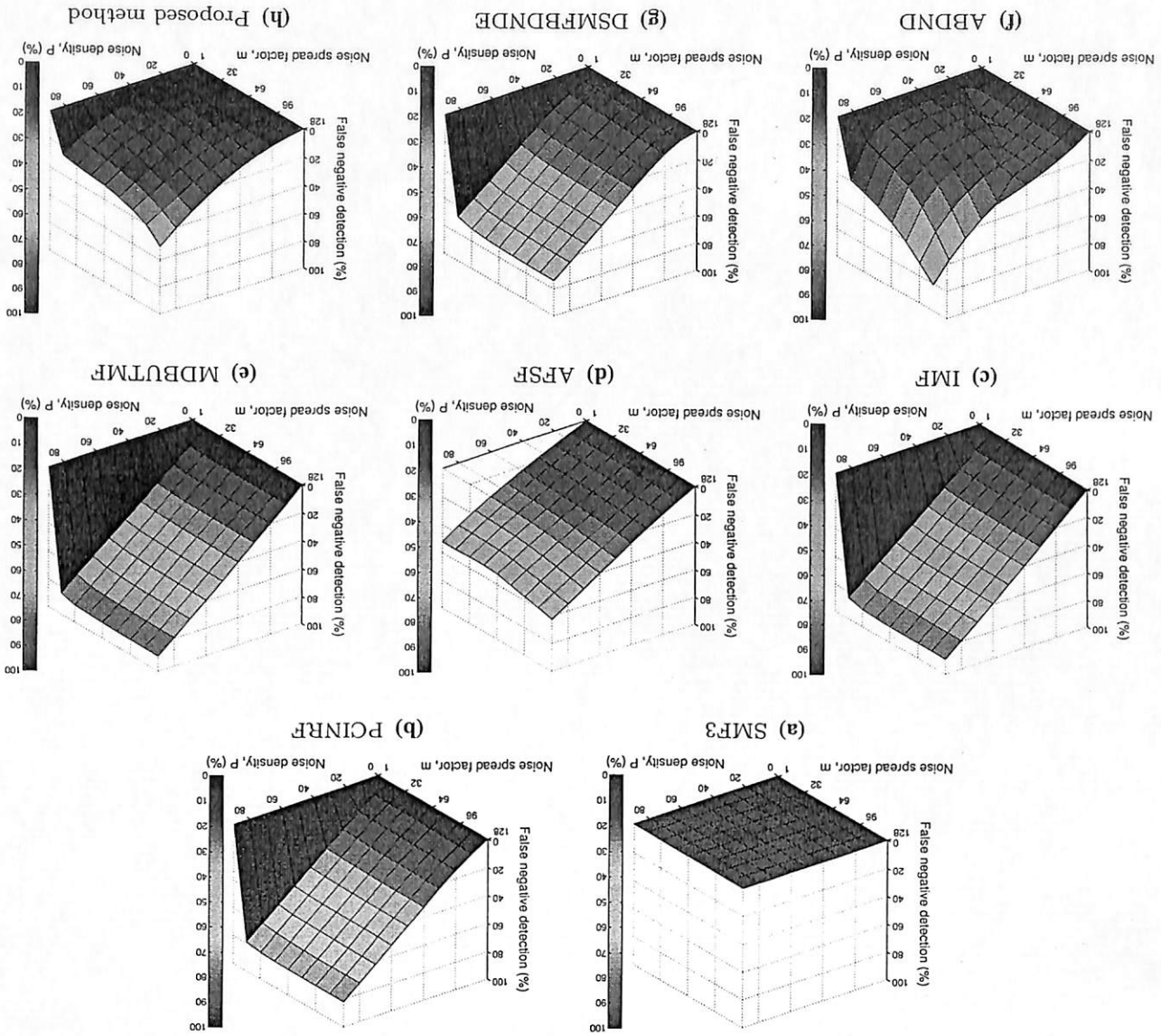


Fig. 8 False negative detection surface plots

Surface plots for false negative detection rate are shown in Fig. 8. As shown by this figure, false negative detection rate for SMF3 is always zero. This is because SMF3 treats all pixels in image **D** as noise pixels. Therefore, all of the actual noise pixels are successfully marked as noisy pixel candidates by SMF3.

In contrary with the results on false positive detection rate, all tested method, except SMF3, have high false negative detection rate when the noise density P is high. This is because when P is high, the number of noise pixels in **D** is also high. Therefore, the probability that the noise pixels will be undetected by the noise detection methods is also increased.

As observed from Fig. 8b, c, e, when $m \neq 1$ (i.e., except salt-and-pepper noise), the false negative detection rate for PCINRF, IMF, and MDBUTMF is almost can be represented as $100 - P$. However, the false positive detection rates for these methods, as can be observed in the corresponding sub-figures in Fig. 7, are very small. These situations indicate that PCINRF, IMF, and MDBUTMF are only work well for salt-and-pepper noise. The similar trend can also be observed in DSMFBDNDE.

In Fig. 8, it is shown that AFSF, ABDND, and the proposed method have low false negative detection rate values. The surface of false negative detection rate for AFSF does not differentiate salt-and-pepper noise, and thus, the surface is more even as compared to others. However, among these three methods, the proposed method has the lowest false negative detection rate at most of the tested samples. Furthermore, similar to ABDND, the proposed method has the high false negative detection rate for highly corrupted random-valued impulse noise. This is may be due that the intensity of the corrupted pixel in **D** is similar to the actual noise-free pixel in image **C**.

3.3.4 Mean structure similarity index (MSSIM)

In order to determine mean structural similarity index (MSSIM) between the filtered image **F** with the ideal clean image **C**, the values of local structural similarity index (SSIM) need to be calculated. The image of size $J \times K$ is divided into blocks of 8×8 pixels, producing $(J/8) \times (K/8)$ non-overlapped sub-images. Then, for each sub-image, indicates by index (i, j) , the value of SSIM is computed by using

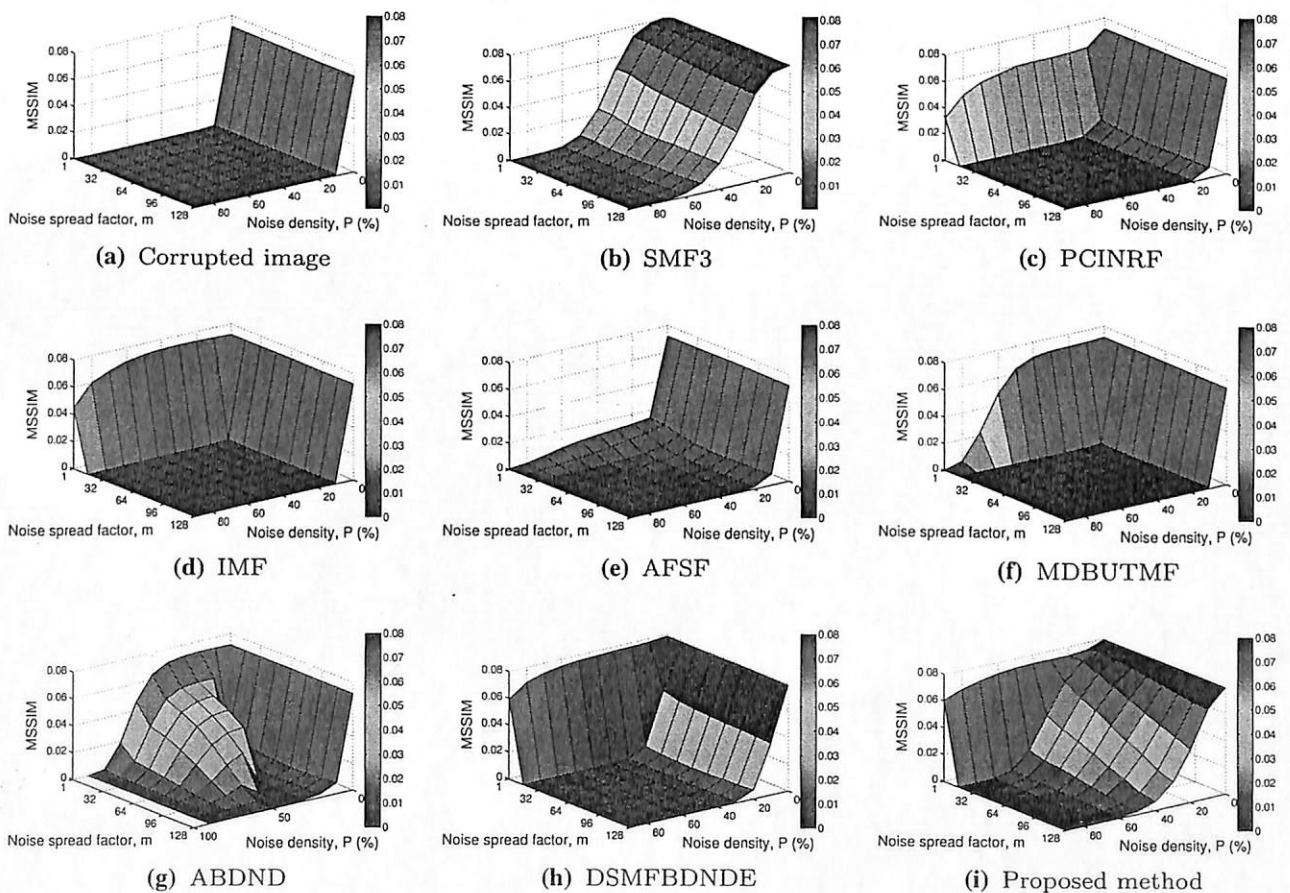


Fig. 9 MSSIM surface plots

the following equations [23]:

$$SSIM(i, j) = \frac{\alpha \times \beta}{\zeta \times \gamma} \quad (13)$$

$$\alpha = (2\mu_C(i, j)\mu_F(i, j) + C_1) \quad (14)$$

$$\beta = (2\sigma_{CF}(i, j) + C_2) \quad (15)$$

$$\zeta = (\mu_C^2(i, j) + \mu_F^2(i, j) + C_1) \quad (16)$$

$$\gamma = (\sigma_C^2(i, j) + \sigma_F^2(i, j) + C_2) \quad (17)$$

where μ_C is the local mean of C , μ_F is the local mean of the restored image F , σ_C is the local standard deviation of C , σ_F is the local standard deviation of F , and σ_{CF} is the local covariance between C and F . These local values are calculated within the sub-image (i, j) . Constant C_1 in this equation is set to $(0.01 \times 255)^2$, while constant C_2 is set to $(0.03 \times 255)^2$. Then, the value of MSSIM is defined as:

$$MSSIM = \frac{g^2}{J \times K} \sum_{i=1}^{J/8} \sum_{j=1}^{K/8} SSIM(i, j) \quad (18)$$

A good noise reduction technique will have a high MSSIM value, as the structures inside image F will be similar to image C .

The surface plots for MSSIM are shown in Fig. 9. As shown in Fig. 9a, the corrupted image D has high MSSIM value only when the noise density P equal to zero. Regardless to noise intensity values, which related to the value of m , the MSSIM values when $P \neq 0$ are almost flat at zero level. This situation indicates that the local structures in D are not anymore similar to the local structures in C , after impulse noise is introduced into the image even at low corruption level.

Figure 9e shows that the MSSIM surface for AFSF is almost similar to Fig. 9a. This means that AFSF cannot restore the image effectively. Figure 9c, d, f, h show that PCINRF, IMF, MDBUTMF, and DSMFBDNDE show only a bit of improvement as compared with AFSF. These methods are just suitable to deal with salt-and-pepper noise (i.e., when m equal to 1). However, when compared Fig. 9b, g, i, it is shown that the proposed method has higher MSSIM values than SMF3 and ABDND for most of the tested samples.

3.3.5 Processing time

Processing time, which is the time needed to complete the filtering process, is used in this work as a measure to indicate the complexity of the method. More complex methods require more processing time. Shorter processing times are desired.

Surface plots of processing time are shown in Fig. 10. As shown by this figure, all methods, except DSMFBDNDE and the proposed method, require less than 5 s to complete the filtering process. However, as indicated by the corresponding

subfigures in Figs. 7 and 8, this short processing time might be due to the failure of the noise detection stage in identifying noisy pixels. Most of these methods have very low false positive detection rate, and high false negative detection rate. This situation indicates that these methods only mark a few pixels as noise pixel candidate. As a consequence, the noise cancellation stage only processes these few pixels and thus requires only a short processing time.

Figure 10g shows that DSMFBDNDE requires the longest processing time. Most of the test samples require more than 2000s (i.e., more than 30 min) to be processed by DSMFBDNDE. This is mostly because DSMFBDNDE uses sorting algorithm for finding median value, and uses relatively large noise detection filter, which is of size 21×21 and 5×5 pixels. On the other hand, as shown by Fig. 10h, although the proposed method requires relatively high processing time compared to the other six noise filtering methods (i.e., for about 10 times longer), the proposed method still has significantly shorter processing time as compared with DSMFBDNDE. Each test sample requires less than 50s (i.e., less than 1 min) to be processed completely by the proposed method.

3.4 Evaluations based on visual inspection

Although there are 90 test samples used to create each surface plot in previous section, only nine sample sets are selected for the visual inspection purpose. These sample sets are shown in Figs. 11, 12, 13, 14, 15, 16, 17, 18 and 19. These nine sample sets are created from a combinations of three values from P (i.e., $P = \{20, 50, 90\} \%$) and three values from m (i.e., $m = \{1, 64, 128\}$). Samples with P equal to 20 % represents low noise corruption, P equal to 50 % represents medium noise corruption, and P equal to 90 % represents high noise corruption. Samples with m equal to 1 are samples with salt-and-pepper noise, while samples with m equal to 128 are samples with random-valued impulse noise.

Figure 11 shows the output images when P equal to 20 % and m equal to 1. In other words, this figure presents the results obtained from filtering an image corrupted by low level of salt-and-pepper noise. Due to this low level of noise corruption, all the tested impulse noise reduction methods, except AFSF method, successfully reduce the impulse noise level from image shown in Fig. 11a. There is no obvious difference between the filtered images with the original uncorrupted image shown in Fig. 4. However, for the case of AFSF method, the output image shown in Fig. 11e still contains impulse noise. Impulse noise can be observed in the region of *Tiffany* sub-image.

The output images when P equal to 50 % and m equal to 1 are shown in Fig. 12. This figure presents the results from medium corruption level of salt-and-pepper noise. As shown by this figure, SMF3 and AFSF are starting to be not able to filter the impulse noise completely. Impulse noise still can be

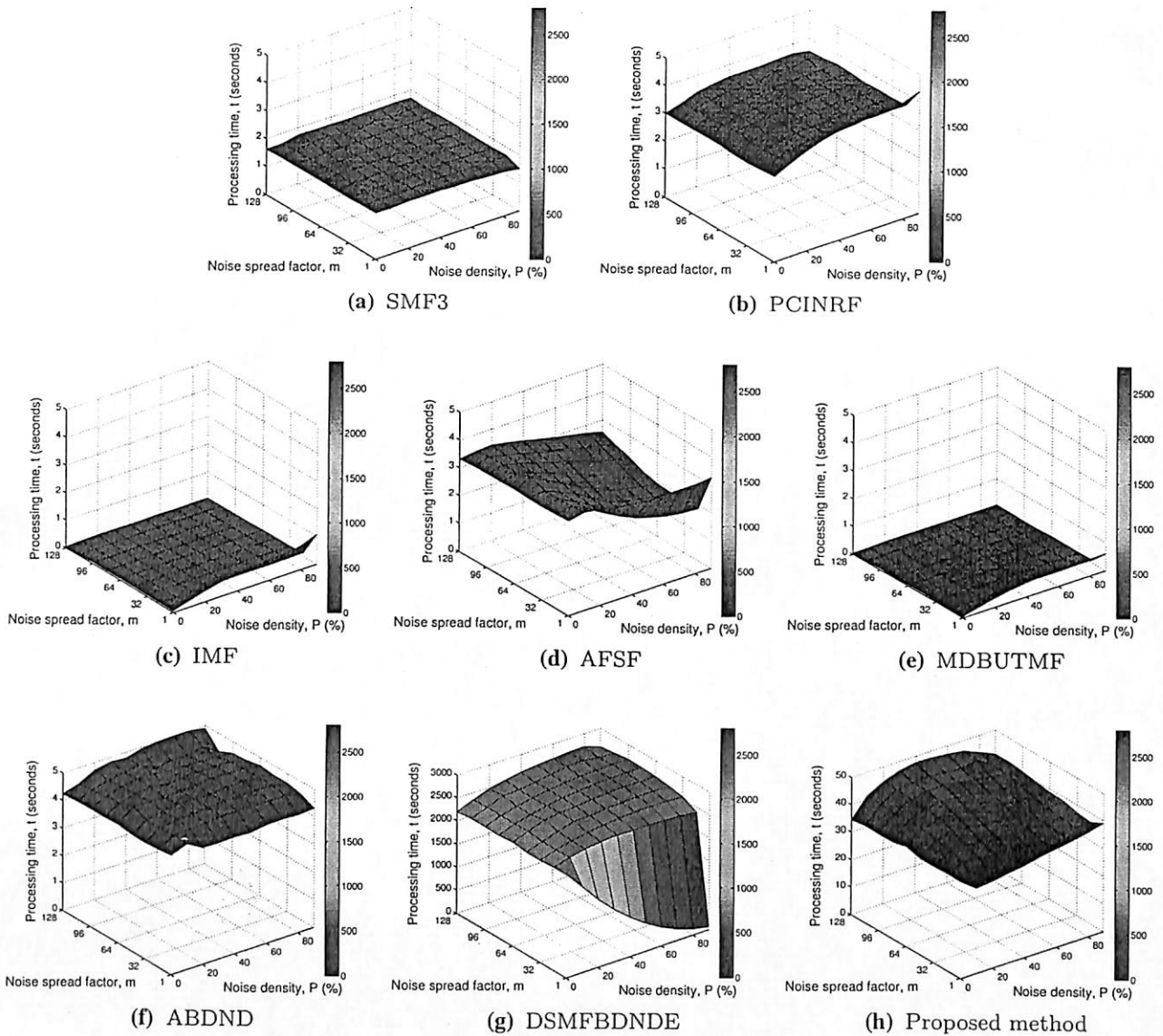


Fig. 10 Processing time surface plots

clearly seen in Fig. 12b, e. However, other methods, which are PCINRF, IMF, MDBUTMF, ABDND, DSMFBDNDE, and the proposed method, successfully remove most of the impulse noise from the image shown in Fig. 12a.

Figure 13 shows the corresponding output images when the input is corrupted by a high level of salt-and-pepper noise (i.e., $P = 90\%$ and $m = 1$). SMF3 does not able to recover the image. Similarly, AFSF failed to filter the image, and makes the image darker. On the other hand, the structures inside the images filtered by MDBUTMF and ABDND are still visible, but the images have undesired small dots due to incomplete removal of impulse noise. Less serious cases can be observed in images by PCINRF and IMF. DSMFBDNDE and the proposed method successfully remove this high level

of salt-and-pepper noise from the image. However, DSMFBDNDE tends to blur the edges. This effect can be observed at the border regions of the sub-images in Fig. 13h.

Figure 14 shows the output images when the input is corrupted by impulse noise with $P = 20\%$ and $m = 64$. By using this parameter, 64 intensity levels are used to present salt noise, and other 64 intensity levels are used to present pepper noise. Although the corruption level for this figure is same as the one in Fig. 11, only SMF3 and the proposed method successfully remove impulse noise and produce clean and sharp images. Although SMF3 is the simplest method used in this work and does not follow switching median filtering approach, in general, the result produced by this method will give an acceptable result if $P \leq 50\%$. With this noise

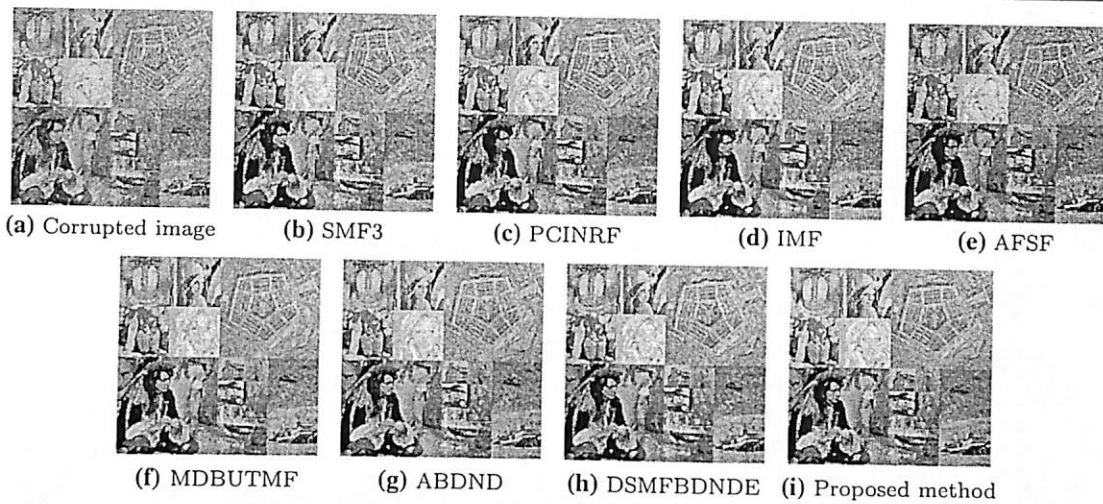


Fig. 11 Output images when P equal to 20 %, and m equal to 1

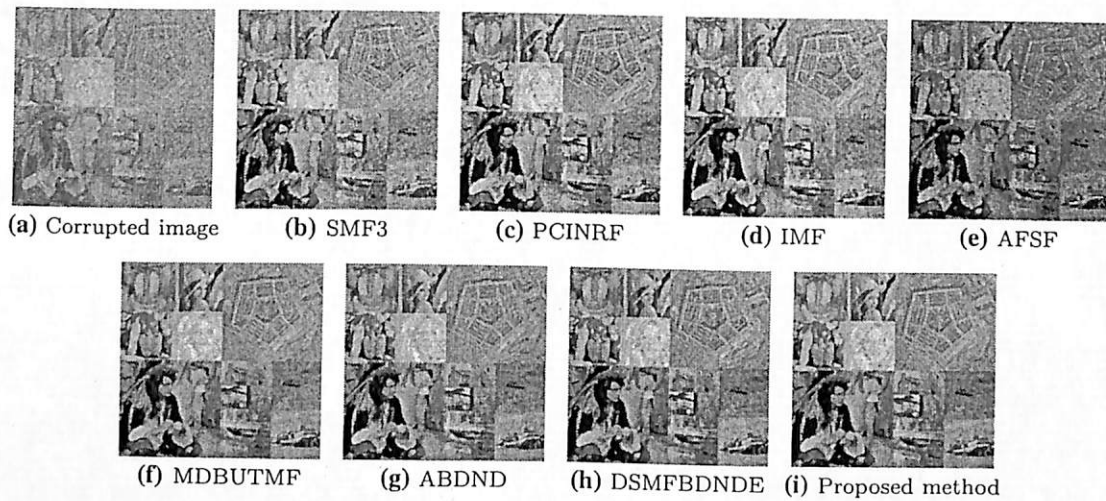


Fig. 12 Output images when P equal to 50 %, and m equal to 1

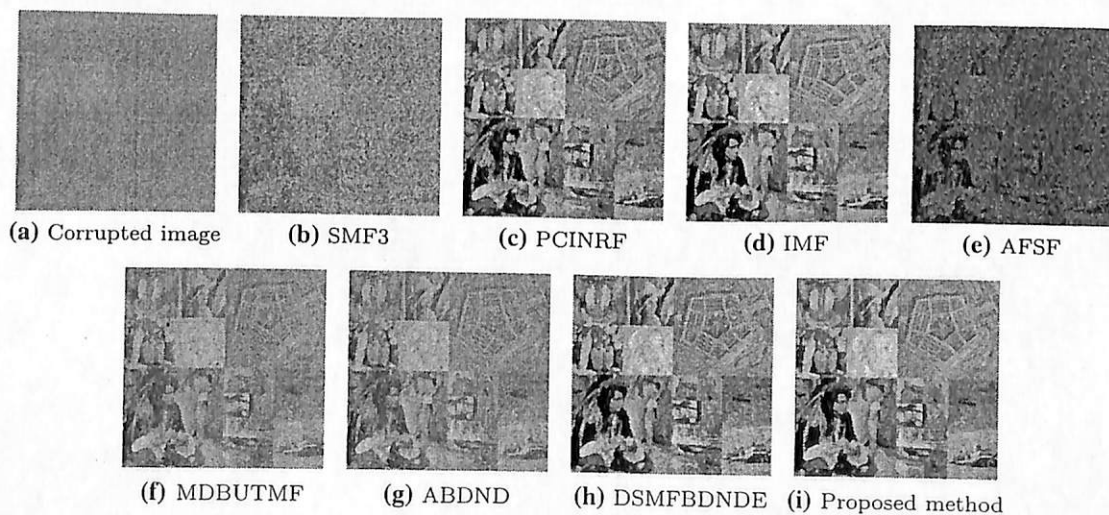


Fig. 13 Output images when P equal to 90 %, and m equal to 1

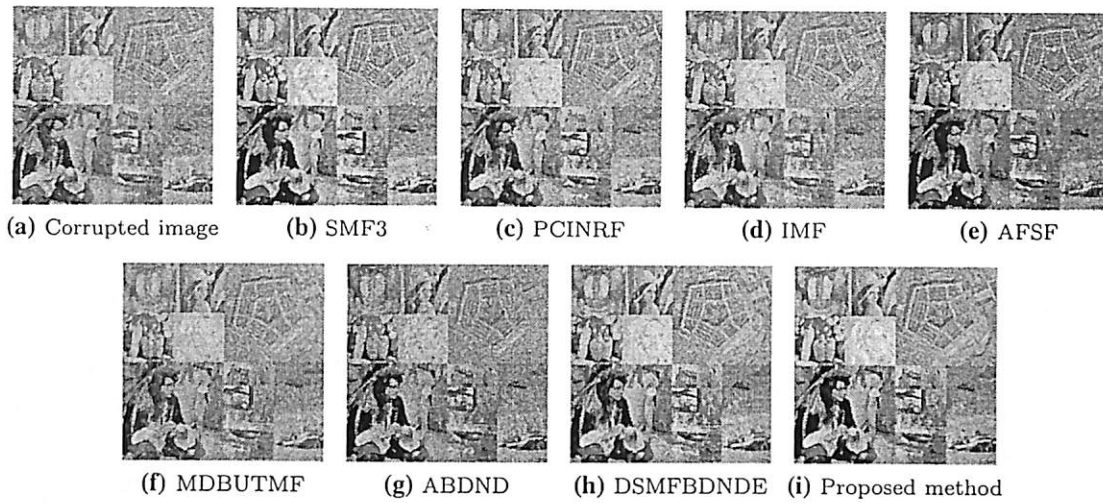


Fig. 14 Output images when P equal to 20 %, and m equal to 64

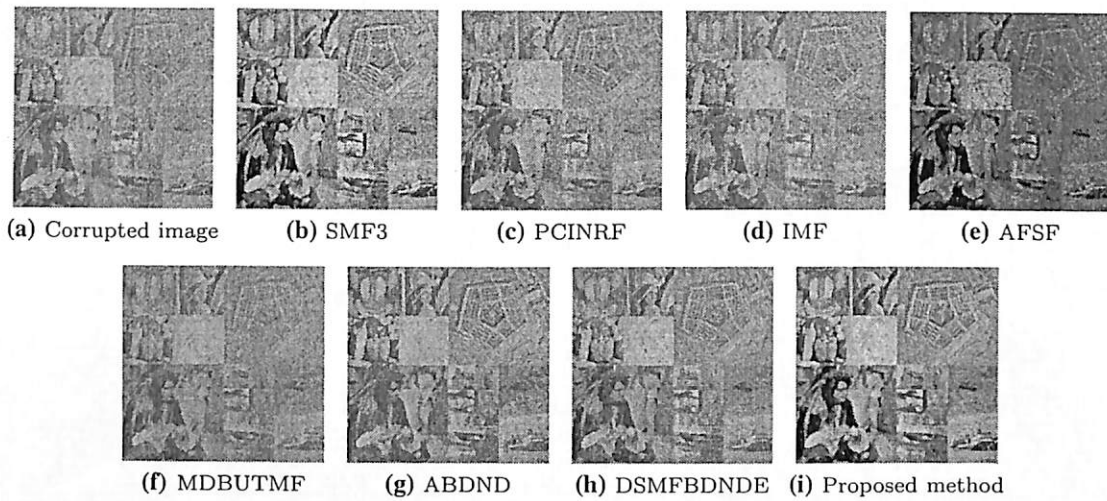


Fig. 15 Output images when P equal to 50 %, and m equal to 64

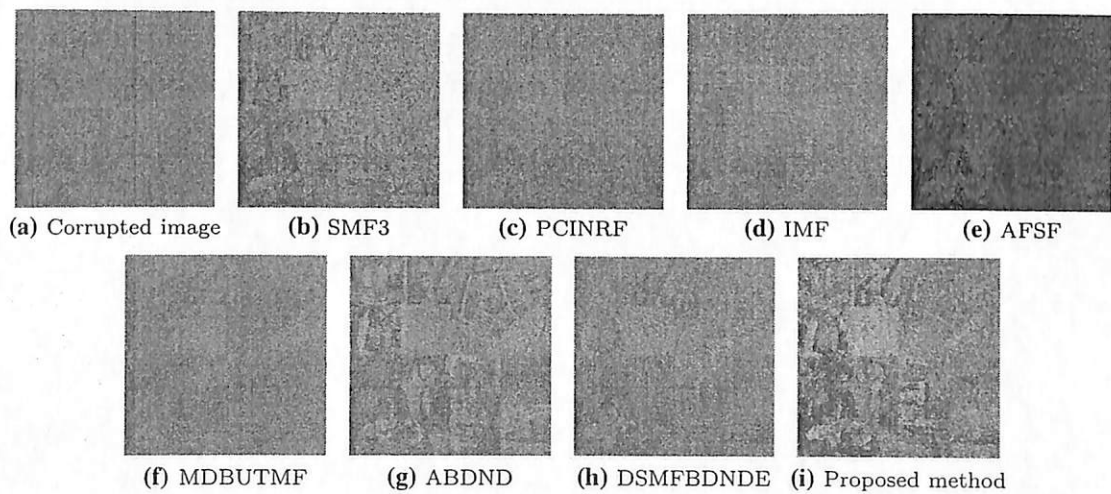


Fig. 16 Output images when P equal to 90 %, and m equal to 64

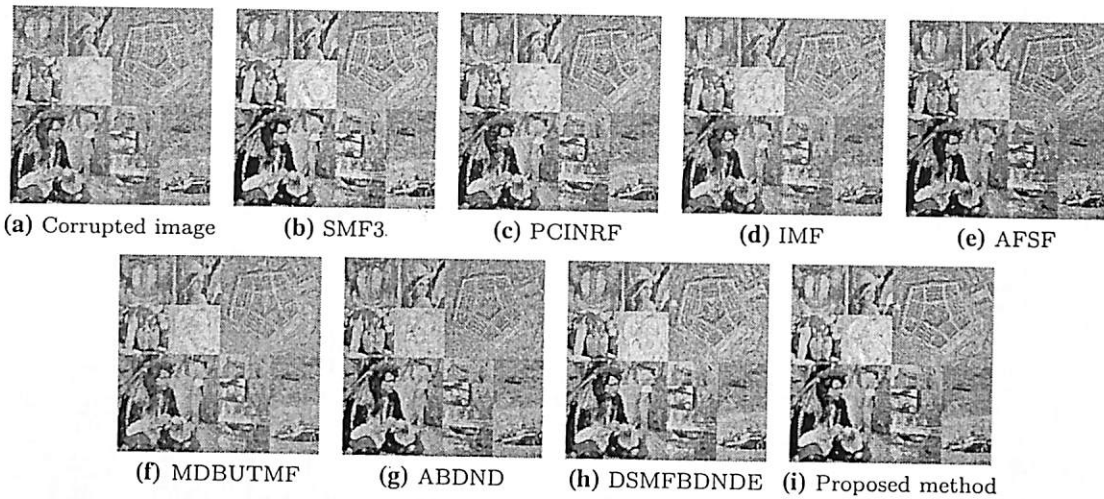


Fig. 17 Output images when P equal to 20 %, and m equal to 128

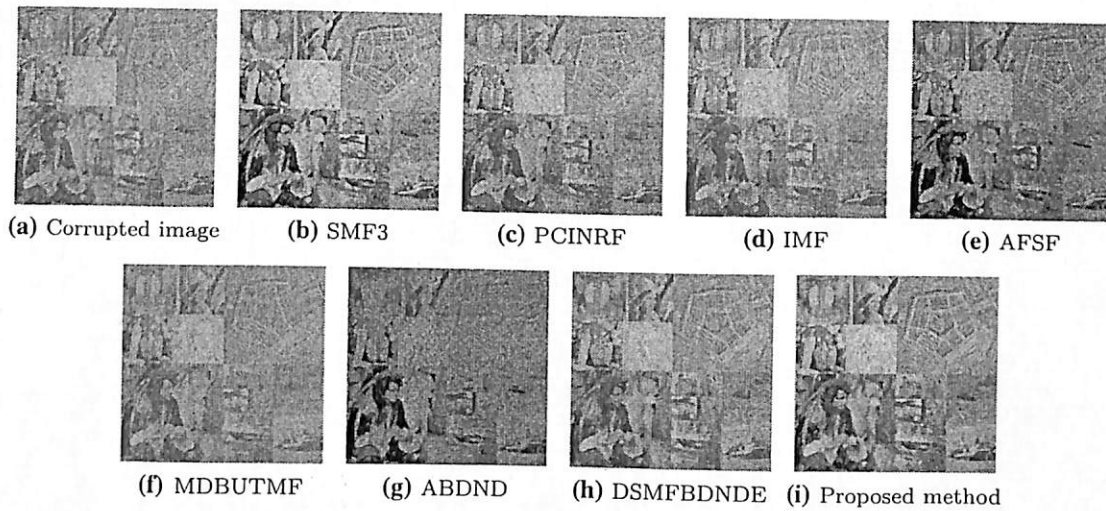


Fig. 18 Output images when P equal to 50 %, and m equal to 128

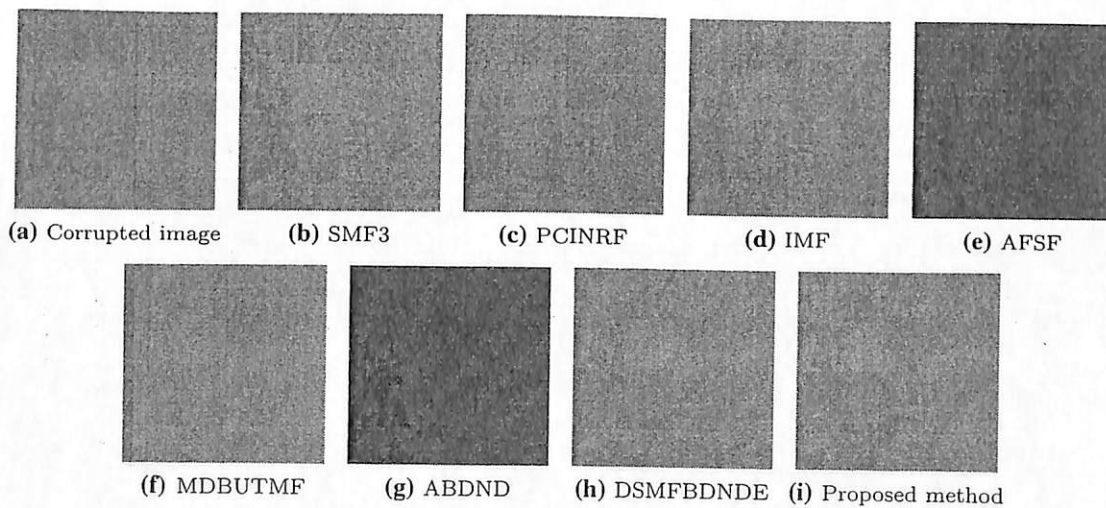


Fig. 19 Output images when P equal to 90 %, and m equal to 128

density, the local median values determined by SMF3 mostly are taken from the clean pixels.

Other tested methods in this work failed to completely remove the added impulse noise. This is mostly due to the failure of the impulse noise detector to detect the noise correctly. For example, in this figure, the result from ABDND is the worst. To explain this situation, we inspect the false positive rate for ABDND from Fig. 7h and found out that the false positive rate at this point is significantly high, which is around 22%. This condition reduces the number of samples that can be used for its noise cancellation stage. Then, Fig. 8h shows that the false negative rate at this point is also relatively high, which is around 12%. In this situation, as some of the good pixels were removed and some of the noise pixels were selected as the sample, noise pixels might contribute more towards the restored pixel values.

With m maintained at 64, the resultant images when the noise density P is increased to 50% are shown in Fig. 15. As shown by this figure, all methods failed to remove the noise completely. The output images from PCINRF, IMF, MDBUTMF, and DSMFBDNDE appear similar to the corresponding corrupted input image, whereas the filtered image by AFSF looks darker. ABDND failed to remove impulse noise especially on the very bright or very dark areas. Impulse noise still visible on images obtained from SMF3 and the proposed method. However, these artefacts are relatively small in number. By observing *Tiffany* region, it can be said that the performance of the proposed method is better than SMF3.

Figure 16a shows the input image after been corrupted with impulse noise with parameter P set to 90% and parameter m set to 64. This high corruption level makes the structures inside the image difficult to be seen. By inspecting output images in Fig. 16, it is shown that all of the tested impulse noise reduction methods in this work have failed to produce excellent filtering results. The results from PCINRF, IMF, MDBUTMF, and DSMFBDNDE are not significant, where the output images are almost similar to the corrupted input image. SMF3 and AFSF produce darker output images. Rough structures can be observed from outputs from ABDND and the proposed method. Structures of *Pentagon*, *House* and *Peppers* are better by ABDND, while structures of *Man*, *Lena*, *Tree*, and *Boats* are better by the proposed method.

The results for a low corruption level of random-valued impulse noise (i.e., $P = 20\%$ and $m = 128$) are shown in Fig. 17. Similar to the results shown in Fig. 14, which is at the same corruption level, only SMF3 and the proposed method successfully remove impulse noise and produce clean and sharp images. The output images from other tested impulse noise reduction methods are still having visible small dots, which correspond to residual impulse noise. The result from ABDND is the worst, as can be seen from region of sub-image *Tiffany*.

Figure 18 shows the results for a medium corruption level of random-valued impulse noise (i.e., $P = 50\%$ and $m = 128$). Although the structures inside the images can be seen clearly, in general, all methods failed to remove impulse noise completely. As expected, the results shown in this figure is inferior than the corresponding results shown in Fig. 15. This can be observed from *Tiffany* sub-image, especially in the results from AFSF and ABDND. In this figure, ABDND produces the worst result. On the other hand, the proposed method produces the relatively sharpest and cleanest output image.

The noise filtering results for the input image corrupted by high density of random-valued impulse noise (i.e., $P = 90\%$ and $m = 128$) are shown in Fig. 19. Because all the results when $P = 50\%$ are already unsatisfactory (see Fig. 18), it is not surprising that all the tested method failed to remove impulse noise in Fig. 19. Unexpectedly, among these results, the result from SMF3 is the best. The structures inside the image produced by SMF3 are more visible than others. This outcome is very different from the outcomes from Figs. 13 and 16, where the outputs from the proposed method are the best.

4 Conclusion

This paper presents the evaluations of the proposed method, as compared to other seven state-of-the-art impulse noise reduction methods. The evaluations have been carried out objectively and also subjectively. It has been shown that the proposed method has the lowest RMSE values for most of the test samples. In terms of false positive detection rate, experimental results show that the proposed method is the second highest, just behind SMF3. However, the good performances of other methods in false positive detection might be due to the inefficiency of the noise detection stage of the methods, where the majority of the pixels will not be classified as noise pixel candidate, even though the pixel is actually a noise pixel. This can be proven by inspecting the false negative detection rate. Among the switching median filtering methods used in this work (i.e., excluding SMF3), the proposed methods has the lowest false negative detection rate, portraying its good noise detection ability. Furthermore, the proposed method also is the best in terms of MSSIM. However, the proposed method require a slightly longer processing time as compared to the majority of the method. It needs around 40–50 s (which is less than 1 min) to completely process one 4-Megapixels image. The proposed method is roughly 60 times faster as compared to DSMFBDNDE. Therefore, the processing time required is still considered reasonable. In terms of the quality of the output image, based on visual inspection, the proposed method mostly will produce good output images, especially for the case of salt-

and-pepper noise. The proposed method has an acceptable performance for other type of impulse noise. Thus, in general, within the scope of this work, it can be concluded that the proposed method is the best impulse noise reduction technique.

Acknowledgments We would like to thank the anonymous reviewers for their constructive comments. We also would like to thank Dr. John Chiverton for helping us to proofread this article. This work was supported in part by the Universiti Sains Malaysia's Short Term Research Grant with account number 304/PELECT/60311013 and Universiti Sains Malaysia's Research University: Individual (RUI) with account number 1001/PELECT/814169.

References

1. Wang, J.-H., Lin, L.D.: Improved median filter using minmax algorithm for image processing. *Electron. Lett.* **33**(16), 1362–1363 (1997)
2. Alajlan, N., Kamel, M., Jernigan, E.: Detail preserving impulsive noise removal. *Signal Process. Image Commun.* **19**(10), 993–1003 (2004)
3. Ibrahim, H., Neo, K.C., Teoh, S.H., Ng, T.F., Chieh, D.C.J., Hassan, N.F.N.: Impulse noise model and its variations. *Int. J. Comput. Electr. Eng. (IJCEE)* **4**(5), 1793–8163 (2012)
4. Gonzalez, R.C., Woods, R.E.: *Digital Image Processing*, 3rd edn. Pearson Prentice Hall, Upper Saddle River, NJ (2008)
5. Pasian, F.: Sorting algorithms for filters based on ordered statistics: performance considerations. *Signal Process.* **14**(3), 287–293 (1988)
6. Walpole, R.E., Myers, R.H., Myers, S.L.: *Probability and Statistics for Engineers and Scientists*, 6th edn. Pearson Prentice Hall, Upper Saddle River, NJ (1998)
7. Srinivasan, E., Ebenezer, D.: New nonlinear filtering strategies for eliminating short and long tailed noise in images with edge preservation properties. *Int. J. Inf. Commun. Eng.* **4**(3), 175–181 (2008)
8. Yang, R., Yin, L.: Optimal weighted median filtering under structural constraints. *IEEE Trans. Signal Process.* **43**(3), 591–604 (1995)
9. Arce, G.: Theoretical analysis of the max/median filter. *IEEE Trans. Acoust. Speech Signal Process.* **35**(1), 60–69 (1987)
10. Teoh, S.H., Ibrahim, H.: Median filtering frameworks for reducing impulse noise from grayscale digital images: a literature survey. *Int. J. Future Comput. Commun.* **1**(4), 323–326 (2012)
11. Song, Y., Han, Y., Lee, S.: Pixel correlation-based impulse noise reduction. In: 17th Korea–Japan Joint Workshop on Frontiers of Computer Vision (FCV), pp. 1–4 (2011)
12. Deivalakshmi, S., Sarath, S., Palanisamy, P.: Detection and removal of salt and pepper noise in images by improved median filter. *IEEE Recent Adv. Intell. Comput. Syst. (RAICS)* **2011**, 363–368 (2011)
13. Saradhadevi, V., Sundaram, W.: An adaptive fuzzy switching filter for images corrupted by impulse noise. *Glob. J. Comput. Sci. Technol.* **11**(4), 29–33 (2011)
14. Esakkirajan, S., Veerakumar, T., Adabala, N.S., PremChand, C.H.: Removal of high density salt and pepper noise through modified decision based unsymmetric trimmed median filter. *IEEE Signal Process. Lett.* **18**(5), 287–290 (2011)
15. Tripathi, A.K., Ghanekar, U., Mukhopadhyay, S.: Switching median filter: advanced boundary discriminative noise detection algorithm. *IET Image Process.* **5**(7), 598–610 (2011)
16. Ng, P.E., Ma, K.K.: A switching median filter with boundary discriminative noise detection for extremely corrupted images. *IEEE Trans. Image Process.* **15**(6), 1506–1516 (2006)
17. Nallaperumal, K., Varghese, J., Saudia, S., Arulmozhi, K., Velu, K.: Salt & pepper noise removal using adaptive switching median filter. In: *Proceedings of IEEE Oceans, Asia Pacific*, Singapore, pp. 1–8 (2006)
18. Nasimudeen, A., Nair, M.S., Tatavarti, R.: Directional switching median filter using boundary discriminative noise detection by elimination. *Signal Image Video Process.* **6**(4), 613–624 (2012)
19. Ibrahim, H., Ng, T.F., Teoh, S.H.: An efficient implementation of switching median filter with boundary discriminative noise detection for image corrupted by impulse noise. *Sci. Res. Essays (SRE)* **6**(26), 5523–5533 (2011)
20. Kong, N.S.P., Ibrahim, H.: Multiple layers block overlapped histogram equalization for local content emphasis. *Comput. Electr. Eng.* **37**(5), 631–643 (2011)
21. Ibrahim, H.: Adaptive switching median filter utilizing quantized window size to remove impulse noise from digital images. *Asian Trans. Fundam. Electron. Commun. Multimed. (ATFECM)* **2**(1), 1–6 (2011)
22. Huang, T.S., Yang, G.J., Tang, G.Y.: A fast two-dimensional median filtering algorithm. *IEEE Trans. Acoust. Speech Signal Process.* **27**(1), 13–18 (1979)
23. Jayaraj, V., Ebenezer, D., Vijayakumar, V.R.: A noise free estimation switching median filter for detection and removal of impulse noise in images. *Eur. J. Sci. Res.* **51**(4), 563–581 (2011)

Research Article

Local Contrast Enhancement Utilizing Bidirectional Switching Equalization of Separated and Clipped Subhistograms

Haidi Ibrahim¹ and Seng Chun Hoo²

¹ School of Electrical & Electronic Engineering, Engineering Campus, Universiti Sains Malaysia, 14300 Nibong Tebal, Penang, Malaysia

² Japan-Malaysia Technical Institute (JMTI), Plot 59, Lorong Perindustrian Bukit Minyak 15, Taman Perindustrian Bukit Minyak, 14100 Simpang Ampat, Penang, Malaysia

Correspondence should be addressed to Haidi Ibrahim; haidi@eng.usm.my

Received 11 October 2013; Revised 26 December 2013; Accepted 5 January 2014; Published 12 February 2014

Academic Editor: Suh-Yuh Yang

Copyright © 2014 H. Ibrahim and S. C. Hoo. This is an open access article distributed under the Creative Commons Attribution License, which permits unrestricted use, distribution, and reproduction in any medium, provided the original work is properly cited.

Digital image contrast enhancement methods that are based on histogram equalization technique are still useful for the use in consumer electronic products due to their simple implementation. However, almost all the suggested enhancement methods are using global processing technique, which does not emphasize local contents. Therefore, this paper proposes a new local image contrast enhancement method, based on histogram equalization technique, which not only enhances the contrast, but also increases the sharpness of the image. Besides, this method is also able to preserve the mean brightness of the image. In order to limit the noise amplification, this newly proposed method utilizes local mean-separation, and clipped histogram bins methodologies. Based on nine test color images and the benchmark with other three histogram equalization based methods, the proposed technique shows the best overall performance.

1. Introduction

Contrast enhancement is currently still one of the active research branches in digital image processing discipline. The main aim of this research branch is to improve the appearance of the acquired image [1]. Although both digital image enhancement and image restoration share the same aim, unlike image restoration, the results obtained from digital image enhancement mostly are evaluate subjectively, where the degree of image quality perceived might be different from person to person [2]. Yet, recent researches in digital image contrast enhancement also include some objective measures in order to evaluate the performance of the algorithms.

Histogram equalization (HE) is one of the popular digital image contrast enhancement methods [3]. This method is simple and easy to be implemented. HE enhances the given input image by using a monotonic mapping function, where this mapping function is derived from the intensity histogram of the input image. The mapping function also can be derived from the probability density function (pdf), which is basically

the normalized version of the histogram [4]. In order to produce an overall contrast enhancement, HE stretches the dynamic range of the image's histogram.

In spite of its simple implementation and popularity, global HE (GHE), which is HE method that uses only one transfer function calculated from the whole pixels in the image, has several drawbacks. These drawbacks include intensity saturation artifacts and washed out appearance. Fortunately, Kim [5] has discovered that these undesired problems can be reduced by simply maintaining the average brightness level (i.e., average intensity level) of the input image into the corresponding output image. As a consequence from this important rule, many variations of GHE have been proposed.

Many of these GHE variations work by equalizing two subhistograms independently in order to preserve the mean brightness. Within this framework, the method splits the input image's histogram into two sections, which is upper and lower subhistograms, by using one splitting point. This splitting point has normally been calculated by using the

input image's statistics, such as the average intensity value [5] or the median intensity value [6].

In order to further improve the performance of the contrast enhancement method in terms of the mean brightness preservation performance, several GHE based methods split the input image's histogram into more than two sections. This multiple separated histogram is obtained by using more than one splitting point. These separating points are typically calculated based on each section's average intensity values [7], median intensity values [8], and local minimum or local maximum values of histogram's bin [9].

Yet, several other GHE based contrast enhancement methods do not put any constrain on preserving the mean brightness. These methods avoid the appearance of unwanted artifacts in their output images by controlling the enhancement rate, which relates to the slope of the intensity mapping function, by modifying the shape of the input histogram. Such modifications are normally been carried out by clipping the histogram [4], applying a weighting function to the histogram's bins [10], or creating a complementary histogram [11].

However, GHE and its derivative methods process the image globally, which mean that these methods use only one monotonically increasing transformation function for each input image. As mentioned in [11], the calculation for this discrete transformation function is done by using discrete values. Therefore, the contrast enhancement is obtained by increasing the spaces between consecutive histogram bins. Yet, mostly the histogram bins with small values will be merged together, which lead to the deterioration of contrast for intensity levels with low probability values.

Local HE, also known as adaptive HE, is still not been fully explored. Unlike GHE based methods, local HE methods generally produce sharper images. As local HE is able to introduce new intensity levels into the output image, they may flatten the image histogram and thus increase the information content (i.e., which normally can be measured by using entropy value) [12]. One of the basic local HE methods is the block overlapped HE (BOHE). BOHE works by using a sliding window of size $W_M \times W_N$, which defines a local contextual region on the image [1]. This local region is treated as a subimage by BOHE, and thus a similar procedure to GHE is applied in order to determine the local intensity mapping function. However, for each windowing operation, only the center pixel of the contextual region is assigned the output value. As a consequence, for a given input image with dimensions $M \times N$ pixels, BOHE needs MN local intensity mapping functions, which leads to high computational time.

Because the computational requirements by BOHE are very high, Pizer et al. [13] have proposed the interpolated adaptive HE (IAHE). IAHE does not use the exact local intensity mapping function to most of the pixels, but it uses the approximation of the function by utilizing bilinear interpolations. Another approximation of BOHE is the method developed by Kim et al. [14] which is called the partially overlapped subblock histogram equalization (POSHE). Unfortunately, the blocking effect reduction filter (BERF) used by POSHE is still not effective on removing some

blocking effect due to the significant difference of intensity mapping functions of neighbouring subblocks.

Another approach to reduce the high complexity of BOHE is by optimizing the way of creating the local intensity histograms [12]. Yet, there is still a major problem associated with BOHE, which is the noise amplification, thus causing the existence of speckle noise in the resultant image. Therefore, a few BOHE based methods that give constrain on noise amplification, such as the contrast clipped adaptive histogram equalization (CLAHE) [15] and multiple layers block overlapped histogram equalization (MLBOHE) [12], were designed.

In this paper, a new variation to BOHE, which is called the local contrast enhancement utilizing bidirectional switching equalization of separated and clipped subhistograms (LCE-BSESCS), has been proposed. This paper is divided into four sections. After this introductory section, Section 2 will explain the methodology of LCE-BSESCS. The next section, which is Section 3, will present the experimental results. Finally, Section 4 will present the conclusion from this research work.

2. Methodology

The main objective of LCE-BSESCS is to increase the image contrast and sharpness, especially to images that suffer from uneven illumination. LCE-BSESCS also aims to preserve the mean brightness of the input image, so that intensity saturation problem can be avoided. The basic ideas of LCE-BSESCS are listed as follows.

- (i) Reducing saturation artefact: LCE-BSESCS uses bidirectional equalization, where the intensity mapping moves towards the local mean value.
- (ii) Reducing noise amplification: LCE-BSESCS utilizes clipped subhistograms in order to avoid abrupt intensity changes.
- (iii) Reducing the processing time: switching approach has been used, so that instead of calculating transfer functions from both subhistograms, LCE-BSESCS calculates one transfer function from one subhistogram only.

The methodology for LCE-BSESCS is explained in the following subsections.

2.1. Define the Contextual Region. Similar to BOHE, the operation of LCE-BSESCS uses a sliding window of size $W_M \times W_N$ pixels, where both W_M and W_N are odd integer numbers (i.e., $W_M = 2W_H + 1$ and $W_N = 2W_W + 1$). Here, W_H and W_W are integer values, presenting the distance from the center pixel of the sliding window to the window's border in vertical direction and horizontal direction, respectively.

This sliding window is used to define the local image, also known as the contextual region (CR), for local processing. Let us assume (i, j) as the spatial coordinates of the pixel, and (y, x) represents the spatial coordinates for the center pixel of the current CR. Using the sliding window, CR will only

occupy the area with coordinates in the range of $y - W_H \leq i \leq y + W_H$ and $x - W_W \leq j \leq x + W_W$.

In the implementation of LCE-BSESCS, truncation of the sliding window has been applied for the pixels located near the image border. For example, when coordinates (y, x) are at position $(0, 0)$, the corresponding CR is truncated to the size of $(W_H + 1) \times (W_W + 1)$ pixels, instead of $W_M \times W_N$ pixels. At this position, the "center pixel" of CR is not located at the middle of CR but located at the top left. By using truncation approach, the size of the original input image can be maintained and we do not need to use any padding operation (e.g., zero padding, padding with global average value, or padding with global median value) toward the input image. We believe that the sampled intensity values from the truncation approach is more accurate than the padding approach, as the sample will not be contaminated by artificially added values.

2.2. Create Local Histogram. As mentioned in previous subsection, at every "center pixel" (y, x) , one CR is defined. If the input image, denoted as $X = \{X(i, j)\}$, has the intensity levels within the range $[0, L - 1]$ (i.e., $X(i, j) = \{X_0, X_1, \dots, X_{L-1}\}$), the subimage defined by CR, $X_{CR(y,x)} = \{X_{CR(y,x)}(i, j)\}$, also has the intensity levels $[0, L - 1]$. Using this CR, a local intensity histogram $H_{CR(y,x)}$ is defined as

$$H_{CR(y,x)}(X_k) = n_k, \quad \text{for } k = 0, 1, \dots, L - 1, \quad (1)$$

where X_k is the k th intensity level and n_k is the number of pixels within CR with intensity level X_k .

2.3. Separate Histogram into Two Subhistograms. With the aim of maintaining the local mean brightness within CR, local mean-separation methodology has been used. The mean-separation methodology was first introduced by Kim [5] in his method known as brightness preserving bi-HE (BBHE). Unlike BBHE that uses global average intensity value as the splitting point, the local splitting point $\bar{X}_{CR(y,x)}$ in LCE-BSESCS is the average intensity value from the samples within CR. This local separating point is defined as

$$\bar{X}_{CR(y,x)} = \left\lfloor \frac{\sum_{k=0}^{L-1} (X_k \times H_{CR(y,x)}(X_k))}{W_M \times W_N} \right\rfloor, \quad (2)$$

where $\lfloor \cdot \rfloor$ is the floor function.

2.4. Clip the Corresponding Subhistogram. A special consideration is given in order to limit the amplification of speckle noise which may degrade the appearance of the resultant contrast enhanced image. In LCE-BSESCS, histogram clipping approach has been utilized. By clipping histogram bins which are exceeding certain threshold value, we can control the enhancement rate defined by the local intensity mapping function. Therefore, the enhanced pixel value at (y, x) will not deviate too much from its surrounding homogenous region. Adapted from bi-HE with a plateau limit (BHEPL) [16], the threshold value $T_{CR(y,x)}$ for the histogram clipping process is obtained by using the average value from subhistogram.

However, unlike BHEPL, a switching approach has been used. The value for $T_{CR(y,x)}$ is defined as

$$T_{CR} = \begin{cases} T_L & X(y, x) \leq \bar{X}_{CR(y,x)}, \\ T_U & \text{otherwise.} \end{cases} \quad (3)$$

Where

$$T_L = \left\lfloor \frac{\sum_{k=0}^{\bar{X}_{CR(y,x)}} H_{CR(y,x)}(X_k)}{\bar{X}_{CR(y,x)} + 1} \right\rfloor + 1, \quad (4)$$

$$T_U = \left\lfloor \frac{\sum_{k=\bar{X}_{CR(y,x)+1}^{L-1} H_{CR(y,x)}(X_k)}{L - \bar{X}_{CR(y,x)} - 1} \right\rfloor + 1.$$

By using this threshold value, LCE-BSESCS clips the histogram bins as follows:

$$H'(X_k) = \begin{cases} T_{CR} & H_{CR(y,x)}(X_k) \geq T_{CR}, \\ H_{CR(y,x)}(X_k) & \text{otherwise.} \end{cases} \quad (5)$$

Next, subhistogram from the clipped histogram H' needs to be normalized, so that pdf of that histogram section can be obtained. In order to do this, the total number of pixels from the modified subhistogram n_T is calculated

$$n_T = \begin{cases} \sum_{k=0}^{\bar{X}_{CR(y,x)}} H'(X_k) & X(y, x) \leq \bar{X}_{CR(y,x)}, \\ \sum_{k=\bar{X}_{CR(y,x)+1}^{L-1} H'(X_k) & \text{otherwise.} \end{cases} \quad (6)$$

2.5. Create the Bidirectional Intensity Mapping Function. After the corresponding normalized clipped subhistogram has been found, intensity mapping function f for the use in LCE-BSESCS is defined. Function f is defined as

$$f(X_k) = \begin{cases} f_L(X_k) & X(y, x) \leq \bar{X}_{CR(y,x)}, \\ f_U(X_k) & \text{otherwise.} \end{cases} \quad (7)$$

Where

$$f_L(X_k) = \left\lfloor \frac{\bar{X}_{CR(y,x)}}{n_T} \times \sum_{j=0}^k H'(X_j) \right\rfloor, \quad (8)$$

$$f_U(X_k) = \left\lfloor \frac{(L - \bar{X}_{CR(y,x)} - 2)}{n_T} \times \left(n_T - \sum_{j=k}^{L-1} H'(X_j) \right) \right\rfloor + \bar{X}_{CR(y,x)} + 1. \quad (9)$$

It is worthnoting that the equalization process defined by (8) propagates from the left to the right side of the subhistogram. On the other hand, equalization process given by (9) propagates in opposite direction. There are two main advantages by using bidirectional equalization. First, by using

this design, the transformed intensities with high histogram values will be given values similar to the local mean value $\bar{X}_{CR(y,x)}$. Therefore, this condition will enable LCE-BSESCS to have a better brightness preservation ability.

The second benefit that can be obtained from bidirectional equalization is the prevention from intensity saturation artifact. In normal local histogram equalization based methods, equalization process always propagates from the left side to the right side of the histogram. Thus, if the "center pixel" $X(y, x)$ has the highest intensity value within CR, the corresponding output pixel $Y(y, x)$ will be assigned the highest intensity level (i.e., intensity X_{L-1}) that normally corresponds to the whitest pixel. As a consequence, the output image might suffer from intensity saturation artifact. However, this is not a problem to LCE-BSESCS as the equalization process by this method is moving towards $\bar{X}_{CR(y,x)}$ instead of X_0 or X_{L-1} .

2.6. Map the Center Pixel. Finally, the output intensity value that corresponds to the "center pixel" $Y(y, x)$ is given as:

$$Y(y, x) = f(X(y, x)). \quad (10)$$

After the value of $Y(y, x)$ is determined, the sliding window slides to the next adjacent pixel and repeats the same procedure until all the pixels in output image Y get their corresponding contrast enhanced values.

As compared with GHE based contrast enhancement methods, which use one monotonic intensity mapping function for each input image, LCE-BSESCS uses $M \times N$ intensity mapping functions. In LCE-BSESCS, each pixel has its own transformation function. As a consequence, LCE-BSESCS is able to introduce new intensity levels into the output image. In this method, the histogram bins can be merged, as well as being broken up into several bins. Therefore, similar to other local HE methods, most of the histogram bins will be filled up with values. Hence, the utilization of the dynamic range in LCE-BSESCS is more effective than GHE based method. It is expected that LCE-BSESCS will produce a larger entropy value.

3. Experimental Results

Nine digital images of size 3264×2448 pixels (i.e., 7.99-megapixel images) are used in this experiment in order to evaluate the performance of LCE-BSESCS. All of these images are 24-bit-per-pixel color images and were acquired using the camera from the same smartphone. This images are shown in Figure 1. In order to process these color images, in this experiment, we treat each color channel (i.e., red (R), green (G), and blue (B) color channel) as an independent 8-bit-per-pixel grayscale image. Therefore, in order to process one color image, LCE-BSESCS will be executed three times, where each execution corresponds to one color channel. Thus, in this experiment, the level of quantization L is set to $2^8 = 256$.

One experiment has been carried out in order to investigate the suitable filter size to be used by LCE-BSESCS. One test image, which is *Image 1*, has been used for this purpose. In this experiment, we has limit the shape of the

filter to be square by setting W_M to be equal to W_N . The enhanced versions of *Image 1* by using different filter sizes are shown in Figure 2. As shown by this figure, LCE-BSESCS successfully sharpens the input image. However, we can see that LCE-BSESCS with smaller filter size does not enhance much contrast as compared to LCE-BSESCS with bigger filter size.

In order to understand the reason for this situation, we have investigated the number of nonempty histogram bins on local histograms versus the size of LCE-BSESCS filter. The statistics from this investigation are presented as box and whisker plots in Figure 3. It is known that for local HE, the contrast of the output image is depending much on the number of nonempty histogram bins [12]. From the graph, it is shown that when the size of the filter is small, the number of nonempty histogram bins is also small, and thus majority of the local histograms have many empty bins. The number of nonempty histogram bins is increasing when the filter size increases. Based on both Figures 2 and 3, we think that LCE-BSESCS with size 129×129 pixels is adequate for the enhancement. With this window size, almost half of the local histograms (i.e., based on the median value) has 128 or more nonempty histogram bins (i.e., more than $L/2$ intensity levels), and the output image is well enhanced.

Then, in order to bench-mark the performance of LCE-BSESCS, three other common HE based contrast enhancement methods have been implemented. These three methods are GHE [1], BOHE [12], and CLAHE [15]. In this implementations, the filter size for both BOHE and CLAHE is set to be exactly the same with the size of the filter used by LCE-BSESCS, which is 129×129 pixels. The plateau limit used in CLAHE is set as 10% from the maximum histogram bin value. Examples of the results are shown in Figures 4, 5, and 6.

Two image quality measures has been used for the evaluation process. As the images are color images, in this research work, the measurements will be carried out on the luminance value of the image. The luminance value I of the pixel at position (y, x) is calculated by using the following equation [1]:

$$I(y, x) = \frac{(R(y, x) + G(y, x) + B(y, x))}{3}, \quad (11)$$

where R is the red color component, G is the green color component, and B is the blue color component.

The first measure is the mean brightness error (MBE) [5]. MBE has been widely used as a quality measure for histogram equalization based methods. MBE is defined as:

$$MBE = \frac{|\bar{I}_Y - \bar{I}_X|}{M \times N}, \quad (12)$$

where M is the height of the image, N is the width of the image, \bar{I}_Y is the average luminance value of the enhanced image, and \bar{I}_X is the average luminance of the original input image. It is expected that a good contrast enhancement method can preserve the mean luminance and therefore has small value of MBE.

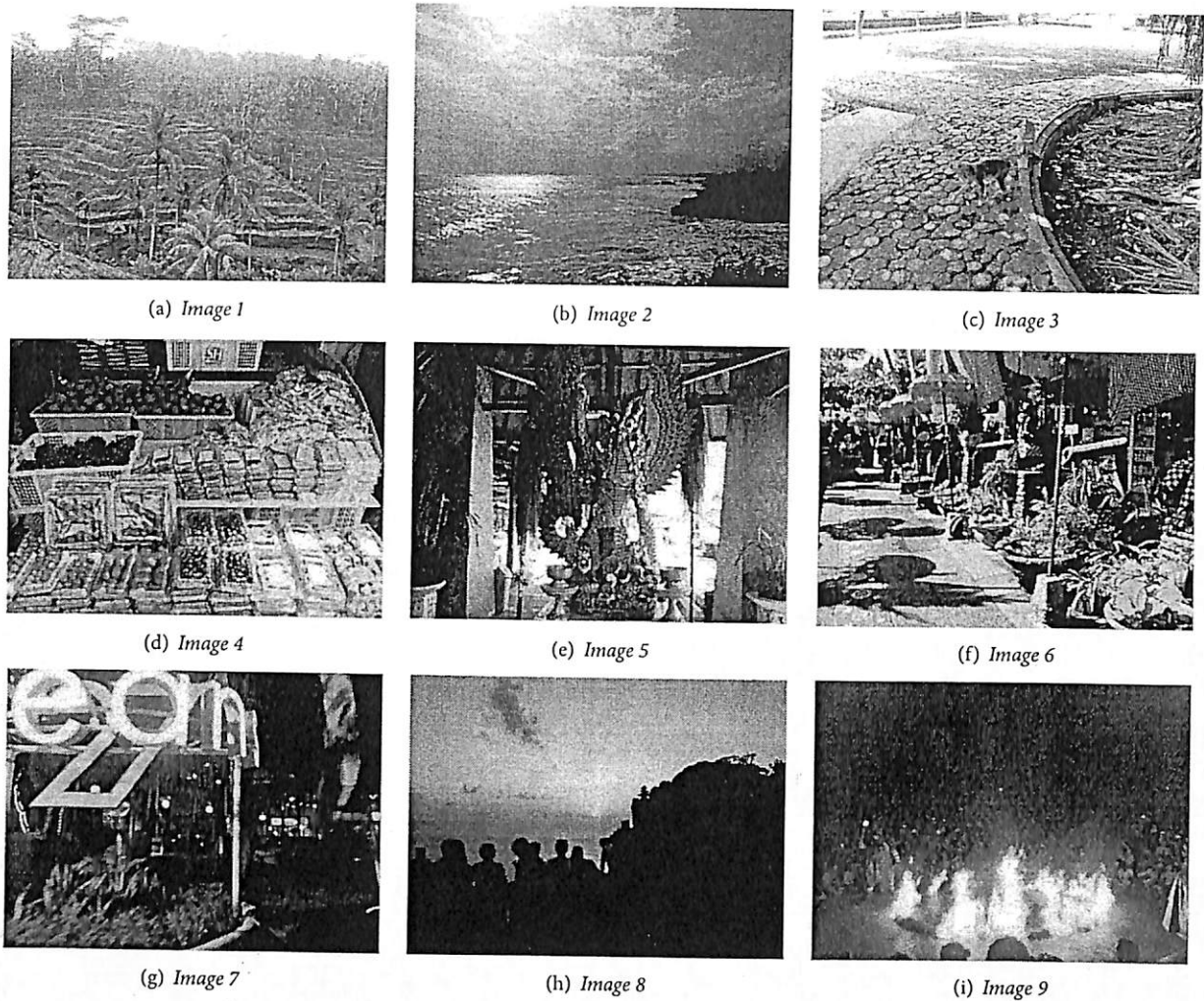


FIGURE 1: Nine input color images used in this experiment.

The second measure is the speckle noise strength (SNS), which is defined as follows:

$$SNS = \frac{\sum_{y=0}^{N-1} \sum_{x=0}^{M-1} |I(y, x) - \hat{I}(y, x)|}{(L - 1) \times M \times N} \times 100\%, \quad (13)$$

where \hat{I} is the approximation to a clean, enhanced image. In this work, \hat{I} is obtained from the version of I that has been filtered by a median filter of size 25×25 pixels. This filter size is still relatively small when compared with the size of the input image (i.e., M and N) and works well even when the image has been corrupted by high density of impulsive noise. Good enhancement method is expected to give small value of SNS.

Tables 1 and 2 show the measured MBE and SNS values, respectively: The bold font in these tables refers to the best result. As shown by Table 1, the proposed method, which is LCE-BSESCS, has the lowest average MBE value. Its average MBE value is significantly lower than others. This outcome shows that LCE-BSESCS has the highest ability to maintain the mean brightness of the image. The mean brightness of the input image is well maintained in the corresponding output image by LCE-BSESCS.

Table 2 shows that all the contrast enhancement methods evaluated in this research increase the strength of the speckle noise. Yet, among these tested methods, LCE-BSESCS produces the lowest average SNS. Although CLAHE also uses clipping histogram approach similar to LCE-BSESCS, LCE-BSESCS has a better performance in SNS. This indicates that a better restriction for noise amplification can be obtained by combining the clipped histogram approach with bidirectional equalization using subhistograms.

Qualitative evaluation, by inspecting the appearance of the output images visually, has also been carried out in this research. Some of the output images are shown in Figure 4 to Figure 6. As shown by these figures, BOHE and CLAHE tend to enhance the edges too much, which make the resultant images lost their global contrast. On the other hand, images produced by LCE-BSESCS appear to be more natural. Furthermore, as also shown by these figures, LCE-BSESCS maintains the basic shape of the original histogram.

4. Conclusions

In this research work, a new contrast enhancement method has been proposed. This method is based on local HE

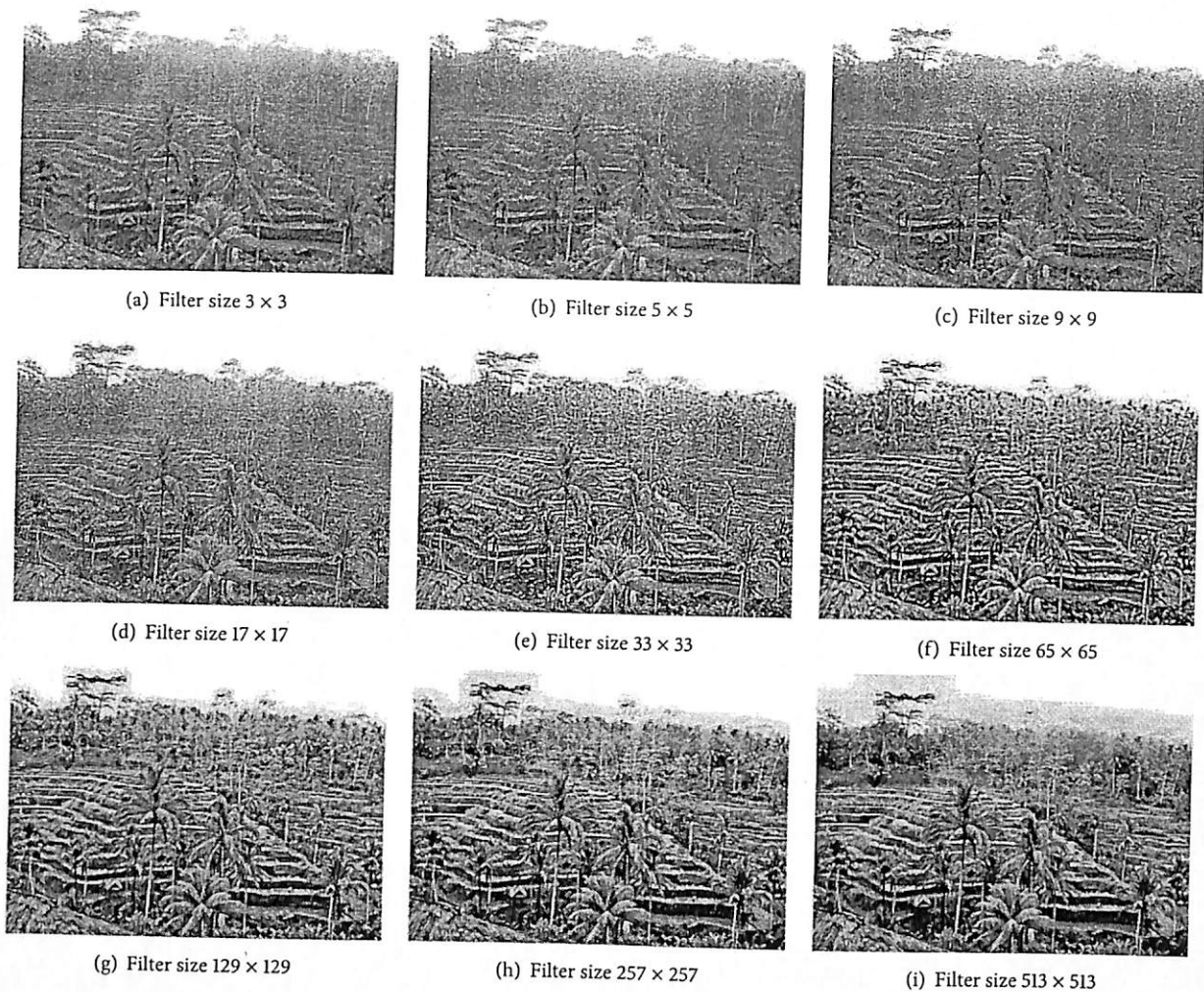


FIGURE 2: Enhanced versions of *Image 1* by using LCE-BSESCS of different filter sizes.

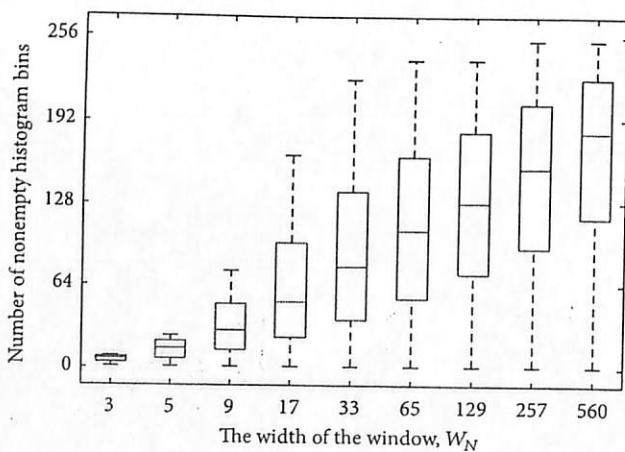


FIGURE 3: Statistics of the number of nonempty histogram bins versus the size of filter used.

method, where the method emphasizes on maintaining mean brightness, while improving contrast of small details on the image. The degree of enhancement can be adjusted by

TABLE 1: MBE values obtained from nine input images.

	GHE [1]	BOHE [12]	CLAHE [15]	LCE-BSESCS
<i>Image 1</i>	11.3669	6.3181	7.0035	4.6966
<i>Image 2</i>	0.6324	6.0483	9.8283	6.8152
<i>Image 3</i>	23.3245	15.2141	10.5754	5.1724
<i>Image 4</i>	10.4738	13.5890	9.3127	1.3990
<i>Image 5</i>	39.4145	45.6867	28.2706	3.1002
<i>Image 6</i>	25.6025	28.3861	11.9334	0.7755
<i>Image 7</i>	52.9224	62.2760	42.9693	4.4040
<i>Image 8</i>	52.4181	80.1929	51.8291	3.4763
<i>Image 9</i>	24.2728	38.7048	30.5922	1.2740
Average	26.7142	32.9351	22.4794	3.4570

changing the filter size, which is the only parameter used for LCE-BSESCS. As shown by the results, the proposed method has the best performance in terms of preserving the mean brightness and avoiding significant noise amplification. Qualitative evaluation shows that the proposed method produces relatively more natural images. Therefore, it can be

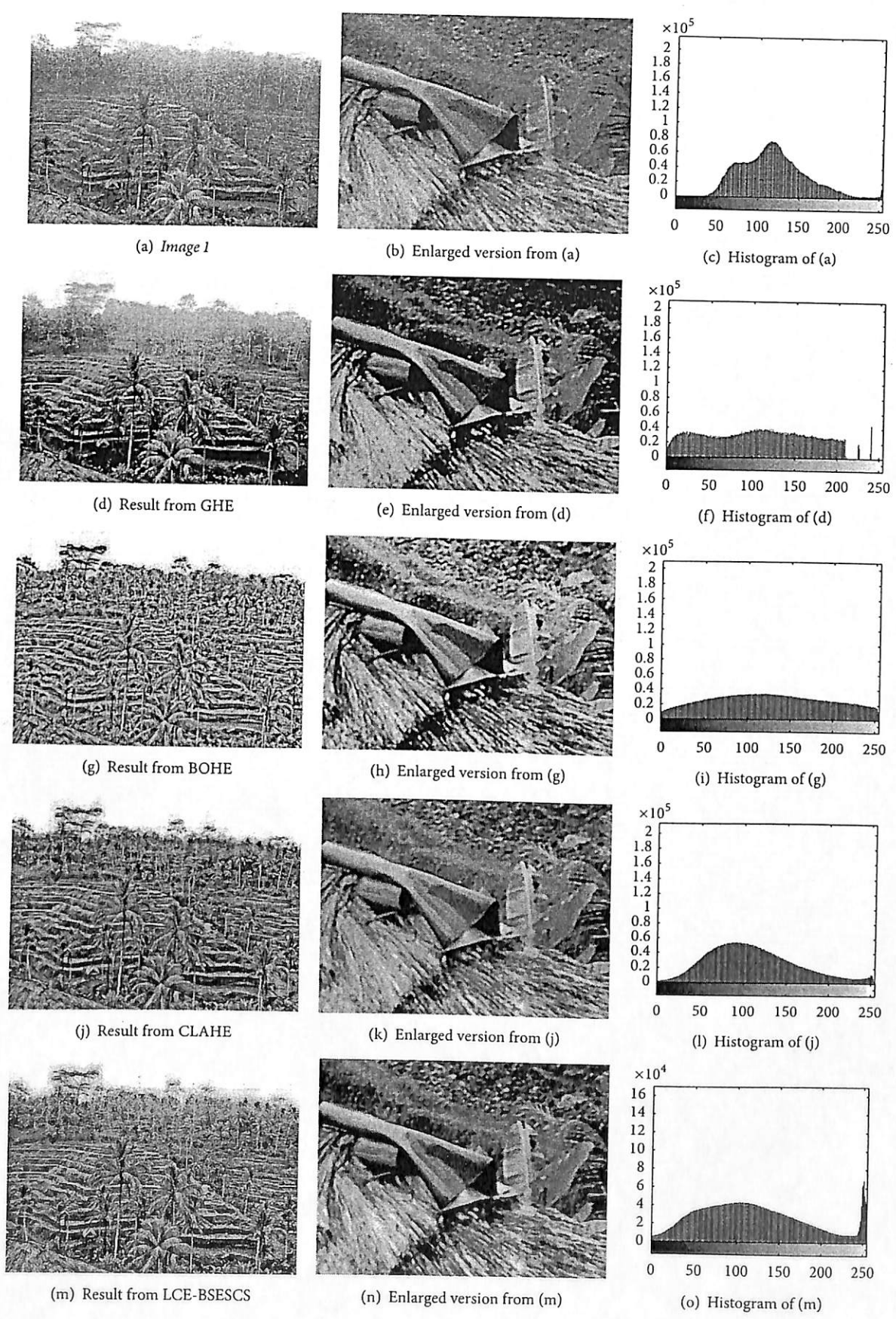
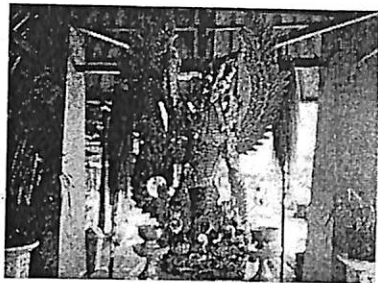
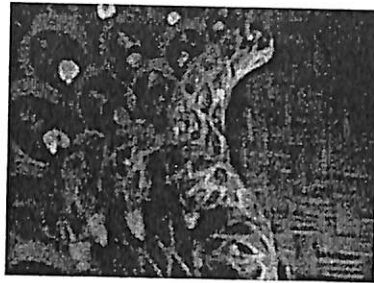


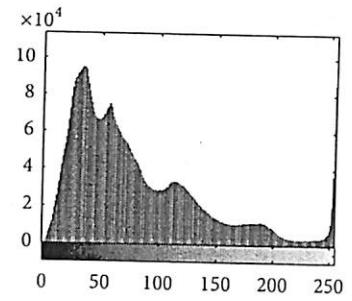
FIGURE 4: *Image 1* and its enhanced versions.



(a) Image 5



(b) Enlarged version from (a)



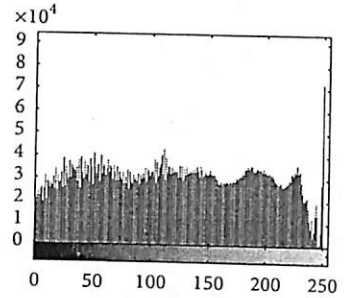
(c) Histogram of (a)



(d) Result from GHE



(e) Enlarged version from (d)



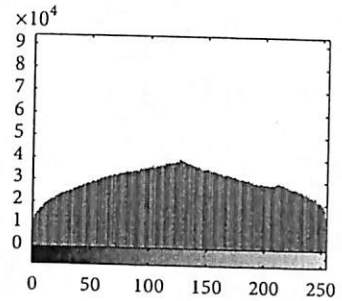
(f) Histogram of (d)



(g) Result from BOHE



(h) Enlarged version from (g)



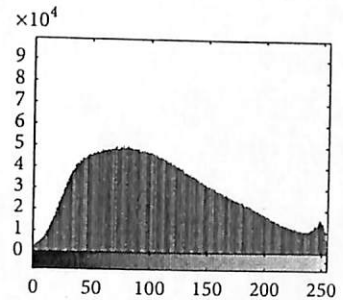
(i) Histogram of (g)



(j) Result from CLAHE



(k) Enlarged version from (j)



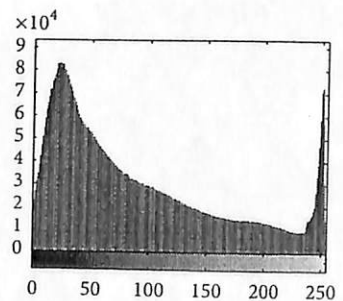
(l) Histogram of (j)



(m) Result from LCE-BSESCS



(n) Enlarged version from (m)



(o) Histogram of (m)

FIGURE 5: Image 5 and its enhanced versions.

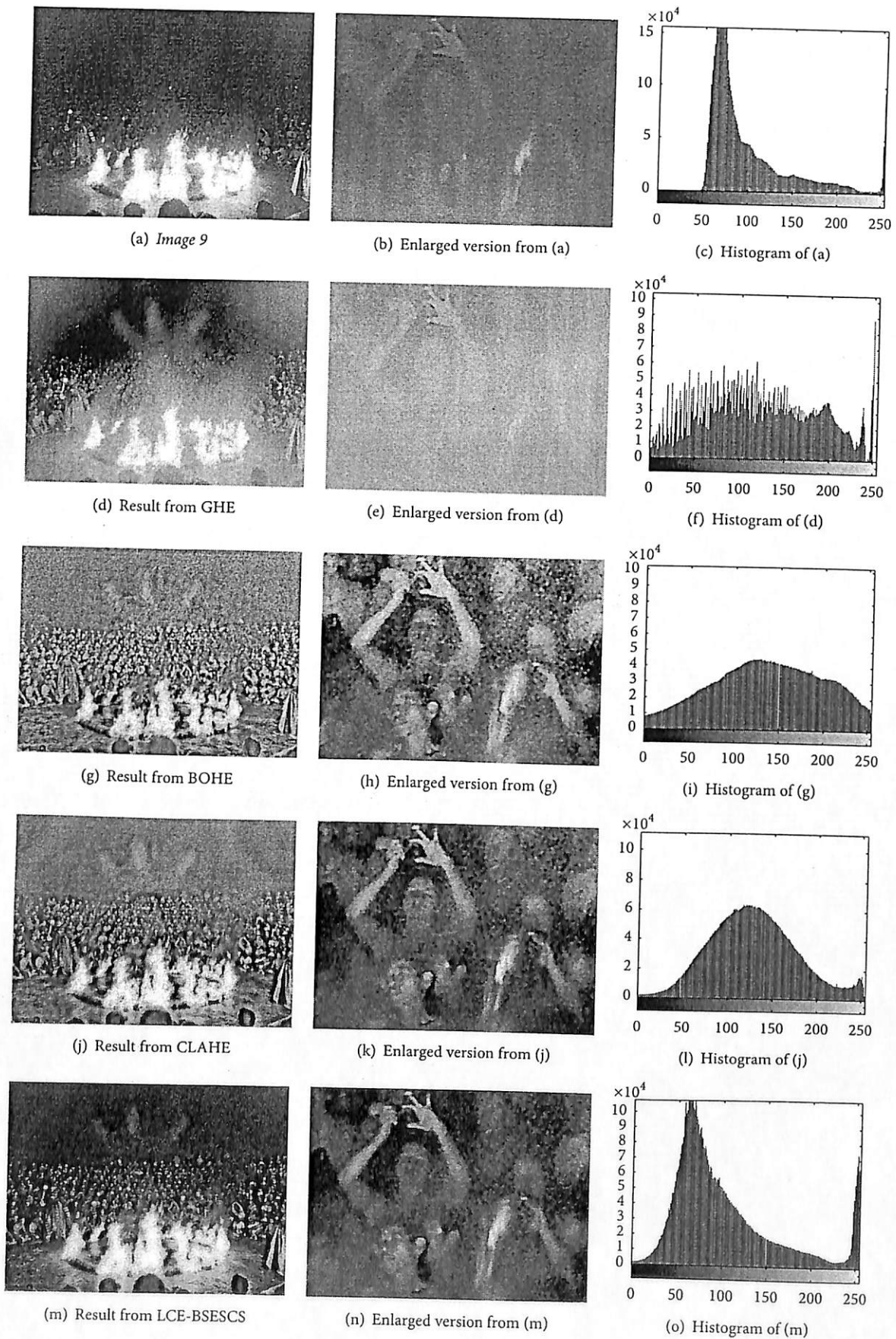


FIGURE 6: Image 9 and its enhanced versions.

TABLE 2: SNS values obtained from nine input images.

	Original	GHE [1]	BOHE [12]	CLAHE [15]	LCE-BSESCS
Image 1	3.4545	7.7319	13.2477	9.5568	6.3514
Image 2	2.2514	7.2053	20.6303	18.9394	8.0975
Image 3	5.0863	10.4602	18.2116	12.6374	7.8931
Image 4	3.9052	15.9535	23.8075	14.9450	6.5358
Image 5	5.2880	7.0348	19.8410	13.8103	7.4881
Image 6	7.8513	13.6009	22.8940	14.1334	9.1318
Image 7	1.3906	20.8070	30.4298	20.1688	5.2793
Image 8	0.5047	20.4854	44.9306	32.5611	3.5101
Image 9	1.0342	12.8723	21.9976	17.5813	3.8881
Average	3.4185	12.9057	23.9989	17.1482	6.4639

concluded that the proposed method shows the best overall performance.

Conflict of Interests

The authors declare that there is no conflict of interests regarding the publication of this paper.

Acknowledgment

This work was supported in part by the Universiti Sains Malaysia's Research University Individual (RUI) with Account no. 1001/PELECT/814169.

References

- [1] R. C. Gonzalez and R. E. Woods, *Digital Image Processing*, Pearson Prentice Hall, Upper Saddle River, NJ, USA, 3rd edition, 2008.
- [2] M. Petrou and P. Bosdogianni, *Image Processing: The Fundamental*, John Wiley & Sons, 2000.
- [3] H. D. Cheng and H. Xu, "A novel fuzzy logic approach to contrast enhancement," *Pattern Recognition*, vol. 33, no. 5, pp. 809–819, 2000.
- [4] S. Yang, J. H. Oh, and Y. Park, "Contrast enhancement using histogram equalization with bin underflow and bin overflow," in *Proceedings of the International Conference on Image Processing (ICIP '03)*, pp. 881–884, September 2003.
- [5] Y.-T. Kim, "Contrast enhancement using brightness preserving bi-histogram equalization," *IEEE Transactions on Consumer Electronics*, vol. 43, no. 1, pp. 1–8, 1997.
- [6] V. Magudeeswaran and C. G. Ravichandran, "Fuzzy logic-based histogram equalization for image contrast enhancement," *Mathematical Problems in Engineering*, vol. 2013, Article ID 891864, 10 pages, 2013.
- [7] S.-D. Chen and A. R. Ramli, "Preserving brightness in histogram equalization based contrast enhancement techniques," *Digital Signal Processing*, vol. 14, no. 5, pp. 413–428, 2004.
- [8] K. S. Sim, C. P. Tso, and Y. Y. Tan, "Recursive sub-image histogram equalization applied to gray scale images," *Pattern Recognition Letters*, vol. 28, no. 10, pp. 1209–1221, 2007.
- [9] K. Wongsritong, K. Kittayaruasiriwat, F. Cheevasuvit, K. Dejhan, and A. Somboonkaew, "Contrast enhancement using multi-peak histogram equalization with brightness preserving," in *Proceedings of the IEEE Asia-Pacific Conference on Circuits and Systems (IEEE APCCAS '98)*, pp. 455–458, November 1998.
- [10] Q. Wang and R. K. Ward, "Fast image/video contrast enhancement based on weighted thresholded histogram equalization," *IEEE Transactions on Consumer Electronics*, vol. 53, no. 2, pp. 757–764, 2007.
- [11] H. Ibrahim, N. S. P. Kong, C. H. Ooi, and D. C. J. Chieh, "Image enhancement with noise suppression ability using histogram manipulations," in *Proceedings of the 1st International Conference on Information Science and Engineering (ICISE '09)*, pp. 579–582, December 2009.
- [12] N. S. P. Kong and H. Ibrahim, "Multiple layers block overlapped histogram equalization for local content emphasis," *Computers and Electrical Engineering*, vol. 37, no. 5, pp. 631–643, 2011.
- [13] S. M. Pizer, E. P. Amburn, J. D. Austin et al., "Adaptive histogram equalization and its variations," *Computer Vision, Graphics, and Image Processing*, vol. 39, no. 3, pp. 355–368, 1987.
- [14] J.-Y. Kim, L.-S. Kim, and S.-H. Hwang, "An advanced contrast enhancement using partially overlapped sub-block histogram equalization," *IEEE Transactions on Circuits and Systems for Video Technology*, vol. 11, no. 4, pp. 475–484, 2001.
- [15] S. M. Pizer, R. E. Johnston, J. P. Ericksen, B. C. Yankaskas, and K. E. Muller, "Contrast-limited adaptive histogram equalization: speed and effectiveness," in *Proceedings of the 1st Conference on Visualization in Biomedical Computing (VBC '90)*, pp. 337–345, May 1990.
- [16] C. H. Ooi, N. P. Kong, and H. Ibrahim, "Bi-histogram equalization with a plateau limit for digital image enhancement," *IEEE Transactions on Consumer Electronics*, vol. 55, no. 4, pp. 2072–2080, 2009.



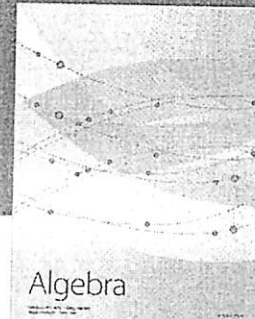
Advances in
Operations Research



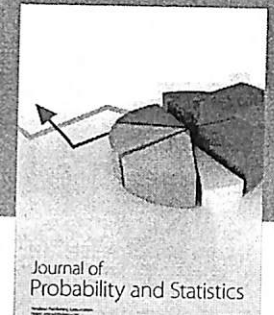
Advances in
Decision Sciences



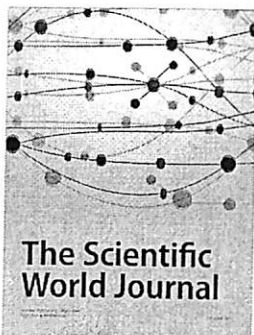
Journal of
Applied Mathematics



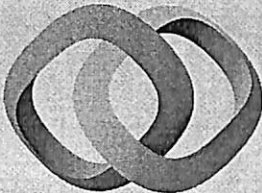
Algebra



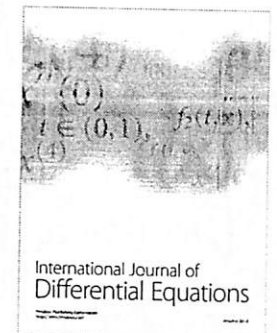
Journal of
Probability and Statistics



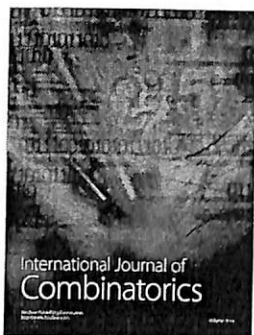
The Scientific
World Journal



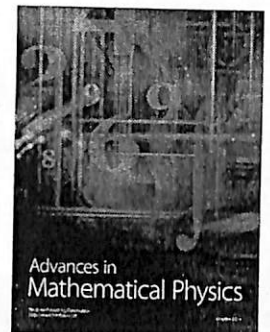
Hindawi
Submit your manuscripts at
<http://www.hindawi.com>



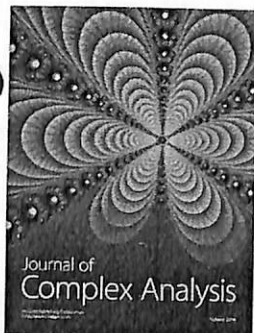
International Journal of
Differential Equations



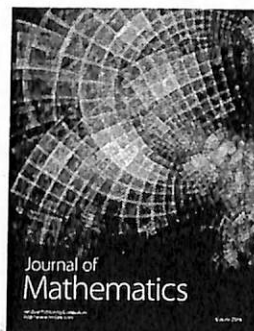
International Journal of
Combinatorics



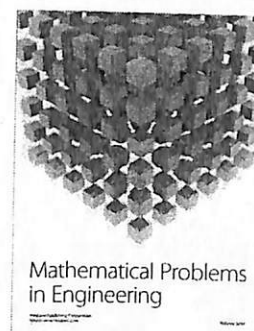
Advances in
Mathematical Physics



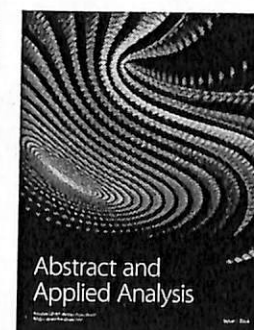
Journal of
Complex Analysis



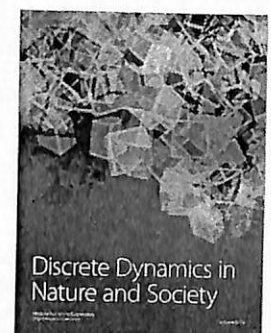
Journal of
Mathematics



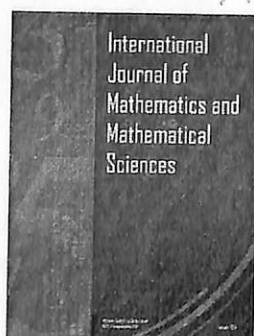
Mathematical Problems
in Engineering



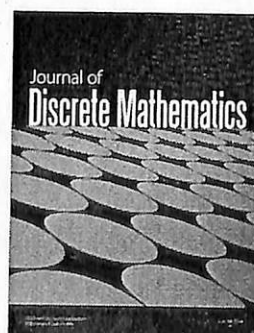
Abstract and
Applied Analysis



Discrete Dynamics in
Nature and Society



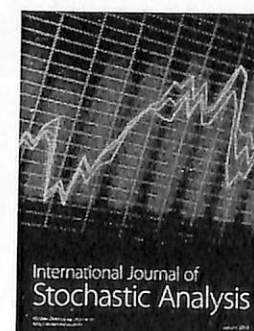
International
Journal of
Mathematics and
Mathematical
Sciences



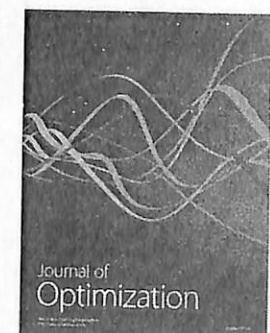
Journal of
Discrete Mathematics



Journal of
Function Spaces



International Journal of
Stochastic Analysis



Journal of
Optimization

Exploration of Current Trend on Median Filtering Methods Utilized in Digital Grayscale Image Processing

Sin Hoong Teoh, Boon Tatt Koik, and Haidi Ibrahim

Abstract—Median filtering is a well known method to deal with impulse noise in digital images. However, due to some limitations associated with the standard median filtering approach, several new improved versions of the median filtering method have been proposed by researchers. The number of methods is expanding from year to year. Therefore, the purpose of this paper is to see the current trend of the median filtering techniques. The trend is observed from the available online literatures; which use or propose new median filtering methods. Because there are thousands of related reliable literatures available online alone, our research concentrates on online literatures only. These literatures were classified according to their search keywords. The scope of our research is limited to IEEEExplore®, ScienceDirect, and Google Scholar databases only. The results confirm that the research regarding to median filtering is still growing at this time. Furthermore, we observed that the weighted median filter is the most popular median filtering research, and it is followed by researches on the adaptive median filter. Based on ScienceDirect database, it is shown that all of the median filtering methods showing an increasing number of publications over year.

Index Terms—Impulse noise, literature survey, median filtering, salt-and-pepper noise.

I. INTRODUCTION

As the demand of the products from the consumers are showing an increasing trend, most of the industries are now employing automatic electronic systems in their production lines. Computerized systems, utilizing optical sensors such as CCD and CMOS, becoming popular in recent years [1]. In order to reduce the burden of human operators in inspection lines, machine vision systems must simulate the human abilities to detect defect products. Therefore, to imitate and put into practice the function of human vision system, the computerized system must use engineering methods, especially from the field of computer, physics and electronic engineering. However, it is worth noting that up to these date, these vision systems are mostly used to assist the work by the human operators, and not completely replacing the human in the production line [2].

Signal acquired by the machine vision system is mostly in the form of digital images, which are two or more dimensional signals. One type of digital images used by the system is the digital grayscale image [3]. Unfortunately, similar to other type of digital images, digital grayscale

images can be corrupted by unnecessary noise signals, including the impulse noise [4]. There are some reasons how the impulse noise can appears in digital grayscale images. Impulse noise can be contributed by malfunctioned image sensors, damaged memory cell in hard disk, and signal corruption during transmission [5]. Impulse noise is a random additive noise, and it has significantly high contrasts towards its surrounding, uncorrupted region. Therefore, even at a very low corruption level of impulse noise, the digital grayscale image might loss its information significantly [6]. As a consequence, the noise mostly will make the automatic vision based systems to give inaccurate outcomes [7].

One of the methods that are used widely to deal with impulse noise in digital grayscale images is the median filtering method [4]. Standard median filtering method works by using a sliding window. It filters the corrupted input image by replacing the corresponding pixel that located on the centre of the window, with the median value determined from the intensity samples, defined by the sliding window at that position [8]. Unfortunately, the standard median filtering method uses all the intensity samples within the sliding window, without considering whether they are noisy pixels, and therefore produce inaccurate results when the input image was damaged by a high degree of impulse noise [9]. On the other hand, as the method changes all the pixel values although the pixels are uncorrupted, the method tends to make unnecessary changes. Therefore, the method will further degrade the image, especially when the input image was corrupted by low level of impulse noise [5]. Furthermore, sharp lines also will be altered by the standard median filter [10].

The limitations of the standard median filter have attracted attention from researchers. In order to overcome these limitations of the standard median filter, many researchers have proposed an extension, or improvement to the method. Hundreds of reliable literatures based on median filtering methods can be found online these days. We believe that there are another hundreds of related literatures that are not available online. According to our past literature survey on the available median filtering method [11], in addition to the standard median filtering method, the improved median filtering methods can be classified into seven categories. They are:

1) Weighted median filter

- First introduced by Justusson in 1981, and further elaborated by Brownrigg [12].
- It has weights to associate with each of its filter element.
- The weight corresponds to the number of sample

Manuscript received December 5, 2012; revised February 6, 2013.

The authors are with the School of Electrical & Electronic Engineering, Engineering Campus, Universiti Sains Malaysia, 14300 Nibong Tebal, Penang, Malaysia (e-mail: tshoong81@yahoo.com, bt5041@gmail.com, haidi_ibrahim@iecc.org).

duplications in the calculation of median value.

2) Iterative median filter

- Iterative method requires the same procedure to be repeated several times.
- Examples are methods in [13]-[15].

3) Recursive median filter

- The output at certain position are determined not only using the input intensities, but also from the pre-calculated output values at previous locations.
- Analogous to infinite impulse response (IIR) filter
- Examples of related methods are [16]-[18].
- Directional median filter
- Works by separating its 2-D sliding window into several 1-D filter components.
- Examples of works are [19]-[21].

4) Switching median filter

- Also known as decision based median filter.
- Normally has two stages; noise detection stage, and noise cancellation stage
- Example of works are [22]-[24].

5) Adaptive median filter

- The filter size is not constant.
- The size is depending to local noise content.
- Examples of works are [25]-[27].

6) Median filter with fuzzy logics

- Uses fuzzy logic to process the image.
- Example of works are [28]-[30].

Each of these abovementioned approaches has its own advantages and disadvantages. As consequences, more and more new methods have been introduced from time to time.

It is worth noting that median filtering method is one of the fundamental methods in digital image processing research. Yet, most of the people, especially those who are outside the field of digital image de-noising, will be surprised when we mentioned that the researches on median filtering technique are still popular these days. Therefore, the aim of this research paper is to show quantitatively that the research on median filtering methods is still expanding. In addition to this, we are also interested to see the current research trend in this area. We want to identify which median filtering approach is now popular, and the trend of the median filtering research towards time.

To ease the presentation of this paper, this paper is organized into four main sections. The first section, which is this section, gives the background and the purposes of this research. Then, Section II explains how this research will be carried out. Section III presents the outcome of this research, while the last section, which is Section IV, concludes our findings.

II. METHODOLOGY

Currently, the number of researches regarding to median filtering for impulse noise reduction from grayscale digital images is very large. Search on internet alone, regarding median filtering method, gave us hundreds of related reliable literatures. As a consequence, it is almost impossible for us to inspect every single literature in details for the methodology

they used or proposed.

To overcome this limitation, we will classify these literatures based on their keywords. We assume that the keywords are used by the literatures reflects exactly the median filtering approach used by that literature. The keywords used are listed in Table I.

TABLE I: THE KEYWORDS USED TO SEARCH RELATED LITERATURES

Method	Keyword
Weighted Median Filter	"Weighted Median Filter Image"
Iterative Median Filter	"Iterative Median Filter Image"
Recursive Median Filter	"Recursive Median Filter Image"
Directional Median Filter	"Directional Median Filter Image"
Switching Median Filter	"Switching Median Filter Image"
Adaptive Median Filter	"Adaptive Median Filter Image"
Median Filter with Fuzzy Logics	"Fuzzy Median Filter Image"
Median Filter (in general)	"Median Filter Image"

We only restricted our research to online literatures. Because there are many online databases are now available, we are then further limiting our searching to these following three well-known databases:

1) IEEExplore® (<http://ieeexplore.ieee.org>)

- Is a well known online database regarding to the researches on electrical, electronic and computer engineering.

2) ScienceDirect (<http://www.sciencedirect.com>)

- Is one of the world's famous database for scientific, technical, and medical full text research papers.

3) Google Scholar (<http://scholar.google.com.my>)

- Provides a search of literatures across many disciplines and sources, including journals, proceedings, abstracts, books, theses, and patents.

In order to see the research trend of each particular median filtering method, the publication year's field, located on the left side of the corresponding webpage will be manipulated. Example of this field, taken from IEEExplore® database, is shown in Fig. 1. Using this useful feature, the number of publication for each year can be determined. Thus, by recording the number of publications versus years, we can see whether the research is expanding, or shrinking. The results then can represent the popularity of each method. The research has been carried out on early December 2012.

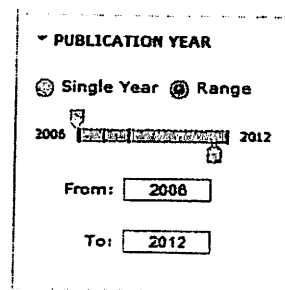


Fig. 1. "Publication Year" feature provided by IEEExplore®.

III. RESULTS

In order to see whether the research regarding median filtering in digital image processing is still popular or not, we utilized the keyword "median filter image" for our search.

The results from three databases are shown in Fig. 2 to Fig. 5. We cannot combine these results together and present it as one figure because the number of publications obtained from each database is significantly very different from each other.

As shown by these figures, the number of publications on median filtering research is the smallest from IEEExplore® database, followed by ScienceDirect, and Google Scholar. This is because the content of IEEExplore® database is only restricted towards electrical, electronic, and computer engineering researches.

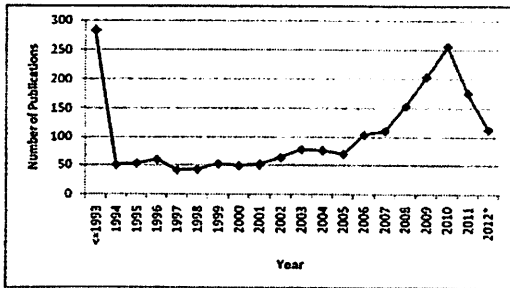


Fig. 2. The trend on the researches regarding to median filtering method, observed from IEEExplore® database.

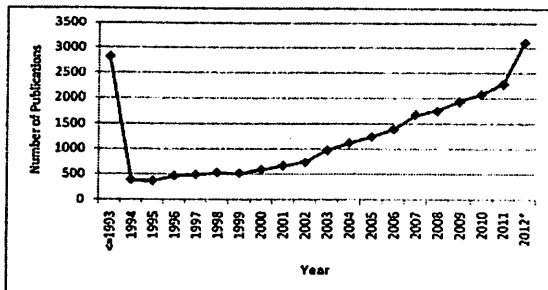


Fig. 3. The trend on the researches regarding to median filtering method, observed from ScienceDirect database.

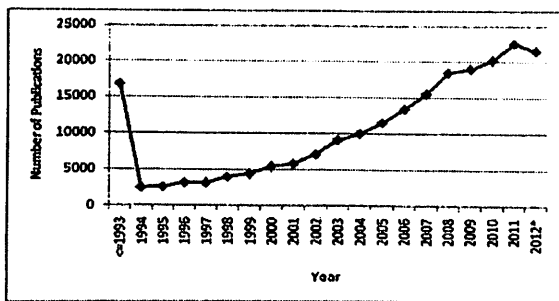


Fig. 4. The trend on the researches regarding to median filtering method, observed from Google Scholar database.

From Fig. 2, it is shows that in IEEExplore database, the research regarding to median filtering is expanding, until 2010, where the rate of the research is slightly reducing after that. However, as shown by Fig. 3 and Fig. 4, the corresponding researches in ScienceDirect and Google Scholar are still expanding. Furthermore, from these figures, we can see that there are more than thousands of related papers introduced in each year. Therefore, this showing that the research related to median filtering method is still expanding these days.

In order to investigate the recent popularity each median filtering method considered in this research, we inputted the keywords shown in Table I to those three databases. By assuming that there is no re-occurrence of literatures between these databases, we plot the accumulated number of

publications versus median filtering methods. Because we want to see the current popularity, our search is restricted to year 2000 and beyond. The result is shown by Fig. 5. We assume that the higher number of publications indicates the popularity. Therefore, from this bar graph, we can say that the weighted median filter has the highest popularity, followed by the adaptive median filter, iterative median filter, directional median filter, switching median filter, fuzzy median filter, and lastly, recursive median filter.

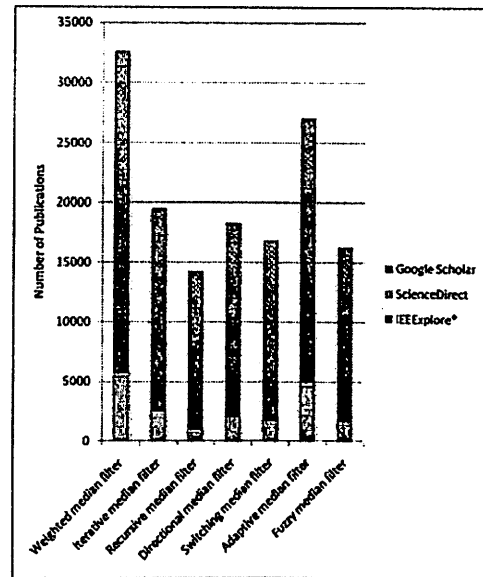


Fig. 5. The bar graph showing the accumulated number of publications versus median filtering methods.

Another question that we want to answer is related to the research trend on each of the median filtering techniques. Therefore, we inspect the trend from ScienceDirect database. The plot of graphs for each median filtering technique, as a function of number of publications versus years was obtained from year 2000 to 2012. This is obtained by utilizing the publication year feature in ScienceDirect. The result is shown in Fig. 6. As shown by this figure, basically all of the methods are showing an increasing in number of publications over years.

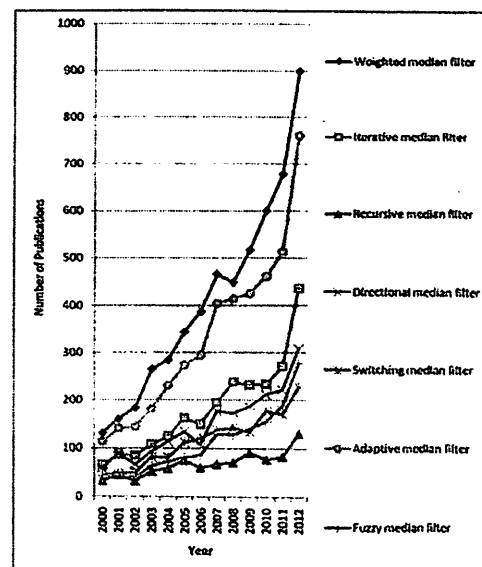


Fig. 6. The trend on the research regarding to each median filtering methods, observed from ScienceDirect database.

IV. CONCLUSION

The results from this survey prove that the researches regarding to median filtering in digital image processing field are still expanding. Majority of the online databases shows an exponentially growth of literatures related to this type of research. Based on the trend observed, the number of materials is expected to continue expanding in the future. The research also successfully shows that the trend for each of the median filtering framework is also expanding as well. It is shown that the weighted median filter is the most popular median filtering framework in current literatures, followed by adaptive median filter, iterative median filter, directional median filter, fuzzy median filter, switching median filter, and lastly recursive median filter.

ACKNOWLEDGMENT

This work was supported in part by the Universiti Sains Malaysia's Short Term Research Grant with account number 304/PELECT/60311013 and Universiti Sains Malaysia's Research University Individual (RUI) Grant with account number 1001/PELECT/814169.

REFERENCES

- [1] C. Y. Wang and D. Lee, "Integration of manufacturing systems: A vision and image processing system perspective," in *Proc. of System Integration*, 1990, pp. 310-316.
- [2] L. Han, F. Xue, Z. Li, and D. Chen, "A generic framework for human-machine hybrid recognition based on wearable visual computing," *Applied Mechanics and Materials*, vol. 39, pp. 317-321, 2011.
- [3] R. C. Gonzalez and R. E. Woods, *Digital Image Processing*, Upper Saddle River, New Jersey, USA, 2008, ch. 2.
- [4] R. C. Gonzalez and R. E. Woods, *Digital Image Processing*, Upper Saddle River, New Jersey, USA, 2008, ch. 5.
- [5] R. H. Chan, C. W. Ho, and M. Nikolova, "Salt-and-pepper noise removal by median-type noise detectors and detail preserving regularization," *IEEE Trans. Image Processing*, vol. 14, no. 10, pp. 1479-1485, 2005.
- [6] H. Ibrahim, K. C. Neo, S. H. Teoh, T. F. Ng, D. C. J. Chieh, and N. F. N. Hassan, "Impulse noise model and its variations," *International Journal of Computer and Electrical Engineering (IJCEE)*, vol. 4, no. 5, pp. 647-650.
- [7] M. E. Yuksel and M. T. Yildirim, "A simple neuro-fuzzy edge detector for digital images corrupted by impulse noise," *AEU-International Journal of Electronics and Communications*, vol. 58, no. 1, pp. 72-75, 2004.
- [8] R. L. Swenson and K. R. Dimond, "A hardware FPGA implementation of a 2D median filter using a novel rank adjustment technique," in *Seventh International Conference on Image Processing and Its Applications*, vol. 1, 1999, pp. 103-106.
- [9] H. Ibrahim, "Adaptive switching median filter utilizing quantized window size to remove impulse noise from digital images," *Asian Trans. Fundamentals of Electronics, Communication & Multimedia*, vol. 2, no. 1, 2012.
- [10] S. Zhang and M. A. Karim, "A new impulse detector for switching median filters," *Signal Processing Letters*, vol. 9, no. 11, pp. 360-363, 2002.
- [11] S. H. Teoh and H. Ibrahim, "Median filtering frameworks for reducing impulse noise from grayscale digital images: A literature review," *International Journal of Future Computer and Communication*, vol. 1, no. 4, pp. 323-326, 2012.
- [12] R. Yang, L. Yin, M. Gabbouj, J. Astola, and Y. Neuvo, "Optimal weighted median filtering under structural constraints," *IEEE Trans. Signal Processing*, vol. 43, no. 3, pp. 591-604, 1995.
- [13] Z. Wang and D. Zhang, "Progressive switching median filter for the removal of impulse noise from highly corrupted images," *IEEE Trans. Circuits and Systems II: Analog and Digital Signal Processing*, vol. 46, no. 1, pp. 78-80, 1999.
- [14] C. Spence and C. Fancourt, "An iterative method for vector median filtering," in *Proc. IEEE International Conference on Image Processing (ICIP 2007)*, vol. 5, 2007, pp. 265-268.
- [15] A. R. Forouzan and B. N. Araabi, "Iterative median filtering for restoration of images with impulse noise," in *Proc. the 2003 10th IEEE International Conference on Electronics, Circuits and Systems*, vol. 1, pp. 232-235, 2003.
- [16] G. R. Arce, "Statistical threshold decomposition for recursive and non-recursive median filters," *IEEE Trans. Information Theory*, vol. 32, no. 2, pp. 234-253, 1986.
- [17] G. R. Arce and N.C. Gallagher Jr., "Stochastic analysis for the recursive median filter process," *IEEE Trans. Information Theory*, vol. 34, no. 4, pp. 669-679, 1988.
- [18] A. Burian and P. Kuosmanen, "Tuning the smoothness of the recursive median filter," *IEEE Trans. Signal Processing*, vol. 50, no. 7, pp. 1631-1639, 2002.
- [19] A. Nasimudeen, M. S. Nair, and R. Tatavarti, "Directional switching median filter using boundary discriminative noise detection by elimination," *Signal, Image and Video Processing*, vol. 6, no. 4, pp. 613-624, 2012.
- [20] A. Hussain, M. A. Jaffar, and A. M. Mirza, "A hybrid image restoration approach: Fuzzy logic and directional weighted median based uniform impulse noise removal," *Knowledge and Information Systems*, vol. 24, no. 1, pp. 77-90, 2010.
- [21] R. N. Czerwinski, D. L. Jones, and W. D. O. Brien Jr., "Ultrasound speckle reduction by directional median filtering," in *Proc. International Conference on Image Processing*, 1995, vol. 1, pp. 358-361.
- [22] S. F. Liang, S. M. Lu, J. Y. Chang, and C. T. Lee, "A novel two-stage impulse noise removal technique based on neural networks and fuzzy decision," *IEEE Trans. Fuzzy Systems*, vol. 16, no. 4, pp. 863-873, 2008.
- [23] V. Saradhadevi and V. Sundaram, "A novel two-stage impulse noise removal technique based on neural networks and fuzzy decision," *International Journal of Computer Applications*, vol. 21, no. 3, pp. 31-42, 2011.
- [24] R. Kubota and N. Suetake, "Distribution distance-based threshold auto-tuning method for switching median filter," *IEICE Electronics Express*, vol. 7, no. 17, pp. 1310-1316, 2010.
- [25] K. M. Moon, M. D. Patil, and B. Parmar, "Image restoration using adaptive switching median filter," in *2010 IEEE International Computational Intelligence and Computing Research (ICCIC)*, 2010, pp. 1-4.
- [26] C. C. Hsieh, P. C. Huang, and S. Y. Hung, "Noisy image restoration based on boundary resetting BDND and median filtering with smallest window," *WSEAS Transactions on Signal Processing*, vol. 5, no. 5, pp. 178-187, 2009.
- [27] P. E. Ng and K. K. Ma, "A switching median filter with boundary discriminative noise detection for extremely corrupted images," *IEEE Trans. Image Processing*, vol. 15, no. 6, pp. 1506-1516, 2006.
- [28] K. K. Anisha and M. Wilscy, "Impulse noise removal from medical images using fuzzy genetic algorithm," *Signal & Image Processing: An International Journal (SIPIJ)*, vol. 2, no. 4, pp. 173-186, 2011.
- [29] A. Toprak and I. Guler, "Suppression of impulse noise in medical images with the use of fuzzy adaptive median filter," *Journal of Medical Systems*, vol. 30, no. 6, pp. 465-471, 2006.
- [30] A. Toprak, and I. Guler, "Impulse noise reduction in medical images with the use of switch mode fuzzy adaptive median filter," *Digital Signal Processing*, vol. 17, no. 4, pp. 711-723, 2007.



Sing Hoong Teoh received his B.Eng. degree in electronic engineering from Universiti Sains Malaysia, Malaysia, in year 2006. He is currently an engineer at Altera Malaysia, and furthering his MSc degree as a part time student at the School of Electrical and Electronic Engineering, Engineering Campus, Universiti Sains Malaysia, Nibong Tebal, Penang, Malaysia. His research interest is impulse noise reduction from digital images.



Boon Tatt Koik received his B.Eng. degree in electronic engineering from Universiti Sains Malaysia, Malaysia, in year 2012. He has published two research papers in international journals, regarding to digital image processing. His research interest includes digital image contrast enhancement, noise reduction, and change detection.



Haidi Ibrahim received his B. Eng degree in electronic engineering from Universiti Sains Malaysia, Malaysia, in year 2000. He then received his Ph.D. degree in digital image processing from the Centre for Vision, Speech, and Signal Processing (CVSSP), University of Surrey, Guildford, Surrey, United Kingdom in year 2005. He is now a senior lecturer at the School of Electrical and Electronic Engineering, Engineering Campus, Universiti Sains Malaysia, Nibong Tebal, Penang, Malaysia. His research interest includes digital image contrast enhancement, noise reduction, image segmentation, 3D visualization, and virtual reality.

A Literature Review on Histogram Equalization and Its Variations for Digital Image Enhancement

Nicholas Sia Pik Kong, Haidi Ibrahim, and Seng Chun Hoo

Abstract—Global Histogram Equalization (GHE) is a well-known image enhancement method. Despite of its simplicity and popularity, GHE still has limitations. GHE usually causes the shifting of the mean luminance of the image, produces artifacts and unnatural enhancements, and does not consider local information in its process. Therefore, these limitations lead to the development of several histogram equalization (HE) methods. This paper surveys some of HE based methods. These methods generally fall into three main families of HE, namely Mean Brightness Preserving HE (MBPHE), Bin Modified HE (BMHE), and Local HE (LHE).

Index Terms—Image enhancement, contrast enhancement, histogram equalization.

I. INTRODUCTION

Histogram is one of the important features which are very related to image enhancement. The histogram does not only gives us a general overview on some useful image statistics (e.g. mode, and dynamic range of an image), but it also can be used to predict the appearance and intensity characteristic of an image. If the histogram is concentrated on the low side of the intensity scale, the image is mostly a dark image. On the other hand, if the histogram is concentrated on the high side of the scale, the image is mostly a bright image. If the histogram has a narrow dynamic range, the image usually is an image with a poor contrast [1].

In order to define a histogram, first, assume that $X = \{X(i, j)\}$ is an image that is composed of L discrete gray levels denoted by $\{X_0, X_1, \dots, X_{L-1}\}$. Here, $X(i, j)$ represents the intensity of the image at spatial location (i, j) with the condition that $X(i, j) \in \{X_0, X_1, \dots, X_{L-1}\}$. As the intensities are all in discrete values, the histogram of a digital image is a discrete function. Then, the histogram h is defined as:

$$h(X_k) = n_k, \quad \text{for } k=0, 1, \dots, L-1 \quad (1)$$

where X_k is the k -th gray level and n_k presents the number of times that the gray level X_k appears in the image. In other words, the histogram is the frequency of occurrence of the gray levels in the image [2].

Alternatively, as used by Wang et al. [3], and Wang and Ye [4], the histogram also can be defined as the statistic probability distribution of each gray level in a digital image. For a given image X , the Probability Density Function (PDF) for intensity X_k , $p(X_k)$, is given by:

$$p(X_k) = n_k / N, \quad \text{for } k=0, 1, \dots, L-1 \quad (2)$$

where N is the total number of samples in the image. By comparing equation (2) with equation (1), the PDF is actually a normalized version of the histogram. Usually, the histogram of an image X is presented as a graph plots of $h(X_k)$ versus X_k , or $p(X_k)$ versus X_k .

There are many Histogram Equalization (HE) methods for digital image contrast enhancement. One of the well-known HE methods is Global Histogram Equalization (GHE), which is also known as Tradisional HE [5] and [6], Classical HE [2] and [7], Conventional HE [8]-[10], and Typical HE [11]-[13]. The basic idea of GHE method is to remap the gray levels of an image based on the image's gray levels cumulative density function.

GHE uses the information of the whole intensity values inside the image for its transformation function and thus this method is suitable for global enhancement [14]. Its goal is to redistribute the intensity of an image uniformly over the entire range of gray-levels (i.e. the image's cumulative histogram is linear) which is very effective for enhancing low contrast detail of an image [15] and maximize the entropy of an image [2] and [4].

GHE attempts to "spread out" the intensity levels belongs to an image to cover the entire available intensity range [16]. GHE flattens and stretches the dynamic range of the resultant image histogram and as a consequence, the enhanced image will optimally utilize the available display levels [17]. This then yields an overall contrast improvement.

A. GHE Algorithm

The sum of all components of a normalized histogram or PDF results a Cumulative Density Function (CDF) of an image. Based on the PDF in equation (2), the CDF for intensity X_k , $c(X_k)$, is defined by the following equation:

$$c(X_k) = \sum_{j=0}^k p(X_j) \quad \text{for } k=0, 1, \dots, L-1 \quad (3)$$

where by definition, $c(X_k)=1$. GHE is a scheme that maps the input image into the entire dynamic range, $[X_0, X_{L-1}]$, by using CDF as its transformation function. Now, let $x=X_k$. The transform function, $f(x)$, is defined based on the CDF as:

$$f(x) = X_0 + (X_{L-1} - X_0).c(x) \quad \text{for } k=0, 1, \dots, L-1 \quad (4)$$

From here, the output image produced by GHE, $Y = \{Y(i, j)\}$, can be expressed as in the following equation:

$$Y = f(X) = \{f(X(i, j)) \mid \forall X(i, j) \in X\} \quad (5)$$

Manuscript received November 25, 2012; revised January 28, 2013.

The authors are with the School of Electrical and Electronic Engineering, Engineering Campus, Universiti Sains Malaysia, 14300 Nibong Tebal, Penang, Malaysia (e-mail: pik_kong@yahoo.com; haidi_ibrahim@ieee.org; hsc852@hotmail.com).

B. Limitations of GHE

Although GHE is suitable for an overall contrast enhancement, practically there are some limitations associated with GHE. Although GHE successfully stretches and expands the dynamic range of the image [1], the histogram is far from being flat. The histogram of the output image may contain many empty bins (A bin is defined as a series of equal intervals in a dynamic range of an image employed to describe the divisions in a histogram.) because the histogram is actually a shifted version of the original histogram [7]. Thus, the entropy value of the GHE enhanced image is almost similar to the original version, and not maximized as expected in theory.

GHE also usually causes level saturation (clipping) effects in small but visually important areas [5]. This happens because GHE extremely pushes the intensities towards the right (bright) or the left (dark) side of the histogram. If the input image is dominated by dark intensity pixels, the histogram is pushed to the right side, and thus bright saturation effect will be clearly visible. On the other hand, if the input is dominated by bright intensity pixels, the output normally suffers from dark saturation effect. This saturation effect, not only degrades the appearance of the image, but also leads to information loss [14].

GHE does the enhancement globally, without considering the local contents of the image. GHE method is effective in enhancing the low contrast image when the input image contains only one big single object, or when there is no appearance contrast change between the object and the background in the image [18]. For other images, GHE mapping often result in undesirable effects such as over enhancement for intensity levels with high probabilities, and loss of contrast for levels with low probabilities [5], [14], [18], [19] and [20]. Thus, the enhancement might be biased towards the depiction of parts of the image which are unimportant for the viewer such as the background area of the image [21] and [22]. As a consequence, GHE algorithm is not applicable to many image modalities, such as infrared image, because this algorithm usually enhances the image's background instead of the object that occupies only a small portion of the image [23].

Furthermore, GHE often causes the shifting on the average (i.e. mean) luminance of the image [3], which is a well-known mean-shift problem [20]. Therefore, GHE is rarely employed in consumer electronic products such as video surveillance, digital camera, and digital television, where the brightness preserving characteristic of the enhancement method is crucial [4]. A dark movie scene displayed on television, for example, should be maintained dark in order to keep its artistic value. Besides, the excessive change in brightness level introduced by GHE leads to annoying artifacts and unnatural enhancement. The noise in the image is also enhanced or magnified [24]. Thus, although GHE can increase the brightness level in the image, this technique might significantly degrade the quality of the image.

II. EXTENSIONS OF HISTOGRAM EQUALIZATION TECHNIQUE

The limitations of GHE as mentioned in Subsection I.B

have encouraged many researchers to actively develop various extensions to Histogram Equalization (HE) method. Generally, variations of HE can be classified into four groups as shown in Fig. 1. In addition to GHE, they are Mean Brightness Preserving HE, Bin Modified HE, and Local HE. Hence, this paper provides a literature review on some of the extensions of HE. Subsection II. A will discuss about the Mean Brightness Preserving HE methods. Then, the Bin Modified HE will be presented in Subsection II. B. After that, Subsection II. C will give in details about the Local HE.

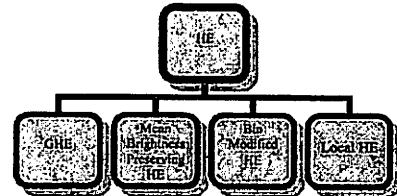


Fig. 1. Block diagram of HE's extensions.

A. Mean Brightness Preserving Histogram Equalization (MBPHE)

MBPHE is a novel extension to HE. This type of enhancement method is specially developed for the use in consumer electronic products such as digital television, digital camera and camcorder. The idea of keeping the mean brightness of an image for consumer electronic products is first introduced by Kim [12]. By preserving the mean brightness, this is not only can maintain the artistic value of the image, but it is also proven that this methodology can reduce the saturation effect, and able to avoid unnatural enhancement and annoying artefacts on the output image.

Commonly, MBPHE decomposes the input image into two or more sub-images, and then it equalizes the histograms of these sub-images independently. The major difference among the MBPHE methods is the criteria used to decompose the input image. Examples of MBPHE methods are Brightness Preserving Bi-HE (BBHE) [12], Quantized Bi-HE (QBHE) [11], Dual Sub-Image HE (DSIHE) [3], Minimum Mean Brightness Error Bi-HE (MMBEBHE) [25] and [26], Recursive Mean-Separate HE (RMSHE) [13] and [26], Recursive Sub-Image HE (RSIHE) [10], Recursive Separated and Weighted HE (RSWHE) [20], Multippeak HE (MPHE) [27], Dynamic HE (DHE) [14], Multi-HE (MHE) [2] and [28], Brightness Preserving Weight Clustering HE (BPWCHE) [29], Brightness Preserving Dynamic HE (BPDHE) [30], and HE with Range Offset (HERO) [31].

B. Bin Modified Histogram Equalization (BMHE)

GHE stretches the contrast of the high histogram region, and compresses the contrast of the low histogram regions [29]. As a consequence, when the object of interest in an image only occupies a small portion of the image, this object will not be successfully enhanced by GHE. Thus, to overcome this limitation, an extension of HE, which is the Bin Modified Histogram Equalization (BMHE) has been introduced.

BMHE modifies the shape of the image histogram by reducing or increasing the value in the histogram's bins based on a threshold limit before the equalization is taking place. Examples of BMHE based methods are Bin

Underflow and Bin Overflow HE (BUBOHE) [32], Weighted and Thresholded HE (WTHE) [5] and Self-Adaptive Plateau HE (SAPHE) [23].

C. Local Histogram Equalization (LHE)

It is known that GHE cannot adapt with the local brightness features of the input image [14]. As a consequence, GHE normally fails to enhance the input image with illumination problem. This is because GHE does the enhancement globally, without considering the local content of the image which is usually contains small or hidden details inside it. GHE uses only one single CDF, which is obtained from the entire pixels in the image, to construct its transform function. Thus, the same transform function is being used by all pixels in that image.

To overcome this limitation, an extension to HE known as Local Histogram Equalization (LHE) has been introduced. The main idea of LHE is to define a local transform function for each pixel based on its surrounding neighbouring pixels [5].

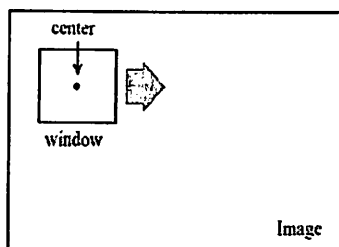


Fig. 2. The basic concept of LHE operation.

Generally, LHE uses a small window to define a Contextual Region (CR) for the center pixel of that window. The relationship between the image and the window is illustrated in Fig. 2. Only the block of pixels that fall in this window is taken into account for the calculation of CDF. Thus, as the window slides, the CDF is modified.

The CDF is the main contributor for the HE transform function. Hence, in LHE, the transform function of a pixel is depending on the statistics of its neighbors in CR. Because the transform function changes as a response to the changes in the contents of CR, LHE is also popularly known as Adaptive Histogram Equalization (AHE) [6] and [33]. Examples of LHE methods are Non-Overlapped Block HE (NOBHE) [1], Block Overlapped HE (BOHE) [1], [19] and [21], Interpolated Adaptive HE (IAHE) [34], Weighted Adaptive HE (WAHE) [34], Contrast Limited Adaptive HE (CLAHE) [34] and [35], Variable Region Adaptive HE (VRAHE) [36], Local Information HE (LIHE) [37], Spatio-Temporally Adaptive HE (STAHE) [19], Partially Overlapped Sub-Block HE (POSHE) [38], Conditional Sub-Block Bi-HE (CSBHE) [39], and Multiple Layers Block Overlapped HE (MLBOHE) [40].

III. REMARKS

In this paper, extensions to HE which are MBPHE, BMHE, and LHE, have been presented. MBPHE methods aim to preserve the overall mean brightness of the original image in the enhanced image, mostly for the implementation in consumer electronic products. After having an extensive review on MBPHE, it is realized that although many

MBPHE methods have been developed, most of them give too much constrain on preserving the mean brightness, rather than enhances the image. Therefore, not much contrast improvement could be obtained from these methods. By altering the input histogram, BMHE methods are able to control the enhancement rate, thus avoid over amplification of noise in an image. However, in order to obtain a good enhancement result, the threshold which is needed to be selected optimally by the user, is difficult to be determined. LHE methods are suitable to be used to reveal small and hidden image content. However, these methods require long processing time, sensitive to noise, and produce unnatural enhancement.

ACKNOWLEDGMENT

This work was supported in part by the Universiti Sains Malaysia's Short Term Research Grant with account number 304/PELECT/60311013 and Universiti Sains Malaysia's Research University Individual (RUI) Grant with account number 1001/PELECT/814169.

REFERENCES

- [1] R. C. Gonzalez and R. E. Woods, *Digital image processing*, 2nd ed. Boston, MA, USA: Prentice-Hall of India, 2002.
- [2] M. L. Najman, J. Facon, and A. de A. Ara'ujo, "Multi-histogram equalization methods for contrast enhancement and brightness preserving," *Consumer Electronics, IEEE Transactions on*, vol. 53, no. 3, pp. 1186–1194, 2007.
- [3] Y. Wang, Q. Chen, and B. Zhang, "Image enhancement based on equal area dualistic sub-image histogram equalization method," *Consumer Electronics, IEEE Transactions on*, vol. 45, no. 1, pp. 68–75, 1999.
- [4] Wang and Z. Ye, "Brightness preserving histogram equalization with maximum entropy: a variational perspective," *Consumer Electronics, IEEE Transactions on*, vol. 51, no. 4, pp. 1326–1334, 2005.
- [5] Q. Wang and R. K. Ward, "Fast image/video contrast enhancement based on weighted thresholded histogram equalization," *Consumer Electronics, IEEE Transactions on*, vol. 53, no. 2, pp. 757–764, 2007.
- [6] Z. Yu and C. Bajaj, "A fast and adaptive method for image contrast enhancement," in *Proc. 2004 International Conference on Image Processing, 2004. ICIP '04*, pp. 1001–1004, vol. 2, 2004.
- [7] M. Eramian and D. Mould, "Histogram equalization using neighbourhood metrics," in *Proc. The 2nd Canadian Conference on Computer and Robot Vision, 2005*, pp. 397–404.
- [8] T. M. Kwon, E. H. Feroz, and H. Cheng, "Preprocessing of training set for backpropagation algorithm: histogram equalization," in *Proc. 1994 IEEE International Conference on Computational Intelligence*, Orlando, FL, USA, pp. 425–430, vol. 1, 1994.
- [9] T. M. Kwon and H. Cheng, "Contrast enhancement for backpropagation," *IEEE Transactions on Neural Networks*, vol. 7, no. 2, pp. 515–524, 1996.
- [10] K. S. Sim, C. P. Tso, and Y. Y. Tan, "Recursive sub-image histogram equalization applied to gray scale images," *Pattern Recognition Letters*, vol. 28, no. 10, pp. 1209–1221, 2007.
- [11] Y. T. Kim, "Quantized bi-histogram equalization," in *Proc. 1997 IEEE International Conference on Acoustics, Speech, and Signal Processing, ICASSP-97*, Munich, Germany, pp. 2797–2800, vol. 4, 1997.
- [12] Y. T. Kim, "Contrast enhancement using brightness preserving bi-histogram equalization," *IEEE Transactions on Consumer Electronics*, vol. 43, no. 1, pp. 1–8, 1997.
- [13] S. D. Chen and A. R. Ramli, "Contrast enhancement using recursive mean-separate histogram equalization for scalable brightness preservation," *IEEE Transactions on Consumer Electronics*, vol. 49, no. 4, pp. 1301–1309, 2003.
- [14] M. Abdullah-Al-Wadud, M. Hasanul Kabir, M. Ali Akber Dewan, and O. Chae, "A dynamic histogram equalization for image contrast enhancement," *IEEE Transactions on Consumer Electronics*, vol. 53, no. 2, pp. 593–600, 2007.
- [15] L. Hall, "Almost uniform distributions for computer image enhancement," *IEEE Trans. Comput.*, vol. 23, no. 2, pp. 207–208, 1973.

- [16] P. C. Cosman, R. M. Gray, and E. A. Riskin, "Combining vector quantization and histogram equalization," in *Data Compression Conference, 1991. DCC '91*, Snowbird, UT, USA, pp. 113-118, 1991.
- [17] A. Iranli, H. Fatemi, and M. Pedram, "HEBS: histogram equalization for backlight scaling," *Design, Automation and Test in Europe, 2005*, pp. 346-351, vol. 1, 2005.
- [18] H. D. Cheng and X. J. Shi, "A simple and effective histogram equalization approach to image enhancement," *Digital Signal Processing*, vol. 14, no. 2, pp. 158-170, 2004.
- [19] T. K. Kim, J. K. Paik, and B. S. Kang, "Contrast enhancement system using spatially adaptive histogram equalization with temporal filtering," *IEEE Transactions on Consumer Electronics*, vol. 44, no. 1, pp. 82-87, 1998.
- [20] M. Kim and M. G. Chung, "Recursively separated and weighted histogram equalization for brightness preservation and contrast enhancement," *IEEE Transactions on Consumer Electronics*, vol. 54, no. 3, pp. 1389-1397, 2008.
- [21] J. B. Zimmerman, S. M. Pizer, E. V. Staab, J. R. Perry, W. McCartney, and B. C. Brenton, "An evaluation of the effectiveness of adaptive histogram equalization for contrast enhancement," *IEEE Transactions on Medical Imaging*, vol. 7, no. 4, pp. 304-312, 1988.
- [22] M. Csapodi and T. Roska, "Adaptive histogram equalization with cellular neural networks," in *Proc. 1996 Fourth IEEE International Workshop on Cellular Neural Networks and their Applications*, CNNA-96, Seville, Spain, pp. 81-86, 1996.
- [23] B. J. Wang, S. Q. Liu, Q. Li, and H. X. Zhou, "A real-time contrast enhancement algorithm for infrared images based on plateau histogram," *Infrared Physics & Technology*, vol. 48, no. 1, pp. 77-82, 2006.
- [24] C. J. Zhang, F. Yang, X. D. Wang, and H. R. Zhang, "An efficient nonlinear algorithm for contrast enhancement of infrared image," in *Proc. 2005 International Conference on Machine Learning and Cybernetics*, pp. 4946-4951, vol. 8, 2005.
- [25] S. D. Chen and A. R. Ramli, "Minimum mean brightness error bi-histogram equalization in contrast enhancement," *IEEE Transactions on Consumer Electronics*, vol. 49, no. 4, pp. 1310-1319, 2003.
- [26] S. D. Chen and A. R. Ramli, "Preserving brightness in histogram equalization based contrast enhancement techniques," *Digital Signal Processing*, vol. 14, no. 5, pp. 413-428, 2004.
- [27] K. Wongsritong, K. Kittayarasiriwat, F. Cheevasuvit, K. Dejhan, and A. Somboonkaew, "Contrast enhancement using multiplex histogram equalization with brightness preserving," in *Proc. The 1998 IEEE Asia-Pacific Conference on Circuits and Systems, APCCAS 1998*, Chiangmai, Thailand, pp. 455-458, 1998.
- [28] Menotti, L., "Contrast enhancement in digital imaging using histogram equalization," Ph.D. dissertation, Federal University of Minas Gerais, Belo Horizonte, Brazil, 2008.
- [29] N. Sengee and H. K. Choi, "Brightness preserving weight clustering histogram equalization," *IEEE Transactions on Consumer Electronics*, vol. 54, no. 3, pp. 1329-1337, 2008.
- [30] H. Ibrahim and N. S. P. Kong, "Brightness preserving dynamic histogram equalization for image contrast enhancement," *IEEE Transactions on Consumer Electronics*, vol. 53, no. 4, pp. 1752-1758, 2007.
- [31] H. Ibrahim, "Histogram equalization with range offset for brightness preserved image enhancement," *International Journal of Image Processing (IJIP)*, vol. 5, no. 5, pp. 599-609, 2011.
- [32] S. Yang, J. H. Oh, and Y. Park, "Contrast enhancement using histogram equalization with bin underflow and bin overflow," in *Proc. 2003 International Conference on Image Processing, ICIP 2003*, pp. 881-884, vol. 1, 2003.
- [33] H. Zhu, F. H. Y. Chan, and F. K. Lam, "Image contrast enhancement by constrained local histogram equalization," *Computer Vision and Image Understanding*, vol. 73, no. 2, pp. 281-290, 1999.
- [34] S. M. Pizer, E. P. Amburn, J. D. Austin, R. Cromartie, A. Geselowitz, T. Greer, B. T. H. Romeny, and J. B. Zimmerman, "Adaptive histogram equalization and its variations," *Comput. Vision Graph. Image Process*, vol. 39, no. 3, pp. 355-368, 1987.
- [35] S. M. Pizer, R. E. Johnston, J. P. Ericksen, B. C. Yankaskas, and K. E. Muller, "Contrast-limited adaptive histogram equalization: speed and effectiveness," in *Proc. the First Conference on Visualization in Biomedical Computing, 1990*, pp. 337-345, 1990.
- [36] A. M. Vossepoel, B. C. Stoel, and A. P. Meershoek, "Adaptive histogram equalization using variable regions," in *Proc. 9th International Conference on Pattern Recognition*, Rome, Italy, pp. 351-353, vol. 1, 1988.
- [37] S. S. Y. Lau, "Global image enhancement using local information," *Electronics Letters*, vol. 30, no. 2, pp. 122-123, 1994.
- [38] J. Y. Kim, L. S. Kim, and S. H. Hwang, "An advanced contrast enhancement using partially overlapped sub-block histogram equalization," *IEEE Transactions on Circuits and Systems for Video Technology*, vol. 11, no. 4, pp. 475-484, 2001.
- [39] N. Saffarian and J. J. Zou, "DNA microarray image enhancement using conditional sub-block bi-histogram equalization," in *proc. IEEE International Conference on Video and Signal Based Surveillance, AVSS '06*, pp. 86-86, 2006.
- [40] N. S. P. Kong and H. Ibrahim, "Multiple layers block overlapped histogram equalization for local content emphasis," *Computers and Electrical Engineering*, vol. 37, no. 5, pp. 631-643, 2011.



Nicholas Sia Pik Kong received his B. Eng degree in electronic engineering from Universiti Sains Malaysia, Malaysia, in year 2006. He then obtained his M.Sc degree in electronic engineering by research mode in year 2010 from the same university. He is currently an engineer at one of the electronic company in Penang. His research interest includes image enhancement and multidimensional signal processing.



Haidi Ibrahim received his B. Eng degree in electronic engineering from Universiti Sains Malaysia, Malaysia, in year 2000. He then received his Ph.D degree in digital image processing from the Centre for Vision, Speech, and Signal Processing (CVSSP), University of Surrey, Guildford, Surrey, United Kingdom in year 2005. He is now a senior lecturer at the School of Electrical and Electronic Engineering, Engineering Campus, Universiti Sains Malaysia, Nibong Tebal, Penang, Malaysia. His research interest includes digital image contrast enhancement, noise reduction, image segmentation, 3D visualization, and virtual reality.



Seng Chun Hoo received his B.Eng degree in electronic engineering from Universiti Sains Malaysia, Malaysia, in year 2008. He is currently pursuing his M.Sc degree by research mode at the same university. He has published two research papers in international journals, regarding to digital image processing. His research interest includes digital image contrast enhancement, noise reduction, and image segmentation.

Variations on Impulse Noise Model in Digital Image Processing Field: A Survey on Current Research Inclination

Sin Hoong Teoh and Haidi Ibrahim

Abstract—As the information from digital images are easier to be evaluated as compared with one dimensional signals, digital images are now commonly used in many research fields. Unfortunately, similar to other digital signals, digital images are also sometimes unintentionally corrupted by unwanted signals, called noise. One of the noises commonly corrupting digital image is the impulse noise. Therefore, impulse noise reduction has become one of the active researches in these recent years. Many impulse noise models have been proposed by researchers for this research purpose. Therefore, the purpose of this paper is to investigate the popularity of these noise models. The research is done by a survey on available online materials. However, because there are more than thousands of related articles available online, the survey was carried out based on the keywords related to those articles. The research was restricted only to IEEEExplore® database. The result from this survey shown that the research related to impulse noise model in digital image processing is still showing an increasing trend. Among the impulse noise models, the salt-and-pepper noise is the most used impulse noise model in current literature.

Index Terms—Impulse noise, salt-and-pepper noise, fixed-valued impulse noise, random-valued impulse noise, uniform noise, universal impulse noise.

I. INTRODUCTION

With the advancement in computers and digital imaging technologies, the costs of digital cameras and computers are lowering each year, and thus these equipments are becoming affordable these days. The usage of digital images in our daily life is turning common. As more information can be extracted from digital images, as compared to one dimensional signal, many research areas, including material researches, are now utilizing digital images, such as microscopic images and X-ray images, as one of their evaluation tools. For example, Brook et al. [1] used radar images in order to inspect aeronautics composite materials and structures. Works by Kumar, Taheri, and Islam [2] used ultrasonic images in order to evaluate and detect several defects in a material. On the other hand, Thai et al. [3] utilizes video sequences to monitor special nuclear material.

Unfortunately, similar to other digital signals, digital images may suffer from unwanted signals known as noise [4]. There are a lot of noise types normally corrupt digital image [5]. One of these noise types is the impulse noise [6].

Impulse noise can be assumed as an additive noise [7], and randomly damages the pixel, at random positions [8]. Normally, impulse noise appears as black and white speckles on the image [9]. Pixels corrupted by impulse noise are normally having either extremely high, or extremely low intensity values [10]. Usually, they have very high contrast towards their clean, uncorrupted smooth surrounding areas [11]. Therefore, impulse noise, even at a low level of degradation, will damage the appearance of digital image dramatically [12]. Many important information will be altered by this noise. As a consequence, the impulse noise also might make a fully automatic vision based system to give inaccurate result.

Based on this problem, many researchers around the globe have put their serious efforts in searching suitable methods that are able to reduce the degree of degradation by the impulse noise. Such type of digital image restoration method requires the researchers to artificially add the impulse noise to set of test images in order to evaluate the performance of their proposed methods. The evaluations normally compare the filtered image with the artificially corrupted image. However, researchers have described impulse noise by many ways. There are many mathematical equations suggested by researcher in literatures to present impulse noise [13]. Several terms have been used to describe impulse noise models in reading materials, such as fixed valued impulse noise, salt-and-pepper noise, uniform impulse noise, random valued impulse noise, and universal impulse noise.

The main aim of this paper is to investigate the current research trend related to impulse noise models. First, we are interested to see whether the research regarding impulse noise in digital image processing is showing a growing trend, or a shrinking trend. Then, we are also interested to investigate which impulse noise model is the mostly used model in current literature.

The organization of this paper is as follows. After this introduction section, we will present our research approach in Section II. Then, we will present the findings from our survey in Section III. Finally, the findings will be concluded in Section IV.

II. METHODOLOGY

As time flies, research areas regarding impulse noise are becoming very large. Currently, when we search for online reading materials from the internet regarding impulse noise, we will be suggested thousands of related literatures. With this situation, it is very impossible to check every single literature to determine which impulse model it used in its

Manuscript received December 1, 2012; revised February 15, 2013.

The authors are with the School of Electrical & Electronic Engineering, Engineering Campus, Universiti Sains Malaysia, 14300 Nibong Tebal, Seberang Perai, Penang, Malaysia (e-mail: tshoong81@yahoo.com; haidi_ibrahim@ieee.org).

experiment. Fortunately, there are keywords attached to these materials. Therefore, we assume that these keywords reflect exactly the noise model used by that literature. Therefore, we will classify the research papers accordingly, based on their keywords.

It is worth noting that currently there are many scientific databases available in internet. Therefore, we need to restrict our search for online materials. To be more specific, we limit our search only to <http://ieeexplore.ieee.org/Xplore/guesthome.jsp>, which is the IEEEExplore® database. This database is one of currently reliable databases, and it is up-to-date. The user interface provided by IEEEExplore® is shown in Fig. 1. There are many features provided in this online database, which can help our research significantly.

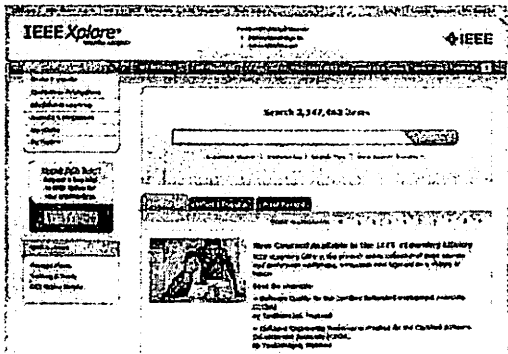


Fig. 1. The user interface of IEEEExplore®.

The related keywords will be typed on the search box, as shown in Fig. 2. The database will then return its search results. Because we want to see the research trend over years, we will utilize the field of "publication year" which is located on the left side of the database, once the search results are been displayed, as shown in Fig. 3. From this field, we can choose to limit our search toward a specific year. The number of publications, based on its types (e.g. conference paper, journal & magazine, etc.) can be obtained from "content type" field, which is located above the "publication year" field.

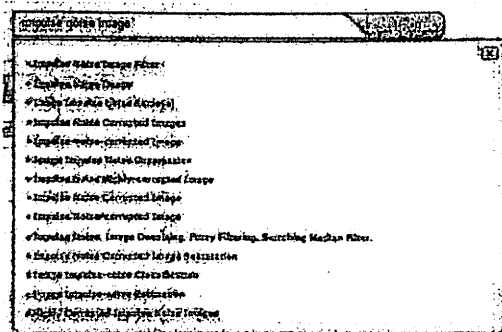


Fig. 2. The search box provided by IEEEExplore®.

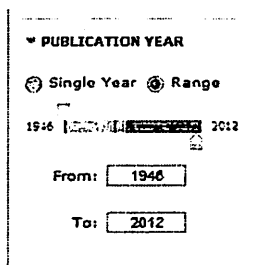


Fig. 3. The "publication year" field provided by IEEEExplore®.

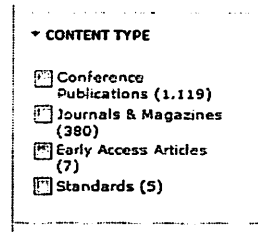


Fig. 4. The "content type" field provided by IEEEExplore®.

III. RESULTS AND DISCUSSIONS

The first observation that we want to achieve through this survey is based on the research trend regarding to the impulse noise, in general, used in digital image processing field. Therefore, we typed "impulse noise image" as the keyword to the search box, shown in Fig. 2. Based on the overall search result, it is shown that the impulse noise based literatures are only available starting from year 1946. Therefore, by selecting "single year" on "publication year" field, shown in Fig. 3, number of publications for each year from 1946 to 2012 is determined. The plot of the findings, plotted as the number of publications versus year, is shown in Fig. 5. From this bar graph, we can witness that the researches related to impulse noise is started to expand dramatically since year 1985. Starting from 1985, there is a significance increment in both journals, magazines, and conference proceedings related to impulse noise based researches. Furthermore, we also can note clearly that the number of conference proceedings is more than the journal and magazine publications. Because the conference proceeding papers normally required relatively shorter time to be published, this outcome suggests that the researches related to impulse noise is expanding very fast in these recent years.

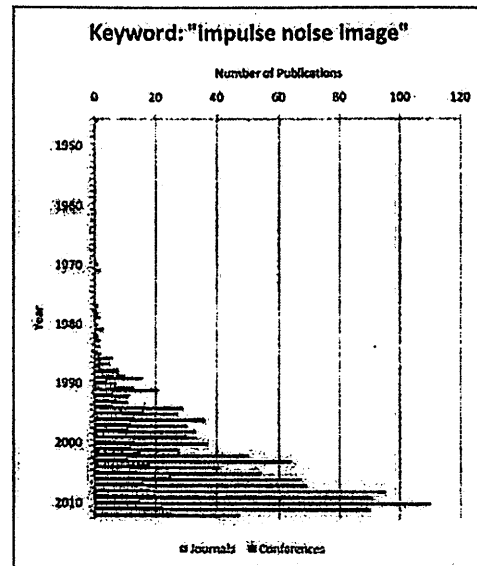


Fig. 5. The trend of research related to impulse noise.

One type of impulse noise is the salt-and-pepper noise. It can be described by either following equations [5]:

$$p(N) = \begin{cases} 0.5P & : \text{pepper; } N = 0 \\ 1 - P & : \text{noise free pixels; } 0 \leq N \leq L - 1 \\ 0.5P & : \text{salt; } N = L - 1 \end{cases} \quad (1)$$

or

$$p(N) = \begin{cases} P_1 & : \text{pepper}; N = 0 \\ 1 - P & : \text{noise free pixels}; 0 \leq N \leq L - 1 \\ P_2 & : \text{salt}; N = L - 1 \end{cases} \quad (2)$$

where p is the noise distribution, P is the noise density (i.e. $0 \leq P \leq 1$), and $P_1 + P_2 = P$. Therefore, in order to observe the trend related to this impulse noise model, we used "salt and pepper noise image" as the keyword for the search in IEEExplore® database. The plot of the graph obtained from this keyword is shown in Fig. 6.

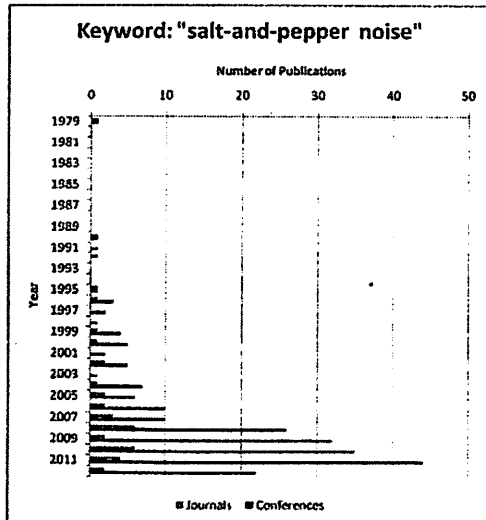


Fig. 6. The trend of research related to salt-and-pepper noise.

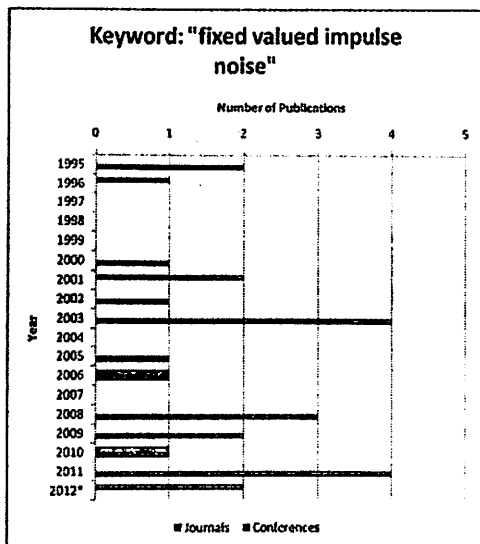


Fig. 7. The trend of research related to fixed valued impulse noise.

Salt-and-pepper noise is also known as the fixed valued impulse noise. Therefore, we also want to investigate the trend related to these terms. We use "fixed valued impulse noise image" as our keyword, and Fig. 7 shows the corresponding result. By comparing Fig. 6 with Fig. 7, we can see that the term salt-and-pepper is more popular than the term fixed valued impulse noise. This is observed from the number of publications. Furthermore, the term salt-and-pepper noise has been used since 1979, whereas the term fixed valued impulse noise started only in 1990. From these bar graphs also, we can observe that the usage of term salt-

and-pepper is showing an increasing trend, while the term fixed valued impulse noise showing an almost constant trend over time.

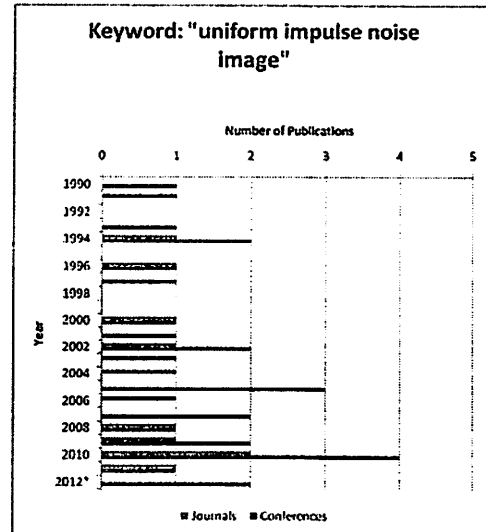


Fig. 8. The trend of research related to uniform impulse noise.

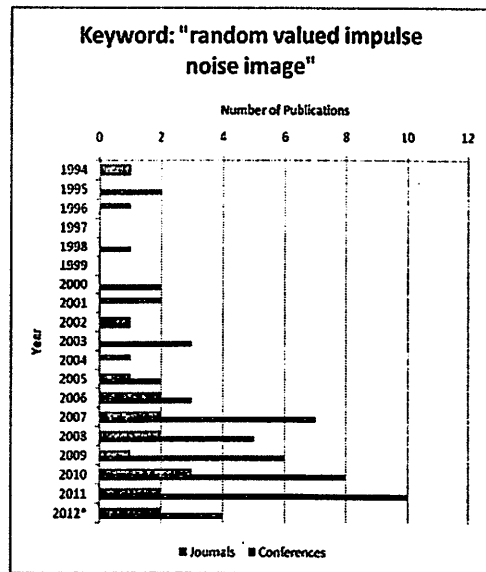


Fig. 9. The trend of research related to random valued impulse noise.

Another type of impulse noise model is known as the uniform impulse noise. This noise can be described by the following equation:

$$p(N) = P/L \quad 0 \leq N \leq L - 1 \quad (3)$$

where L is the quantization level of the image. In this noise model, the distribution of the impulse noise is equally distributed. We used "uniform impulse noise image" as the keyword to IEEExplore® database, and obtained the result as shown in Fig. 8. As the uniform impulse noise is also known as the random-valued impulse noise, we also investigate the use of this term. We use the term "random valued impulse noise" for this purpose. The graph obtained from this keyword is shown in Fig. 9.

From Fig. 8 and Fig. 9, although both the uniform impulse noise and the random-valued impulse noise are presenting the same type of impulse noise, the term random-valued impulse noise is more popular in the literature. The term random-valued impulse noise is showing an increasing

trend of its usage. On the other hand, the term uniform impulse noise is showing an almost constant pattern over time.

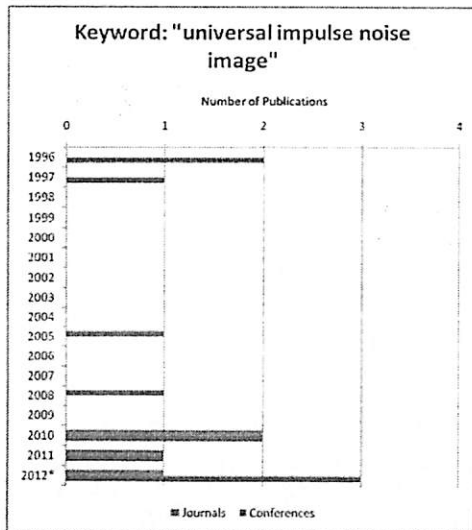


Fig. 10. The trend of research related to universal impulse noise.

Another type of impulse noise is the universal impulse noise. It can be considered as a weighted combination between the fixed valued impulse noises with the random valued impulse noise. In order to inspect the trend related to this impulse noise model, we use the keyword "universal impulse noise image" for our search. The bar graph obtained from this keyword is shown in Fig. 10. From this figure, we can observe that this type of noise model is seldom been used in research publications. However, this noise model is showing an increasing trend for the last three years.

By inspecting bar graphs shown in Fig. 5 to Fig. 10, we can see that the term salt-and-pepper noise is the most popular terms used by research literatures in this field. This is judged based on the quantity of the publications. Furthermore, this type of impulse noise is still showing an increasing trend. We also can assume that the researches related to salt-and-pepper noise, or fixed-valued impulse noise is more popular than the researches related to uniform impulse noise, or random-valued impulse noise.

IV. SUMMARY

This research investigates the current trend regarding to impulse noise models. It is found that the research related to impulse noise in image processing is still an interesting research field, and attracts more and more researchers in recent years. The research also shown that the salt-and-pepper noise is the most popular impulse noise model used in literature.

ACKNOWLEDGMENT

This work was supported in part by the Universiti Sains Malaysia's Short Term Research Grant with account number 304/PELECT/60311013 and Universiti Sains Malaysia's Research University Individual (RUI) Grant with account number 1001/PELECT/814169.

REFERENCES

- [1] A. Brook, E. Cristofani, M. Vandewal, C. Matheis, and J. Jonuscheit, "3-D radar image processing methodology for non-destructive testing of aeronautics composite materials and structures," *2012 IEEE Radar Conference (RADAR)*, pp. 806-811, 2012.
- [2] S. S. Kumar, F. Taheri, and M. R. Islam, "Artificial intelligence and image processing approaches in damage assessment and material evaluation," in *Proc. International Conference on Computational Intelligence for Modeling, Control and Automation, 2005 and International Conference on Intelligence Agents, Web Technologies and Internet Commerce*, vol. 1, pp. 307-313, 2005.
- [3] T. Thai, J. Carlson, D. Urenda, and T. Cooley, "An image processing system for the monitoring of special nuclear material and personnel," in *Proc. International Carnahan Conference on Security Technology*, pp. 39-42, 1994.
- [4] M. Petrou and P. Bosdogianni, *Image Processing: The Fundamentals*, John Wiley & Sons, England, 1999.
- [5] R. C. Gonzalez and R. E. Woods, *Digital Image Processing*, New Jersey: Pearson Prentice Hall, 3rd Edition, 2008.
- [6] R. L. Stevenson and S. M. Schweizer, "Nonlinear filtering structure for image smoothing in mixed-noise environments," *Journal of Mathematical Imaging and Vision*, vol. 2, no. 2-3, pp. 137-154, November 1992.
- [7] E. Abreu, M. Lightstone, S. K. Mitra, and K. Arakawa, "A new efficient approach for the removal of impulse noise from highly corrupted images," *IEEE Transactions on Image Processing*, vol. 5, no. 6, pp. 1012-1025, Jun 1996.
- [8] H. Ibrahim, T. F. Ng, and S. H. Teoh, "An efficient implementation of switching median filter with boundary discriminative noise detection for image corrupted by impulse noise," *Scientific Research and Essays (SRE)*, vol. 6, no. 26, pp. 5523-5533, November 2011.
- [9] N. S. P. Kong and H. Ibrahim, "The effect of shape and weight towards the performance of simple adaptive median filter in reducing impulse noise level from digital images," in *Proc. 2nd International Conference on Education Technology and Computer (ICETC)*, vol. 5, pp. 118-121, June 2010.
- [10] K. K. V. Toh, H. Ibrahim, and M. N. Mahyuddin, "Salt-and-pepper noise detection and reduction using fuzzy switching median filter," *IEEE Transactions on Consumer Electronics*, vol. 54, no. 4, pp. 1956-1961, November 2008.
- [11] H. Ibrahim, "Adaptive switching median filter utilizing quantized window size to remove impulse noise from digital images," *Asian Transactions on Fundamentals of Electronics, Communication & Multimedia*, vol. 2, no. 1, pp. 1-6, March 2012.
- [12] H. Ibrahim, N. S. P. Kong, and T. F. Ng, "Simple adaptive median filter for the removal of impulse noise from highly corrupted images," *IEEE Transactions on Consumer Electronics*, vol. 54, no. 4, pp. 1920-1927, November 2008.
- [13] H. Ibrahim, K. C. Neo, S. H. Teoh, T. F. Ng, D. C. J. Chieh, and N. F. N. Hassan, "Impulse noise model and its variations," *International Journal of Computer and Electrical Engineering (IJCEE)*, vol. 4, no. 5, pp. 647-650, October 2012.



images.

Sing Hoong Teoh received his B. Eng degree in electronic engineering from Universiti Sains Malaysia, Malaysia, in year 2006. He is currently an engineer at Altera Malaysia, and furthering his MSc degree as a part time student at the School of Electrical and Electronic Engineering, Engineering Campus, Universiti Sains Malaysia, Nibong Tebal, Penang, Malaysia. His research interest is impulse noise reduction from digital



Haidi Ibrahim received his B. Eng degree in electronic engineering from Universiti Sains Malaysia, Malaysia, in year 2000. He then received his Ph.D degree in digital image processing from the Centre for Vision, Speech, and Signal Processing (CVSSP), University of Surrey, Guildford, Surrey, United Kingdom in year 2005. He is now a senior lecturer at the School of Electrical and Electronic Engineering, Engineering Campus, Universiti Sains Malaysia, Nibong Tebal, Penang, Malaysia. His research interest includes digital image contrast enhancement, noise reduction, image segmentation, 3D visualization, and virtual reality.

Exploration of Current Trend on Blur Detection Method Utilized in Digital Image Processing

Boon Tatt Koik and Haidi Ibrahim

School of Electrical & Electronic Engineering, Engineering Campus, Universiti Sains Malaysia, 14300 Nibong Tebal, Penang, Malaysia

Email: btkoik@gmail.com, haidi_ibrahim@ieee.org

Abstract—Detection of blur in digital image, which is commonly preliminary step for de-blurring process, has becoming one of the growing research areas these days and has attracted many attentions from researchers. Research scholars have proposed new methods, or improved blur detection algorithms, based on edge sharpness analysis, low Depth of Field analysis, blind de-convolution, Bayes discriminant function, reference or non-reference block and wavelet based histogram with Support Vector Machine (SVM). The purpose of this paper is to explore the research trends (before year 1993 to year 2012) regarding the usage of blur detection algorithms for digital image processing researches. Because there are thousands of reliable literatures available, the trend is observed from the available online literature alone. Our scope of research has been limited only to search engine of IEEExplore®, ScienceDirect, and Google Scholar database. The searching for literatures will be classified according to their respective keyword for each method being utilized. We observed that low Depth of Field blur detection analysis is currently the most popular method, followed by edge sharpness analysis of blur detection. Google Scholar also has the most abundance source of online literature compared with IEEExplore® and ScienceDirect. Based on the trending graph, we observed that the researches in blur detection method are very positive, showing an overall increasing number of publication from year to year.

Index Terms—Blur detection, literature survey, edge sharpness analysis, low depth field analysis, blind de-convolution, Bayes discriminant function, non-reference block, wavelet based histogram

1. INTRODUCTION

Blur detection, one of the popular research areas in computer vision system is showing an increasing research trend. It is expected that computer vision technology will be the future of the manufacturing line, replacing most of the human operator works and cut operational cost in long term basis [1]. However, it is worth noting that up to this day, human work still has an upper hand on most of the industries over computer vision work [2]. Blur detection method can be applied as initial stage for de-blurring when the machine vision of manufacturing line is out of focus or due to rapid movement of the inspected product. Besides,

there are applications for blur detection method for crime solving purposes, as part of the image enhancement for video surveillance system for a clearer picture of the criminal. In daily life routine, blur detection application can be used to de-blur precious image which is blurred. The blurring of image may due to many causes; the two commonly studied classification of the blur type is near-isotropic blur, which includes out of focus blur, and directional motion blur.

As study of the characterization and detection for blur region are needed in order to understand image information and evaluating image quality [3], developing of the blur detection algorithms for automatic detection and classification has become very functional in terms of computation and cost. Rugna and Konik [4] have shown in their work that blurry regions in image are more invariant to low pass filter process. The idea of their works has been widely accepted by researchers and it becomes an interesting research feature to classify blurry and non-blurry region. Works in [5] by Levin used a method based on inferred kernel to build an energy function to separate the image into two distinctive layers of blur and non-blur for further classifications. Other algorithm proposed by Elder and Zucker [6] only measures the blur extend of the blurry image, without classify the blurry and non-blurry regions of the image input.

The restriction of blur detection method has attracted many researchers to extend the edge of limitation. Many researchers have proposed extension, composite or improved algorithms which contributed to the development of the blur detection method. Thousands of reliable literatures based on blur detection method can be found online these days. Although we belief that there are much more research papers available but not online, the online literature alone is sufficient to give an overview of the research trend. Based on analysis on the past researches on the blur detection methods, blur detection can be classified in to seven categories. They are:

A. Edge Sharpness Analysis Blur Detection in Digital Image

- Common edge sharpness analysis methods use the contrast edge of object in the image for blur analysis.
- Using the Harr wavelet transform, to detect blur and extend of blurring [7].

Manuscript received July 21, 2013; revised September 18, 2013.

- Using perceptual-based no-reference objective image sharpness/blurriness metric by integrating the concept of just noticeable blur into a probability summation model [8].
- Using standard deviation of the edge gradient magnitude profile and the value of the edge gradient magnitude with weighted average [9].

B. Depth of Field (D.o.F.) Blur Detection in Digital Image

- Focusing on object detection in Object of Interest (OOI) technique in image by photographer.
- Works on low Depth of Field.
- Related methods in [10-12].

C. Blind De-Convolution Blur Detection in Digital Image

- Blind de-convolution works more efficient with correctly estimated blurring Point spread Function (PSF).
- Blind de-convolution can be non-iterative or iterative process.
- Related methods in [13]-[18].

D. Bayes Discriminant Function Blur Detection in Digital Image

- Based on statistical analysis of the image gradient of both sharp and blur regions.
- Examples of works are [19].

E. Non-Reference Block Blur Detection in Digital Image

- No reference to the original image signal information.
- Most convenient and robust compared with reduce-reference and full-reference methods.
- Examples of works in [20]-[24].

F. Directional Frequency Energy Blur Detection in Digital Image

- Direction estimation of the blur region is performed.
- Blur detection without PSF.
- Example of works in [25].

G. Wavelet-Based Histogram Blur Detection in Digital Image

- Discrimination of the gradient distributions between blurred and non-blurred image regions.
- Probability map can be constructed with wavelet gradient histograms
- Examples of works in [26]-[28].

Each of the blur detection method has its own advantages and disadvantages. Therefore, each of the application has their research value based on the type of application and signal input of data. We will analysis the research trend of above-mentioned blur detection method to give an understanding on how the researched method popularity goes.

To ease the presentation of this paper, this paper is organized into four main sections. The first section, which is this section, gives the background and the purposes of this research. Then, Section II explains the methodology on how this research will be carried out. Section III

presents the outcome of this research, while the last section, which is Section IV, concludes our findings.

II. METHODOLOGY

As the number of research literature available online is very large, it is almost impossible for us to inspect every single literature in detail for the methodology they used or proposed as every single research paper is unique. In order to smooth the research and also for standardization of this review paper, we will classify these literatures based on their keywords. We assume that the keywords used by the literatures reflect exactly the blur detection approach used by that literature. The keywords used are listed in Table I.

TABLE I. THE KEYWORDS USED TO SEARCH RELATED LITERATURES

Method	Keyword
Edge Sharpness Blur Detection in Digital Image	"Edge Sharpness Blur Detection Digital Image"
Low Depth Field Blur Detection in Digital Image	"Low Depth Field Blur Detection Digital Image"
Blind De-Convolution Blur Detection in Digital Image	"Blind De-Convolution Blur Detection Digital Image"
Bayes Discriminant Blur Detection in Digital Image	"Bayes Discriminant Blur Detection Digital Image"
Non-Reference Block Blur Detection in Digital Image	"Non-Reference Block Blur Detection Digital Image"
Directional Frequency Energy Blur Detection in Digital Image	"Directional Frequency Energy Blur Detection Digital Image"
Wavelet Based Histogram Blur Detection in Digital Image	"Wavelet Based Histogram Blur Detection Digital Image"
Blur Detection in Digital Image (In General)	"Blur Detection Digital Image"

As there is abundance of reliable online literatures available, this paper will be restricted to three well-known database sources, which are Google Scholar, ScienceDirect and IEEEExplore®:

A. Google Scholar (<http://scholar.google.com.my>)

- Google Scholar provides searching of literatures across almost all disciplines and sources, including journals, proceedings, abstracts, books, theses, and patents.

B. ScienceDirect (<http://www.sciencedirect.com>)

- ScienceDirect is one of the world's famous database for scientific, technical, and medical full text research papers.

C. IEEEExplore® (<http://ieeexplore.ieee.org>)

- IEEEExplore® is a well-known online database containing more specific scope regarding to the researches on electrical, electronic and computer engineering.

In order to check the popularity of each blur detection method, we will utilize the search engine of each corresponding website. Fig. 1 shows the different search engine interface available for IEEEExplore®, Google Scholar and ScienceDirect. These user friendly interfaces are located on the left hand side of the corresponding website. By collecting data and presenting in graphical

form, the popularity of the research trend can be interpreted by the number of research paper published.

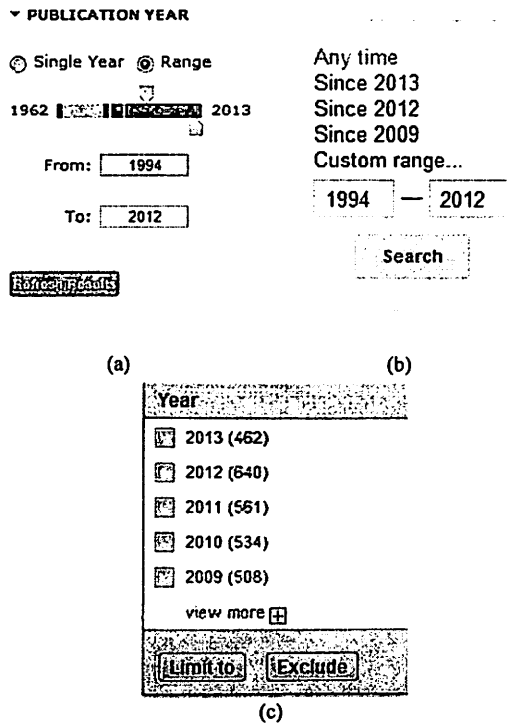


Figure 1. "Publication Year" feature provided by (a) IEEExplore®, (b) Google Scholar and (c) ScienceDirect

III. RESULTS

To see whether the research on blur detection method in digital image is still a popular topic among researchers, keyword of "blur detection digital image" is used for data collections via corresponding database website. The number of publication from these three databases is then displayed as line graphs. Fig. 2 shows the trend extracted from IEEExplore® database, Fig. 3 shows the results from ScienceDirect, whereas Fig. 4 shows the publication trend of Google Scholar. A composite graph is not suitable to represent the data collected as the search results of publication number have a very high contrast with each other.

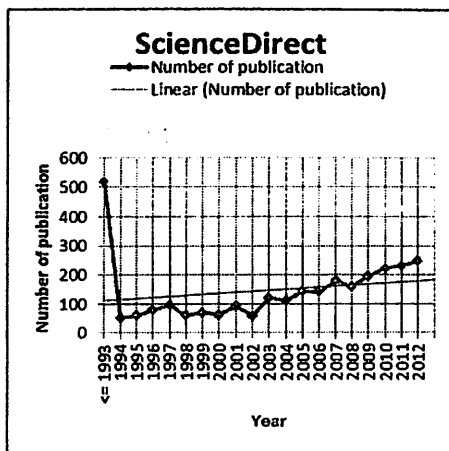


Figure 2. The trend on the researches regarding to blur detection method, observed from ScienceDirect database

As shown by these figures, the number of publications on blur detection method is the highest from Google Scholar database, followed by ScienceDirect, and IEEExplore®. This is because the content of IEEExplore® database is only restricted towards electrical, electronic, and computer engineering researches. However, if we observe the overall linear trend, which shows the growth of the research topic, we can see that ScienceDirect experience the lowest growing index and Google Scholar has the highest growing index on this research topic.

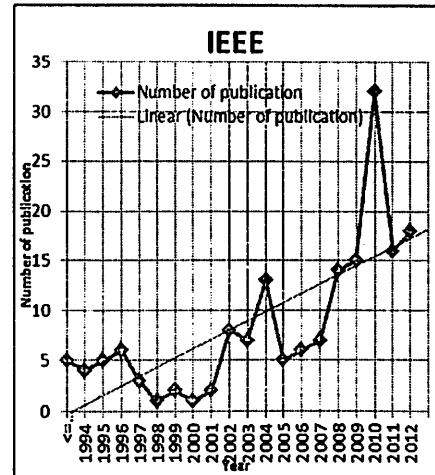


Figure 3. The trend on the researches regarding to blur detection method, observed from IEEExplore® database

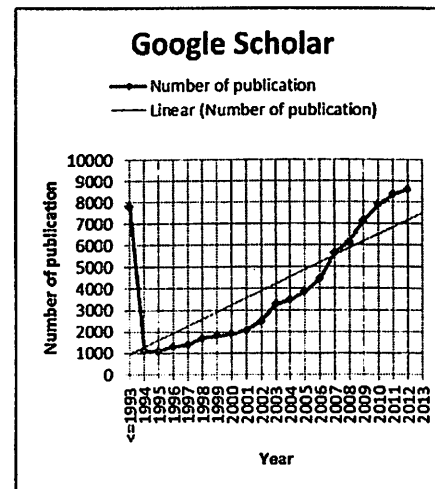


Figure 4. The trend on the researches regarding to blur detection method, observed from Google Scholar database

From Fig. 2, it shows that the research on blur detection in digital image in IEEE experienced fluctuation in the number of published paper regarding blur detection in digital image but it experienced a large boost in year 2010 and since then, steadily grow at year 2011 and year 2012. In ScienceDirect, the publication number had smaller fluctuation compared with IEEE but remains a growing trend over the years from year before 1993 to year 2012. Google Scholar had the fastest growing database over the year and it is expected to maintain its high growing linear gradient index. From the graphical presentations, we can see that blur detection methods are still growing and

thousands of publications being published each year, therefore we can expect that more and more new and hybrid methods being introduced in the years to come.

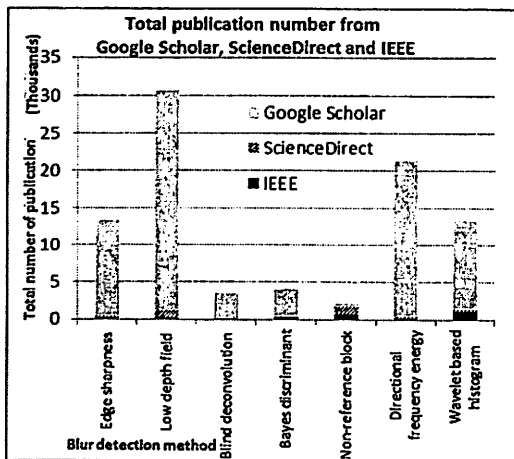


Figure.5. The bar graph showing the accumulated number of publications versus blur detection methods

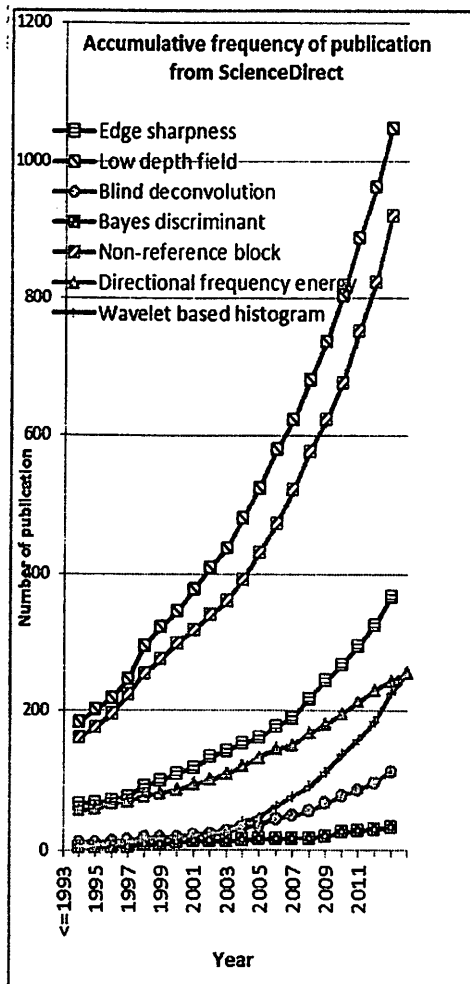


Figure.6. The trend on the research regarding to each blur detection method, observed from ScienceDirect database

In order to investigate the popularity each blur detection methods considered in this research, we inputted the

keywords shown in Table I into the three respective search engines. The results are shown in Fig. 5. We assumed that there is no reoccurrence exists in the database. The range of year presented is from year before 1993 to year 2012. The popularity is measured by the number of publication available for each year. We can see from the composite graph shown in Fig. 5, low Depth of Field analysis on blur detection has the highest popularity and it followed by directional frequency analysis, edge sharpness analysis, wavelet-based histogram analysis, Bayes discriminant analysis, blind de-convolution analysis and finally non-reference block analysis.

Besides the total publication from each database, we need to know the popularity of each of the blur detection method in digital image. A composite graph is plotted using the ScienceDirect database for each of the blur detection method in this review paper. The range of data collection is from year before 1993 to year 2012, as shown in Fig. 6.

IV. CONCLUSION

From this survey, we can conclude that blur detection is still a popular research area with potential of further advancement in the future. This review also shows that each of the blur detection method has active research value and expected to increase for years to come.

REFERENCES

- [1] T. Brosnan and D. W. Sun, "Inspection and grading of agricultural and food products by computer vision systems—A review," *Computers and Electronics in Agriculture*, volume 36, issues 2–3, pp. 193–213, November 2002.
- [2] L. Han, F. Xue, Z. Li, and D. Chen, "A generic framework for human-machine hybrid recognition based on wearable visual computing," *Applied Mechanics and Materials*, vol. 39, pp. 317–321, 2011.
- [3] B. Su, S. Lu, and C. L. Tan, "Blurred image region detection and classification," in *Proc. Association for Computing Machinery, ACM Multimedia*, 2011, pp. 1397–1400.
- [4] J. D. Rugna, and H. Konik, "Automatic blur detection for metadata extraction in content-based retrieval context," *International Professional Society for Optics and Photonics Technology SPIE*, vol. 5304, pp. 285–294, 2003.
- [5] A. Levin, "Blind motion de-blurring using image statistics," *Neural Information Processing Systems*, pp. 841–848, 2006.
- [6] J. H. Elder and S. W. Zucker, "Local scale control for edge detection and blur estimation," *Pattern Analysis and Machine Intelligence*, vol. 20, no.7, pp. 699–716, 1998.
- [7] H. H. Tong, M. J. Li, H. J. Zhang, and C. S. Zhang, "Blur detection for digital images using wavelet transform," in *Proc. IEEE International Conference on Multimedia and Expo*, 2004, vol. 1, pp.17–20.
- [8] R. Ferzli and L. J. Karam, "A no-reference objective image sharpness metric based on the notion of just noticeable blur," *Image Processing, IEEE Transactions*, vol.18, no.4, pp. 717–728, April 2009.
- [9] Y. C. Chung, J. M. Wang, Bailey, S. W. Chen, and S. L. Chang, "A non-parametric blur measure based on edge analysis for image processing applications," in *Proc. IEEE Conference on Cybernetics and Intelligent Systems*, 2004, vol. 1, pp. 356–360.
- [10] F. Graf, H.-P. Kriegel, and M. Weiler, "Robust segmentation of relevant regions in low depth of field images," in *Proc. 18th IEEE International Conference on Image Processing*, 2011, pp. 2861–2864.
- [11] G. Rafiee, S. S. Dlay, and W. L. Woo, "Automatic segmentation of interest regions in low depth of field images using ensemble

- clustering and graph cut optimization approaches," in *Proc. IEEE International Symposium on Multimedia*, 2012, pp. 161-164.
- [12] Y. G. Kang, M. C. Kim, and H. Jeong, "Segmentation with low depth of field images," in *Proc. 6th International Conference on Computer Sciences and Convergence Information Technology*, 2011, pp. 249-252.
- [13] C. Yi and T. Shimamura, "A blind image deconvolution method based on noise variance estimation and blur type reorganization," in *Proc. International Symposium on Intelligent Signal Processing and Communications Systems*, 2011, pp. 1-6.
- [14] Y. C. Lai, C. L. Huo, Y. H. Yu, and T. Y. Sun, "PSO-based estimation for Gaussian blur in blind image deconvolution problem," in *Proc. IEEE International Conference on Fuzzy Systems*, 2011, pp. 1143-1148.
- [15] P. E. Robinson and Y. Roodt, "Blind deconvolution of Gaussian blurred images containing additive white Gaussian noise," in *Proc. IEEE International Conference on Industrial Technology*, 2013, pp. 1092-1097.
- [16] U. Qidwai, "Blind De-convolution for retinal image enhancement," in *Proc. IEEE EMBS Conference on Biomedical Engineering and Sciences*, 2010, pp. 20-25.
- [17] J. Xie, W. Y. Lin, H. X. Li, K. Guo, B. Jin, Y. H. Zhang, and D. H. Liu, "A new algorithm for improving De-blurring effects and addressing spatially-variant blur problems for image motion de-blurring," in *Proc. 4th International Congress on Image and Signal Processing*, 2011, vol. 2, pp. 651-655.
- [18] S. Ramya and T. M. Christial, "Restoration of blurred images using Blind De-convolution Algorithm," in *Proc. International Conference on Emerging Trends in Electrical and Computer Technology*, 2011, pp. 496-499.
- [19] J. Ko and C. Kim, "Low cost blur image detection and estimation for mobile devices," in *Proc. International Conference on Advanced Computing Technologies*, 2009, vol. 3, pp. 1605-1610.
- [20] D. B. Liu, Z. B. Chen, H. D. Ma, F. Xu, and X. D. Gu, "No reference block based blur detection," in *Proc. Quality of Multimedia Experience, QoMEX, International Workshop*, 2009, pp. 75-80.
- [21] N. D. Narvekar and L. J. Karam, "A no-reference image blur metric based on the Cumulative Probability of Blur Detection (CPBD)," *Image Processing, IEEE Transactions*, vol.20, no.9, pp. 2678-2683, Sept. 2011.
- [22] N. D. Narvekar and L. J. Karam "A no-reference perceptual image sharpness metric based on a cumulative probability of blur detection," in *Proc. International Workshop on Quality of Multimedia Experience*, 2009, pp. 87-91.
- [23] D. Marijan, V. Zlokolica, N. Teslic, V. Pekovic, and T. Tekcan, "Automatic functional TV set failure detection system," *Consumer Electronics, IEEE Transactions*, vol.56, no.1, pp. 125-133, February 2010.
- [24] R. M. Bora and N. M. Shahane, "Image forgery detection through motion blur estimates," in *Proc. IEEE International Conference on Computational Intelligence & Computing Research*, 2012, pp. 1-4.
- [25] X. G. Chen, J. Yang, Q. Wu, and J. J. Zhao, "Motion blur detection based on lowest directional high-frequency energy," in *Proc. 17th IEEE International Conference on Image Processing*, 2010, pp. 2533-2536.
- [26] V. Kanchev, Tonchev, and O. Boumbarov. "Blurred image regions detection using wavelet-based histograms and SVM," in *Proc. IEEE 6th International Conference on Intelligent Data Acquisition and Advanced Computing Systems*, 2011, vol.1, pp. 457-461.
- [27] L. L. Pei, Y. H. Zhao, and H. B. Luo, "Application of wavelet-based image fusion in image enhancement," in *Proc. 3rd International Congress on Image and Signal Processing*, 2010, vol. 2, pp. 649-653.
- [28] K. S. Ni, Z. Z. Sun, and N. T. Bliss, "Real-time global motion blur detection," in *Proc. 19th IEEE International Conference on Image Processing*, 2012, pp. 3101-3104.



Boon Tatt Koik received his B.Eng degree in electronic engineering from Universiti Sains Malaysia, Malaysia, in year 2012. He has published two research papers in international journals, regarding to digital image processing. His research interest includes digital image contrast enhancement, noise reduction, and change detection.



Haidi Ibrahim received his B. Eng degree in electronic engineering from Universiti Sains Malaysia, Malaysia, in year 2000. He then received his Ph.D degree in digital image processing from the Centre for Vision, Speech, and Signal Processing (CVSSP), University of Surrey, Guildford, Surrey, United Kingdom in year 2005. He is now a senior lecturer at the School of

Electrical and Electronic Engineering, Engineering Campus, Universiti Sains Malaysia, Nibong Tebal, Penang, Malaysia. His research interest includes digital image contrast enhancement, noise reduction, image segmentation, 3D visualization, and virtual reality.

A Literature Survey on Blur Detection Algorithms for Digital Imaging

Boon Tatt Koik

School of Electrical & Electronic Engineering,
Engineering Campus, Universiti Sains Malaysia,
14300 Nibong Tebal, Penang, Malaysia
Email: btkoik@gmail.com

Haidi Ibrahim

School of Electrical & Electronic Engineering,
Engineering Campus, Universiti Sains Malaysia,
14300 Nibong Tebal, Penang, Malaysia
Email: haidi_ibrahim@ieec.org

Abstract—Development of blur detection algorithms has attracted many attentions in recent years. The blur detection algorithms are found very helpful in real life applications and therefore have been developed in various multimedia related research areas including image restoration, image enhancement, and image segmentation. These researches have helped us in compensating some unintentionally blurred images, resulted from out-of-focus objects, extreme light intensity, physical imperfection of camera lenses and motion blur distortion. Overview on a few blur detection methods will be presented in this paper. The methods covered in this manuscript are based on edge sharpness analysis, low depth of field (DOF) image segmentation, blind image de-convolution, Bayes discriminant function method, non-reference (NR) block, lowest directional high frequency energy (for motion blur detection) and wavelet-based histogram with Support Vector Machine (SVM). It is found that there are still a lot of future works need to be done in developing an efficient blur detection algorithm.

Keywords—component—Digital image, blur detection, literature review, literature survey, image restoration, image enhancement, image segmentation, blur classification

I. INTRODUCTION

Studies on characterization and detection for blur regions from digital image have become one of the important research branches in recent years. In addition to the use as a part of de-blurring process, automatic detection and classification of the blurred regions from digital image are very functional in order to understand the image information, and also useful for evaluating image quality [1] for further enhancement processes.

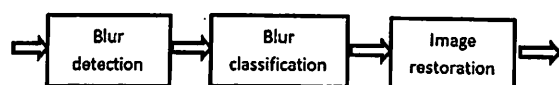


Figure 1. Block diagram to relate blur detection, blur classification, and image restoration.

Researches regarding blur phenomena in digital image can be narrowed down into three main branches. These branches are blur detection, blur classification, and image restoration. However, we can also describe these three research branches as a series of consequence processes, as

shown in Fig. 1. The initial process is the blur detection, where the blurred regions are identified. Then, it is followed by blur classification, where the blurred regions are categorized and classified according to their blurring nature. Finally, image restoration will take place, where the blurred image will be processed by de-blurring operation, in order to obtain a sharper image.

Being the first branch or the initial stage in improving the quality of digital image that suffers from blur, blur detection algorithm is very useful because it is used as the preliminary processes to detect the specific regions which require de-blurring operations. Many blur detection algorithms have been proposed by researchers in recent years. The research presented by Rugna and Konik [2] had showed that blurry regions are more invariant to low pass filtering process. As a consequence, this interesting fact has been chosen as one of the features to classify image regions into either blurry or non-blurry areas.

Algorithm proposed by Levin in 2006 [3], on the other hand, uses a method based on inferred blur kernel. This kernel is used to build an energy function to divide the image into two distinctive layers; which are the blur layer, and the non-blur layer. On the other hand, in works by Elder and Zucker [4], only the blur extent is being measured; without designing a method that distinctly labels the image's region into blurry or non-blurry areas.

Blur classification is the second branch of the research related to blur in digital images. This research branch's objective is to classify the blur areas according to their characteristics, or types. The two common studied classification of the blur type is near-isotropic blur, which includes out of focus blur, and directional motion blur. Hough transform and error-parameter can be used to estimate the blur parameter for linear motion blur. Other directional motion blur is curve motion blur, which is using curve fitting approach and polar transformation to estimate the motion parameter values [5]. Blur detection algorithms are also useful in segmenting the digital image into a few regions, based on blurring characteristics.

The third research branch is the blur image restoration, or de-blurring process. The main objective of this research branch is to improve or repair the blur image by using various algorithms and methods. This research branch is very useful for real life applications. For example, they are applicable to forensic or crime solving, by restoring blurred digital images captured by the mostly low-cost, low-quality surveillance camera into a clearer picture of the criminal.

Besides, image restoration can be used in image enhancement researches. For example, blur image restoration algorithms can be used as a preliminary process in an advanced image enhancement algorithms to increase the contrast of a digital image captured from consumer electronic products, such as digital camera, smart phones, and video camcorder.

The work by Razligh and Kehtarnavaz [6] proposed an image de-blurring method for the use in cell phone. This de-blurring method takes considerations on the brightness and the contrast of the blurred input images and also corrects low exposure images. Other examples of de-blurring algorithms are the works by Fergus et. al [7] and Shan, Jia, and Agarwala [8]. These methods show reasonable results of de-blurring process, and robustness to noisy image. However, algorithm processing in [7] and [8] are computationally expensive and time consuming which adding disadvantages to their algorithms.

Based on the above mentioned facts, as the research related to blur in digital images are very wide and active, this paper will give more attention and review on blur detection methods. This review is limited only to the methods used for digital images and digital video sequences. The review will be presented in the next section.

II. BLUR DETECTION METHODS FOR DIGITAL IMAGE

Researches on blur detection are very useful for improving the digital image quality, possible aiding in crime solving with video quality improvement and restoration of some precious images in our daily life. Based on our readings, in general, we can divide blur detection methods into seven main categories, which are:

- Edge sharpness analysis.
- Low depth of field (DOF) image segmentation.
- Blind image de-convolution.
- Bayes discriminant function method.
- Non-reference (NR) block.
- Lowest directional high frequency energy (for motion blur).
- Wavelet-based histogram and Support Vector Machine (SVM).

Each of the category will be explained briefly in the following subsections.

A. Blur Detection using Edge Sharpness Analysis

Fig. 2 presents an example to show the effect of blur towards the slope of the object's edges in the image. Sharp images contain step edges. However, when the image become blurred, the step edges become ramp edges. The slope of the edge is depending to the degree of blurring. Therefore, the blur detection can be carried out using the information of the object's edges.

Blur detection and estimation using this method aim at measuring the blur extend by inspecting the object edges

inside the image. In the work by Chung et. al [9], gradient magnitude and edge direction are fitted to a normal distribution. The gradient magnitude, with the standard deviation of the normal distribution is regarded as the blur measure[10].

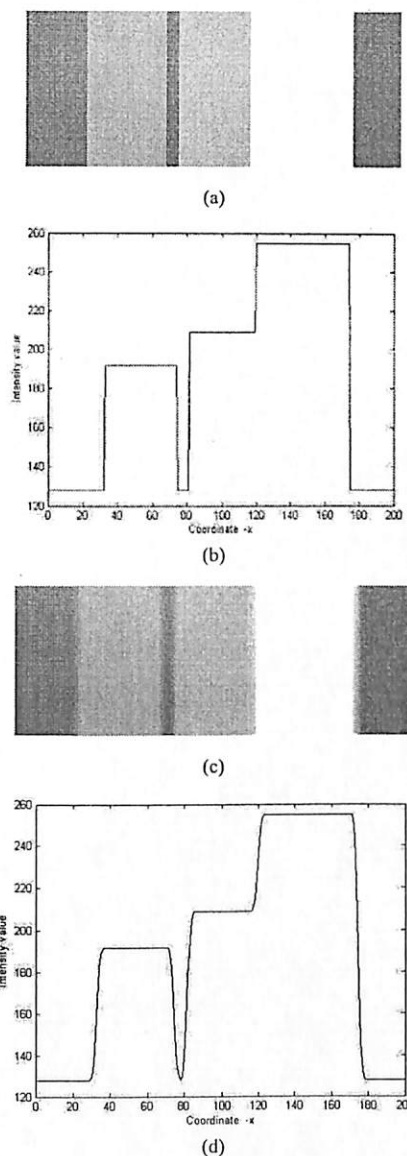


Figure 2. Example of blur edges. (a) The original, sharp image. (b) Horizontal profile of image (a). (c) The blur version of image (a). (d) Horizontal profile of image (c).

On the other hand, the degree of blur which is measured through thickness of object contours is made in the work by Elder and Zucker [4]. This is done by modeling focal blur by a Gaussian blur kernel and calculations of the response using the first and second derivative order of steerable

Gaussian basic filters [11]. Similar to first derivative of the Gaussian, the works by Zhang and Bergholm [12] defines a Gaussian different signature to measure the diffuseness of out-of-focus object in digital images.

B. Blur Detection using Low Depth of Field (DoF)

This blur detection method is suitable for low DoF image, where center image containing focused object with out-of-focus background. An example of an image with low DoF is shown by Fig. 3. Object of interest (OOI) focusing, which is a photography technique by photographer, can be extracted through works by Kim [13] and Wang et. al [14]. As expected, these methods work on images with low DoF.

Other researches that detect the low DoF images using a low DoF indicator shown in works in [15]. The indicator is defined using the ratio of the center region's high frequency wavelet coefficient of the input image. This method is suitable to be used to extract focal image that is done intentionally by photographer for further refining process. However, implementation of only this method without integration of other methods such as edge based segmentation method often resulted in incomplete classification of interest object [16].

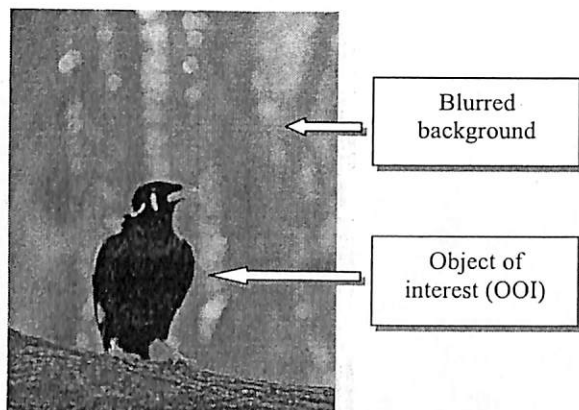


Figure 3. Example of image, with sharp object of interest (OOI) located at the centre of the image. The image contains out-of-focus background.

C. Blur Detection using Blind Image De-Convolution

Methods by Fergus et. al [17] and Jia [18] use blind de-convolution methods in their works. Estimation of the blur filter and latent un-blurred image is the main objective of these works. In the work by Kovacs and Sziranyi [19], un-blur regions are extracted out in order to distinguish them from blur regions.

In the proposed works in Bar et. al [20] and Levin [21], user interaction or blur kernel assumption is used to solve the partial blur issues. Example of image with partial blur problem is shown in Fig. 4. Estimation by user interaction is subject to the number of sample data being taken and the object data. Blind de-convolution works with satisfactory

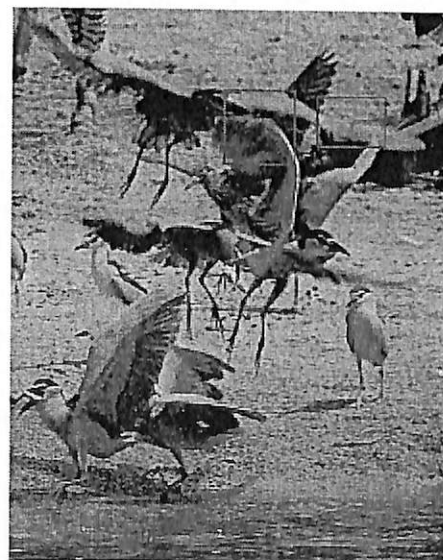
results with correctly estimated Point Spread Function (PSF) and kernel structures.

D. Blur Detection using Bayes Discriminant Function

In the works by Ko and Kim in 2009 [22], Bayes discriminant function is constructed based on the statistic of the gradients of the input image. Mean and standard deviation's statistic are taken for all blur and sharp regions. Blur image tends to have a smaller value of mean and standard deviation in the distribution compared with sharp image. By utilizing this concept, blur region in images can be detected for further de-blurring processes.



(a)



(b)

Figure 4. Example of images with partial blur problem (region bracketed by red rectangular frame).

E. Blur Detection using No Reference (NR) Block

Sometimes, in researches regarding to digital image processing, we need to measure the degree of blur introduced into the image after we applied certain type of processes. Therefore, blur degree can become one of the qualitative measures to evaluate the quality of an image. Therefore, the degree of blurring is important for researcher to evaluate the robustness and effectiveness a few of the image processing algorithms. If the measurement requires both the processed and the original sharp image, this measurement method is known as full-reference (FR) method.

No reference block based blur detection method does not require the original signal information which is more convenience in real scenario, compared with full-reference (FR) and reduced-reference (RR) block based. Image blur region is obtained via averaging the local blur of macro blocks in the images. Texture influence of the image is reduced via a content dependent weighting scheme. This method has lower complexity, higher robustness for variety of image contents compared with traditional edge based blur metrics [23].

F. Motion Blur Detection using Lowest Directional High Frequency Energy

The proposed direction estimation is based on measurement of lowest directional high frequency energy [24]. Motion blur detection based on lowest directional high frequency energy has less computational cost without usage of point spread function estimation. The main contribution of this paper is that a closed-form solution is derived. This method detect the blur motion blurred region by analyzing high frequency energy and estimate the motion direction of the image, making it more accurate and more robust compared with other learning-based methods [25].

The closed form solution that stated above is based on concept that high frequency energy decrease significantly along the motion direction in blurred image. Energy is regarded as sum of the squared derivative of image. The closed-form solution is developed based on this concept. This method has efficiently detect blurred regions without performing simultaneous algorithms of point spread function and de-blurring, which are advanced optimization normally used to restore motion blurred image. The advantages of this method over the stated advanced optimization method is that this method has less computational cost and still can detect blur region effectively.

G. Out-Of-Focus Blur Detection using Wavelet-Based Histogram and Support Vector Machine (SVM)

The main idea of algorithm of wavelet-based histogram and support vector machine is on discrimination of the gradient distributions between blurred and non-blurred

image regions [26]. The proposed algorithm does not need the prior knowledge about the input image and is oriented to out-of-focus blur, unlike motion blur detection as described in section 2.6.

This algorithm works on feature extraction in wavelet space by applying wavelet decomposition of input image, calculating wavelet gradient map and construction of gradient histograms. Fig. 5 shows an example of gradient distribution of blurred and non-blurred images.

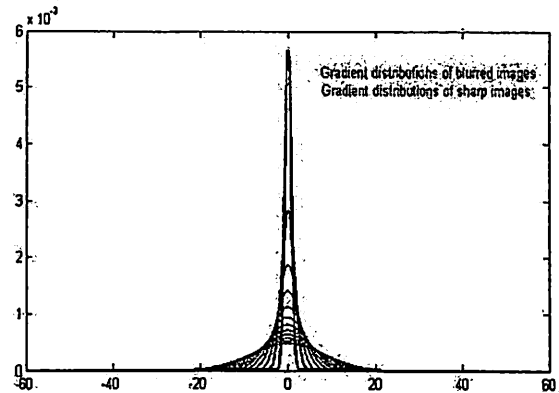


Figure 5. Example of gradient histograms of blurred and non-blurred images. The thick red lines are the areas where high probability of gradient distribution of the blurred images being located, while thin and scattered blue lines indicate the areas where high probability of gradient distribution for sharp images. (Modified from [26].)

Probabilistic SVM is used to apply on each patch of the gradient histogram to further analysis and generate a global probability map with SVM predicted probability value. Laplace distribution [27] has been used to model the wavelet gradient histogram and the kernel parameter of SVM is estimated by cross validation applied only to the training set. This proposed method has achieved its objective in detecting out-of-focus blur, which closely related to Gaussian blur.

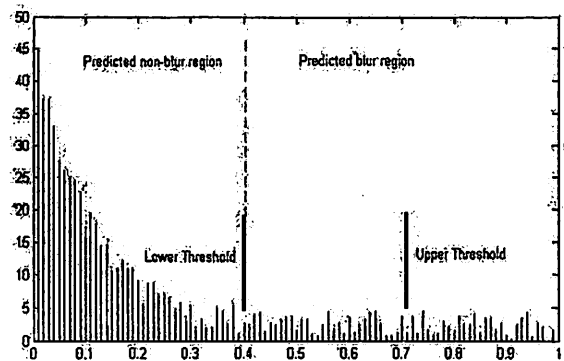


Figure 6. Example of histogram level of probabilistic SVM predicted value of image patches. X-axes: SVM predicted values of image patches, Y-axes: Distribution of SVM probability

TABLE I: TABULATION FOR ALL THE REVIEWED METHODS

Method	Application	Advantages	Disadvantages
Edge sharpness analysis [9][10][11][12].	Blur extent measurement based on image intensity profile.	Lower computational cost and time.	Not effective for complex image.
Low depth of field (DOF) image segmentation [13][14][15][16].	Photography.	OOI (object of interest) able to be identified effectively.	Only effective for low DoF (Depth of field) image.
Blind image de-convolution [17][18][19][20][21].	Preliminary step for de-blurring process.	Potential blur region in image can be detected effectively.	User interaction is needed for correctly estimated PSF and kernel structure.
Bayes discriminant function method [22].	Preliminary step for de-blurring process.	Fast computation and effective blur identification.	Sampling of large database needed prior to detection.
Non-reference (NR) block [23].	Blur measure.	Lower complexity and does not need original signal information.	Not very effective for complex image.
Lowest directional high frequency energy (for motion blur) [24] [25].	Motion blur detection.	A robust closed form solution is derived for motion blur detection.	Only effective to motion blur image.
Wavelet-based histogram and Support Vector Machine (SVM) [26] [27].	Out of focus blur detection.	Effective and robust in detecting out of focus blur.	Only effective to out of focus image.

III. SUMMARY

This literature review can be summarized as given by Table I. From the review, we can observe that most of the methods deal with specific type of blur and cannot work efficiently if the input image contains complex feature. Therefore, there are still a lot of future works needed to be done in developing blur detection algorithms. Through variety of techniques and methods such as high-level image segmentation, object extraction, content-based image retrieval and image enhancements, many of the researches have provided foundation and improvement for solving many blur-oriented and region based computer vision area. Future researches will be done to develop more robust blur detection methods and also new approaches to have a more effective processing in terms of quality, computing time and cost.

ACKNOWLEDGMENT

This work was supported in part by the Universiti Sains Malaysia's Research University Individual (RUI) Grant with account number 1001/PELECT/814169.

REFERENCES

[1] B. Su, S. Lu, and C. L. Tan, "Blurred image region detection and classification," In: ACM Multimedia 2011, MM'11, pp. 1397-1400, 2011.
 [2] J. D. Rugna, and H. Konik, "Automatic blur detection for metadata extraction in content-based retrieval context," In: Proc. SPIE, vol. 5304, pp. 285-294, 2003.
 [3] A. Levin, "Blind motion deblurring using image statistics," In Neural Information Processing Systems, NIPS, pp. 841-848, 2006.

[4] J. H. Elder, and S. W. Zucker, "Local scale control for edge detection and blur estimation," Pattern Analysis and Machine Intelligence, PAMI, vol. 20, no.7, pp. 699-716, 1998.
 [5] Wang Wei, Zheng Jin-jin, Liu Xing, and Hen Lian-guan, "Adaptive detection method of degraded parameters in motion blur image," 2011 Eighth International Conference on Fuzzy Systems and Knowledge Discovery (FSKD), pp. 2158-2162, 2011.
 [6] Q. R. Razligh, and N. Kehtarnavaz, "Image blur reduction for cell-phone cameras via adaptive tonal correction," In International Conference on Image Processing, ICIP, pp. 113-116, 2007.
 [7] R. Fergus, B. Singh, A. Hertzmann, S. T. Roweis, and W. T. Freeman, "Removing Camera Shake from a Single Photograph," Association for Computing Machinery, ACM Transactions on Graphics, vol. 25, pp. 787-794, 2006.
 [8] Qi Shan, Jiaya Jia, and A. Agarwala, "High-quality motion deblurring from a single image," Association for Computing Machinery, ACM Transactions on Graphics, vol. 27, Article No. 73 2008.
 [9] Y. Chung, J. Wang, R. Bailey, S. Chen, and S. Chang, "A non-parametric blur measure based on edge analysis for image processing applications," Institute of Electrical and Electronics Engineers, IEEE Conference on Cybernetics and Intelligent Systems, pp. 356 - 360 vol.1, 2004
 [10] Smith and Leslie N. Estimating an image's blur kernel from edge intensity profiles. Naval Research Lab Washington D.C. Applied Optics Branch, No. NRL/MR/5660-12-9393, 2012.
 [11] W. T. Freeman and E. H. Adelson, "The design and use of steerable filters," Pattern Analysis and Machine Intelligence, PAMI, vol. 13, no. 9, pp. 891-906, 1991.
 [12] W. Zhang and F. Bergholm, "Multi-scale blur estimation and edge type classification for scene analysis," International Journal of Computer Vision, vol. 24, no. 3, pp. 219-250, 1997.
 [13] C. Kim, "Segmenting a low-depth-of-field image using morphological filters and region merging," Institute of Electrical and Electronics Engineers, IEEE Transactions on Image Processing, vol. 14, no. 10, pp. 1503-1511, 2005.
 [14] J. Z. Wang, J. Li, R. M. Gray, and G. Wiederhold, "Unsupervised multi-resolution segmentation for images with low depth of field," Pattern Analysis and Machine Intelligence, PAMI, vol. 23, no. 1, pp. 85-90, 2001.
 [15] R. Datta, D. Joshi, J. Li, and J. Z. Wang, "Studying aesthetics in photographic images using a computational approach," In European Conference on Computer Vision, ECCV, vol. 3, pp. 288-301, 2006.

- [16] Jufeng Zhao, Huajun Feng, Zhihai Xu, Qi Li, and Xiaoping Tao. Automatic blur region segmentation approach using image matting. *Signal, Image and Video Processing*, pages 1–9, 2012.
- [17] R. Fergus, B. Singh, A. Hertzmann, S. T. Roweis, and W. T. Freeman, "Removing camera shake from a single photograph," *Association for Computing Machinery, ACM Trans. Graph.*, vol. 25, no. 3, pp. 787–794, 2006.
- [18] J. Jia, "Single image motion de-blurring using transparency," In *Computer Vision and Pattern Recognition, CVPR*, pp. 1-8, 2007.
- [19] L. Kovács and T. Szirányi, "Focus area extraction by blind deconvolution for defining regions of interest," *Institute of Electrical and Electronics Engineers, IEEE Transaction on Pattern Analysis and Machine Intelligence*, vol. 29, pp. 1080–1085, 2007.
- [20] L. Bar, B. Berkels, M. Rumpf, and G. Sapiro, "A variational framework for simultaneous motion estimation and restoration of motion-blurred video," In *International Conference on Computer Vision, ICCV*, pp. 1-8, 2007.
- [21] A. Levin, "Blind motion de-blurring using image statistics," In *Neural Information Processing Systems, NIPS*, pp. 841–848, 2006.
- [22] Jaeseung Ko, and Changick Kim, "Low cost blur image detection and estimation for mobile devices," *Advanced Communication Technology, 2009. International Conference on Advanced Computing Technologies, ICACT 2009. 11th International Conference on*, vol. 3, pp. 1605-1610, 15-18 Feb. 2009.
- [23] Liu Debing, Chen Zhibo, Ma Huadong, Xu Feng, and Gu Xiaodong, "No reference block based blur detection," *Quality of Multimedia Experience, QoMEx. International Workshop on*, pp. 75-80, 29-31 July 2009.
- [24] Xiaogang Chen; Jie Yang; Qiang Wu; Jiajia Zhao, "Motion blur detection based on lowest directional high-frequency energy," *Image Processing (ICIP), 2010 17th IEEE International Conference on*, vol., no., pp 2533-2536, 26-29 Sept. 2010.
- [25] R. Liu, Z. Li, J. Jia, "Image partial blur detection and classification," *CVPR*, June, pp. 1-8, 2008
- [26] Kanchev, V.; Tonchev, K.; Boumbarov, O., "Blurred image regions detection using wavelet-based histograms and SVM," *Intelligent Data Acquisition and Advanced Computing Systems (IDAACS), 2011 IEEE 6th International Conference on*, vol.1, no., pp. 457-461, 15-17 Sept. 2011
- [27] Moorthy, A.K.; Bovik, A.C., "Statistics of natural image distortions," *Acoustics Speech and Signal Processing (ICASSP), 2010 Institute of Electrical and Electronics Engineers, IEEE International Conference on*, vol., no., pp. 962-965, 14-19 March 2010

Image Thumbnail Based on Fusion for Better Image Browsing

Boon Tatt Koik

School of Electrical & Electronic Engineering,
Engineering Campus, Universiti Sains Malaysia,
14300 Nibong Tebal, Penang, Malaysia.
Email: btkoik@gmail.com

Haidi Ibrahim

School of Electrical & Electronic Engineering,
Engineering Campus, Universiti Sains Malaysia,
14300 Nibong Tebal, Penang, Malaysia.
Email: haidi_ibrahim@ieee.org

Abstract— Thumbnail image is a smaller version of higher resolution image. It is used to represent the information contained in the original larger image. Thumbnail image gives basic information about the image composition, so that rough judgment on the original image can be done by the user. Yet, common thumbnail algorithms are not sensitive towards blur. Therefore, in order to overcome this problem, we propose a simple image fusion algorithm for thumbnail image. Experimental results carried out in this research show that the thumbnail images generated from the proposed algorithm are more informative as compared with some other common image thumbnails.

Keywords—digital image thumbnail; image down-sampling; image down-scaling; blur detection

I. INTRODUCTION

Nowadays, due to the advances in computer technologies and consumer electronics, many photos are been captured digitally. It is expected that in year 2014, there will be as many as 880 billion digital photos captured. In every one minute, 27800 photos are uploaded to Instagram, whereas 208300 photos are uploaded to Facebook [1]. With this vast amount of information, we need to have a better multimedia management system.

Although the process of taking picture by digital camera is relatively easy, it will be difficult for the user to search back the images. Usually, in order to help the users to find the photos that they want in digital storage, image thumbnails are provided. Many consumer electronics, such as smart phones and digital camera, are also using thumbnail images to display the captured images due to their limited display screen resolution [2].

Pixel-based Down-Sampling with Anti-aliasing Filter (PDAF) is one of the common methods to generate image thumbnail [3]. There are two main stages involved in PDAF. The first stage is to filter the original image with a low pass filter. The low pass filter is used to reduce the frequency bandwidth of the image [4]. This band-limited image is then down-scaled to the size of the desired image thumbnail.

PDAF method has some disadvantages. First, because PDAF applies low pass filter to the image, high frequency components of the image will be eliminated from the image.

Digital noise normally occupies high frequency portion, and thus, PDAF not able to fuse the noise information into its thumbnail [3]. With inappropriate low-pass filter parameters, PDAF sometimes smooth the image thumbnail slightly [5]. PDAF is also not able to accurately present the blur regions of the original image [3].

Direct Pixel Down-sampling (DPD) is other alternative algorithm that is available to generate image thumbnail [5]. DPD creates image thumbnail by using directly the down-sampling equation. If the thumbnail image f is generated from an original high resolution image F using down-sampling factor L , the relationship is given as follows:

$$f(x, y) = F(Lx, Ly) \quad (1)$$

where $f(x,y)$ is the intensity value at coordinate (x,y) on the output image thumbnail, while F is the intensity value of the high resolution input image.

As compared with the image thumbnail generated by PDAF, image thumbnail generated by DPD is relatively sharper. This is because image thumbnail generated by DPD has higher frequency components, which are not removed by low-pass filtering process. Unfortunately, DPD shares the same problem with PDAF, which is it does not able to present the blur of the original image [2].

Fang and Au in 2011 [5] has proposed an algorithm to generate image thumbnail known as Direct Sub-pixel-based Down-sampling (DSD). This method only valid, if both original high resolution and low resolution image thumbnail are color images. This algorithm has been designed in order to strengthen the apparent resolution of an LCD display.

Consider that the images are in Red, Green, Blue (RGB) color space. Then, image F has three layers, which are R , G , and B layers. DSD then will process these three color layers individually, using slight different equations. Lets the output from this algorithms are three color components r , g and b . The equations used to generate r , g , and b from R , G , and B , are [5]:

$$r(x, y) = R(Lx, Ly) \quad (2)$$

$$g(x, y) = G(Lx + 1, Ly) \quad (3)$$

$$b(x, y) = B(Lx + 2, Ly) \quad (4)$$

where L is the down-sampling factor.

However, DPD and DSP produce image thumbnails which are suffers from aliasing [2]. This is because the original signal is not band limited, which makes the violation towards the Nyquist sampling rule.

In order to create a better image thumbnail, in this paper, we propose a simple, yet effective method for image thumbnail generation. As the method wants to give more emphasize on blur region, blur detection is employed in this technique. Blur detection used is based on the edge width.

This paper is arranged as follows. Section II presents the methodology. Experimental results are shown in Section III. Conclusion is given in Section IV.

II. METHODOLOGY

The basic methodology of the proposed method is presented by Figure 1. As shown by this figure, the method can be divided into two stages, which are global processing stage, and local processing stage.

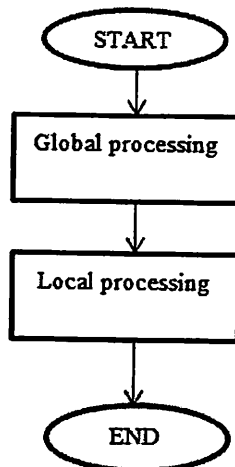


Fig. 1. The general flowchart of the proposed method.

The process involved in the global processing are presented in Figure 2. The input for this stage are the original high resolution image F . Two image thumbnail versions are obtained from this stage. One image thumbnail, which is image thumbnail p , is obtained from PDAF algorithm, whereas another thumbnail image, which is image thumbnail d , is obtained from DPD algorithm.

Another output from this global processing is the edge width map W . Unlike image thumbnail p and image thumbnail

d , which are down-sampled version of F , edge width map W is at the same resolution with F .

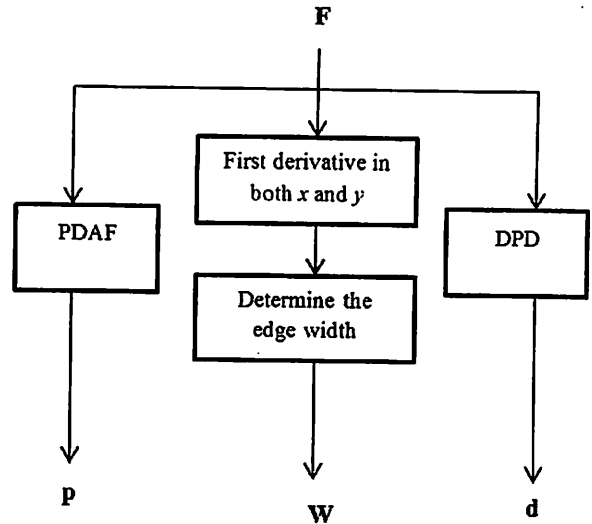


Fig. 2. The processes involved in global processing stage.

Assume that the high resolution images (i.e. F and W) are of size $M \times N$ pixels, while the image thumbnails (i.e. p and d) at resolution $m \times n$ pixels. If the image thumbnails are generated by using a down-sampling factor L , then:

$$m = M / L \quad (5)$$

$$n = N / L \quad (6)$$

In order to create W , original image F is convolved with two Sobel operators, which is in x and y directions. This convolution process with Sobel operator is performed to get the approximation to the first derivative of image F .

First derivative emphasize the location of the edges on image F . Edges play an important role in our blur detection stage, as blur effect can be easily observed on object edges. The sharp region on the image has sharp edges (i.e., step edges), and thus the width of the edge is short. On the other hand, the blurred region on the image has ramp edges, which means a longer edge width.

The edge width is determined based on the work proposed by Chung et al. in year 2004 [6]. From the first derivative estimation, the edge is identified by finding the local maximum gradient values. The width of an edge element is defined as the distance between two distinct local minimum gradient values, where the route for this distance calculation must pass through this edge element (i.e. local maximum gradient value). The calculation started at the local maximum to the "left" side, and then continues to another edge portion at the "right" side. The

route of this process is determined from the edge direction, which is also calculated from the information obtained from the first derivation. In this proposed method of thumbnail generating algorithm, all the pixels involved with the route will be given the value of the edge width.

Next, local processing is carried out. If down-sampling factor of L is used, then, local processing is defined in every contextual region defined by $L \times L$ pixels on the original input resolution. We define another variable, α , which presents the average edge width within that contextual region.

$$\alpha(x, y) = \frac{1}{L \times L} \sum_{i=x}^{x+L-1} \sum_{j=y}^{y+L-1} w(i, j) \quad (7)$$

Yet, in order to reduce the processing burden, α can be approximated by β , which is a sum of edge width:

$$\beta(x, y) = \sum_{i=x}^{x+L-1} \sum_{j=y}^{y+L-1} w(i, j) \quad (8)$$

Then, the local processing is presented by Figure 3.

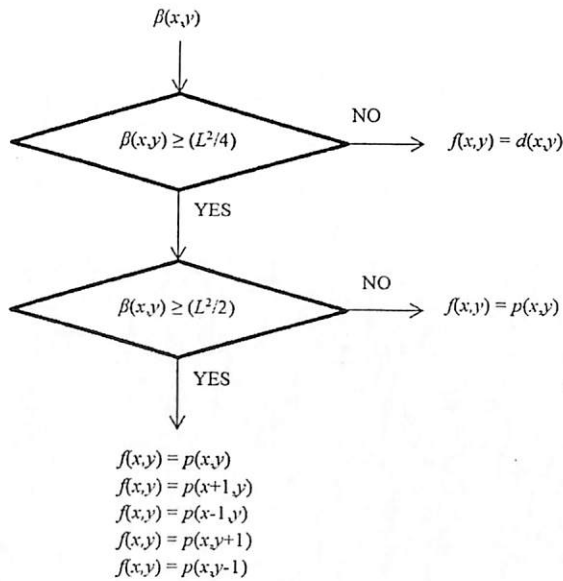


Fig. 3. The processes involved in global processing stage.

As shown by this Figure 3, the intensity of the image thumbnail f at location (x, y) , $f(x, y)$, is depending to the value of $\beta(x, y)$. Switching method is utilized. If $\beta(x, y)$ is less than $L^2/4$, the contextual region is considered as sharp region, and thus, information from DPD is more applicable (i.e., $f(x, y) = d(x, y)$). Otherwise, the contextual region is considered as blurred, and therefore, image thumbnail f will take the value from PDAF. Yet, we further classified the region as blurred region, and seriously blurred region. If $\beta(x, y)$ is less than $L^2/2$, the contextual region is considered as blurred region, and thus, $f(x, y)$ takes the value from $p(x, y)$. For the seriously blurred region, where $\beta(x, y)$ is equal or greater than $L^2/2$, the

corresponding pixel at (x, y) and its four neighboring pixels will take the value from p . This approach is used to give emphasize on the seriously blurred region into the image thumbnail.

III. EXPERIMENTAL RESULTS



(a)



(b)



(c)



(d)



(e)

Fig. 4. Test image 1 (a) The original image. (b) Image thumbnail generated using PDAF. (c) Image thumbnail generated using DPD. (d) Image thumbnail generated using DSD. (e) Image thumbnail generated using the proposed method.

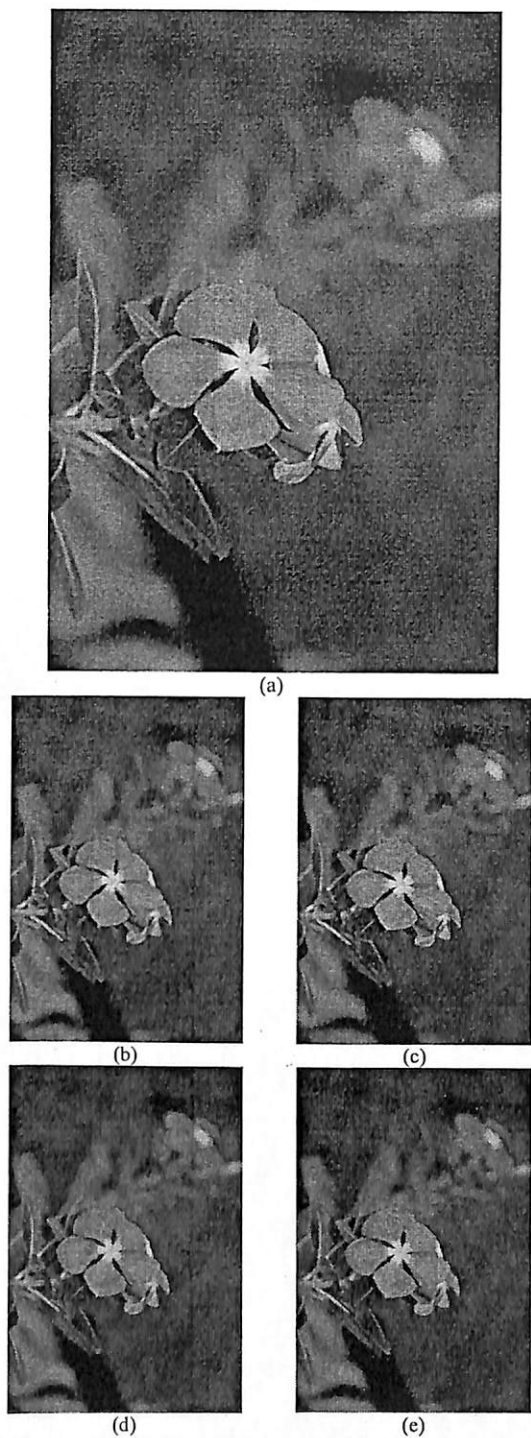


Fig. 5. Test image 2 (a) The original image. (b) Image thumbnail generated using PDAF. (c) Image thumbnail generated using DPD. (d) Image thumbnail generated using DSD. (e) Image thumbnail generated using the proposed method.

In order to evaluate the performance of the proposed method, the image thumbnails generated from the proposed method have been compared with the responding image thumbnails from PDAF, DPD and DSD. Two test images have been used. The down-sampling factor L is set to 8. The results are shown in Figure 4 to Figure 5.

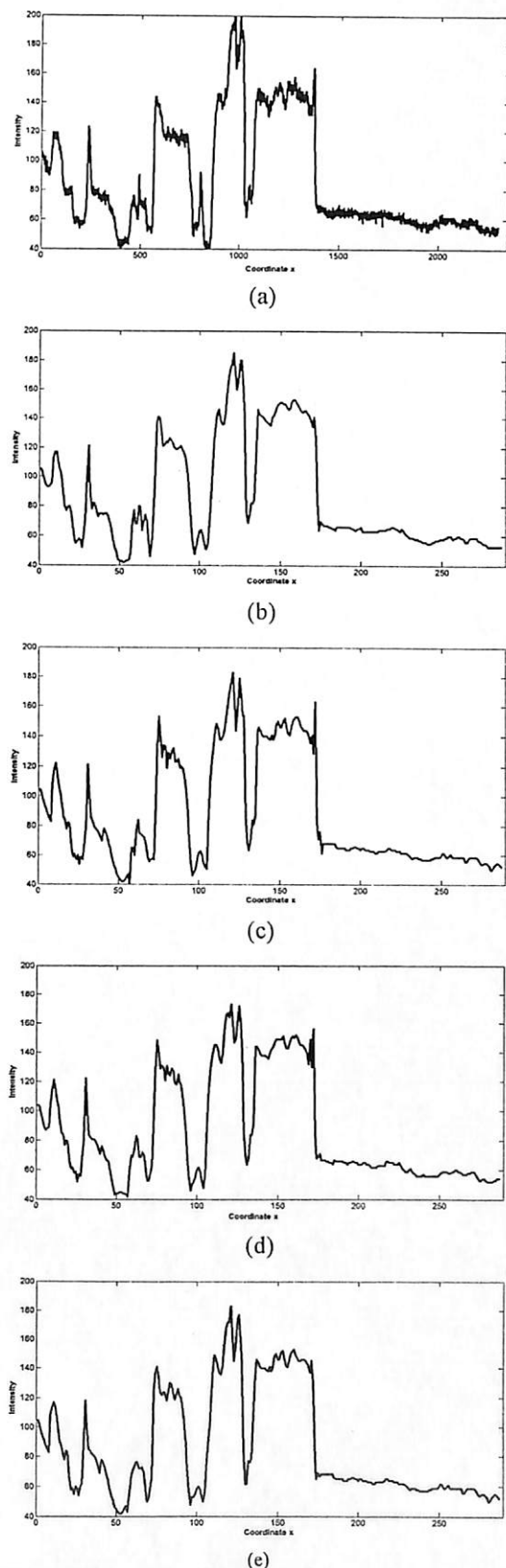


Fig. 6. The respective image profiles showing blur and sharp region of Fig. 5.

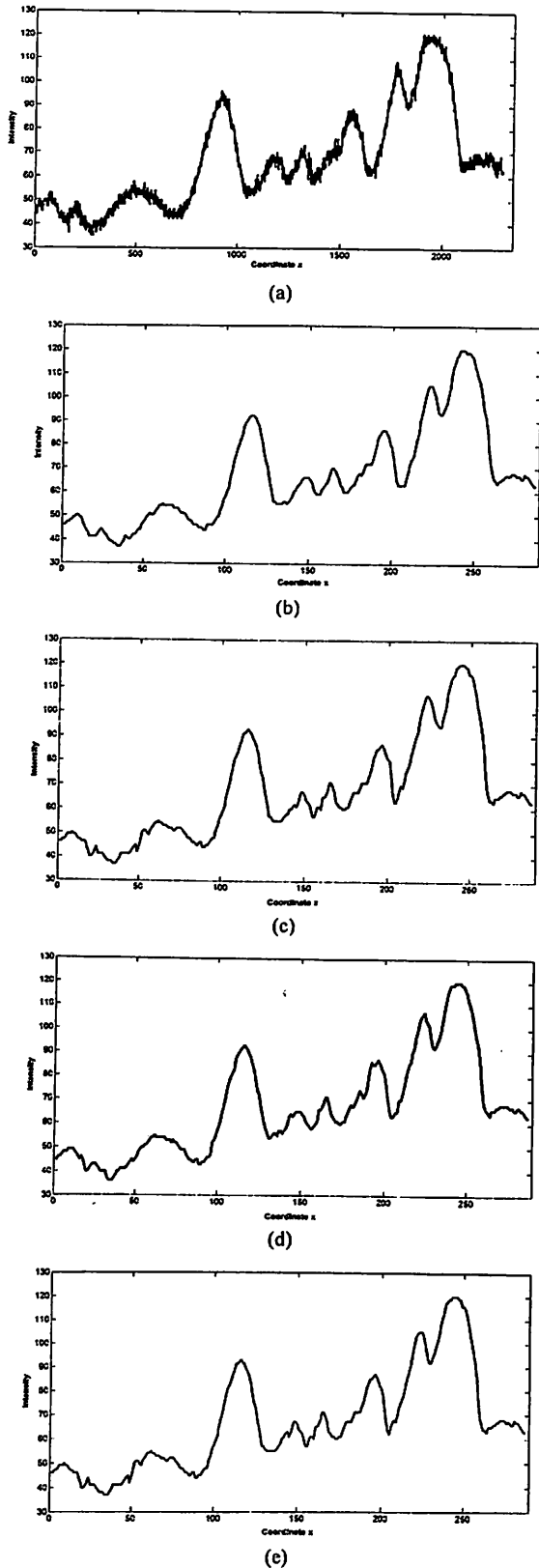


Fig. 7. The respective image profiles for total blur region of Figure 5.

As shown in Figure 4, Test image 1 is an indoor picture. Object of interest in this photo is the face of the boy. This region is sharp. Some regions of the image are blurred. This is because due to the movement. For example, the person that walked behind the boy was moving when this photo taken, thus appears blurred. The boy also clapping his hands, thus his hands also appears blurred in this image.

In Figure 4, the person who walked behind the boy appears blurred in all image thumbnails. Yet, the blur on the hands region are easier to be seen in the thumbnail image generated by PDAF and the proposed method.

Figure 5 shows Test image 2, which is blurred due to focus of the camera. Similar to Figure 4, the results from DPD and DPD are slightly sharper. This can be observed on the edges of the flowers and leaves located on the front portion. The results from PDAF and the proposed algorithm are better as the thumbnail images appear smoother.

In order to further evaluate the performance of the proposed algorithm, profiles of images shown in Figure 5 are shown in Figure. 6. The profiles are taken at $y=1728$ for the original image, while $y = 216$ for the image thumbnails, which is equal to half of the y-axes in the resultant image. Figure 7 shows the image profile of coordinate x across quarter value of $y = 108$ for thumbnail image and $y=864$ for original image.

As shown by Figure 6, information of the original image has been reduced by all image thumbnails. Yet, the profiles for DPD and DSD suggest that many edges on these images thumbnail are step edges, which make the object appears sharper. For smoother thumbnails, the thumbnail by the proposed method is smoother than thumbnail by PDAF method as it has less step edges.

For Figure 7, as the cross-line is in a fully blur region, the fluctuation of the step edge is hard to be noticeable as compared with Figure 6, which the cross-line included the sharp object, the flower and blur background.

IV. CONCLUSION

This paper presents a new method to generate image thumbnail. The performance of the proposed method is better than DPD and DSD method. Yet, there are still improvements that can be done in order to increase the sensitivity of the algorithm towards blur and noise.

ACKNOWLEDGMENT

This work was supported in part by the Universiti Sains Malaysia's Research University Individual (RUI) Grant with account number 1001/PELECT/814169.

REFERENCES

- [1] Stan Horaczek. (2013, May 27). *How many photos are uploaded to the internet every minute?* [Online]. Available: www.poppphoto.com/news/2013/05/how-many-photos-are-uploaded-to-internet-every-minute
- [2] Haidi Ibrahim, "Image thumbnail with blur and noise information to improve browsing experience", *Advances in Multimedia - An International Journal (AMIJ)*, vol. 2, no. 3, pp. 39-48, 2011.

- [3] Ramin Samadani, Suk Hwan Lim and Dan Tretter, "Representative image thumbnails for good browsing", *IEEE International Conference on Image Processing, ICIP 2007*, pp. II-193-II-196, 2007.
- [4] Johannes Kopf, Ariel Shamir, and Pieter Peers, "Content-adaptive image downscaling", *ACM Transactions on Graphics (TOG)*, vol. 32, no. 6, 8 pages, 2013.
- [5] Lu Fang and Oscar C. Au, "Subpixel-based image down-sampling with min-max directional error for stripe display", *IEEE Journal of Selected Topics in Signal Processing*, vol. 5, no. 2, pp. 240-251, 2011.
- [6] Yun-Chung Chung, Jung-Ming Wang, R. R. Bailey, Sei-Wang Chen, and Shyang-Lih Chang, "A non-parametric blur measure based on edge analysis for image processing applications", *IEEE Conference on Cybernetics and Intelligent Systems 2004*, vol. 1, no. 1, p. 356-360, 2004.

Accentuate of Bright Structures onto Image Thumbnail using Dilated Intensity Projection

Boon Tatt Koik¹, Haidi Ibrahim¹ and Theam Foo Ng²

¹School of Electrical & Electronic Engineering, Engineering Campus, Universiti Sains Malaysia, 14300 Nibong Tebal, Penang, Malaysia,

²Centre for Global Sustainability Studies (CGSS), 5th Floor, Hamzah Sendut Library (New Wing), Universiti Sains Malaysia, 11800 Penang, Malaysia.

btkoik@gmail.com, haidi_ibrahim@iccc.org, tfng@usm.my

Abstract: Thumbnail image, which is a relatively small image, is used to represent a larger, original image. Thumbnail image gives a basic idea to the user about the general quality of the original image. Due to limited information that can be embedded onto thumbnail image, small or thin structures normally have been eliminated in this small image version. Thus, in this paper, we proposed a new, yet simple method to accentuate small or thin bright structures into image thumbnail. Our method uses grayscale mathematical morphology operation, where the thumbnail is presented by the projection of dilated intensity values. Experimental results show that this new thumbnail generation approach is able to highlight small or thin bright structures.

Keywords: Digital image thumbnail, image down-sampling, image down-scaling, mathematical morphology operations.

1. Introduction

Currently, images can be captured digitally by using semiconductor charge-coupled devices (CCD) or complementary metal-oxide-semiconductor (CMOS) sensors [1]. With the advancement of technologies, digital cameras are now affordable and becoming a common tool in our daily life. It is expected that within this year, as many as 880 billion digital photos will be captured [2]. In order to fulfill the requirements from the user, in addition to digital cameras and digital camcorder, many other consumer electronic products, such as laptops and smart phones are now been equipped with digital camera.

When we capture the image using these electronic products, normally we will check the quality of the captured image right after we took the picture. The captured images are commonly shown on the display screen of the product. Basically, the display is with limited spatial resolutions, thus the captured images have to down-sampled, or down-scaled, in order to fit those image to the display screen [3]. This down-sampled version is called as the thumbnail image.

The common method to generate image thumbnail is by using a method known as Pixel-based Down-sampling with Anti-aliasing Filter (PDAF) [4]. This method contains two stages. The first stage, an anti-aliasing filter, which is a low pass filter, is applied to the original image, in order to reduce the frequency range of the image. This approach is used in order to avoid aliasing effect due to the violation of Nyquist sampling rate. The second stage of the method is the down-scaling process, where the originally larger image is down-sampled to smaller image representative.

Unfortunately, PDAF method has some disadvantages. Due to the usage of low pass filter, the image becoming blurred. Small or thin structures, which are dominated by high frequency components, will be reduced, or even eliminated from the thumbnail images. Therefore, PDAF is not able to embed information of the image noise onto the thumbnail image [4]. In addition, thumbnail images generated by PDAF are sometimes too smooth, especially when the parameters for the low-pass filter are not been tuned properly [5].

Thumbnail image also can be generated from Direct Pixel Down-sampling (DPD) method [5]. This method, unlike PDAF, only has one stage, which is down-scaling stage. The down-scaling process of DPD is given by the following equation:

$$f(x, y) = F(Lx, Ly) \quad (1)$$

where F is the originally high spatial resolution image, f is output thumbnail image, (x, y) are the spatial coordinates, and L is the down-sampling factor.

DPD method produces thumbnail images, which are relatively sharper than the one produced by PDAF. The implementation of DPD is also simple. Unfortunately, similar to PDAF method, DPD method is also has several drawbacks. Thumbnail images generated by DPD suffer from aliasing artifact [3]. Furthermore, as shown by equation (1), only information from one pixel from the original image is taken to represent one pixel on the thumbnail image. Information from other L^2-1 are been ignored by DPD, make it difficult to presents small and thin structures.

A modification to DPD method, known as Direct Sub-pixel-based Down-sampling (DSD), has been proposed by Fang and Au in 2011 [5]. This method only works for color images, and has been designed for the use in LCD display. DSD considers both F and f are in red, green and blue color space. The processes involved in DSD method are given by Equations (2) to (4):

$$r(x, y) = R(Lx, Ly) \quad (2)$$

$$g(x, y) = G(Lx+1, Ly) \quad (3)$$

$$b(x, y) = B(Lx+2, Ly) \quad (4)$$

where r , g , and b are the red, green, and blue channel for image f , respectively. On the other hand, R , G , and B are the red, green, and blue channel for image F .

Similar to DPD, only limited information is taken by DSD. Considering three color channel, for a down-sampling process with factor L , DSD only takes the information from

three pixels, while ignoring $3(L^2-1)$ pixels. Therefore, DSD is also not suitable to present small and thin structure on the image.

In this paper, we propose a new, yet simple method. This method utilizes grayscale mathematical morphology operation, which is the dilation operation. By using this operation, the method gives more emphasize to the bright structures, and accentuate them onto image thumbnail.

The arrangement of this manuscript is as follows. We begin with Section II, which will present the methodology of the proposed method. Then, the experimental results will be presented in Section III. The last section, which is Section IV, will conclude our research findings.

2. Methodology

If F is with resolution $M \times N$ pixels, f is with resolution $m \times n$ pixels (i.e, $m = M/L$ and $n = N/L$). Therefore, in generating the thumbnail, our aims is to project $M \times N$ pixels onto $m \times n$ grid. In other words, we want to accurately project $L \times L$ pixels from image F to one single pixel on image f . This is shown by Figure 1.

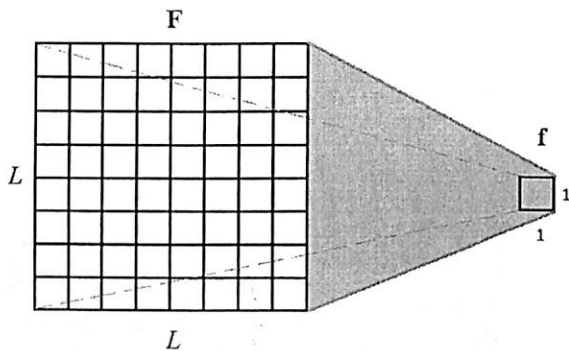


Figure 1. Projecting information from high spatial resolution grid to lower resolution grid

The proposed method consists of two stages. The first stage is the accentuation of bright structures by using grayscale morphology operation. The second stage is the down-scaling process.

In order to emphasize bright structure in the image, we use grayscale morphological operations, which is erosion operation \ominus . This operation is given as [6]:

$$D(x, y) = [F \ominus S](x, y) = \max_{(s,t) \in b} \{F(x-s, y-t)\} \quad (5)$$

where S is the structuring element, and D is the dilated image. In this work, we use a flat structuring element, with size $L \times L$ pixels. The reason why we choose a flat structuring element is because we want to take equal contributions from all samples. We set the structuring element to size of $L \times L$ pixels in to completely cover the area defined by the down-sampling factor L , as shown by Figure 1.

The second stage of this method is to down sample image D . This process is given as:

$$f(x, y) = D(Lx, Ly) \quad (6)$$

The method can be used for grayscale and also color images. If the image is color image, the proposed method will process each color channel independently.

It is noted from Equation (6), the proposed method only takes use one pixel from image D to assign it to image f . Thus, in order to reduce the processing time, Equation (5) can be simplified as follows:

$$D(x, y) = \begin{cases} [F \oplus S](x, y) & \begin{cases} x = 0, L, 2L, 3L, \dots \\ y = 0, L, 2L, 3L, \dots \end{cases} \\ 0 & \text{Otherwise} \end{cases} \quad (7)$$

By using Equation (7) instead of Equation (5), the computational requirement of the proposed method is reduced significantly.

3. Experimental Results

In this experiment, two test images have been used. The first result, which is using Test Image 1, is shown in Figure 2. The original size of Test Image 1 is 3456×2304 pixels. The down-sampling factor used in this experiment is set to value 8 (i.e., $L=8$). Thus, the output thumbnail image is at size 432×288 pixels.

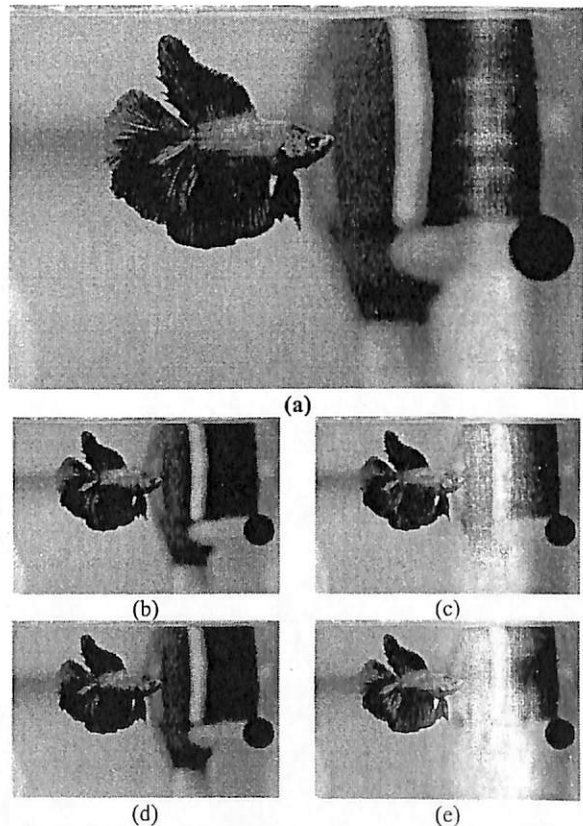


Figure 2. Test image 1. (a) Input image. (b) Output from PDAF. (c) Output from DPD. (d) Output from DSD. (e) Output from the proposed method.

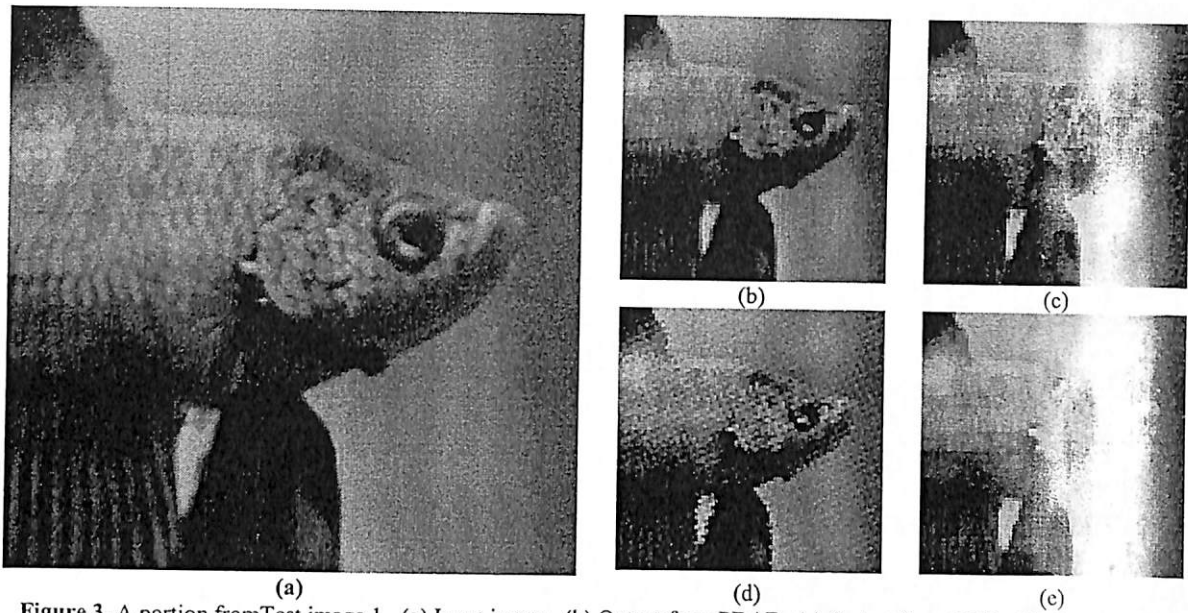


Figure 3. A portion from Test image 1. (a) Input image. (b) Output from PDAF. (c) Output from DPD. (d) Output from DSD. (e) Output from the proposed method.

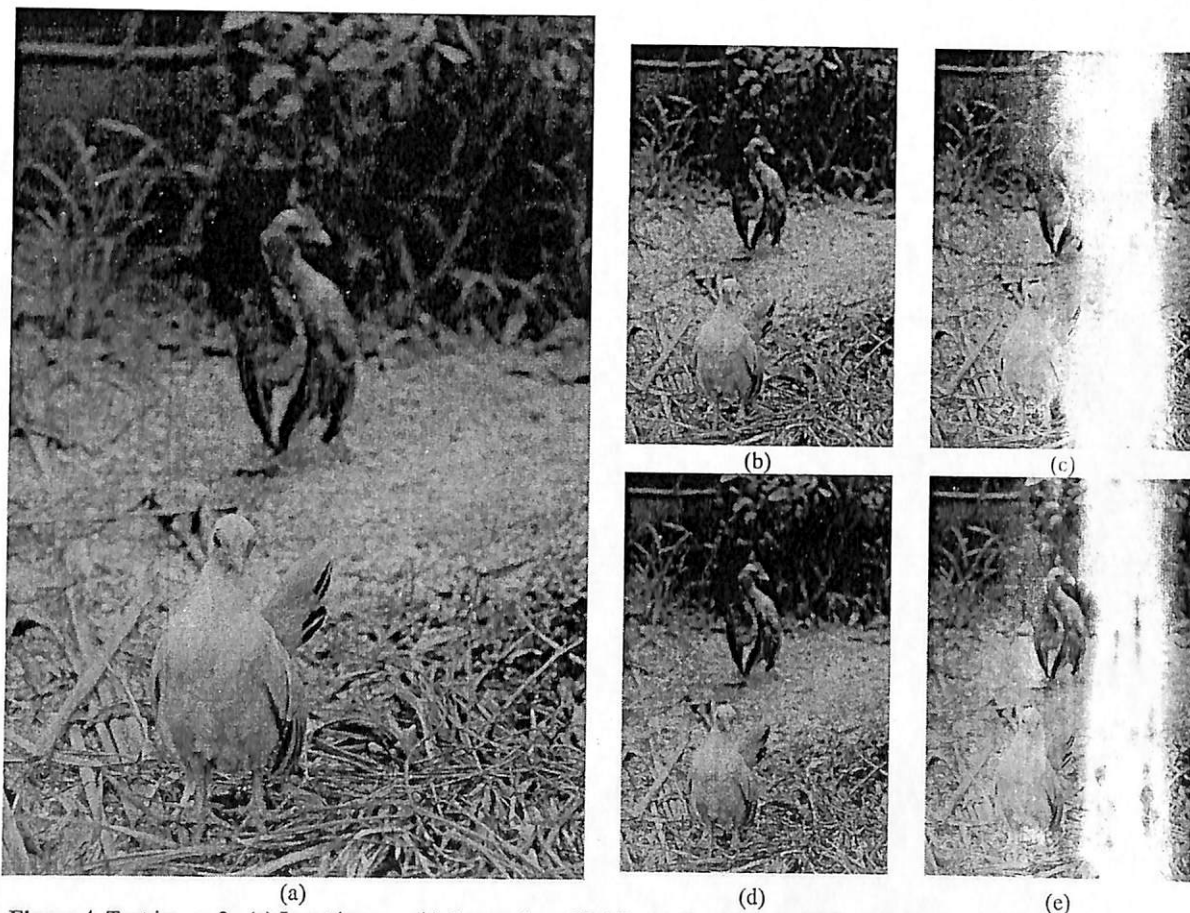


Figure 4. Test image 2. (a) Input image. (b) Output from PDAF. (c) Output from DPD. (d) Output from DSD. (e) Output from the proposed method.

As shown by Figure 2, all methods successfully generate the thumbnail versions of the original images. The basic structure and the composition of the original image can be represented by all thumbnail images. Yet, the proposed method successfully emphasizes the bright structure of the image. This can be observed by comparing the body and tail of the fish in Figure 2(e) with other subfigures.

Zoom in image regions from the images shown in Figure 2 are given in Figure 3. This square region is defined by two coordinates, which are (x_{start}, y_{start}) and (x_{end}, y_{end}) . For image F, $(x_{start}, y_{start}) = (1360, 170)$ and $(x_{end}, y_{end}) = (2007, 1207)$, whereas for image f, $(x_{start}, y_{start}) = (170, 70)$ and $(x_{end}, y_{end}) = (250, 150)$. The size for the cropped original image is 648×648 pixels, while the size for the cropped thumbnail images is 81×81 pixels.

In Figure 3, we can see that both thumbnail images from DPD (see Figure 3(c)) and DSD (see Figure 3(d)) suffer from aliasing artifacts, where the edges are not smooth. The thumbnail image from PDAF produce more natural image. However, the thumbnail image from the proposed method is more accurate. This is because, if we compare Figure 3(e) with Figure 3(a), we can see that the proposed method successfully embeds the bright small dots near the fish's mouth onto its thumbnail image.

The second result, which is using Test Image 2, is shown in Figure 4. The original size of Test Image 2 is 3456×5184 pixels. The down-sampling factor used in this experiment is set to value 8 (i.e., $L=8$). Thus, the output thumbnail image is at size 432×648 pixels.

Similar to the results obtained in Figure 2, the same observation can be obtained from Figure 4. All thumbnail versions can give a basic idea to the users, regarding to the basic composition of the original image. However, the proposed method successfully emphasizes the bright structure on the image, as what can be seen from Figure 3(e). In this figure, the white hen appears brighter in this thumbnail, as compared with other thumbnail images.

4. Conclusion

A new method, utilizing grayscale mathematical morphological dilation operation, has been proposed in this paper. The method is simple and easy to be implemented. Compared to other thumbnail image algorithms, the proposed method has better ability to highlight bright structure into the thumbnail images.

Acknowledgment

This work was supported in part by the Universiti Sains Malaysia's Research University Individual (RUI) Grant with account number 1001/PELECT/814169.

References

- [1] Gerald C. Holst and Terrence S. Lomheim, CMOS/CCD Sensors and Camera Systems. *SPIE Press Book*, 2007.
- [2] Stan Horaczek, How many photos are uploaded to the internet every minute? [Online, Accessed on 31st August 2014] www.popphoto.com/news/2013/08/how-many-photos-are-uploaded-to-internet-every-minute
- [3] Haidi Ibrahim, "Image thumbnail with blur and noise information to improve browsing experience," *Advances in Multimedia - An International Journal (AMJ)*, vol. 2, no. 3, pp. 39-48, 2011.
- [4] Ramin Samadani, Suk Hwan Lim and Dan Greter, "Representative image thumbnails for good browsing", *IEEE International Conference on Image Processing (ICIP 2007)*, pp. II-193-II-196, 2007.
- [5] Lu Fang and Oscar C. Au, "Subpixel-based image down-sampling with min-max directional error for stripe display," *IEEE Journal of Selected Topics in Signal Processing*, vol. 2, no. 2, pp. 240-251, 2011.
- [6] Rafael C. Gonzalez and Richard E. Woods, *Digital Image Processing*, Third Edition. *Pearson Prentice Hall*, 2008.